Universidade do Minho
Escola de Engenharia

César Javier Chácara Espinoza

Macro-Element Nonlinear Dynamic Analysis
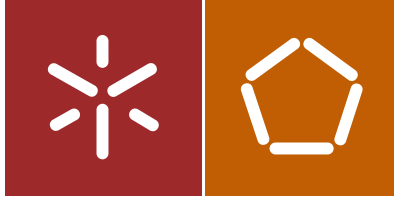for the Assessment of the Seismic Vulnerability
of Masonry Structures

César Javier Chácara Espinoza

Macro-Element Nonlinear Dynamic Analysis for the Assessment of the Seismic Vulnerability of Masonry Structures
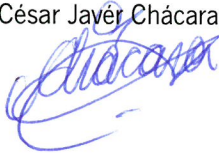
STATEMENT OF INTEGRITY

I hereby declare having conducted my thesis with integrity. I confirm that I have not used plagiarism or any form of falsification of results in the process of the thesis elaboration.

I further declare that I have fully acknowledged the Code of Ethical Conduct of the University of Minho.

University of Minho, 16/02/2018

Full name: César Javér Chácara Espinoza

Signature:

ACKNOWLEDGMENTS

ABSTRACT

Earthquakes constitutes one of the most devastating natural hazards since they lead to the collapse of buildings; and consequently, a significant number of human losses. Some typologies of buildings, namely historical and masonry constructions, are one of the most vulnerable elements at risk due to their weak performance when subjected to seismic actions. For instance, historic structures were built based on simple rules since seismic codes were not properly established at the time of their construction. On the other hand, many masonry structures, especially in developing countries, are usually constructed without taking into consideration the specifications provided by current seismic codes. These constructions are mainly characterised by a poor connection between orthogonal walls and between walls and horizontal diaphragms which lead to the occurrence of out-of-plane mechanisms. This behaviour is considered one of the most vulnerable, yet one of the most neglected failure mechanisms when assessing the seismic performance of these constructions.

This thesis aims at the assessment of the out-of-plane behaviour as well as the seismic vulnerability of masonry structures with a predominant out-of-plane collapse. For this purpose, a simplified computational tool, based on a macro-element modelling approach, was extended into the dynamic field by the definition of cyclic constitutive laws and the introduction of a consistent mass matrix. This modelling approach is capable of accurately simulating the main in-plane and most importantly out-of-plane mechanisms of this type of constructions with a reduced computational burden. These features are validated by the comparison of the linear and nonlinear dynamic response of three case studies investigated by means of differential equations and sophisticated computational tools. This validation demonstrated the capability of this simplified modelling approach of accurately estimating dynamic properties and simulating the rocking motion of a rigid block and the nonlinear hysteretic behaviour of masonry structures.

After validation, this modelling approach was employed for the assessment of the out-of-plane behaviour of two unreinforced masonry structures previously tested by means of shaking table tests. This

investigation was carried out in the static and dynamic nonlinear fields by the application of a mass distributed lateral force and a recorded input from the experimental campaign. The unreinforced masonry structures were also investigated considering a more sophisticated numerical approach, namely Finite Element models. A comparison between these two numerical models was conducted in terms of maximum load capacity, post-elastic behaviour and hysteretic response demonstrating significant resemblance. An additional comparison was conducted taken into consideration numerical and experimental failure mechanisms. A good agreement was obtained when comparing the in-plane response of these structures. Nevertheless, the out-of-plane mechanisms were not successfully simulating evidencing the complexity of this behaviour, especially in a dynamic context. Based on these results, it was demonstrated that this simplified numerical tool can be considered as an alternative computational tool for the assessment of this type of structures since the computational burden was significantly reduced.

Finally, the seismic vulnerability of one of these unreinforced masonry structures was investigated by the derivation of analytical fragility curves. For this purpose, the simplified model of such structure was subjected to a set of nonlinear dynamic analyses based on accelerogram artificially generated. In addition, three limit states, whose definition was based on an alternative procedure consisting of the application of nonlinear static analyses, were considered for the assessment of the seismic vulnerability of such structure. This was conducted concentrating the uncertainty initially on the seismic input (artificial accelerograms), and subsequently, on additional parameters such as mechanical properties, thickness of walls, and damping ratio by the definition of probabilistic models. From these assessments, it was possible to determine the probability of exceeding the three limit states due to the application of dynamic loading to masonry structures that are characterised by out-of-plane collapse mechanisms.

RESUMO

Os sismos constituem um dos perigos naturais mais devastadores, uma vez que envolvem o colapso de edifícios e, consequentemente, um número significativo de perdas humanas. Algumas tipologias de edifícios, nomeadamente construções históricas e de alvenaria, são um dos elementos mais vulneráveis devido ao seu fraco desempenho quando submetidas a ações sísmicas. Por exemplo, as estruturas históricas foram construídas com base em regras simples, uma vez que os regulamentos sísmicos não foram adequadamente estabelecidos aquando a sua construção. Por outro lado, muitas estruturas de alvenaria, especialmente em países em desenvolvimento, são geralmente construídas sem ter em consideração as especificações fornecidas pelos códigos sísmicos atuais. Essas construções são caracterizadas, principalmente, por uma deficiente ligação entre paredes ortogonais e entre paredes e diafragmas horizontais que levam à ocorrência de mecanismos para fora do plano. Esse comportamento é considerado um dos mais vulneráveis e, também, um dos mecanismos de colapso mais negligenciados na avaliação do desempenho sísmico dessas construções.

Esta tese tem como objetivos principais a avaliação quer do comportamento para fora do plano, quer a vulnerabilidade sísmica das estruturas de alvenaria com um colapso predominante para fora do plano. Para isso, uma ferramenta computacional simplificada, baseada numa abordagem de modelação de macro-elemento, foi alargada ao comportamento dinâmico pela definição de leis constitutivas cíclicas e a introdução de uma matriz consistente de massa. Esta abordagem de modelação é capaz de simular com precisão os mecanismos principais no plano e, mais importante, os mecanismos para fora do plano deste tipo de construções com um esforço computacional reduzido. Essas características foram validadas pela comparação da resposta dinâmica linear e não-linear de três casos de estudo investigados por meio de equações diferenciais e outras ferramentas computacionais sofisticadas. Esta validação demonstrou a capacidade da presente abordagem para estimar com precisão as propriedades dinâmicas e simular o movimento de corpo rígido e o comportamento histerético não-linear das construções em alvenaria.

Após a validação, esta abordagem de modelação foi utilizada para a avaliação do comportamento para fora do plano de duas estruturas de alvenaria simples, previamente testadas numa mesa sísmica. Esta investigação foi realizada nos regimes estáticos e dinâmicos não-lineares pela aplicação de uma força de massa lateralmente distribuída e através de registos da campanha experimental. As estruturas de alvenaria simples também foram investigadas considerando uma abordagem numérica mais sofisticada, nomeadamente modelos de elementos finitos. Uma comparação entre esses dois modelos numéricos foi realizada em termos de capacidade de carga máxima, comportamento pós-elástico e resposta histerética demonstrando uma semelhança significativa. Uma comparação adicional foi realizada levando em consideração os mecanismos de rotura numéricos e experimentais. Foi obtido um bom acordo na comparação da resposta no plano dessas estruturas. No entanto, os mecanismos para fora do plano não foram simulados com sucesso, evidenciando a complexidade desse comportamento, especialmente num contexto dinâmico. Com base nesses resultados, foi demonstrado que esta ferramenta numérica simplificada pode ser considerada como uma ferramenta computacional alternativa para a avaliação deste tipo de estruturas, uma vez que o esforço computacional foi significativamente reduzido.

Finalmente, a vulnerabilidade sísmica de uma dessas estruturas de alvenaria simples foi investigada através da obtenção analítica de curvas de fragilidade. Para esse fim, o modelo simplificado dessa estrutura foi submetido a um conjunto de análises dinâmicas não-lineares através de acelerogramas gerados artificialmente. Para a avaliação da vulnerabilidade sísmica foram considerados três estados limite, cuja definição foi baseada num procedimento alternativo baseado na aplicação de análises estáticas não-lineares. Esta avaliação foi conduzida concentrando, inicialmente, a incerteza na ação sísmica (acelerogramas artificiais) e, subsequentemente, em parâmetros adicionais como propriedades mecânicas, espessura das paredes e rácio de amortecimento com definição de modelos probabilísticos. A partir dessas análises, foi possível determinar a probabilidade de atingir os três estados limite devido à aplicação do carregamento dinâmico a estruturas de alvenaria que são caracterizadas por mecanismos de rotura para fora do plano.

RESUMEN

Los sismos constituyen uno de los peligros naturales más devastadores, ya que implican el colapso de edificios y, por consiguiente, un número significativo de pérdidas humanas. Algunas tipologías de edificios, en particular construcciones históricas y de albañilería, son uno de los elementos más vulnerables debido a su débil desempeño cuando se someten a acciones sísmicas. Por ejemplo, las estructuras históricas se construyeron sobre la base de reglas simples, ya que los códigos sísmicos no fueron establecidos adecuadamente en su construcción. Por otro lado, muchas estructuras de albañilería, especialmente en países en desarrollo, generalmente se construyen sin tener en cuenta las especificaciones proporcionadas por los códigos sísmicos actuales. Estas construcciones se caracterizan principalmente por una conexión deficiente entre muros ortogonales, y entre muros y diafragmas horizontales, lo que conlleva a la ocurrencia de mecanismos por fuera del plano. Este comportamiento es considerado uno de los más vulnerables y, también, uno de los mecanismos de colapso menos considerados en la evaluación del desempeño sísmico de esas construcciones.

Esta tesis tiene como objetivos principales la evaluación tanto del comportamiento por fuera del plano como la vulnerabilidad sísmica de las estructuras de albañilería con un colapso predominante por fuera del plano. Para ello, una herramienta computacional simplificada, basada en un enfoque de modelado de macro-elemento, se ha ampliado al comportamiento dinámico mediante la definición de leyes constitutivas cíclicas y la introducción de una matriz consistente de masa. Este enfoque de modelado es capaz de simular con precisión los mecanismos principales en el plano y, más importante, los mecanismos por fuera del plano de este tipo de construcciones con una demanda computacional reducida. Estas características fueron validadas mediante la comparación de la respuesta dinámica lineal y no lineal de tres casos de estudio investigados por medio de ecuaciones diferenciales y otras herramientas computacionales sofisticadas. Esta validación demostró la capacidad del presente enfoque para estimar con precisión las propiedades dinámicas, y simular el movimiento de cuerpo rígido y el comportamiento histerético no lineal de las construcciones en albañilería.

Después de la validación, este enfoque de modelado fue utilizado para evaluar el comportamiento por fuera del plano de dos estructuras de albañilería simples, previamente ensayadas en una mesa sísmica. Esta investigación se realizó en los regímenes estáticos y dinámicos no lineales mediante la aplicación de una fuerza de masa lateralmente distribuida, y por medio de registros de la campaña experimental. Las estructuras de albañilería simple también fueron investigadas considerando un enfoque numérico más sofisticado, en particular modelos de elementos finitos. Una comparación entre estos dos modelos numéricos se llevó a cabo en términos de capacidad de carga máxima, comportamiento post-elástico y respuesta histerética demostrando una semejanza significativa. Una comparación adicional fue realizada tomando en cuenta los mecanismos de falla numéricos y experimentales. Se obtuvo una buena correspondencia en la comparación de la respuesta en el plano de estas estructuras. Sin embargo, los mecanismos por fuera del plano no fueron simulados con éxito, evidenciando la complejidad de este comportamiento, especialmente en un contexto dinámico. En base a estos resultados, se ha demostrado que esta herramienta numérica simplificada puede considerarse como una herramienta computacional alternativa para la evaluación de este tipo de estructuras, ya que el esfuerzo computacional se redujo significativamente.

Finalmente, la vulnerabilidad sísmica de una de esas estructuras de albañilería simple fue investigada a través de la obtención analítica de curvas de fragilidad. Para este fin, el modelo simplificado de esa estructura fue sometido a un conjunto de análisis dinámicos no lineales en base a acelerogramas generados artificialmente. Para la evaluación de la vulnerabilidad sísmica se consideraron tres estados límite, cuya definición se basó en un procedimiento alternativo basado en la aplicación de análisis estáticos no lineales. Esta evaluación se llevó a cabo concentrando inicialmente la incertidumbre en la acción sísmica (acelerogramas artificiales) y, posteriormente, en parámetros adicionales como propiedades mecánicas, espesor de las paredes y coeficiente de amortiguamiento, mediante la definición de modelos probabilísticos. A partir de estos análisis, fue posible determinar la probabilidad de alcanzar los tres estados límite debido a la aplicación de carga dinámica a estructuras de albañilería que se caracterizan por mecanismos de falla por fuera del plano.

CONTENTS

CHAPTER 3

MACRO-ELEMENT MODELLING APPROACH

CHAPTER 4

MODEL VALIDATION

CHAPTER 5

ANALYSIS OF URM STRUCTURES

INDEX OF FIGURES

INDEX OF TABLES

CHAPTER 1

INTRODUCTION

1.1 MOTIVATION

The construction of masonry structures made of bricks, stones or adobes, dates back over 10,000 years making it one of the oldest and most widely used building materials in the world. Nowadays, this type of structures is still being used, mainly in developing countries due to its easy accessibility and affordability, but also in many European countries for housing structures or infills. Nevertheless, it has been evidenced that many of these constructions present a weak performance when subjected to seismic actions, especially when the collapse mechanism is associated with an out-of-plane response. This type of behaviour usually occurs due to the inadequate connection between walls and diaphragms, or the weak behaviour of these horizontal elements since many of these constructions, including the historical ones, were built without taking into consideration seismic codes. In this regard, the assessment of the seismic behaviour of this type of structures as well as their vulnerability constitutes an important concern in regions with significant seismic hazard.

During the last decades, the assessment of the seismic behaviour of masonry structures has been conducted by means of experimental campaigns, numerical simulations, and analytical formulations. Most of these investigations have been focused on the study of the in-plane response assuming the prevention of out-of-plane mechanisms, adopting a box-type behaviour. A reduced number of studies has also been carried out regarding the out-of-plane response of this type of structures, demonstrating its complex behaviour, especially in the dynamic field. On the other hand, the seismic vulnerability of masonry constructions has also been investigated in the last years. However, the literature

regarding this type of structures is limited and, again, mostly focused on in-plane mechanisms following the same box-type behaviour assumption; therefore, neglecting the out-of-plane mechanisms. In this regard, it can be noted that these investigations have been mainly oriented to modern reinforced masonry structures, built either under the guidelines of recent seismic codes or before such codes.

The seismic assessment of masonry structures by means of numerical simulations has been conducted using advanced and simplified approaches. These different computational tools are characterised by advantages as well as disadvantages when assessing the seismic behaviour of this type of structures. For instance, numerical models based on the Finite Element (FE) method constitute one of the most versatile tools capable of predicting and understanding the nonlinear behaviour of masonry structures. This modelling approach has been implemented with a diversity of computational frameworks as well as sophisticated constitutive laws. However, the application of nonlinear analysis mainly in the dynamic field usually requires a significant computational burden due to the degree of detail of the mesh refinement, which constitutes a major drawback for the seismic vulnerability assessment. In this regard, the introduction of simplified computational tools was conceptualised aiming at overcoming this limitation. Nevertheless, expedite numerical strategies also present some drawbacks mainly associated with the oversimplification of their mechanical scheme, and most importantly with neglecting the complex out-of-plane behaviour of masonry structures without box behaviour. Due to the limitations just addressed, the seismic assessment of UnReinforced Masonry (URM) structures is still considered a complex task, and a simplified numerical tool capable of properly simulating the out-of-plane mechanisms with a reduced computational burden is needed.

In this regard, a simplified numerical tool based on a macro-element modelling approach was proposed by Caliò, et al. [1] aiming at assessing the seismic behaviour of masonry structures in the nonlinear static field. Based on an initial mechanical configuration, this modelling approach was capable of simulating the main in-plane mechanisms of this type of structures namely rocking, toe-crushing, shear-diagonal, and shear-sliding. Furthermore, this initial mechanical scheme was upgraded by Pantò, et al. [2] aiming at incorporating the out-of-plane mechanisms of URM structures. The seismic behaviour of this typology of constructions has been investigated by means of such a numerical tool demonstrating its accuracy despite the simplicity of its mechanical configuration. It is worth noting that these investigations were limited to a static context in which the material degradation and energy dissipation were not taken into consideration.

1.2   FOCUS OF THE THESIS

URM structures are characterised by a poor performance under seismic excitations in which one of the most complex and dangerous types of failures corresponds to out-of-plane mechanisms. In addition, this constitutes one of the major causes of human and building losses having a significant impact from a socio-economic point of view. Thus, there is a necessity of better understanding the seismic response of URM structures together with their corresponding vulnerability aiming at managing and reducing the risk associated with the occurrence of earthquakes. This thesis aims at assessing the seismic vulnerability of

an URM structure by means of the application of time history analyses and the corresponding derivation of analytical fragility functions. For this purpose, the thesis involves five main topics, as detailed next:

1) Compilation of the state of the art regarding the available computational tools for the assessment of masonry structures, as well as the different investigations regarding their out-of-plane response and seismic vulnerability;

2) Extension of a macro-element model into a dynamic context by the introduction of a consistent mass matrix and appropriate cyclic constitutive laws;

3) Validation of macro-element model in the nonlinear dynamic field considering analytical and experimental investigations;

4) Assessment of the out-of-plane behaviour of URM structures subjected to static and dynamic nonlinear analyses;

5) Assessment of the seismic vulnerability of an URM structure by means of time history analyses and an alternative procedure for the definition of its displacement capacity.

1.3 Outline

This document presents the research proposal for the implementation of a practical and simplified approach for the assessment of the dynamic behaviour of unreinforced masonry structures in the nonlinear field. In order to provide a better description and explanation of the topics regarding the research proposal, this document has been partitioned into five chapters, as follows:

1. **Chapter 1**, which is this chapter, consists of a brief introduction of the work in which the motivation associated with the seismic vulnerability and behaviour of URM is briefly addressed. In addition, the focus of the thesis and well as the outline related to its content are reported.

2. **Chapter 2** presents a literature review concerning three topics associated with the investigation of masonry structures. The first one is related to the different computational tools, advanced and simplified, that are employed for the seismic assessment of these structures. The second topic is related to the investigation conducted regarding the out-of-plane behaviour of masonry structures by means of analytical formulations and experimental campaigns. Finally, the third topic is oriented to the assessment of the seismic vulnerability of masonry structures by means of empirical and analytical formulations.

3. **Chapter 3** aims at describing the simplified numerical tool used in this thesis. The different improvements, as well as the calibration procedure and cyclic constitutive laws, are reported. Finally, this chapter ends with the introduction of a generic formulation associated with the computation of a consistent mass matrix.

4. **Chapter 4** is dedicated to the validation of the cyclic constitutive laws and the generic formulation of a macro-element consistent mass matrix. Three case studies were considered for this validation. The first one is related to the estimation of the dynamic properties of cantilever beams. The second one corresponds to the assessment of the free rocking motion. Finally, the last one is associated with the seismic behaviour of a two-story masonry wall by means of the application of time history analysis.

5. **Chapter 5** presents the assessment of the out-of-plane behaviour of two URM structures previously tested by means of shaking table tests. For this purpose, two numerical strategies, namely FE and macro-element modelling approaches, were taken into consideration. The out-of-plane behaviour of these structures was investigated in the static and dynamic nonlinear fields. A comparison between the numerical approaches, in terms of maximum load capacity, horizontal displacement and failure mechanisms, is also reported.

6. **Chapter 6** is associated with the assessment of the seismic vulnerability of one of the masonry structures. In this case, the definition of the displacement capacities associated with three Limit States was conducted by means of an alternative procedure based on the application of pushover analyses. The derivation of analytical fragility curves was carried out by the application of time history analyses based on the generation of artificial accelerograms and the definition of probabilistic models. The seismic vulnerability of the URM structure was assessed taking into consideration two approaches in which the uncertainty was focused on the seismic input and on mechanical properties,.

7. **Chapter 7** presents the main conclusions from this work together with proposal for future works.

CHAPTER 2

STATE OF THE ART

2.1 INTRODUCTION

In this Chapter, a literature review regarding three topics associated with masonry structures is presented. The first topic is related to the variety of available numerical tools employed for the seismic assessment of this type of structures. In this regard, the numerical tools were classified initially in accordance with three different modelling approaches, namely Finite Element (FE), Discrete Element, and Macro-element. Subsequent subdivisions associated with the FE and macro-element approaches were conducted based on the degree of refinement when modelling masonry, and the typology of macro-elements used for the representation of structural components, respectively. The second topic corresponds to the assessment of the out-of-plane behaviour of masonry structures in the absence of rigid diaphragms. This topic is of significant importance within the structural and earthquake engineering community since unreinforced masonry (URM) structures present a complex out-of-plane behaviour, especially in the dynamic field. In this Chapter, investigations associated with the assessment of the out-of-plane behaviour by means of analytical formulations, experimental (in-situ and laboratory) campaigns, and numerical simulations are reported. Finally, the last topic is related to the assessment of the seismic vulnerability of masonry structures by means of fragility functions. Several studies associated with the seismic vulnerability of civil engineering structures have been conducted aiming at providing relevant information for the decision making, vulnerability prediction, and management of seismic risk. Nevertheless, the studies associated with masonry structures are still limited in spite of these being one of the major causes of human losses due to earthquakes. Therefore, this Chapter reports in detail recent investigations related to the seismic vulnerability of masonry structures.

2.2 COMPUTATIONAL TOOLS FOR THE ASSESSMENT OF MASONRY STRUCTURES

There is a great number of computational tools available in the literature, which have been employed for the assessment and understanding of the complex response of masonry structures when subjected to seismic loading. Numerical models based on the Finite Element (FE) method are considered one of the most well-known computational approaches, since the FE method is capable of representing masonry structures with complex geometric configurations. Nevertheless, this numerical tool is based on the definition of sophisticated constitutive laws for an accurate simulation of the nonlinear response of this type of structures, and the application of advanced procedures requires substantial computational efforts. In this regard, alternative numerical tools based on discrete or macro elements approaches have been implemented in order to overcome the limitations of FE models. The application of these numerical tools has demonstrated a significant accuracy for the assessment of the seismic response of masonry structures.

2.2.1 FINITE ELEMENT MODELS

The FE modelling approach corresponds to one of the most popular and versatile numerical tools used for the evaluation of the seismic response of masonry structures. This tool allows the modelling of different typologies of masonry structures due to the availability of a wide range of one-, two- and three-dimensional computational elements. In addition, the nonlinear response can be accurately simulated through a significant variety of constitutive laws that aim at describing the tensile and compressive behaviour of these structures. This computational tool can assess the seismic response of masonry structures taking into consideration different strategies namely micro- and macro-modelling approaches, as reported by Lourenço [3]. The first strategy consists on the modelling of these structures considering the actual masonry arrangement and the interaction between units and mortar joints. On the other hand, the latter is focused on the modelling of masonry as a homogeneous material. In the following paragraphs, these strategies are briefly described.

a. Micro-modelling strategy

This strategy corresponds to a numerical approach consisting of a thorough representation of masonry structures in which the constituent elements, namely units and mortar joints, are modelled individually. This strategy is considered as a reliable tool for the assessment of the seismic response of this typology of structures since it allows the simulation of failure mechanisms such as crushing of masonry units as well as cracking or sliding of mortar joints, as reported by Lourenço [4]. This approach is generally applicable for small structures since it requires a considerably large computational demand when performing sophisticated analyses. This numerical strategy can be further subdivided into two groups depending on the level of refinement, namely detailed and simplified micro-modelling strategies, respectively. The former consists of the representation of masonry units and mortar joints as continuum elements, whereas the interaction between these components is conducted by means of interface (discontinuous) elements as illustrated in Figure 2.1a. The latter, depicted in Figure 2.1b, follows a similar

approach as the detailed one, considering the masonry units as blocks bonded by potential fracture/slip planes simulating the interaction between the joints and masonry units [5-8], without full representation of the mortar. The mechanical behaviour of the continuum elements can be considered linear elastic, whereas the nonlinearity of the material usually focuses on the interface elements since they present a weaker behaviour.
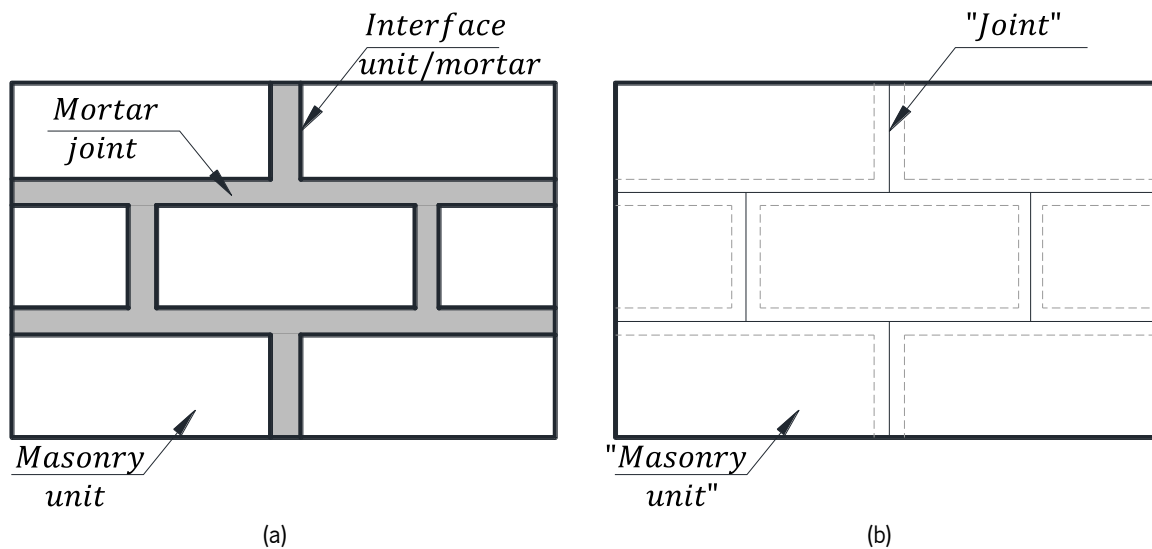
Figure 2.1. Computational tool for the assessment of masonry structures based on the Finite Element method based on (a) detailed and (b) simplified micro-modelling strategies [3].

The effectiveness of this modelling strategy was investigated considering two case studies reported in the work conducted by Lourenço [3]. The first one was associated with the modelling of a shear wall subjected initially to a vertical pre-compression pressure, and subsequently to a horizontal force up to failure. The observed failure mechanism consisted of a diagonal stepped crack and crushing on the compressed toe [8]. The second case study corresponded to a pier-wall connection initially subjected to a uniformly distributed vertical load, and later a horizontal force was applied at the top of the wall until failure was reached. In this case, an accurate correlation between experimental and numerical responses was established [9]. In addition, the response of historical stone masonry shear walls subjected to axial compression and lateral shear loading by means of the micro-modelling approach was investigated by Senthivel and Lourenço [10]. In such investigation, three walls with different configurations were assessed by means of two-dimensional micro models aiming at replicating the response from experimental tests in terms of deformation, shear capacity and failure mechanisms. The first wall consisted of dry-stone masonry without bonding mortar, the second wall consisted of irregular stone masonry with bonding mortar and the last one consisted of rubble masonry with irregular bonding mortar thickness. A good correspondence was obtained between the numerical and experimental responses, both in terms of failure mechanism and force-displacement curves.

b. Macro-modelling strategy

This modelling strategy consists on the representation of masonry as an equivalent continuum and homogeneous composite, without distinguishing units, mortar joints and their corresponding interaction, as depicted in Figure 2.2. The formulation of masonry as an anisotropic inelastic material is a complicated task when considering a macro-modelling strategy. In this regard, Lourenço, et al. [4] proposed a constitutive model capable of reproducing an anisotropic behaviour of masonry taking into account different hardening and softening responses along each axis of the material. Lourenço [3] conducted additional numerical simulations on two case studies aiming at demonstrating the accuracy of this modelling approach. The first case study was related to the assessment of a confined shear wall initially subjected to vertical pre-compression, and further to a lateral force up to failure [11]. The failure mechanism of the macro model was governed by a tensile nonlinear response. The second case corresponded to the assessment of a masonry panel with a window opening subjected to out-of-plane pressure [12]. Based on such investigation, a good agreement in terms of failure mechanism (diagonal cracking from the lower part of the panel to the bottom part of the opening) was obtained when comparing the numerical results to the experimental response.
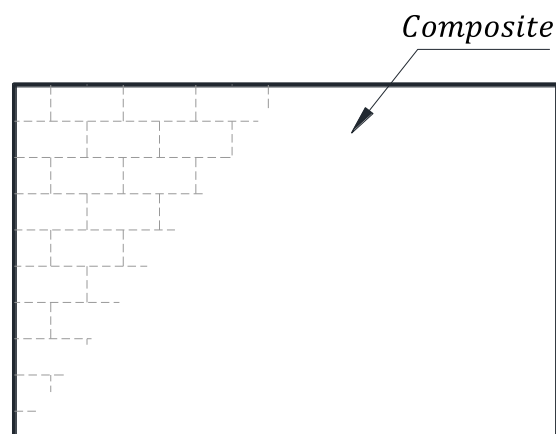
Figure 2.2. Computational tool for the assessment of masonry structures based on the Finite Element method based on macro-modelling strategy [3].

2.2.2 DISCRETE ELEMENT MODELS

The Discrete Element (DE) modelling approach corresponds to an alternative computational tool for the assessment of the seismic behaviour of masonry structures. This modelling approach was initially introduced by Cundall [13] aiming at the evaluation of the behaviour of rocks and soils using plane elements, and further upgraded by means of the introduction of spatial elements [14, 15]. The DE modelling approach consists of the assemblage of rigid or deformable elements, meaning blocks whose interaction is conducted using contact constraints which can be discretised by two different hypothesis, namely point contact, and edge on edge formulations. The former presents a simple mechanical scheme in which the contacts are assigned in length and area for two- and three-dimensional models, respectively.

The DE method based on this hypothesis enables an independent meshing of the blocks without the necessity of node matching; and therefore, allows different typologies of geometric interactions. The determination of the state of stresses is based on the definition of suitable constitutive laws for the joints. In the second formulation, the discretisation of the contacts is conducted by means of interacting lines allowing a linear variation of stresses. The discretisation of contacts for a three-dimensional modelling can be conducted by using a combination of faces, edges and vertexes which leads to an increment of the complexity of the model and its numerical solution. The mechanical behaviour of the contacts can be classified into two groups, namely hard and soft contacts, as reported by Cundall and Hart [16]. The first group, characterised by rigid contacts, is based on an assumption that the blocks do not experience any overlapping. On the contrary, the second group, also known as deformable contacts, allows a small overlapping of blocks in the compressive phase. In this sense, this type of contact requires the definition of stiffness in normal and tangential directions.

The solution of this modelling approach is based on a numeric integration of the equation of motion considering the hypothesis of large displacements and the updating of the current position of the constituent blocks. This modelling approach is characterised by a relatively small number of DOFs leading to a reduced computational demand when performing sophisticated nonlinear analyses (at least in 2D). The number of DOFs is associated with the density of rigid or deformable elements, without considering the interacting contacts. It is worth noting that the simulation of deformable blocks requires an internal division into finite compounds such as triangular and tetrahedral elements for two- and three-dimensional modelling approaches, respectively.

Boffi and Casolo [17] developed a DEM based on rigid elements connected by contact elements which aimed at the simulation of the axial, flexural and shear responses governed by different hysteretic constitutive laws. In addition, Casolo [18] presented a simplified DEM aiming at assessing the seismic behaviour of masonry structures in which a portion of masonry (see Figure 2.3a) can be simulated by a set of rigid blocks as depicted in Figure 2.3b. This approach falls into the category of Rigid Body Spring Model (RBSM) in which blocks or rigid bodies are assembled by means of springs as illustrated in Figure 2.3c. Each contact of the rigid body is composed of a couple of orthogonal links together with an additional longitudinal one. The stiffnesses related to orthogonal and longitudinal links are denoted respectively as k_x and k_v for vertical contacts, and k_y or k_s for contacts in a horizontal direction. The kinematic parameters that describe each rigid block are composed by three DOFs: two of them are associated with horizontal and vertical displacements u and v, and the remaining one is related to the rotation φ of the rigid block.

The axial and flexural mechanisms are governed by the two orthogonal springs located at the edges of the rigid blocks presenting a value of stiffness, k_x and k_y in Figure 2.3c, associated with the Young's modulus of masonry without considering the effects of the Poisson's ratio. As reported by Casolo [18], the axial mechanism, depicted in Figure 2.4a, is characterised by an equal response of the two orthogonal springs. On the other hand, the proper simulation of the flexural response requires the estimation of an optimum distance d from at which the orthogonal springs are placed as illustrated in Figure 2.4b. Such distance is generally considered as a third of the middle length of the rigid block e in a given contact direction. The shear behaviour of the rigid blocks is ruled by the additional longitudinal

links whose values of stiffness k_s and k_v are related to the shear modulus of the masonry material. The flexural and shear mechanisms of the deformable elements are influenced by the Poisson's ratio. The deformations associated with these elements can be classified into three groups, namely pure shear deformation, mixed shear-bending deformation, and local rigid rotation. Each of these deformations can be described by the ratio between the Young's Modulus of masonry units E_{unit} and mortar joints E_{mortar}. In this sense, the pure shear deformation is characterised by a ratio E_{unit}/E_{mortar} equal to 1, whereas the mixed shear-bending deformation and local rigid rotation present a ratio of 10 and 1000, respectively.

| (a) | (b) | (c) |
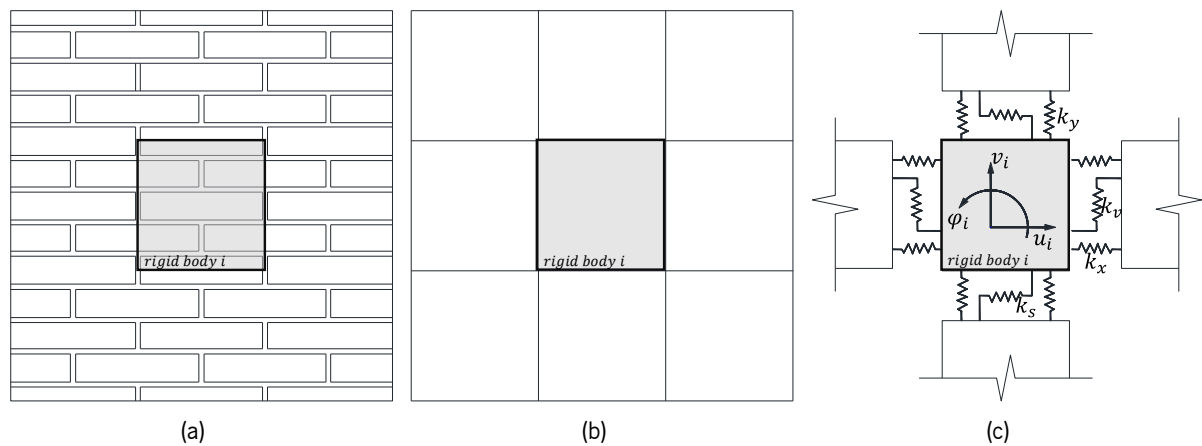
Figure 2.3. Rigid body spring model (RBSM): (a) masonry structure with regular texture, (b) assemblage of rigid bodies for the modelling of masonry structure, and (c) mechanical scheme of the model [18].

The RBSM was further upgrader for the assessment of the seismic response of masonry structures in the dynamic field as reported by Casolo and Peña [19]. The post-elastic response of these models is ruled by nonlinear behaviour associated with flexural and shear mechanisms. The constitutive law that governs the flexural response consist firstly on a low value of tensile strength f_t in which the post-peak branch is described by a rapid degradation of the strength. Due to the brittle behaviour that characterises the flexural response, the dissipation of hysteretic energy during unloading cycles related to the tensile response does not present a significant value. On the other hand, the compressive behaviour is described by a limited ductility once it reaches the value of compressive strength f_c. The shear behaviour is associated with the mechanical behaviour of the mortar joints, and it is governed by a Mohr-Coulomb yielding criterion in which the residual shear capacity depends on the vertical axial load.

Alternative computational tools based on the DEM such as hybrid discrete-finite element models [20-22] and Distinct Deformation Analysis (DDA) [23, 24] have been also implemented for the seismic assessment of masonry structures The former corresponds to a combined method in which concepts of the discrete and finite element methods are taken into consideration. In these models, the blocks are represented by a set of triangular or quadrilateral deformable finite elements. The latter consists of the representation of blocks as deformable elements characterised by a uniform state of strain and stress. This approach does not allow the overlapping of blocks since it considers a rigid behaviour of the contacts. The work conducted by Lemos [25] presents a detailed description of the concepts and application of the discrete element method.
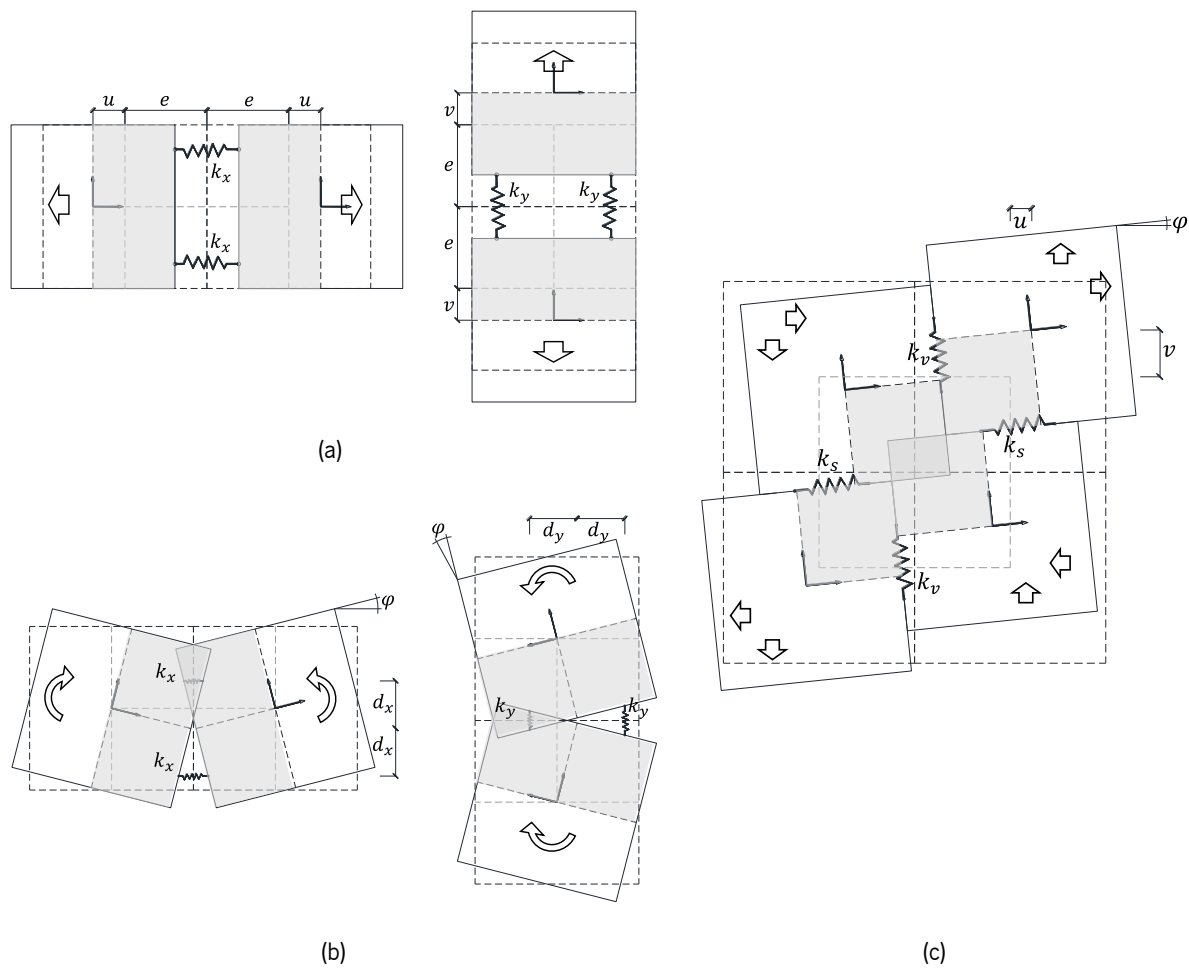
Figure 2.4. Failure mechanism simulated by means of the rigid body spring model (RBSM) due to: (a) horizontal and vertical axial loading, (b) in-plane bending loading, and (c) shear loading.

2.2.3 MACRO-ELEMENT MODELS

During the last decades, the seismic response of masonry structures has been investigated by means of numerical models based on simplified mechanical schemes in which masonry can be modelled by the assemblage of macro-elements. These numerical models have been implemented as an alternative to sophisticated computational tools aiming at overcoming the substantial computational demand required for the application of complex nonlinear analyses. In this regard, these simplified models are described by a reduced number of DOFs making them suitable for the assessment of masonry structures for practical applications. An additional advantage associated with these models corresponds to the definition of the nonlinear response by means of simple constitutive laws. Despite the simplicity of the mechanical scheme of these numerical models, an accurate simulation of the overall response of masonry structures requires a proper calibration of the mechanical parameters.

The macro-element modelling approaches can be classified into two groups namely frame and plane models. The former consists of the modelling of masonry wall by means of equivalent frames which are composed of rigid elements connected to deformable ones. This type of modelling is generally applied

to masonry structures with a regular distribution of openings. Approaches such as the POR method and the Equivalent Frame model classify into this category. On the other hand, the plane models consider a two-dimensional representation of masonry structures. This type of modelling allows a more detailed description of the overall behaviour of the structure. Approaches such as the Multi-fan Panel, Variable Geometry, Three-layer, and Strut-and-tie models belong to this category. The macro-models mentioned are briefly described in this Chapter.

a. POR method

The POR method is considered as one of the first frame macro-element models used for the seismic assessment of masonry structures. This modelling approach is based on a simplified formulation that allows the practical assessment of masonry structures with a rigid diaphragm. However, the POR method neglects the contribution of the out-of-plane mechanisms making it an unsuitable tool for structures characterised by a deformable diaphragm or by the absence of it. The initial development of the POR method was capable of simulating the shear-diagonal failure mechanisms of masonry structures. It was subsequently upgraded aiming at the simulation of coupled axial flexural mechanisms. In this approach, masonry walls are modelled as a set of parallel nonlinear springs connected to two adjacent diaphragms whose axial and flexural stiffnesses are assumed infinite. The contribution of partition walls in terms of axial stiffness is not taken into consideration In this sense, so each story is described by three DOFs. The nonlinear response of this frame macro-element model is governed by an elasto perfectly plastic constitutive law adopted for the spring elements.

The assessment of masonry structures by means of the POR method consists of the application of an incremental horizontal force in the centre of mass of the diaphragms. Such force is initially distributed in accordance with the stiffness of each nonlinear spring, and it is applied until the yield strength is reached. Subsequently, each nonlinear spring starts to deform up to its ultimate displacements without experiencing any increment or reduction of the load capacity. The nonlinear spring is excluded from the model once its ultimate displacement is reached since it is not capable of bearing any more load. Nonlinear static analyses may continue until equilibrium can no longer be achieved. The ultimate load obtained from this method presents an overestimated value when compared to the real one due to the assumption of infinite rigid diaphragms. Further details of the POR method can be found in Tomaževič [26].

b. SAM model

The SAM model corresponds to an equivalent frame model which was initially proposed by Magenes and Calvi [27] and further implemented into a computational code by Magenes and Della Fontana [28]. This approach is based on the modelling of masonry by means of a frame system composed of deformable and rigid elements. The deformable elements aim at simulating the behaviour of vertical and horizontal components of masonry structures, namely piers and spandrels, respectively. The deformable elements are characterised by a linear behaviour until the maximum value of shear strength is reached. The nonlinear behaviour of these elements is governed by an elasto-plastic constitutive model in which the ultimate shear strength is given by the lowest value from different failure

mechanisms. The displacements are assessed in terms of distortion, and the ultimate value is associated with the one corresponding to a sliding failure mechanism [29]. On the other hand, the rigid elements aim at connecting the vertical and horizontal components of masonry structures (deformable elements). Nevertheless, this model focuses mainly on the in-plane failure mechanisms associated with masonry structures.

The assessment of masonry structures by means of the SAM model is conducted by the application of fixed increments of load. As a first step, it is required to determine the shear distribution associated with the stiffness of the vertical deformable elements of the masonry structure. Subsequently, the bending moments at both ends of these elements are calculated based on the distributed increment of lateral force. The solution of this procedure is conducted by imposing a rotational equilibrium of the nodes in order to estimate the moments at the ends of the horizontal deformable elements together with the corresponding shear and normal stresses. If the shear stress exceeds its maximum value, a redistribution within adjacent elements is required. The deformable elements involved in this redistribution are subjected to a variation of the bending moment diagram with constant shear strength. Once the redistribution is concluded, the normal stresses of the vertical deformable elements are computed by imposing a vertical equilibrium. Based on such equilibrium, the shear stress of each vertical element is computed. If its value is again higher than the shear strength, an additional redistribution is required within the vertical elements still capable of bearing load. This procedure is repeated throughout all the fixed load increments. However, the elements in which the ultimate shear strength has been exceeded are not taken into consideration for the equilibrium of the system. It is worth noting that the SAM model is capable of capturing the variation of normal and shear stresses in the vertical elements, whereas the POR method ignores it.

c. **Multi-fan panel model**

The multiple-fan panel model was presented by Braga and Liberatore [30] aiming at a first introduction of a two-dimensional macro-element approach for the assessment of masonry structures. In this simplified strategy, each macro-element is composed of two free lateral edges together with two additional rigid faces, and it presents a series of compressed triangular blocks as illustrated in Figure 2.5. This modelling approach is based on a multi-fan stress pattern in which the tensile and compressive responses are characterised by elasto-plastic and non-reacting behaviours, respectively. In this regard, this macro-element is capable of simulating some local structural response with high accuracy and a reduced computational demand. On the contrary, the model does not allow the reproduction of some failure mechanisms associated with the sliding of mortar joints which may lead to an overestimation of the maximum load capacity of the structure. It is also worth mentioning that this modelling approach is not able to describe hysteresis loops or material degradation. An accurate simulation of the local mechanisms of masonry structure is obtained by means of careful calibration of the mechanical properties such as Young's modulus and compressive strength f_c. This macro-element modelling approach was subsequently implemented into a computer software by Braga, et al. [31].
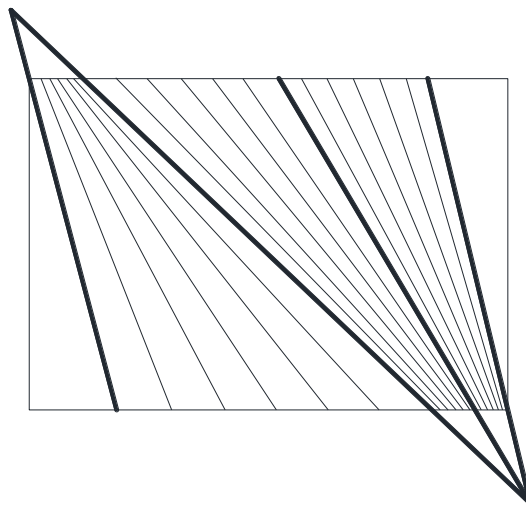
Figure 2.5. Multi-fan panel model: macro-element with compressed triangular blocks.

d.   Variable geometry model

The variable geometry modelling approach was introduced by D'Asdia and Viskovic [32] aiming at the assessment of the response of two-dimensional masonry structures subjected to in-plane horizontal loading. The evaluation of the response of three-dimensional structures was carried out considering an upgrade of this simplified macro-element model conducted by D'Asdia and Viskovic [33]. As illustrated in Figure 2.6a, the modelling of masonry structures by means of this simplified macro-element strategy consists of the assemblage of triangular finite elements. Two types of geometric configurations of these macro-elements can be identified for the simulation of masonry elements. The first type is associated with the modelling of deformable elements such as piers and spandrels, and its geometric configuration is depicted in Figure 2.6b. The second type is related to the modelling of rigid elements used for the connection of the deformable ones. The geometric configuration corresponding to these rigid elements is illustrated in Figure 2.6c.

The response of masonry structures by means of this modelling approach is not based on the nonlinearity of the mechanical properties, but a nonlinearity focused on the geometric configuration of each deformable macro-element. Such nonlinearity is related to the variation of the shape of each triangular finite element at a certain load step allowed by the geometrical arrangement of these macro-elements as illustrated in Figure 2.7. For instance, when a deformable element with an initial geometric configuration (see Figure 2.7a) is subjected to a certain load increment, the nodes of the triangular finite elements are translated from its original position aiming at establishing the equilibrium of the system as depicted in Figure 2.7b. In this sense, due to the variation of the shape of the deformable macro-elements, the parts of masonry in which positive stresses present a higher value than the tensile strength of the material are excluded from the element as illustrated in Figure 2.7c. The external triangles from the rigid macro-element also present a variable geometry in accordance with the deformation of the finite elements of the interacting deformable macro-element. On the other hand, the remaining triangular finite elements of the rigid macro-elements present a fixed geometry. During this non-iterative geometric procedure, the load step should present a small value aiming at a significant reduction of numerical errors.
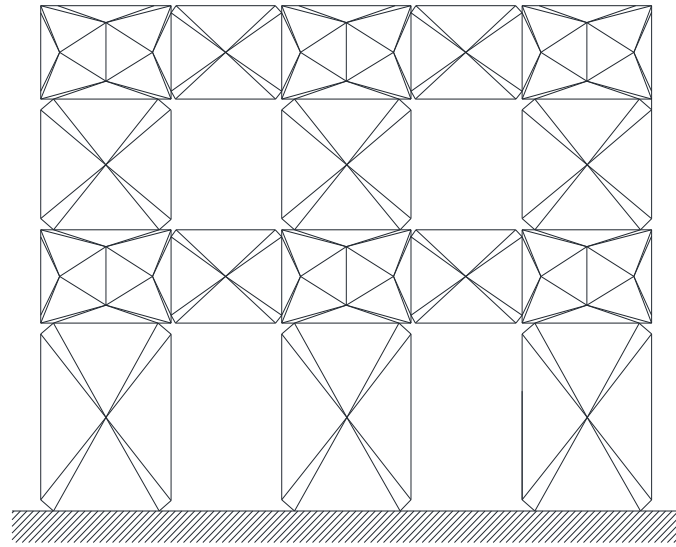
(a)
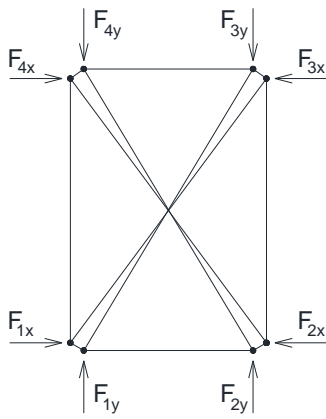
(b)
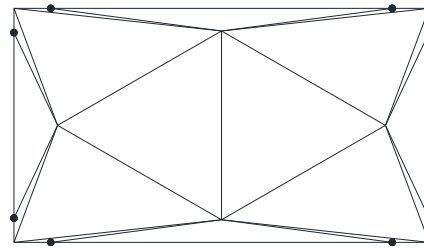
(c)

Figure 2.6. Variable geometry model: (a) mechanical representation of a masonry wall, and macro-element for (b) piers and spandrels, and (c) rigid elements.
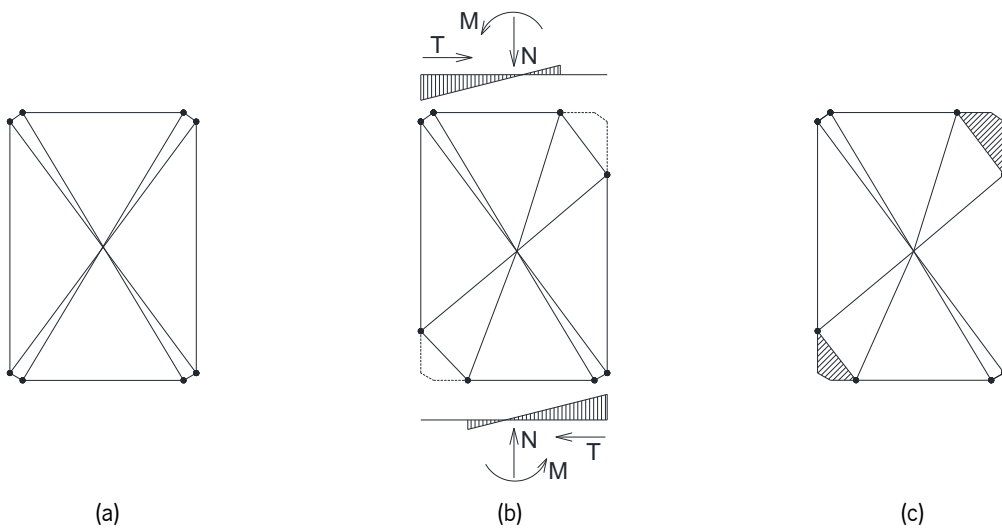
(a)

(b)

(c)

Figure 2.7. Geometrical procedure: (a) undeformed macro-element, (b) state of stress (c) deformed macro-element (node translation with exclusion of damaged area).

e. Three-layer model

The three-layer model corresponds to a plane macro-element approach introduced by Brencich, et al. [34] for the assessment of the seismic response of masonry structures. In this modelling approach, shear walls are modelled by means of deformable panels connected by means of rigid elements as illustrated in Figure 2.8a and Figure 2.8b for two- and three-dimensional masonry structures, respectively. The deformable panels or macro-elements aim at simulating the behaviour of masonry components such as piers and spandrels which are characterized by a localised failure mechanism. On the other hand, the rigid elements connecting the deformable panels do not experience any significant damage concentration. Each deformable macro-element is divided into three layers aiming at simulating the flexural behaviour and shear deformation of masonry walls. The flexural mechanism is governed by top and bottom zero-thickness layers, whereas the shear mechanism is ruled by an additional central layer.

Rigid element   *Deformable element*

(a)   (b)
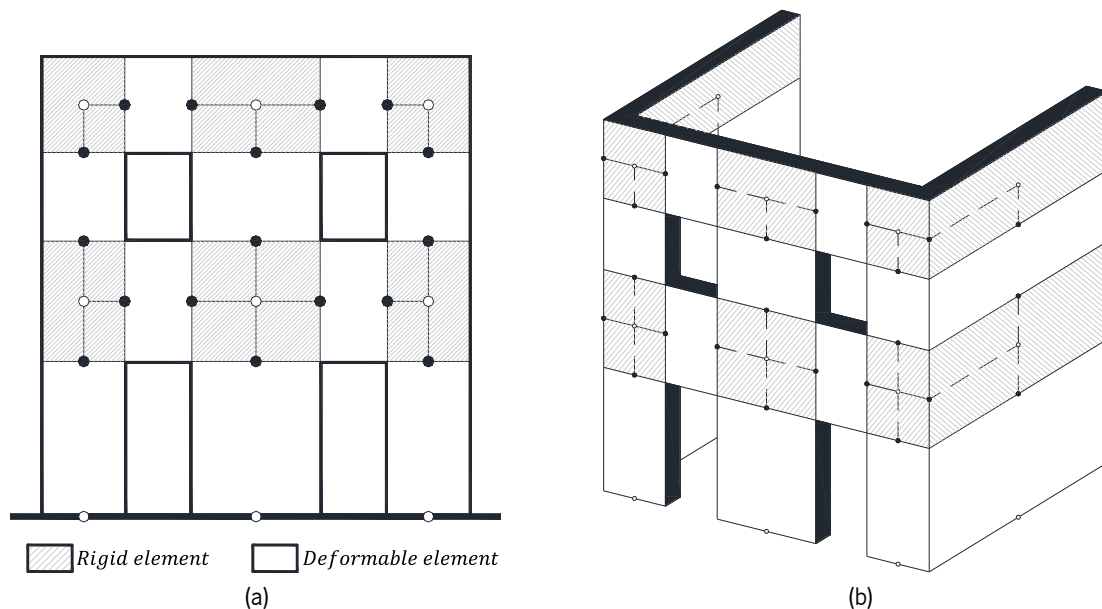
Figure 2.8. Three-layer model: (a) two- and (b) three-dimensional representation of masonry structures [34].

Each macro-element is described by eight kinematic variables as illustrated in Figure 2.9a. Six kinematic variables consisting of horizontal and vertical translational DOFs (u, w) together with an additional rotational DOF (φ) are placed in nodes i and j at both ends of the deformable macro-element. The remaining two kinematic variables in the central layer correspond to additional translational and rotational DOFs denoted as δ and ϕ, respectively. In this sense, each deformable panel is characterised by a vector **a** expressed in equation 2-1, in which u is associated with horizontal displacements, w and δ to vertical displacements, and φ and ϕ to rotations of the system. In this regard, the static variables of a deformable macro element are described by eight components as illustrated in Figure 2.9b, and given by the vector **q** in equation 2-2. Additional contributions associated with the self-weight components (ρg) and the interaction with adjacent elements (t_l and t_r) are also taken into consideration. Due to the simplified mechanical scheme, this numerical tool is characterized by a reduced number of DOFs, and therefore, the application of sophisticated nonlinear analyses require a low computational demand.

$$\mathbf{a} = \begin{Bmatrix} u_i \\ w_i \\ \varphi_i \\ u_j \\ w_j \\ \varphi_j \\ \delta \\ \phi \end{Bmatrix} \qquad \text{2-1} \qquad\qquad \mathbf{q} = \begin{Bmatrix} t_i \\ n_i \\ m_i \\ t_j \\ n_j \\ m_j \\ v \\ m \end{Bmatrix} \qquad \text{2-2}$$
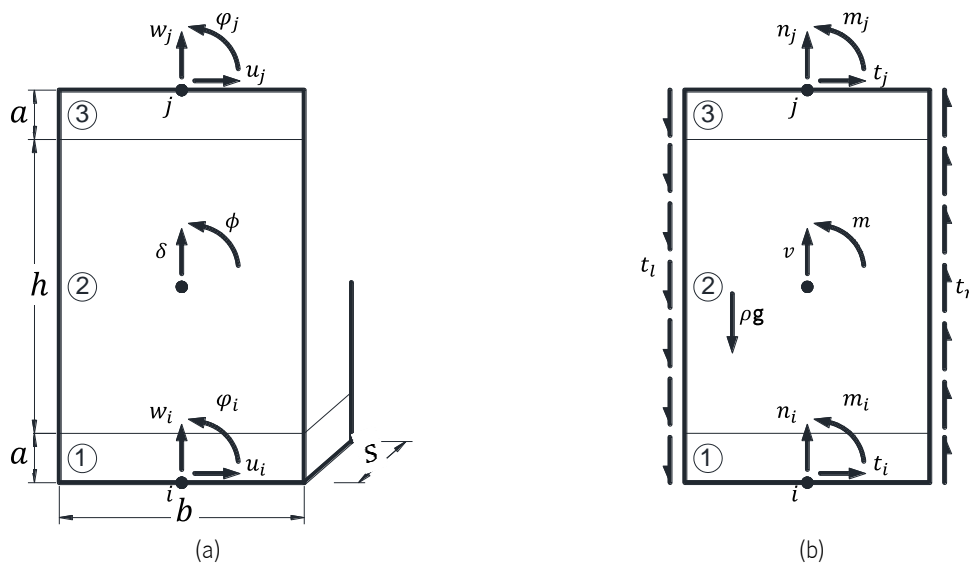
Figure 2.9. Three-layer model: (a) kinematic and (b) static variables of the deformable macro-elements [34].

This macro-element model is described by a constitutive model governed by Young's and shear modulus, shear strength, global friction coefficient, and two additional non-dimensional coefficients denoted as c, and β, respectively. The first coefficient is associated with the elastic deformation, whereas the second one is related to the softening phase. As reported in equation 2-3, such constitutive model is partially composed of an elastic response, a nonlinear contribution, and the initial conditions of the system denoted as $\mathbf{K\,a}$, $\mathbf{q}^*$, and $\mathbf{q}^0$, respectively. The initial stiffness matrix $\mathbf{K}$, given by equation 2-4, remains constant throughout the entire analysis. The axial and flexural responses of the deformable macro-elements are decoupled from the shear mechanism. The mechanical behaviour at the top and bottom layers of the deformable panel is governed by a unilateral elastic response subjected to a nonlinear contribution for axial and flexural responses. The shear mechanism is described by a uniform shear strain distribution, in the central layer of the deformable panel. The overall shear response is also given by elastic and nonlinear contributions.

$$\mathbf{q} = \mathbf{K} \cdot \mathbf{a} + \mathbf{q}^{*} + \mathbf{q}^{0}$$

<div align="right">2-3</div>

$$\mathbf{K} = \begin{bmatrix} GA/h & 0 & 0 & -GA/h & 0 & 0 & 0 & -GA \\ 0 & kA & 0 & 0 & 0 & 0 & -kA & 0 \\ 0 & 0 & \frac{1}{12}kAb^2 & 0 & 0 & 0 & 0 & -\frac{1}{12}kAb^2 \\ -GA/h & 0 & 0 & GA/h & 0 & 0 & 0 & GA \\ 0 & 0 & 0 & 0 & kA & 0 & -kA & 0 \\ 0 & 0 & 0 & 0 & 0 & \frac{1}{12}kAb^2 & 0 & -\frac{1}{12}kAb^2 \\ 0 & -kA & 0 & 0 & -kA & 0 & 2kA & 0 \\ -GA & 0 & -\frac{1}{12}kAb^2 & GA & 0 & -\frac{1}{12}kAb^2 & 0 & GAh+\frac{1}{6}kAb^2 \end{bmatrix}$$

<div align="right">2-4</div>

Based on this macro-element model, different applications and implementations have been conducted aiming at improving its accuracy when simulating the actual response of masonry structures [35-37]. The implementations of this macro-element model have been validated by means of the comparison between experimental and numerical results. The nonlinear degradation of the rocking response was reported by Penna, et al. [38] by means of the introduction of a limited compressive strength. On the other hand, an optimum height of the deformable elements was proposed by Marques and Lourenço [39] by assessing its influence on the in-plane seismic response of masonry structures.

f. Strut-and-tie Model

A numerical tool based on a strut-and-tie modelling approach was introduced by Foraboschi and Vanin [40] aiming at the assessment of masonry structures. In this simplified approach, a masonry structure is divided into stories in which the vertical elements are modelled by means of panels whose assessment is conducted individually. This modelling approach is based on a maximum stiffness or minimum deformation energy criteria, and a lower bound theorem of the limit analysis. In addition, this model is based on the assumption of no-tension behaviour together with an elasto-plastic behaviour in compression. The strut-and-tie model is capable of simulating the in-plane flexural and shear mechanisms of masonry structures illustrated in Figure 2.10a, and Figure 2.10b, respectively. The proper simulation of these mechanisms is conducted by means of evolutive strut-and-tie procedures depicted in Figure 2.10c and Figure 2.10d.
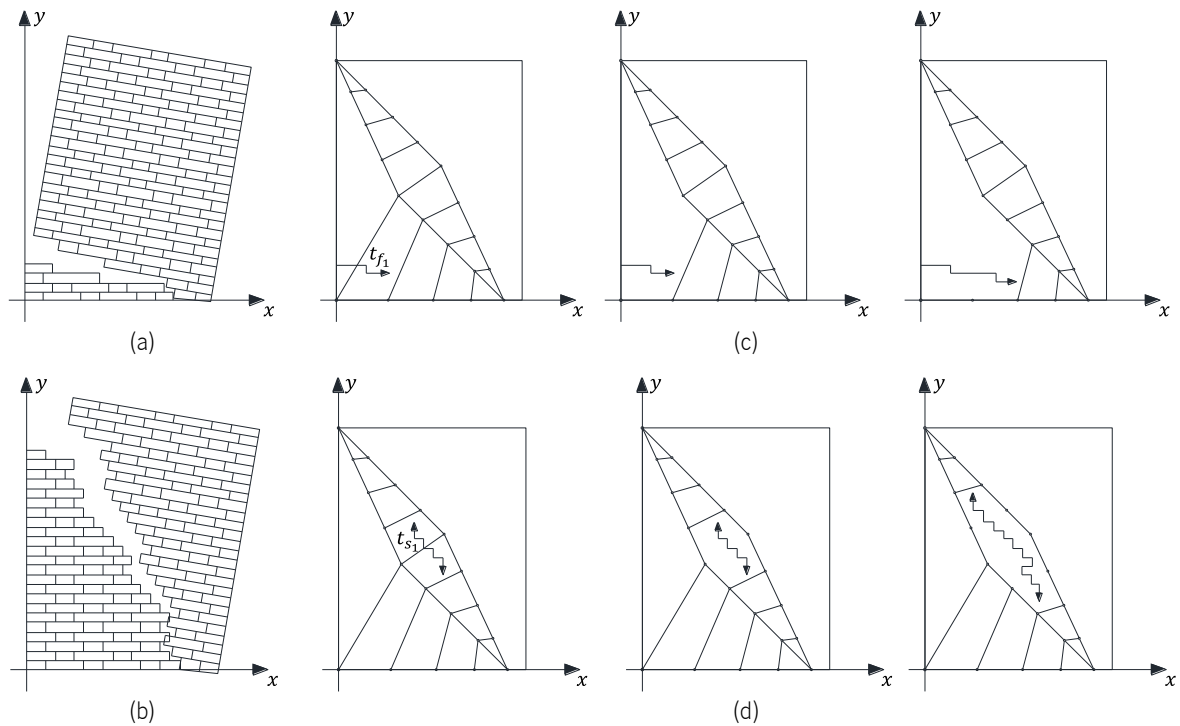
Figure 2.10. Modification of the equivalent strut-and-tie due to: (a) flexural, and (b) shear failure with diagonal crack [40].

The assessment of a masonry structure using this modelling approach is conducted firstly by means of the application of nonlinear static analysis on each vertical element. Subsequently, the assessment of each story is conducted by determining its capacity curve taking into consideration the response of the vertical elements. In this regard, the ratio between the seismic demand and the load capacity of each story is calculated. Finally, the overall assessment associated with the seismic safety of the masonry building is carried out by the computation and evaluation of ratios corresponding to all the constituent stories.

2.3   OUT-OF-PLANE BEHAVIOUR OF MASONRY STRUCTURES

Investigations regarding the response of masonry structures have been mainly focused on the study and understanding of the in-plane mechanisms when subjected to seismic loading. Nevertheless, these structures present a more vulnerable behaviour when the failure due to seismic loading is related to the occurrence of out-of-plane mechanisms. In spite of this, the out-of-plane failure mechanisms are still considered one of the most complex and neglected topics associated with the seismic evaluation of masonry structures. In this regard, a recent literature review about the assessment of the out-of-plane behaviour of these structures by means of analytical formulations, numerical approaches, and experimental campaigns was reported by Ferreira, et al. [41].

2.3.1 ANALYTICAL FORMULATIONS

In accordance with the work conducted by Ferreira, et al. [41], the analytical formulations are classified into two groups in accordance with force- or displacement-based approaches, respectively. In the former, the out-of-plane response of masonry structures was early investigated using limit state theories based on the assumption of no tensile strength and no sliding failure mechanism as reported by Heyman [42]. In this regard, two constitutive models for the seismic assessment of masonry structures were implemented by Giaquinta and Giusti [43] and Del Piero [44] following the same assumption. One of the most utilised force-based formulations corresponds to graphic statics in which equilibrium can be established graphically by means of vectors and closed force polygons, allowing an explanation of experimental results [45]. This method was applied for the assessment of the stability of different components and structural typologies such as vaults, arches and buttresses. This formulation does not usually consider failure mechanisms such as local crushing, crack propagation, or sliding of joints; and therefore, it overestimates the capacity of the structure leading to non-conservative results [46-48].

An alternative force-based analytical formulation used for the assessment of the out-of-plane behaviour of masonry structures corresponds to the kinematic limit analysis. As reported by D'Ayala and Speranza [49], the application of this type of formulation requires a preliminary definition of all the possible out-of-plane failure mechanisms associated with masonry structures. However, due to the complexity of the out-of-plane failure mechanisms, this assessment should be conducted on an individual basis taking into consideration the different load patterns as well as the geometric and boundary conditions [50]. In this regard, a set of expressions associated with the out-of-plane overturning of masonry walls was reported in the work conducted by Hobbs, et al. [51]. Two additional out-of-plane failure mechanisms together with their corresponding analytical formulations were introduced by De Felice and Giannini [68]. In such investigation, a collapse multiplier λ given by the ratio between lateral and gravitational forces (horizontal forces and self-weight) was established for both out-of-plane mechanisms. An additional out-of-plane failure mechanism which involves friction forces was initially proposed by Casapulla [52] and further modified by Picchi [53]. As illustrated in Figure 2.11, a wide variety of out-of-plane mechanisms assessed using limit analysis was presented by D'Ayala and Speranza [49]. The assessment of these mechanisms was conducted by modelling masonry as rigid bodies connected with hinges, and the subsequent determination of the collapse multiplier or load factor λ. In this sense, the failure mechanism presenting the lowest corresponds to the most likely to occur.

New analytical formulations for the estimation of the collapse multiplier for complex out-of-plane mechanisms were implemented in the study conducted by Restrepo-Vélez [54]. These formulations were further validated by means of a comparison with results from experimental campaigns. The simplicity of these procedures together with the limited number of input parameters make the kinematic limit analysis a suitable approach for the assessment of the out-of-plane behaviour of masonry structures. Nevertheless, the collapse multipliers obtained by means of this analytical procedure usually present a conservative value when compared to the one obtained under dynamic conditions [49].
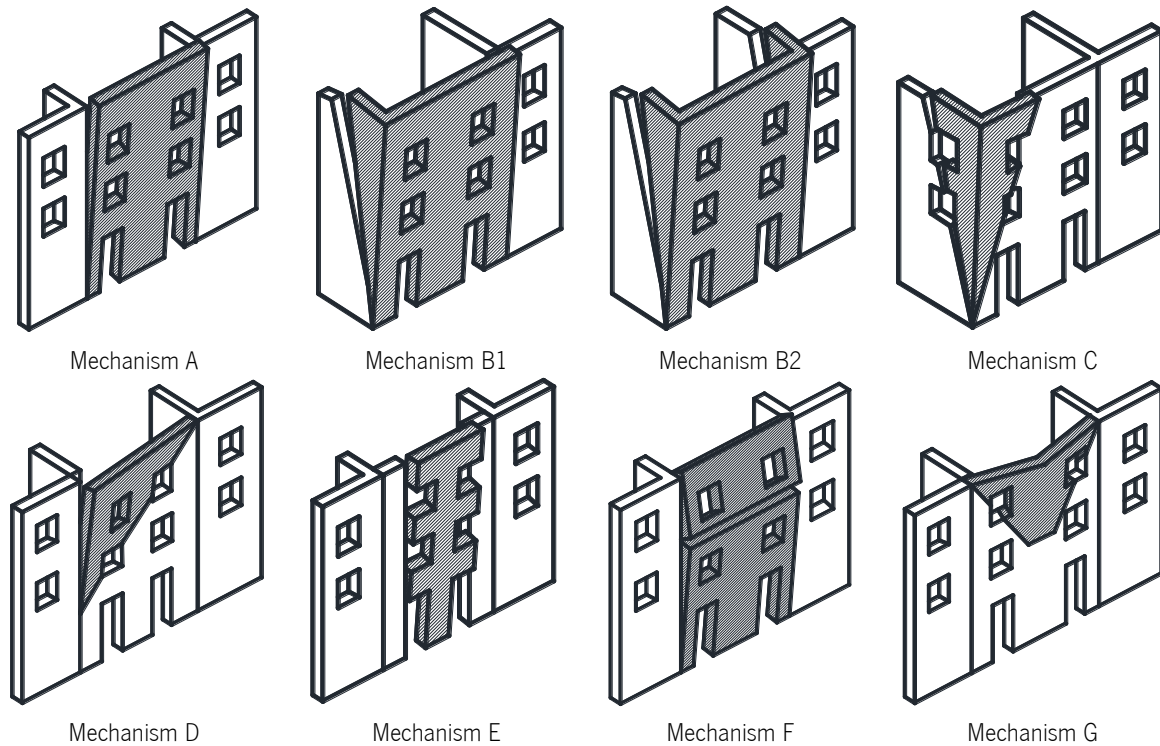
Figure 2.11. Out-of-plane failure mechanisms of masonry structures evaluated by means of kinematic limit analysis [49].

On the other hand, it has been evidenced that the seismic response of this type of constructions when subjected to dynamic loading is characterised by a rigid body motion in which the actual resistance of the structure presents a higher value than the one obtained from force-based formulations. In this sense, the seismic assessment of masonry structures based on displacement-based formulation is considered a more reliable approach since it was demonstrated that maximum displacements are a key aspect in the overall stability of these structures as stated by Abrams, et al. [55]. A linearized displacement-based procedure was introduced by Doherty, et al. [56] aiming at the out-of-plane assessment of unreinforced masonry walls. This procedure is based on the estimation of a trilinear relationship that described the actual nonlinear force-displacement response of masonry walls. In the same investigation conducted by Doherty, et al. [56], the modelling of cracked masonry walls by means of a set of rigid blocks characterised by large displacements was also reported. In addition, the assessment of the seismic response of unreinforced masonry structures by means of a trilinear force-displacement curve was also conducted by Griffith, et al. [57]. Based on such study, it was demonstrated that the maximum strength and ultimate displacement play a significant role in the failure mechanisms of these structures. In addition, an accurate simulation of the response of this type of structures was determined when subjected to low values of axial loading.

An assessment of the dynamic response of unreinforced masonry walls was conducted by Housner [58] in which the walls were modelled by means of rigid blocks subjected to horizontal acceleration at the base consisting on free and forced excitations. The response was assessed by means of an energy approach, and it was possible to evidence that this approach is capable of providing good approximation regarding the response of this type of structures when subjected to dynamic loading. In addition, a significant sensitivity associated with small changes in geometry was determined when

assessing the rocking and overturning mechanisms of rigid blocks with different sizes and aspect ratios subjected to high-intensity seismic actions as reported by Aslam, et al. [59]. Another investigation regarding the formulation and application of nonlinear equations for the assessment of the rocking motion of rigid blocks subjected to horizontal and vertical loading was conducted by Yim, et al. [60]. From such investigation, it was also evidenced that small changes in size and slenderness ratio have a significant influence on the rocking response of rigid blocks when subjected to random excitations. On the other hand, Makris and Konstantinidis [78] conducted an investigation regarding the responses of a SDOF system and a slender rigid block demonstrating that these approaches cannot be correlated since these results were slightly different. In an investigation conducted by Sorrentino [61], a high vulnerability was determined regarding the out-of-plane rocking mechanism of unreinforced masonry façades with lateral restrains assessed by means of rigid bodies. The out-of-plane behaviour of masonry façades was investigated in the dynamic field by Al Shawa, et al. [62] through the development of a modelling strategy based on a SDOF approach and the definition of analytical formulations for the rocking motion. Based on the results obtained from such study, the proposed modelling strategy provided accurate results comparable to experimental tests conducted on masonry wall subjected to free rocking motion.

The out-of-plane behaviour of unreinforced masonry structures has not been deeply investigated by means of multi-degree of freedom rigid blocks, and limited literature can be found about this topic. For instance, Psycharis [63] assessed the rocking response of a system composed of two stacked rigid blocks subjected to horizontal and vertical loading. Nevertheless, this approach demonstrated high complexity when assessing the rocking response since it required the definition of equations of motions and energy dissipation for every possible mode. In this regard, Spanos, et al. [64] presented a similar investigation in which nonlinear equations were formulated for the rocking response in the dynamic field based on the application of horizontal and vertical excitations. D'Ayala and Shi [65] also developed a simple dynamic model for the evaluation of the rocking response of masonry walls which consisted of the analysis of two stacked rigid blocks based on three different patterns of relative rotation. Such assessment was conducted by means of nonlinear equations formulated and implemented in a commercial software, and it evidenced the complexity of this particular response. In 2013, Gabellieri, et al. [66] investigated the influence of deformable diaphragms on the out-of-plane response of a masonry wall modelled by means of a 2DOF system. In this study, equations of motion were formulated for numerical integration aiming at determining the influence of the stiffness of the deformable diaphragm on the rocking response of the wall in the dynamic field.

On the other hand, an investigation regarding the out-of-plane behaviour of unreinforced masonry wall by means of an analytical model involving the influence of crack height, overburden loads as well as mortar compressive strength was conducted by Derakhshan, et al. [67]. It was demonstrated that this analytical model was suitable for describing the rocking behaviour of double or triple leaf solid masonry walls. In 2015, Ferreira, et al. [68] developed a new approach for the assessment of the out-of-plane response of unreinforced masonry structures based on a linearized four-branch model. Such model is capable of characterising the linear and nonlinear response of the masonry structures by means of a moment-rotation relationship. The development of this model was based on the experimental determination and assessment of certain parameters that rule its formulation.

In 2017, Derakhshan, et al. [69] investigated the out-of-plane behaviour of two URM buildings subjected to shaking table tests. This investigation was conducted taking into consideration a displacement-based approach in which the URM structures were modelled as a SFOD system. Trilinear curves were defined for these structures; and subsequently, their corresponding secant stiffnesses were computed. Based on the effective mass and the secant stiffness, the period of a SOFD system was determined. In addition, spectra of displacement were generated from the history of acceleration recorded in the shaking table tests considering three damping ratios (2%, 5% and 10%). In this sense, the maximum displacement of each structure was determined as the spectral displacement corresponding their corresponding period. A good agreement was obtained when comparing the spectral displacements with a 5% of damping ratio with the experimental results.

2.3.2 LABORATORY AND IN-SITU EXPERIMENTAL WORKS

During the last decades, a significant number of experimental campaigns (laboratory and in-situ testing) has been conducted aiming at the assessment of the seismic response of masonry structures. In this regard, the studies related to the out-of-plane behaviour of masonry structures were obtained as a by-product of extensive experimental programmes as stated by Restrepo-Vélez [54]. Nevertheless, some laboratory and in-situ campaigns have been carried out focusing mainly on the evaluation of the out-of-plane response of masonry structures.

An extensive experimental campaign based on laboratory testing was conducted by ABK [70] aiming at the development of a methodology for the seismic hazard mitigation of masonry structures. In such investigation, the influence of the slenderness ratio of the out-of-plane response of twenty unreinforced masonry wall was evaluated by means of the application of dynamic excitations with values of PGA ranging from 0.1 g to 0.4 g. In addition, the authors of such investigation demonstrated that the resistance of the masonry walls presented a significant dependency on peak velocities. In 1991, Tomaževič, et al. [71] investigated the influence of the roof rigidity on the out-of-plane behaviour of stone masonry buildings by the application of shaking table tests on scaled specimens. From such experimental campaign, it was possible to determine the crack pattern and failure mechanisms associated with masonry structures in the presence of flexible diaphragms. Another extensive laboratory programme was conducted by Benedetti, et al. [72] aiming at the evaluation of the response of masonry structures before and after the application of a retrofitting procedure. For the purpose of such investigation, fourteen half-scaled specimens were subjected to seismic inputs until a considerable damage pattern was identified. In addition, static and dynamic tests were conducted to URM walls aiming at the development of a SDOF macro model for the assessment of the one-way bending response due to out-of-plane inertial forces [73]. In this regard, the URM walls were subjected to a static load by means of a hydraulic jack as well as simple pulse and earthquake ground motions in a dynamic context. Griffith, et al. [74] performed laboratory tests aiming at assessing the out-of-plane behaviour of URM structures subjected to two-way bending loading. In such investigation, specimens with different configurations associated with aspect ratio, position and dimensions of openings, and pre-compression state were subjected to half and full cyclic tests by means of a system of airbags. From such study, a force-displacement relationship was

established for the development of a nonlinear inelastic hysteretic model in two-way bending. Similar studies regarding two-way bending were also conducted by Ghobarah and El Mandooh Galal [75] and Vaculik, et al. [76]. A recent investigation was conducted by Candeias, et al. [77] aiming at assessing the out-of-plane behaviour of two URM structures by means of shaking table testing. In this investigation, the structures were characterised by a U-shape configuration: one main gable wall and two return walls. A uniaxial seismic input was increasingly applied in the direction perpendicular to the main gable wall up to failure. A briefly description of this investigation is presented in Chapter 5.

Laboratory testing has also been conducted for the development and enhancement of analytical formulations. For instance, Restrepo-Vélez [54] conducted static tests on 1:5 scaled dry stone masonry walls in order to validate analytical expressions and to implement new formulations for the definition of collapse multipliers associated with out-of-plane failure mechanisms and ultimate static displacements. The scaled dry stone masonry walls were characterised by different configurations related to the length, presence and position of openings, staggering ratio, etc. In addition, D'Ayala and Shi [65] conducted shaking table tests for the validation of simple models for the assessment of masonry structures in the dynamic field. From the results obtained in that investigation, it was evidenced that strength and ductility predictions based on limit state analyses as well as damage indicator cannot be accurately determined. The influence of the seismic input on the out-of-plane overturning of masonry walls was assessed in investigations conducted by Al Shawa, et al. [62] and Costa, et al. [78]. In the former, a single volcanic stone masonry façade with two return walls (U-shape configuration) was subjected to shaking table tests. In the latter study, another U-shaped stone masonry specimen composed of a gable wall with a window opening was also subjected to shaking table tests using seismic input previously selected. The selection of the input was based on numerical analyses by means of a rigid body simplification considering three failure mechanisms and no severe damage in the occurrence of overturning. The results obtained by means of the experimental campaign presented similar values in terms of PGA from force-based formulations with an increased energy dissipation and ultimate displacement.

Experimental programmes based on laboratory testing have also been conducted for the assessment of the effectiveness of strengthening techniques to improve the out-of-plane behaviour of masonry structures. For instance, static tests on eighteen masonry panels externally strengthened FRP composites were conducted by Hamoush, et al. [79] aiming at assessing the influence of the composites on the out-of-plane shear strength of the masonry panels. A similar investigation was carried out by Anania, et al. [80] aiming at assessing the enhancement of the out-of-plane behaviour of masonry walls due to the application of externally bonded FRP composites. Mosallan [81] performed laboratory tests to four full-scale masonry walls by the application of uniform pressure through water bags. In such investigation, one of the walls was tested in as-built conditions for comparison purposes, whereas the remaining three were strengthened with FRP composites in order to improve the out-of-plane flexural response. In addition, Anil, et al. [82] evaluated the effectiveness of CFRP strips for the strengthening of the out-of-plane behaviour of eleven masonry walls with hollow units subjected to static four-point loading up to failure. One specimen was tested in as-built conditions whereas the others were retrofitted with CFRP strips. Moreover, Dizhur, et al. [83] tested five full-scale masonry walls by means of airbag loading

in order to investigate the effectiveness of near-surface mounted (NSM) CFRP inserts as a strengthening solution for the improvement of the out-of-plane behaviour.

On the other hand, the out-of-plane behaviour of masonry structures has also been assessed by means of in-situ experimental testing. However, the literature regarding this topic is quite limited. An in-situ experimental campaign was conducted by Costa [84] in which stone masonry walls were subjected to cyclic out-of-plane loading by means of an attached device composed of steel frames. In this regard, buckets were suspended from the steel bar at each side of the walls, and subsequently filled with sand in order to induce bending moments. The results were assessed in terms of the variation of the natural frequencies of the stone masonry walls due to the application of incremental cyclic out-of-plane loading. Another in-situ campaign was conducted by Tumialan, et al. [85] in which seven masonry specimens were subjected to out-of-plane loading up to failure by means of a hand driven hydraulic jack. Two walls were tested as-built, whereas the remaining five were strengthened before testing. It is worth noting that some limitations associated with the control of the cyclic reversal loading were experienced during the experimental campaign. Furthermore, Arêde, et al. [86] also performed in-situ tests on abandoned houses after the 1998 earthquake in the Azores, Portugal. Non-strengthened and strengthened walls were subjected to a quasi-static incremental force by means of a self-equilibrium device. The out-of-plane loading was applied at the top of the wall in repeated and alternate cycles. In 2009, Dizhur, et al. [87] conducted in-situ based experimental tests on two partition walls from a historic house in New Zealand. One of the walls was tested in as-built conditions, whereas the remaining one was reinforced by using externally bonded FRP sheets together with NSM FRP bars. The walls were subjected to a uniform distribution of out-of-plane loading and unloading by means of an arrangement of airbags, placed centrally and symmetrically to the walls in order to assess the stiffness degradation. A similar investigation was conducted by Ismail and Ingham [88] aiming at evaluating the out-of-plane behaviour of masonry structures. Masonry walls from a historic house in New Zealand in as-built conditions and strengthened with near surface mounted twisted steel bars were tested in-situ by means of an airbag system. An additional laboratory experimental programme was conducted for the validation of the results obtained in-situ.

2.3.3 NUMERICAL APPROACHES

Section 2.2 was mainly dedicated to the description of different computational tools available in literature used for the assessment of the seismic response of masonry structures. However, this Section focuses on numerical investigations associated with the assessment of the out-of-plane behaviour of URM structures. As reported by Ferreira, et al. [41], the assessment of this complex behaviour by means of numerical tools can be classified into three groups, namely Finite Element, Discrete Element, and Multibody dynamics based approaches. Here, an additional group related to a recently developed macro-element modelling approach for the assessment of the out-of-plane behaviour of URM structures is also addressed.

Based on the level of accuracy, the FE models can be further classified into three additional categories (detailed-micro modelling, simplified micro-modelling or meso-modelling in [41], and macro-

modelling strategies), as discussed in Section 2.1. Investigations regarding the detailed micro-modelling strategy, such as the work conducted by Lourenço and Rots [8] and Lourenço [12], were mainly focused on the nonlinear behaviour of the interface elements that simulate the interaction between masonry units and mortar joints. Another investigation was conducted by Cecchi, et al. [89] in which a kinematic limit analysis approach was reported. In such investigation, the interaction between blocks and interface elements was described by a two-dimensional Reissner-Mindlin plate. The interface elements were governed by a Mohr-Coulomb yielding criterion in which a compressive gap and tension cut-off were taken into account, whereas the blocks were characterised by an infinite resistance. The kinematic limit analysis approach was applied to a masonry wall under cylindrical flexure, and to a rectangular plate with a central opening, out-of-plane loaded, obtaining an accurate simulation of rocking and shear mechanisms. In addition, Zuccarello, et al. [90] investigated the behaviour of unbonded masonry panels subjected to out-of-plane loading by means of experimental campaigns and numerical simulations. Two approaches associated with a heterogeneous upper bond model [91] and homogeneous limit analyses approach [92] were taken into consideration for the numerical simulations.

Investigations associated with a simplified micro- or meso-modelling strategy have been conducted for the seismic assessment of masonry structures. Nevertheless, it was stated by Macorini and Izzuddin [93] that this modelling strategy is not suitable for the structural assessment of URM buildings since it is not capable of properly simulating the out-of-plane mechanisms. In this regard, an interface element characterized by geometric and material nonlinearities was introduction aiming at the in-plane and out-of-plane assessment of URM structures [93]. The geometric nonlinearity was governed by a co-rotational approach, whereas the material nonlinearity was ruled by a multi-surface softening plasticity model capable of simulating the main in-plane and out-of-plane mechanisms of URM structures. Furthermore, the definition of the interface element was validated considering several comparisons with experimental results.

On the other hand, studies related to a macro-modelling strategy aim at implementing efficient constitutive models capable of accurately simulate the nonlinear behaviour of masonry as well as the corresponding mechanisms of this type of buildings. For instance, a 3D model based on a homogenization procedure was introduced by Cecchi and Sab [94] aiming at investigating masonry walls subjected to out-of-plane loading. Based on such 3D model, the effects of joints size and deformability ratio of mortar and blocks on macroscopic constitutive functions were taken into consideration. A similar investigation considering a simplified homogenization technique was conducted by Milani, et al. [92] aiming at the assessment of the out-of-plane behaviour of masonry structures. On the other hand, the bucking behaviour of slender URM walls subjected out-of-plane loads by means of a simplified homogenization approach was conducted by [95]. This procedure was characterised by geometric and material nonlinearity, and it was capable of approximately simulating the post-elastic and post-buckling response of URM walls. In 2013, Casolo and Milani [96] also conducted an assessment in which three FE homogenization techniques were formulated and investigated for the out-of-plane assessment of three-leaf masonry walls.

Recent investigations were carried out in order to assess the out-of-plane behaviour of two experimentally tested URM structures based on FE modelling approaches. For instance, Gams, et al. [97]

presented a two-step procedure for the evaluation of the out-of-plane response of these structures. The first step consisted on the definition of the crack pattern and collapse mechanism of a FE macro-model. Based on these results, the second step consisted on modelling of a set of multibody systems connected by means of contact elements. Each multibody system corresponded to a portion of the masonry structure delimited by a significant crack pattern. These multibody systems were characterised by an elastic behaviour, whereas the nonlinearity was focused on the contact element. Nonlinear dynamic analyses were conducted to these models considering a damping ratio equal to 0%. The response of these analyses in terms of displacement was in reasonable agreement when compared to the ones obtained experimentally. The same URM structures were also investigated by means of macro- and meso-modelling approaches by Chácara, et al. [98]. A detailed description of this investigation is reported in Chapter 5.

The out-of-plane behaviour of masonry structures has also been deeply studied by means of Discrete Element models during the last decades. For instance, [99] investigated the out-of-plane failure mechanisms of circular and pointed arches and intersecting arches with different cross sections subjected to seismic loading. In addition, the seismic out-of-plane behaviour of pillars from a stone masonry aqueduct was investigated by Sincraian, et al. [100] using two-dimensional DE models. In the same regard, the dynamic response of another aqueduct was investigated by [101]. Such assessment was conducted by means of a rigid block DE model allowing a more realistic representation of the structure. A simplified approach for the assessment of masonry walls modelled by a series of plane rigid elements subjected to seismic loading was presented by Casolo [102]. The interaction between adjacent rigid elements was conducted by means of deformable hinges simulating flexural and torsional mechanisms of masonry walls. Casolo [103] also introduced a new modelling approach for the assessment of masonry when subjected to dynamic loading. Such approach takes into consideration strength and stiffness degradation due to hysteresis. In addition, shear and membrane effect are neglected since a hypothesis of in-plane rigidity is assumed, focusing only on the occurrence of out-of-plane mechanisms. A comparison regarding the application of nonlinear dynamic analyses based on such modelling approach and static nonlinear analyses on historical and monumental buildings was conducted by Casolo and Uva [104]. Based on such investigation, it was concluded that nonlinear dynamic analysis corresponds to a more accurate and effective numerical procedure for the assessment of this typology of structures. Roberti and Spina [105] investigated the out-of-plane behaviour of the ancient Sardinian Nuraghe structure "Santu Antine" by means of discrete elements composed of polygonal blocks. This modelling approach was capable of simulating the discontinuities of the dry-stone masonry characteristic of this building. Alexandris, et al. [106] investigated the collapse mechanisms of one- and two-story buildings subjected to seismic loading. Based on such investigation it was demonstrated that two-dimensional models are not a suitable approach for the assessment of URM structure since they are not capable of properly capturing out-of-plane mechanisms. It was also evidenced that the adopted numerical tool could not accurately simulate the post-yielding stiffness degradation. A three-wall URM structure, previously subjected to shaking table tests, was investigated by means of a Discrete Element model in the work conducted by Lemos and Campos Costa [107]. The numerical model consisted of rigid blocks connected by contact elements whose nonlinear behaviour was described by a Mohr-Coulomb law. The numerical model was subjected to nonlinear dynamic analyses aiming at reproducing the experimental response. A good

agreement was obtained in terms of collapse mechanisms as well as deformations. A sensitivity analysis regarding the influence of the friction coefficient was also taken into consideration.

AlShawa, et al. [108] used a combined Finite-Discrete Element numerical strategy for the assessment of the out-of-plane response of two URM structures. The numerical models were composed of block discretised by means of solid finite elements characterized by a linear-elastic behaviour. These elements were connected by means of nonlinear contact interfaces. These models were capable of reproducing the experimental results of the URM structures. An additional sensitivity analysis was conducted aiming at assessing the influence of different parameters on the overall response of these structures. The parameters that were taken into consideration for this sensitivity analyses were the associated with the accumulation of damage, the amplitude of the seismic input, the discretization of blocks and of the finite elements, and the variability of mechanical properties.

The concepts of the multi-body dynamics theory have also been employed for the assessment of the out-of-plane behaviour of URM structures since it is capable of simulating complex local mechanisms. The suitability of this approach is mainly related to the definition of the input parameters required for the simulation of those mechanisms, namely geometric and mass-related properties of the elements as well as friction and energy restitution coefficients. Nevertheless, a previous definition of realistic out-of-plane mechanisms is required for the construction of multibody models [41]. In this regard, Costa [109] assessed the out-of-plane behaviour of URM buildings by means of a kinematic chain approach. Such approach is based on the assumption of infinite rigid bodies, and the nonlinearity is based on a sliding frictional phenomenon in the contact elements. The contacts are governed by a Mohr-Coulomb criterion in which compression is considered infinite, and tension and cohesion present a null value.

Finally, a novel macro-element model was initially introduced by Caliò, et al. [1], but further upgraded by Pantò, et al. [2] for the out-of-plane behaviour of URM structures. In this modelling approach, the out-of-plane mechanisms, namely flexural and sliding, are simulated by two sets of nonlinear links. This modelling approach has been validated by means of comparison with sophisticated FE numerical models and experimental results. This macro-element modelling approach was also employed for the assessment of the out-of-plane behaviour of two URM structures in the static field [110]. Two different numerical strategies were taken into consideration, namely macro- and meso-modelling. An acceptable agreement was obtained in terms of maximum load capacity and failure mechanisms when comparing them to experimental results. A detailed description of this macro-element modelling approach is presented in Chapter 3.

2.4 SEISMIC VULNERABILITY OF MASONRY STRUCTURES

It is well known that masonry structures correspond to one of the most diffused structural typologies of low-rise buildings since they are characterized by inexpensive and rapid construction, commonly without considering any seismic design standard. In addition, masonry structures made of stone, brick or adobe also constitute the vast majority of heritage buildings still standing nowadays. This typology of structures is often located in areas characterised by a frequent occurrence of earthquakes, which corresponds to one of the principal threats for its disappearance, but also an important cause of human losses. In this regard, the assessment of the seismic vulnerability of existing buildings has become

a relevant topic within the earthquake engineering community and other professionals associated with the decision making, risk prediction, and management of seismic hazard.

The assessment of the seismic vulnerability is usually conducted by means of practical statistical tools such as fragility or vulnerability curves. This statistical tool is capable of providing the probability of reaching or exceeding a specified limit state LS due to a given level of Intensity Measure IM [111]. The derivation of fragility functions can be conducted by means of different procedures, namely judgement based, analytical, empirical and hybrid methods [13]. Judgement based procedures are commonly derived from a substantial and detailed assessment of an estimate of damage level provided by a team of experts [112]. However, a uniform estimate of the damage level may not be reached since these formulations are based on individual experience of experts [113]. On the other hand, fragility functions obtained by analytical formulations rely on results of numerical analyses conducted on structural models. Simplified numerical tools have been employed for this purpose since refined models require a substantial computational demand and an extensive knowledge of the input parameters. The assessment of the seismic vulnerability by means of analytical formulations may increase the reliability of the estimate of damage since they overall reduce the bias associated with judgement based procedures. Nevertheless, they still present limitations since they may require a significant computational effort and they may not fully reproduce the real state of the structure or may neglect the contribution of non-structural components. Finally, the empirical formulations are based on a statistical elaboration of data obtained from post-earthquake surveys. As stated by Rota, et al. [113], this formulation provides a more accurate assessment of the seismic vulnerability since the results are based on a more realistic source of information regarding actual structural typologies, soil effects, site profile characteristics and other relevant factors. The reliability of the fragility functions also relays on a suitable definition of the limit states, together with the proper definition of the intensity measure. Regarding the former, different codes or standards provide detailed limit states associated with the functionality of the structure based on inter-story drifts or resistance—based approaches [114-123]. These limit states are mainly determined by means of the amount of damage, inter-story drifts or structural demand. On the other hand, several parameters such as peak ground velocity, spectral acceleration, spectral displacement, Arias intensity, and Housner intensity have been proposed as intensity measures for the assessment of seismic vulnerability [124]. Still, the most common parameters used for the derivation of fragility curves correspond to the macroscale intensity and peak ground acceleration of ground motion, as reported by Rota, et al. [113].

Despite the significant relevance regarding the assessment of the seismic vulnerability for risk management of civil engineering structures, a limited number of investigations have been conducted for masonry buildings [125]. In this regard, recent studies on masonry structures have been conducted mainly taking into consideration simplified structural models and analysis methods [126-130]. For instance, the seismic vulnerability of a typical two-story stone masonry building in the north of Italy was investigated by Pasticier, et al. [131]. In such investigation, the masonry building was modelled based on an equivalent frame approach using the software SAP2000 [132] in which the post-elastic behaviour was focused on plastic hinges and nonlinear links. Aiming at reducing the computational burden, it was decided to conduct nonlinear analyses only on an equivalent frame model of the façade. In this regard,

pushover analyses were initially conducted to the simplified model in order to establish three limit states based on inter-story drifts in accordance with the EC8 – Part 3 [116]. The first one, denoted as Limited Damage LS, corresponded to the point in the pushover curve associated with a yielding displacement. The second one, denoted as Significant Damage LS, was established as ¾ of the ultimate displacement provided by the last limit state. The latter LS is achieved when the structure experiences a 20% reduction of its shear capacity, and it is denoted as Near Collapse LS. The assessment of the seismic vulnerability of the façade of the stone masonry building was conducted considering the PGA as intensity measure by means of the application of Incremental Dynamic Analysis. For this purpose, fourteen earthquake ground motion records with different scale factors were applied to the simplified model aiming at obtaining dynamic pushover curves. The uncertainty in this investigation was focused on the seismic input, whereas geometric and mechanical properties were considered as deterministic parameters.

In 2008, Altug Erberik [133] assessed the seismic vulnerability of Turkish masonry buildings by means of the application of nonlinear analyses. These analyses were conducted using the software SAM [134] focused on the in-plane seismic assessment of masonry structures, neglecting the occurrence of out-of-plane mechanisms. These masonry buildings were classified according to the number of stories, material properties, regularity in plan, and finally criteria based on length of walls and openings. In addition, the fragility curves were derived aiming at assessing the capacity and the demand of Turkish buildings by static and dynamic nonlinear analyses, respectively. The pushover analyses for the assessment of the capacity the masonry buildings consisted of the application of a triangular lateral force. In that case, the uncertainty of the model was focused on the compressive strength which was characterized by a normal probability distribution function in which different mean values and standard deviation were defined for each class of material properties. The seismic vulnerability was assessed taking into consideration two limit states associated with the value of shear capacity. The first one corresponded to the value at the threshold of the elastic behaviour, whereas the second one was related to the ultimate shear capacity of the masonry buildings. The demand associated with the masonry buildings was investigated by the application of time history analysis based on fifty ground motion records with values of PGA ranging from 0.01 g to 0.80 g. In this case, the uncertainty also focused on the shear modulus and viscous damping. The results of the fragility functions, with PGA as intensity measure, demonstrated a high sensitivity of the seismic response with respect mainly to the height of the masonry building as well as the quality of the material properties. In addition, the fragility curves were used to estimate the seismic performance of masonry buildings in Dinar, Turkey after the 1995 earthquake.

Fragility curves based on empirical formulations were derived from damage data of Italian typological structures in the work conducted by Rota, et al. [113]. In such investigation, an initial database, composed of 163,479 buildings surveyed after five recent earthquakes, was considered. Due to missing data as well as additional factors taken into account by the authors, the number of buildings used for vulnerability assessment was reduced to 91,934. The buildings were initially divided according to the type of vertical bearing elements present, with reference to the RISK-EU building typology matrix [135]. Additional subdivisions associated with the number of stories, the type of horizontal diaphragm (rigid or flexible), and other structural and technical characteristics, were conducted leading to a total of twenty-three structural typologies. For the assessment of the seismic vulnerability of those buildings, PGA was

established as intensity measure, and five damage limit states in accordance with the European Macroseismic Scale [136] were defined. The limit states corresponded to negligible to slight damage (DS1), moderate damage (DS2), substantial to heavy damage (DS3), very heavy damage (DS4), and destruction (DS5). The computation of the fragility curves required initially the formulation of damage probability matrices which represent the probability of occurrence of the different limit states associated with each building typology and PGA interval. Subsequently, the estimation of the probability of reaching or exceeding a certain damage level is conducted by frequencies from the highest to the lowers level of damage. A similar investigation associated with empirical formulation was conducted by Omidvar, et al. [137] aiming at assessing the seismic vulnerability of Iranian buildings.

Rota, et al. [125] carried out another investigation regarding the seismic vulnerability of masonry buildings by means of the application of pushover and time history analyses. For the purpose of such investigation, a single three-story masonry building was considered as representative of a structural typology of the Rione Libertà, Italy. The computational model, as well as the numerical simulations, were conducted using an equivalent frame model implemented in the software TreMuri [138]. This macro-element modelling approach allows an accurate assessment of the seismic response with a reasonable computational demand. Nevertheless, it based on the assumption of a box-type behaviour in which out-of-plane mechanisms are neglected from the overall response of the structure. In this regard, two sets of 1000 static nonlinear analyses based on a lateral force proportional to the first vibration mode were conducted in the weakest direction of the masonry building. The first set of analyses considered uncertainty on the mechanical properties, assuming a normal probability distribution function, whereas in the second set of analyses, mechanical properties from 30 different materials were randomly assigned to 165 structural elements. On the other hand, the application of time history analysis required the selection of a proper set of seven real accelerograms obtained through an online database. These accelerograms were properly scaled aiming at matching the target PGA (0.25 g) of a Type 1 response spectrum [116]. In addition, two sets of time history analyses were conducted to the simplified model of the masonry structure. In the first one, the average values of mechanical properties, whereas the intensity measure (PGA) was considered deterministic, presenting values ranging from 0.05 g and 0.30 g. In the second set of analysis, the uncertainty focused on the material by generating 100 realisations of mechanical properties by means of Monte Carlo simulations. The derivation of the fragility function considered four damage limit states: two with the response of a bilinear approximation o the capacity curve of a single masonry pier (DS1 and DS2), and two related to the global pushover curve of the building (DS3 and DS4). DS1 and DS2 were defined as the yielding displacement and the displacement associated with the first shear crack of the masonry pier, respectively. On the other hand, DS3 and DS4 were established as the displacements associated with the maximum shear capacity and a reduction of 20% of its value.

An investigation associated with the seismic vulnerability of low-rise URM masonry structures located in the central and southern United States regions was conducted by Park, et al. [130] in 2009. The typology of buildings in such area is characterised by one or two stories in which the bearing walls are usually connected by timber roof diaphragms. The seismic vulnerability was conducted to a benchmark structure representative of such typology of building which was experimentally tested aiming

at determining its lateral resistance [139]. In such investigation, the influence of the out-of-plane wall stiffness on the seismic vulnerability of this typology of buildings was also taken into account. For this purpose, three hypotheses regarding the out-of-plane wall stiffness were considered. In the first one, the stiffness associated with the out-of-plane walls are neglected. The second one was based on the assumption that top and bottom ends of the out-of-plane walls are fully connected (fixed). The last hypothesis, and the most conservative one, assumed that the connection between out-of-plane walls with in-plane walls and horizontal diaphragms are in perfect conditions (box behaviour). The modelling of the masonry structure was based on the assemblage of nonlinear springs. The in-plane walls are modelled by means of an arrangement of springs in series and in parallel, whereas the out-of-plane walls and horizontal diaphragms were modelled by a single spring. The three-dimensional modelling of masonry structures also considered the utilization of lumped masses. For the computation of the fragility curves, four limit states were defined in terms of inter-story drift in accordance with HAZUS [140]. The limit states are namely slight, moderate, extensive and complete damage, and present inter-story drifts of 0.2%, 0.5%, 1.2%, and 2.8% respectively. On the other hand, the uncertainty of the model was described by lognormal probability distribution functions associated with mechanical properties such as specific weight, compressive strength and cohesion. The application of time history analyses was based on synthetic ground motions developed by Wen and Wu [141]. These synthetic ground motions were generated taking into consideration 2% and 10% of probability of exceedance in 50 years. In addition, the simulation of the ground motion took into consideration local site effects and amplification representative of the location. It was demonstrated by means of the fragility functions that the seismic response of URM structures is highly sensitive to the stiffness of walls loaded out-of-plane, and its contribution should not be neglected. A further comparison of the derived fragility curves to the ones obtained by HAZUS was also conducted.

A more recent investigation based on an equivalent frame model implemented in the software SAP2000 [132] was conducted by Kappos and Papanikolaou [142] aiming at assessing the seismic vulnerability of a single-story elementary school in Limassol, Cyprus. The numerical model was subjected to time history analyses by the application of three artificial accelerograms generated based on response spectrum for a soil type B in accordance with the EC8 [116]. In addition, the artificial accelerograms were scaled taking into consideration fifteen values of PGA ranging between 0.01 g and 1.20 g. For the assessment of the seismic vulnerability of the elementary school, the authors of such investigation established four damage limit states based on displacements obtained from pushover curves are reported in Table 2-1. It is worth mentioning that the masonry building was also assessed taking into consideration retrofitting techniques.

Table 2-1. Damage limit states reported by Kappos and Papanikolaou [142]

Damage States	Description	Displacement from pushover curve [128]
DS1	Negligible structural damage, low non-structural damage	$0.7 \cdot \Delta_y$
DS2	Minor structural damage and/or moderate non-structural damage	$0.7 \cdot \Delta_y + 5 \cdot \left(\dfrac{\Delta_u - 0.7 \cdot \Delta_y}{100} \right)$
DS3	Significant structural damage and extensive non-structural damage	$0.7 \cdot \Delta_y + 20 \cdot \left(\dfrac{\Delta_u - 0.7 \cdot \Delta_y}{100} \right)$
DS4	Collapse, repairing the building not feasible	Δ_u

In 2014, the seismic vulnerability of three European historical masonry buildings was investigated by Asteris, et al. [143]. The first one, located in Chania, Greece, corresponded to a two-stone masonry building made of stone units, wooden roof, and steel element. The second structure was located in Aveiro, Portugal, and it corresponded to a two-story adobe building with timber roofs. The remaining one corresponded to a church in Askas, Cyprus, and it was made of stone units, mud, and brick gallets. The 3D FE numerical models of such structures were built using the commercial software SAP2000 [132], and its seismic vulnerability was investigated by means of the application of time history analyses. The uncertainty of the structures mainly focused on PGA and tensile strength of the material. The definition of the damage limit states was based on the work conducted by Asteris [144] in which a damage index based on the percentage of damaged area is provided. In this regard, three limit states were established namely insignificant damage (< 10%), moderate damage (>10%, < 20%), and heavy damage (>20%), respectively. It is worth mentioning that the fragility functions were derived before and after retrofitting. Regarding the assessment of the seismic vulnerability of existing masonry churches, Milani and Venturini [145] implemented a limit analysis software based on 3D homogenized FE procedure aiming at the automatic generation of fragility curves. In such investigation, Monte Carlo simulations were conducted for the assessment of the global failure mechanisms as well as the overall strength of the masonry buildings. For the seismic vulnerability, the uncertainty focused on the mechanical properties of the masonry material and on the direction of an equivalent seismic load.

2.5 FINAL CONSIDERATIONS

This Chapter addresses a state of the art regarding three relevant topics associated with the seismic behaviour of URM structures, namely the variety of numerical tools available in the literature, the out-of-plane behaviour of these structures, and the tools for assessment of their seismic vulnerability.

The numerical tools were classified based on three different modelling approaches. The first one is related to a FE approach which can be further divided into three groups depending on the degree of detail used for the modelling of masonry structures: detailed micro-, simplified micro, and macro-modelling strategies. This modelling approach is considered as one of the most versatile tools since it can provide a wide range of computational elements as well as a diverse material library. Nevertheless, the application of models based on this approach requires a significant computational effort. The second one is associated with a discrete element modelling approach as an alternative tool for the assessment

of masonry structures. This modelling approach is based on the assemblage of rigid or deformable blocks whose interaction is conducted by contact constraints. It has been demonstrated that this modelling approach is suitable for the assessment of this type of structures despite the challenges related to 3D modeling of a large number of blocks and the use of explicit solution procedures. Finally, the last group is associated with a simplified approach in which masonry structures components can be modelled by means of one- (beam) and two- (plate) dimensional macro-elements. The simplified mechanical scheme of these numerical models leads to a significant reduction of the computational demand. Despite their simplicity, these models are capable of properly simulating the in-plane response of masonry structures. Nevertheless, they are based on the hypothesis of a box-type behaviour in which the out-of-plane mechanisms are neglected.

The assessment of the out-of-plane behaviour of URM structure has been conducted by means of analytical formulations, experimental campaigns and numerical simulations. In this Chapter, different force- and displacement-based formulations implemented during the last decades are briefly reported. It is worth noting that since the out-of-plane behaviour of URM structures in the dynamic field can be described as a rigid body, the displacement-based formulations correspond to a more accurate approach. On the other hand, the assessment of the out-of-plane behaviour by means of experimental campaigns is limited, and in most cases, it comes as a by-product of other investigations. In this Chapter, laboratory and in-situ investigations focusing on the out-of-plane behaviour as well as on the efficiency of retrofitting techniques are briefly reported. In addition, the numerical simulations, as well as modelling implementations based on the finite element, discrete element, macro-elements as well as multibody dynamics approaches, are also addressed.

Finally, this Chapter includes recent investigations regarding the seismic vulnerability of masonry structures as a relevant topic associated with decision making and risk management. Most of the investigations conducted were based on the hypothesis of a box-type behaviour of masonry structures, considering that the occurrence of out-of-plane mechanisms was prevented. This assumption can be considered as a drawback when assessing the seismic vulnerability of existing (non-strengthened) URM structures since it was evidenced that the out-of-plane response corresponds to a more dangerous and complex mechanism. In the same regard, different damage limit states, as well as intensity measures for the assessment of the seismic vulnerability, have been established by different authors. Moreover, the definition of damage limit states based on a displacement approach has been carried out taking into consideration mostly in-plane failure mechanisms. In this sense, a more rational approach needs to be taken into consideration which accounts for the complex out-of-plane behaviour of URM structures. Therefore, it is evident that there is still work to be done regarding this important topic.

CHAPTER 3

MACRO-ELEMENT MODELLING APPROACH

3.1 INTRODUCTION

This Chapter aims at presenting a novel simplified modelling approach for the seismic assessment of URM masonry structures which was initially introduced by Caliò, et al. [1]. Such modelling approach, implemented in the software 3DMacro [146], is focused on a typology of masonry structures whose response is characterised by a box-type behaviour. In this sense, a two-dimensional macro-element, described by four DOFs, is capable of simulating the main in-plane nonlinear behaviour of such typology. It is noteworthy that this two-dimensional modelling approach is also capable of simulating the response of infilled frame structures by using lumped plasticity elements [147]. The initial scheme of this modelling approach was extended for the investigation of the seismic response of URM structure by the introduction of a three-dimensional or spatial macro-element [2]. In addition, unlike other simplified approaches, this simplified numerical tool allows the modelling of curved masonry structures by irregular spatial macro-elements [148]. This spatial macro-element, implemented in the software HiStrA [149], is described by seven DOFs, and it is capable of simulating the main in-plane and out-of-plane mechanisms of URM structures. Each mechanism is governed by a specific set of nonlinear links. An accurate simulation of these mechanisms requires an adequate calibration of their linear and nonlinear parameters. Moreover, a more recent implementation was conducted for the assessment of the seismic behaviour of URM structures in the dynamic field. For this purpose, a description of the adopted procedure for the computation of the mass matrix based on this modelling approach as well as the definition of cyclic constitutive laws for the nonlinear links are presented in this Chapter.

3.2 MECHANICAL SCHEME

This modelling approach in the initial two-dimensional formulation presented a mechanical configuration in which plane macro-elements or panels are composed of four rigid edges connected by four hinges and two additional diagonal nonlinear links. The interaction between adjacent panels is carried out by means of one-dimensional interface elements as illustrated in Figure 3.1a. These interface elements are composed of two sets of nonlinear links. The first one corresponds to a single link placed parallel to the edges of the connected panels, whereas the second one is related to a discrete distribution of nonlinear links positioned in the direction perpendicular to the edges in interaction. Based on this mechanical scheme, the kinematics of a single macro-element is described by four DOFs. Three of these DOFs are related to the in-plane rigid body motion: two translations u_1, u_2, and one rotation φ. The corresponding deformed configurations of these DOFs are depicted in Figure 3.1b, Figure 3.1c, and Figure 3.1d, respectively. On the other hand, the remaining DOF is associated with the shear deformability of the panel denoted as $\Delta\alpha$. The deformed configuration of this last DOF is shown in Figure 3.1e, with respect to a reference configuration in which one edge is constrained. It is worth noting that the kinematics of each interface element is described by six translational DOFs, two along its length and the remaining four in the perpendicular direction. However, the behaviour of these elements is characterized by a relative displacement between the connected panels; and therefore, no additional DOFs are introduced.
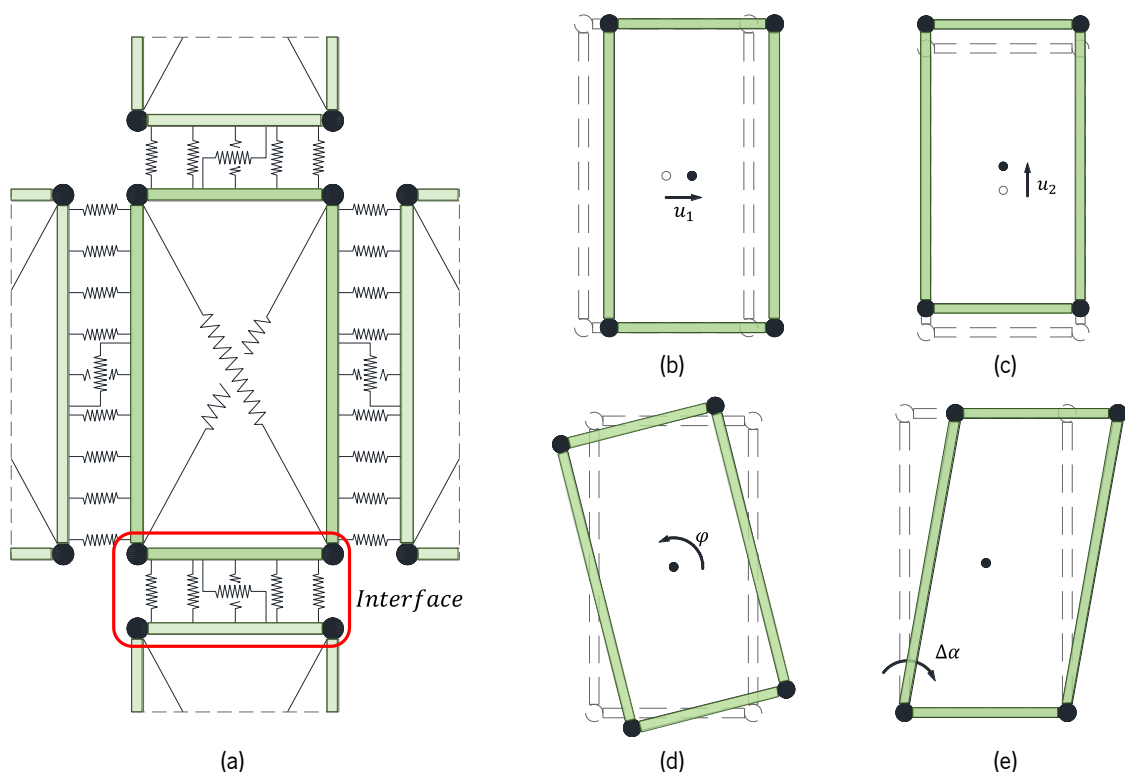
Figure 3.1 Two-dimensional macro-element: (a) mechanical scheme, kinematics associated with (b, c and d) rigid body motion, and (e) shear deformability DOFs

The initial mechanical scheme of this macro-element modelling approach was conceptualised on the assumption of a box-type behaviour; therefore, neglecting the response of masonry structures for which the out-of-plane response is not prevented. Based on this assumption, these two-dimensional macro-elements are capable of accurately simulating the main in-plane mechanisms of this type of structures when subjected to horizontal loading. It is worth mentioning that each of these in-plane mechanisms, namely flexural, shear-diagonal, and shear-sliding, are governed by a specific set of nonlinear links. The in-plane flexural mechanism is associated with the rocking of masonry in its plane (see Figure 3.2a), in which the crushing of the panel in the compressive zone as well as the progressive rupture of the panel in the tensile region lead to the loss of the bearing capacity. This mechanism is simulated by the discrete distribution of nonlinear links placed at the interface elements. Figure 3.2b illustrates the corresponding simulation of the flexural response by means of this set of links, denoted as transversal nonlinear links.
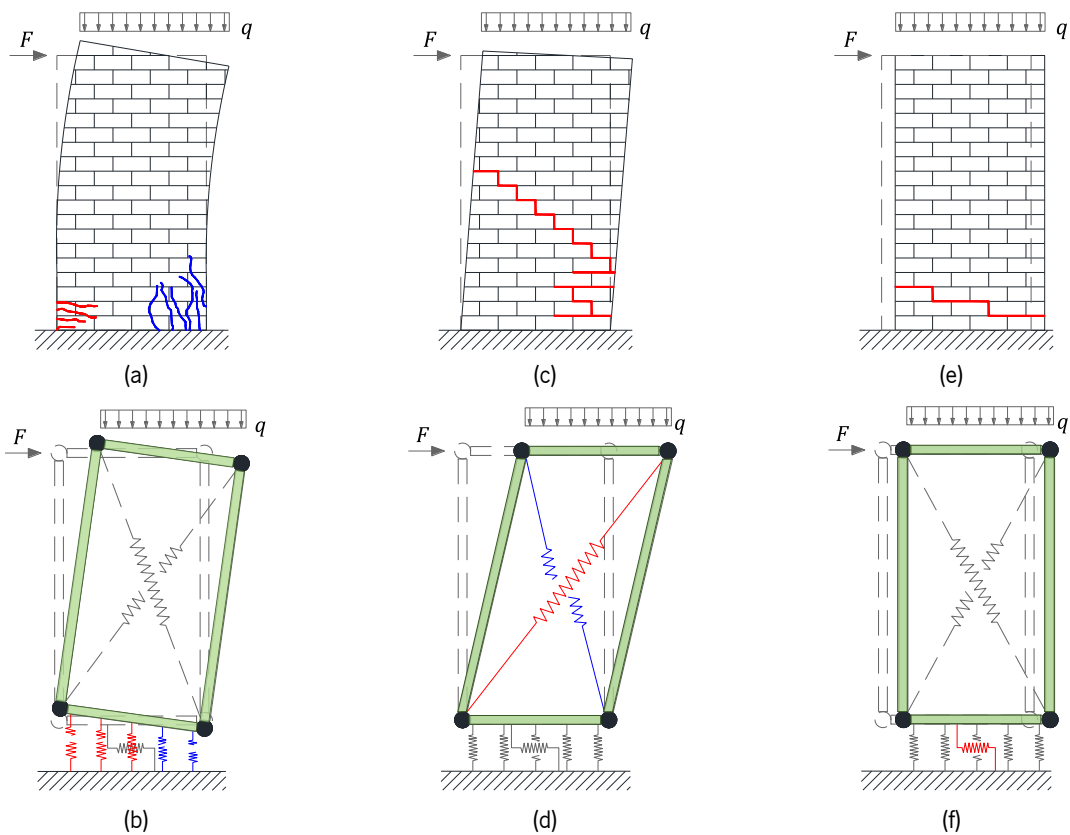
Figure 3.2 Main in-plane mechanisms of masonry structures and the corresponding simulation using the macro-element modelling approach: (a,b) flexural, (c,d) shear-diagonal, and (e,f) shear sliding.

On the other hand, the shear-diagonal mechanism is associated with the formation of diagonal cracks due to the loss of bearing capacity from excessive shear deformations and limited tensile strength. In this modelling approach, the diagonal nonlinear link placed at each macro-element aims at governing the shear-diagonal response of masonry structures. This mechanism and its corresponding simulation by means of a single macro-element are depicted in Figure 3.2c and Figure 3.2d, respectively. Finally, the shear-sliding mechanism is related to the slipping of masonry due to the formation of cracks parallel to

the bed joints as a consequence of the loss of bearing capacity due to the low values of cohesion or friction coefficient of mortar (see Figure 3.2e). As shown in Figure 3.2f, this mechanism is controlled by an additional nonlinear link placed along the length of the interface element. The adequate simulation of the in-plane response of masonry structures, using this discrete-macro modelling approach, requires an accurate calibration of the mechanical properties of each set of nonlinear links.

3.2.1 MODELLING OF INFILLED FRAME STRUCTURES

As reported by Caliò and Pantò [147], this modelling approach was implemented by introducing beam-column lumped plasticity elements for the assessment of the nonlinear response of infilled frame structures. Their interaction with two-dimensional panels is modelled by means of interface elements also composed by a discrete distribution of transversal links and an additional in-plane sliding link. The implementation of this type of elements required the introduction of additional DOFs for the proper definition of the kinematics of the system, increasing the complexity of the mechanical scheme. The mechanical scheme for the modelling of infilled frame structures is characterised by eleven fixed DOFs together with an additional number of DOFs whose variability depends on the discretisation of the interface element. From these eleven fixed DOFs, four of them are related to the two-dimensional panel, and the remaining seven are associated with the beam-column element. These seven DOFs consist of four displacements u_1, v_1, u_2, v_2, and two rotations φ_1, φ_2 located at both ends of the beam-column lumped plasticity element, together with an additional middle span displacement u_m as illustrated in Figure 3.3. On the other hand, the variable amount of DOFs depends on the number of transversal links placed in the interface element. In this sense, for each transversal link, two additional DOFs, one displacement v_o, and one rotation φ_o, are introduced as kinematic variables of the system.
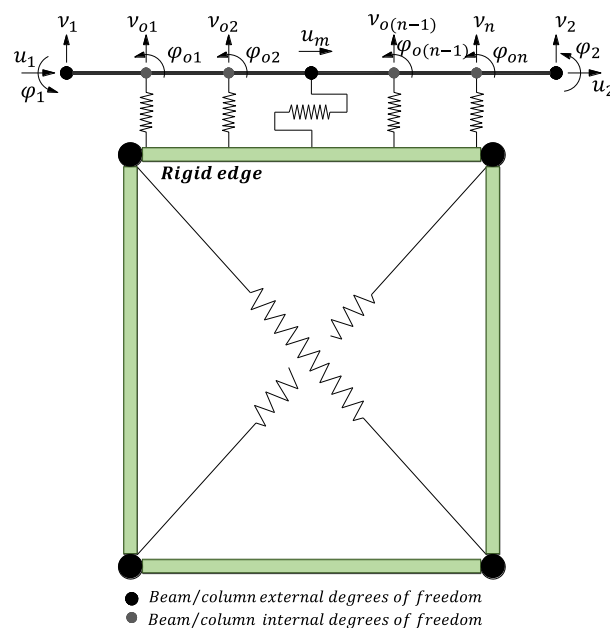
Figure 3.3. Mechanical scheme and kinematics of a macro-element for infilled frame structures by means of the introduction of a beam-column lumped plasticity element.

Based on this implementation, a single infilled frame structure (see Figure 3.4a) can be easily modelled by means of this macro-element approach considering different mesh refinements as depicted in Figure 3.4b. It is noteworthy that this macro-element modelling approach is capable of simulating the main in-plane mechanisms related to this typology of structures. Mechanisms associated with the masonry panel such as corner crushing, diagonal cracking, and shear-sliding, together with the occurrence of plastic hinges along the frame structure can be appropriately reproduced. The corner crushing mechanism is associated with the rupture of the masonry panel caused by its weak behaviour and a poor connection between this element and the frame structure (see Figure 3.4c). This mechanism is simulated by means of the transversal nonlinear links at the interface element as illustrated in Figure 3.4d. Moreover, the diagonal cracking mechanism is related to the shear-diagonal collapse of the masonry panel, and its behaviour is governed by the diagonal nonlinear links. This mechanism and its corresponding simulation using this modelling approach are shown in Figure 3.4e, and Figure 3.4f, respectively. The sliding mechanism (see Figure 3.4g) consists on the collapse of the bed joints due to the weak behaviour of the mortar joints, and it is simulated by the additional nonlinear link at the interface element (see Figure 3.4h). Finally, the mechanism of the frame structure related to the progressive occurrence of plastic hinges is mainly governed by the interaction of axial forces and flexural moments. Figure 3.4i and Figure 3.4j illustrate the mechanisms associated with the frame structure and its corresponding representation by two-dimensional macro-element model, respectively. It is worth noting that a more detailed response and a better representation of the collapse mechanisms are obtained when using a more discretised macro-element model (refined mesh).
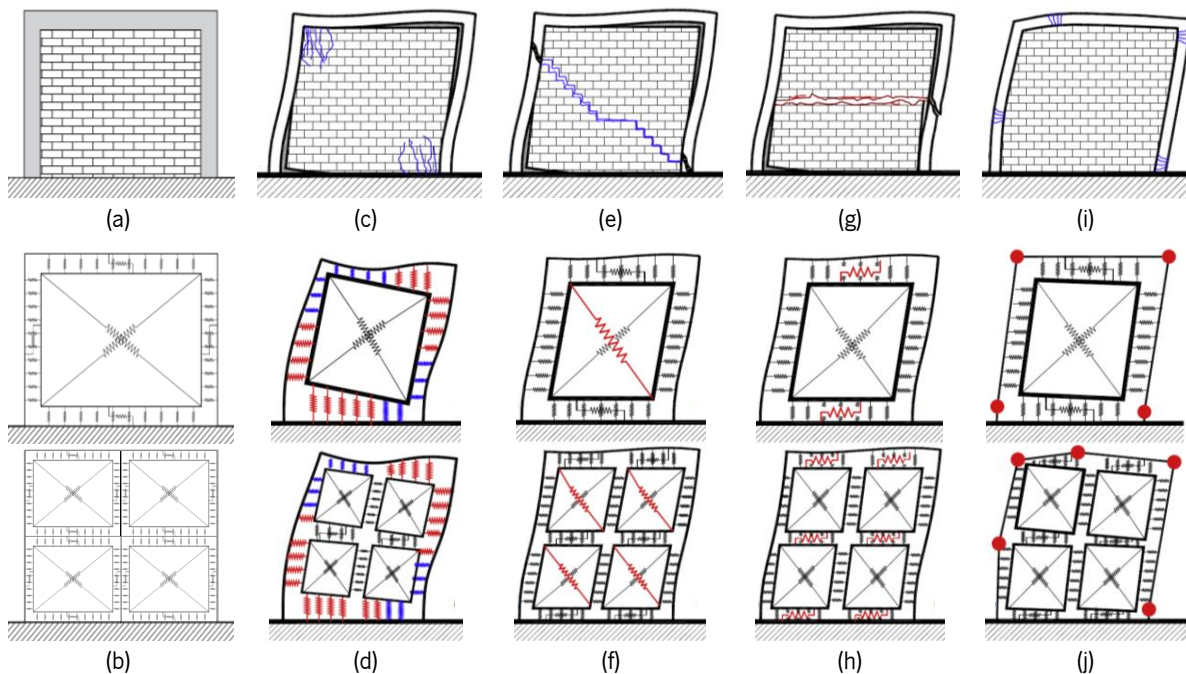
Figure 3.4 Discrete macro-element approach: (a) infilled frame structure, (b) simplified models, in-plane mechanisms and simulation by means of this modelling approach: (c,d) flexural, (e,f) shear-diagonal, (h,i) shear-sliding and (i,j) plastic hinges.

The latter applications of this simplified approach have been focused on the modelling of masonry as a continuum and homogeneous material. However, this mechanical scheme also allows the modelling of this type of structures by means of discrete elements, in which each unit is simulated by a single macro-element or panel, and the interaction between mortar joints and units can be described by means of the interface elements (mesoscale modelling). A portion of masonry (see Figure 3.5a) can be discretised in accordance with the specific arrangement of units together with half of the surrounding mortar joints as illustrated in Figure 3.5b. In this sense, each discretized section is modelled by means of a single macro-element as depicted in Figure 3.5c. Due to the detailed mesh refinement required for the modelling of masonry structures, this discretisation leads to a significant increment of the computational demand as a result of the number of DOFs. Nevertheless, this macro-element mesoscale strategy is characterised by a reduced number of degrees of freedom if compared to the already proposed mesoscale strategies presented in the literature [93] and can be used for the validation and a numerical calibration of the macro model parameters.

(a) (b) (c)
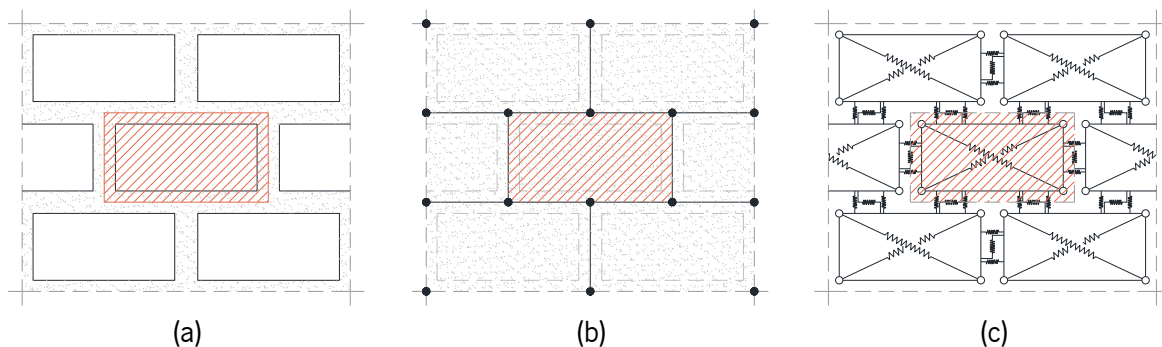
Figure 3.5 Discrete macro-element modelling approach: (a) portion of masonry, (b) simplified discretized representation, and (c) macro-element mechanical scheme.

3.2.2 MODELLING OF OUT-OF-PLANE MECHANISMS

This macro-element modelling approach was further upgraded aiming at the simulation of the out-of-plane response of URM structures by means of the introduction of additional sets of nonlinear links in three-dimensional panels [2]. The mechanical scheme that describes this upgraded approach is composed of four rigid plates connected by hinges and a single diagonal nonlinear link as illustrated in Figure 3.6a. The connection between adjacent elements is still conducted by means of a plane interface element which is now discretised into a matrix of transversal nonlinear links as depicted in Figure 3.6b. In addition, this two-dimensional interface element is also composed by a single nonlinear link along its length and two additional nonlinear links along its thickness as depicted in Figure 3.6c.

This upgraded modelling approach is capable of simulating the main in-plane and out-of-plane mechanisms of UMR structures. The single diagonal nonlinear link located at each three-dimensional macro-element governs the in-plane shear-diagonal mechanism, whereas as the single nonlinear link along the length of the interface element controls the in-plane shear-sliding mechanism. On the other hand, the discretised matrix of transversal nonlinear links rules the bi-flexural and axial mechanisms corresponding to this type of structures. Finally, the additional couple of nonlinear links along the

thickness of the interface element controls the out-of-plane shear-sliding mechanism and the torsion response around the axis perpendicular to the interface element surface. It is worth noting that the mesh refinement can influence the proper simulation of the out-of-plane and torsion mechanisms of URM as reported by Pantò, et al. [2], since the number of element has to guarantee a proper description of the out-of-plane kinematics.
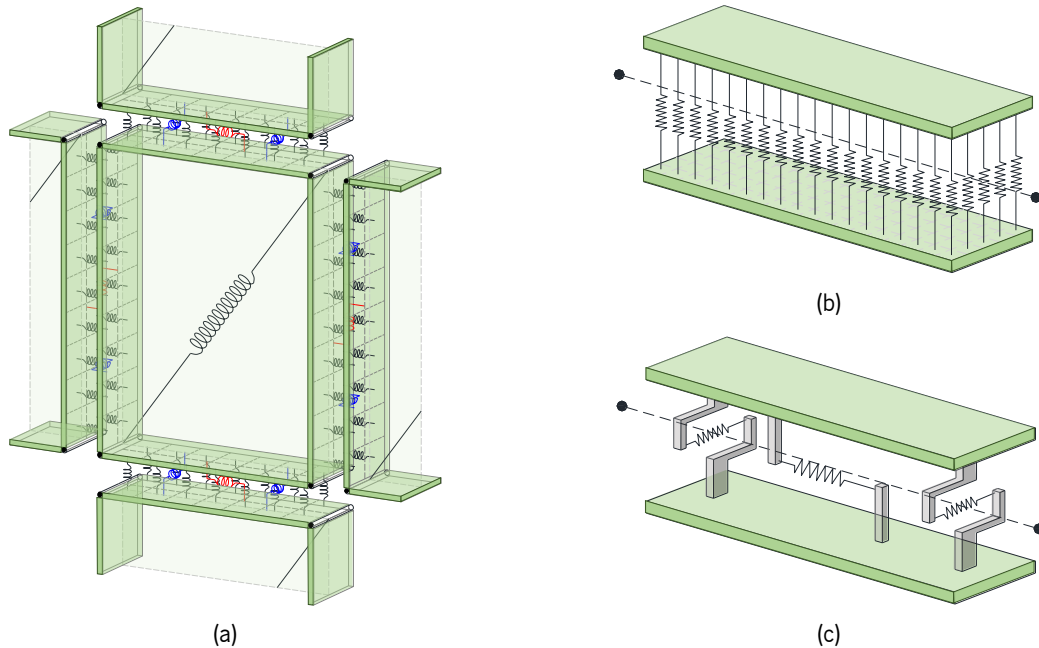
Figure 3.6 Three-dimensional macro-element: (a) mechanical scheme, (b) discretised matrix of transversal nonlinear links, and (c) additional nonlinear links along its length and thickness

The kinematics of each spatial macro-element is characterised by seven DOFs, in which six of them are related to the in-plane and out-of-plane rigid body motion, and the remaining one is associated to the in-plane shear deformability ($\Delta\alpha$). The six DOFs related to the rigid body motion correspond to three translations u_1, u_2, u_3 and three rotations $\varphi_1, \varphi_2, \varphi_3$, whose deformed configurations are illustrated in Figure 3.7a, and Figure 3.7b, respectively. In the case of the DOF associated with the shear deformability of the panel, its deformed configuration by means of a spatial macro-element is depicted in Figure 3.7c. These seven DOFs in a local reference system are located in the vector $\mathbf{u}$ as reported in equation 3-1 in which the notation of the components associated with the rotation of a rigid body (u_4, u_5, u_6) and the shear deformability (u_7) were modified aiming at a more consistent and simplified expression.

$$\mathbf{u} = \begin{bmatrix} u_1 \\ u_2 \\ u_3 \\ u_4 \\ u_5 \\ u_6 \\ u_7 \end{bmatrix} \qquad \text{3-1}$$
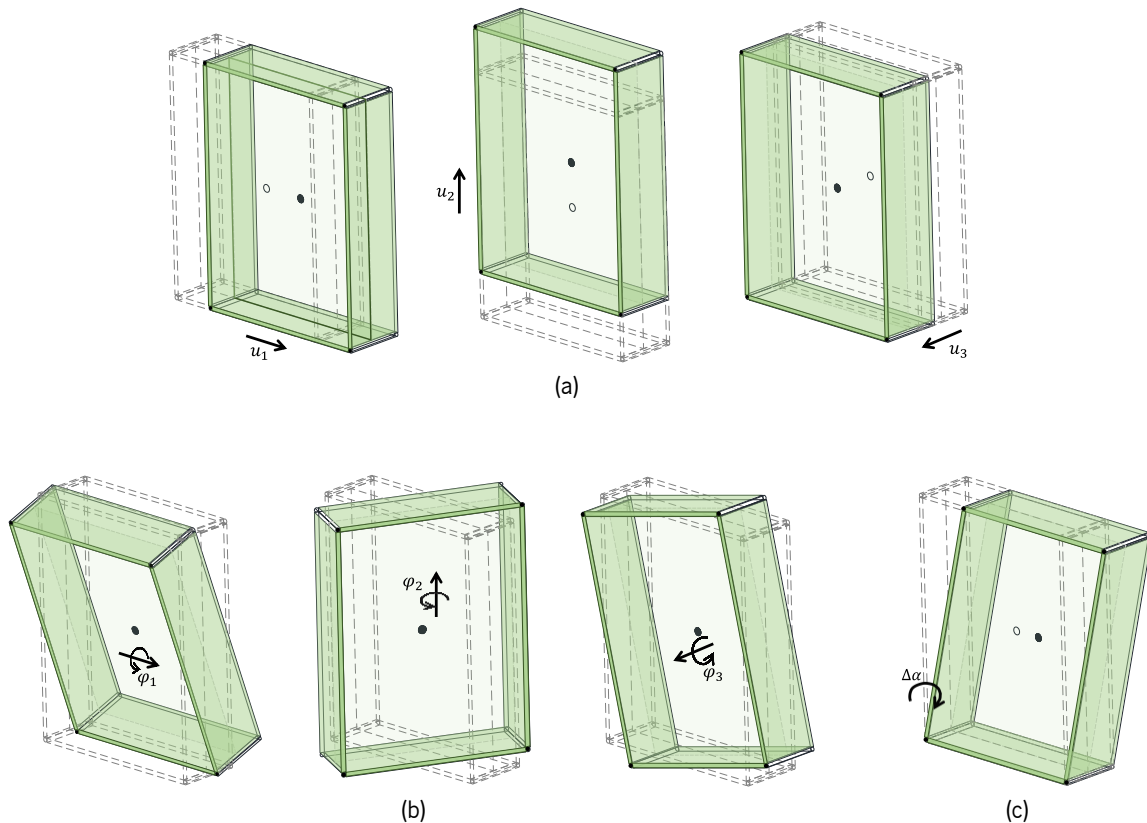
Figure 3.7 Kinematic associated with three-dimensional macro-element: (a) translational, (b) rotational, and (c) shear deformability DOFs

3.2.3 MODELLING OF CURVED MASONRY STRUCTURES

As reported by Cannizzaro [150], an additional implementation was conducted to this macro-element modelling approach aiming at the representation of curved masonry structures, such as vaults or domes, using three-dimensional panels with an irregular geometry. The discretization of this type of structures is conducted taking into consideration two different sets of grids. The first set of grids is composed of curved lines (red lines in Figure 3.8a) defined by means of horizontal planes distributed along the height of the masonry element. On the other hand, the second set of grids, also composed of curved lines (blue lines in Figure 3.8a), is defined by vertical planes that rotate around a fixed axis in the masonry element. Based on this procedure, a single discretised element, depicted in Figure 3.8b, is characterized by four middle vertexes $n = 1...4$ together with their corresponding thickness s_i and unit vector m_i, normal to the element surface. The parameters that define each discretized element are better illustrated in Figure 3.8c. In this regard, the central plane surface of an irregular macro-element is defined by connecting the four middle vertexes of the discretised element as shown in Figure 3.8d. The thickness of the irregular macro-element is obtained by the projection of the original configuration of the discretised element into the new defined central plane surface. If the orientation of the thickness of each vertex is coplanar to the initial unit vector of the discretised element, the definition of the unit vector t_i corresponding to the irregular macro-element is required (see Figure 3.8e).
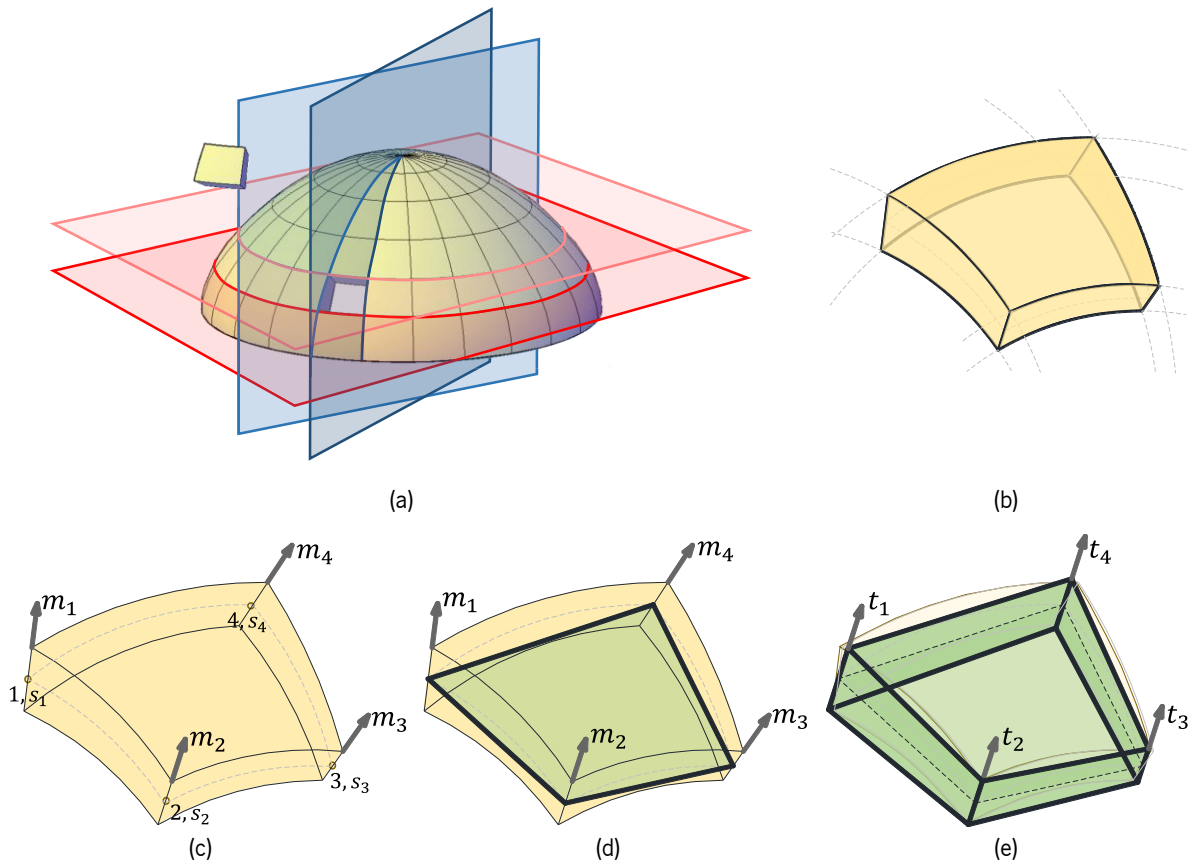
Figure 3.8 Modelling of curved structures: (a) discretisation procedure, (b) discretised element, definition of (c) middle vertexes, (d) central surface, and (e) unit vectors of irregular macro-element

The mechanical scheme of this irregular macro-element presents no major modifications with respect to the regular one. It is still composed of four rigid plates connected by four hinges and one diagonal nonlinear link. However, the orientation and dimensions of each panel are governed by the geometric characteristics of the curved masonry structures to be modelled. The connection between adjacent elements is still governed by two-dimensional interface elements composed by a grid of transversal nonlinear links together with three sliding nonlinear links. The kinematics of this type of panels is still described by seven DOFs: six related to the rigid body motion, and one to the shear deformability. It is worth noting that this kinematics presents a more sophisticated behaviour associated with the seventh DOF due to the irregularity in geometry.

Based on the mechanical scheme of this modelling approach, a relation between the displacements at each of the vertexes of an irregular macro-element in a local reference system and the seven DOFs can be established. This relation is partially contributed by the rigid body motion DOFs (translation and rotations) and the additional DOF associated with shear deformability. In this sense, the displacement vector $\hat{\mathbf{v}}_n$ of the nth vertex associated with the first six kinematic variables are given by a general formulation expressed in equation 3-2. It is worth noting that this formulation can also be applied to macro-elements with a regular geometric configuration.

$$\hat{v}_{nx} = u_1 + \left(z_n - z_g\right) \cdot u_5 - \left(y_n - y_g\right) \cdot u_6$$

$$\hat{v}_{ny} = u_2 + \left(x_n - x_g\right) \cdot u_6 - \left(z_n - z_g\right) \cdot u_4 \qquad\qquad \text{3-2}$$

$$\hat{v}_{nz} = u_3 + \left(y_n - y_g\right) \cdot u_4 - \left(x_n - x_g\right) \cdot u_5$$

where $\hat{v}_{nx}$, $\hat{v}_{ny}$, and $\hat{v}_{nz}$ are related to the displacements of the nth vertex, x_n, y_n, and z_n are the local coordinates of the nth vertex, x_g, y_g, z_g are the local coordinates of the centre of gravity g, and u_1, u_2, u_3, u_4, u_5, and u_6 are the first six DOFs associated with a rigid body motion.

On the other hand, the contribution associated with the remaining DOF (shear deformability) is strongly influenced by the geometric characteristics of each panel. This behaviour is presented by means of the deformed shape of an irregular panel due to the application of u_7 ($\Delta\alpha$) as depicted in Figure 3.9. It can be observed that vertexes 1 and 2 do not present any displacement; and therefore, the contribution of this DOF is neglected. On the other hand, the remaining two vertexes are described by the deformations δ_3 and δ_4, respectively, whose definition is related to the length l_4 at the fourth edge of the panel as well as the angles α_n formed at each of the vertexes. In this regard, the displacements at vertexes 3 and 4 require the definition of a contribution associated with the shear deformability DOF. The local displacements at each vertexes considering the contribution of this DOF are now expressed in equations 3-3, 3-4, 3-5, and 3-6 for vertexes 1, 2, 3, and 4, respectively. A detailed description of the kinematics of irregular macro-elements based on a global reference system can be found in [150]. Nevertheless, in this investigation, the kinematics of the elements was considered in a local reference system for more simplified and manageable mathematical procedures.
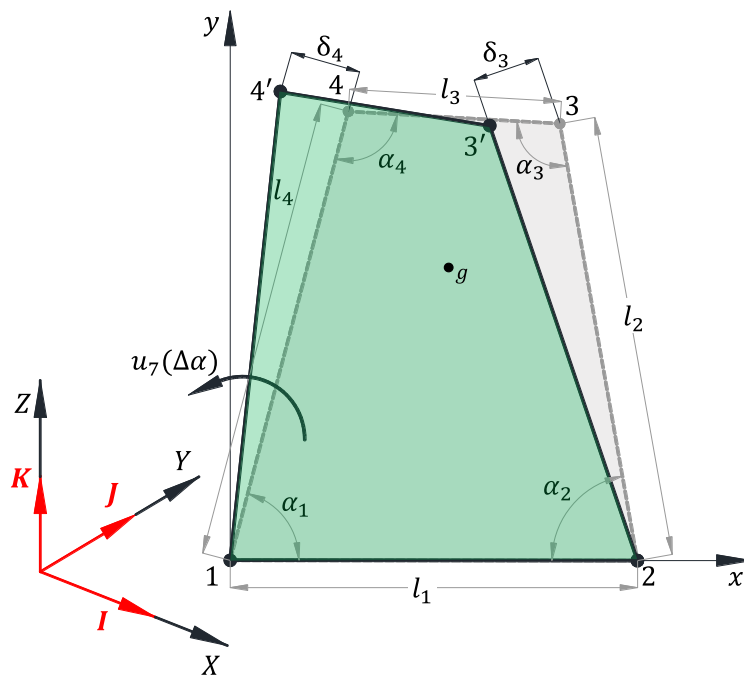
Figure 3.9. Kinematic of an irregular element associated with the shear deformability DOF

Vertex 1

$$\hat{v}_{1x} = u_1 + \left(z_1 - z_g\right)\cdot u_5 - \left(y_1 - y_g\right)\cdot u_6$$

$$\hat{v}_{1y} = u_2 + \left(x_1 - x_g\right)\cdot u_6 - \left(z_1 - z_g\right)\cdot u_4 \qquad\qquad 3\text{-}3$$

$$\hat{v}_{1z} = u_3 + \left(y_1 - y_g\right)\cdot u_4 - \left(x_1 - x_g\right)\cdot u_5$$

Vertex 2

$$\hat{v}_{2x} = u_1 + \left(z_2 - z_g\right)\cdot u_5 - \left(y_2 - y_g\right)\cdot u_6$$

$$\hat{v}_{2y} = u_2 + \left(x_2 - x_g\right)\cdot u_6 - \left(z_2 - z_g\right)\cdot u_4 \qquad\qquad 3\text{-}4$$

$$\hat{v}_{2z} = u_3 + \left(y_2 - y_g\right)\cdot u_4 - \left(x_2 - x_g\right)\cdot u_5$$

Vertex 3

$$\hat{v}_{3x} = u_1 + \left(z_3 - z_g\right)\cdot u_5 - \left(y_3 - y_g\right)\cdot u_6 - \left(\frac{l_4\cdot\sin\alpha_4\cdot\sin\alpha_2}{\sin\alpha_3}\right)\cdot u_7$$

$$\hat{v}_{3y} = u_2 + \left(x_3 - x_g\right)\cdot u_6 - \left(z_3 - z_g\right)\cdot u_4 - \left(\frac{l_4\cdot\sin\alpha_4\cdot\cos\alpha_2}{\sin\alpha_3}\right)\cdot u_7 \qquad\qquad 3\text{-}5$$

$$\hat{v}_{3z} = u_3 + \left(y_3 - y_g\right)\cdot u_4 - \left(x_3 - x_g\right)\cdot u_5$$

Vertex 4

$$\hat{v}_{4x} = u_1 + \left(z_4 - z_g\right)\cdot u_5 - \left(y_4 - y_g\right)\cdot u_6 - \left(l_4\cdot\sin\alpha_1\right)\cdot u_7$$

$$\hat{v}_{4y} = u_2 + \left(x_4 - x_g\right)\cdot u_6 - \left(z_4 - z_g\right)\cdot u_4 + \left(l_4\cdot\cos\alpha_1\right)\cdot u_7 \qquad\qquad 3\text{-}6$$

$$\hat{v}_{4z} = u_3 + \left(y_4 - y_g\right)\cdot u_4 - \left(x_4 - x_g\right)\cdot u_5$$

In this regard, the local displacements of a vertex of a macro-element can be expressed in the vector form as reported in equation 3-7, in which the vector $\hat{\mathbf{v}}_n$ corresponds to local displacements of the nth vertex, the vector $\mathbf{u}$ is related to the seven DOFs, and $\hat{\boldsymbol{\psi}}_n$ is a matrix operator which contains the displacements of each of the nth vertexes in a local reference system. This matrix operator is better specified throughout equations 3-8, 3-9, 3-10, and 3-11 for vertexes 1, 2, 3, and 4, respectively.

$$\hat{\mathbf{v}}_n = \hat{\boldsymbol{\psi}}_n \cdot \mathbf{u}$$

$$\begin{bmatrix} \hat{v}_{nx} \\ \hat{v}_{ny} \\ \hat{v}_{nz} \end{bmatrix} = \hat{\boldsymbol{\psi}}_n \cdot \begin{bmatrix} u_1 \\ u_2 \\ u_3 \\ u_4 \\ u_5 \\ u_6 \\ u_7 \end{bmatrix}$$

3-7

$$\hat{\boldsymbol{\psi}}_1 = \begin{Bmatrix} 1 & 0 & 0 & 0 & z_1 - z_g & y_g - y_1 & 0 \\ 0 & 1 & 0 & z_g - z_1 & 0 & x_1 - x_g & 0 \\ 0 & 0 & 1 & y_1 - y_g & x_g - x_1 & 0 & 0 \end{Bmatrix}$$

3-8

$$\hat{\boldsymbol{\psi}}_2 = \begin{Bmatrix} 1 & 0 & 0 & 0 & z_2 - z_g & y_g - y_2 & 0 \\ 0 & 1 & 0 & z_g - z_2 & 0 & x_2 - x_g & 0 \\ 0 & 0 & 1 & y_2 - y_g & x_g - x_2 & 0 & 0 \end{Bmatrix}$$

3-9

$$\hat{\boldsymbol{\psi}}_3 = \begin{Bmatrix} 1 & 0 & 0 & 0 & z_3 - z_g & y_g - y_3 & -\dfrac{l_4 \sin\alpha_4 \cdot \sin\alpha_2}{\sin\alpha_3} \\ 0 & 1 & 0 & z_g - z_3 & 0 & x_3 - x_g & -\dfrac{l_4 \sin\alpha_4 \cdot \cos\alpha_2}{\sin\alpha_3} \\ 0 & 0 & 1 & y_3 - y_g & x_g - x_3 & 0 & 0 \end{Bmatrix}$$

3-10

$$\hat{\boldsymbol{\psi}}_4 = \begin{Bmatrix} 1 & 0 & 0 & 0 & z_4 - z_g & y_g - y_4 & -l_4 \cdot \sin\alpha_1 \\ 0 & 1 & 0 & z_g - z_4 & 0 & x_4 - x_g & l_4 \cdot \cos\alpha_1 \\ 0 & 0 & 1 & y_4 - y_g & x_g - x_4 & 0 & 0 \end{Bmatrix}$$

3-11

The transformation of the matrix operator from a local to a global reference system $\boldsymbol{\psi}_n$ is conducted by the introduction of a rotational matrix as expressed in equation 3-12. This rotational matrix contains information about the global unit vectors given in a local reference system which are denoted as $\mathbf{I} = [I_x, I_y, I_z]$, $\mathbf{J} = [J_x, J_y, J_z]$ and $\mathbf{K} = [K_x, K_y, K_z]$, and it is given by equation 3-13.

$$\boldsymbol{\psi}_n = \mathbf{R} \cdot \hat{\boldsymbol{\psi}}_n$$

3-12

$$\mathbf{R} = \begin{Bmatrix} I_x & I_y & I_z \\ J_x & J_y & J_z \\ K_x & K_y & K_z \end{Bmatrix}$$

3-13

All in all, the mechanical scheme of a single macro-element has been object of different upgrades aiming at improving its accuracy and effectiveness when assessing the seismic response of URM structure. In this sense, Figure 3.10a depicts the initial two-dimensional scheme of regular panels used for the in-plane assessment of this typology of structures. On the other hand, Figure 3.10b and Figure 3.10c illustrate the mechanical schemes for three-dimensional panels used for the in-plane and out-of-plane evaluation of these structures based on regular and irregular geometric configurations, respectively.

(a) (b) (c)
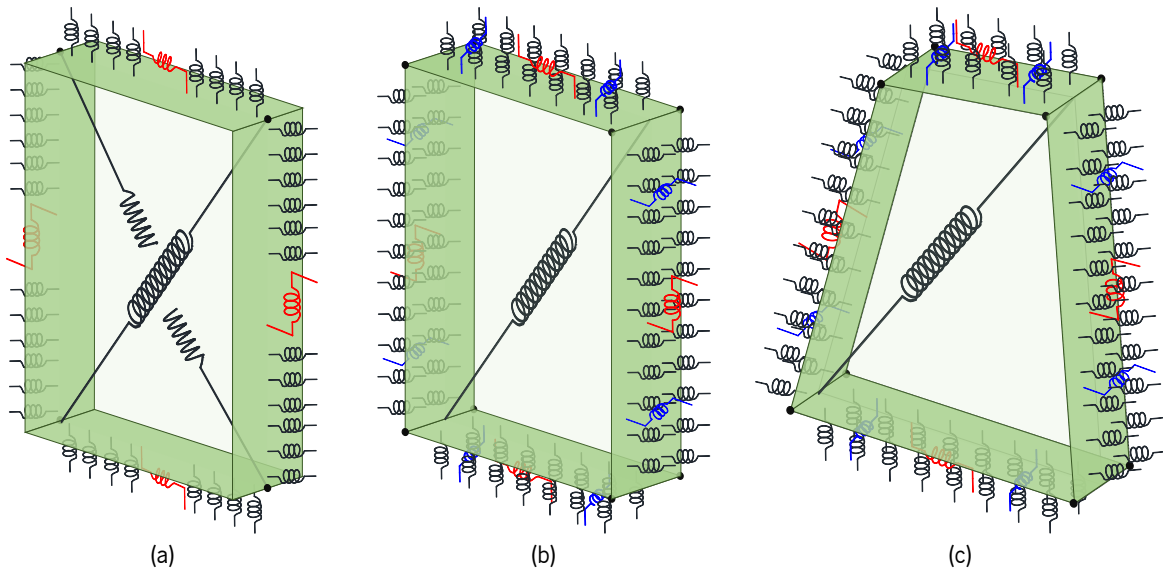
Figure 3.10 Macro-element modelling approach: (a) two-dimensional scheme, and (b) regular and (c) irregular three-dimensional schemes

3.2.4 MODELLING OF FIBRE REINFORCED POLYMERS

A more recent upgrade was conducted to this macro-element approach for the modelling of Fibre Reinforced Polymer FRP elements as reported by Pantò, et al. [148]. This reinforcement is simulated by the introduction of zero-thickness rigid flat elements connected partially or entirely to one of the macro-element surfaces as illustrated in Figure 3.11. The connection between these flat elements and the coincident surfaces of panels is conducted by means of two-dimensional interface elements. Such fibre-masonry interface element is composed of a two-dimensional grid of transversal links and a set of sliding links for the simulation of an adhesive, organic or cementitious behaviour of reinforcement, and the delamination phenomenon, respectively. It is worth noting that the interaction based on these interface elements allows the simulation of normal and tangential stresses between reinforcement and masonry. On the other hand, the connection between rigid flat elements (reinforcement) is carried out considering a different approach. This connection is conducted by means of a particular one-dimensional interface element composed by a discrete linear distribution of nonlinear links which is involved in the generation of additional tangential stresses between reinforcement and masonry.
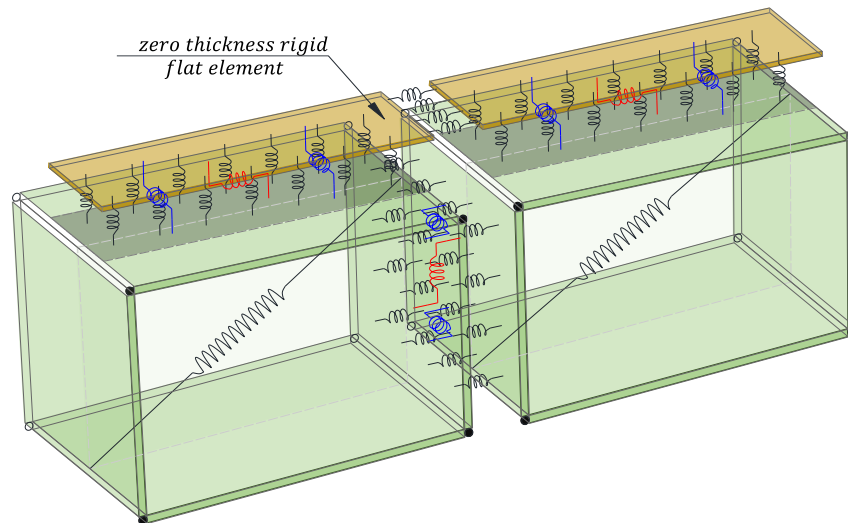
Figure 3.11 Modelling of FRP by means of rigid flat elements.

3.3 CALIBRATION OF TRANSVERSAL NONLINEAR LINKS

This section reports the calibration procedure associated with the transversal links which simulate, with reference to the spatial regular panels, the axial and bi-directional flexural responses of masonry structures. It is worth noting that this calibration procedure is suitable for two-dimensional or three-dimensional models characterised by regular elements. Nevertheless, the calibration of transversal links associated with irregular three-dimensional panels present a more sophisticated procedure which is beyond the scope of this thesis. A detailed description of the calibration procedure for irregular macro-elements can be found in [150].

The definition of the elastic mechanical properties of this set of links is based on a fibre calibration procedure in which a single equivalent link represents a masonry strip corresponding to two adjacent panels as illustrated in Figure 3.12a. Initially, the interface element connecting two adjacent macro-elements (e.g. panels l and k), in a given material direction, is composed by a set of discretised nonlinear links in series characterised by an influence area As_n together with half of the length of the corresponding panel. In this sense, each couple of transversal nonlinear links in series is further replaced by a single equivalent one as depicted in Figure 3.12b. It is worth noting that the behaviour of masonry as an orthotropic material is conducted by a separate calibration of horizontal and vertical interface elements using the corresponding mechanical properties in the given direction.

Based on this fibre calibration procedure, the initial stiffness of each link in series is related to the axial rigidity of its corresponding masonry strip which is characterised by Young's modulus E_n, the influence area As_n, and the half-length L_n of the panel n. The initial stiffness K_{in} of each of the links in series and the initial stiffness K_i of the equivalent link are given by equations 3-14 and 3-15, respectively. On the other hand, the yielding forces in tension F_{ytn} and compression F_{ycn} of each transversal link in series (equations 3-16 and 3-17) are related to their influence area together with the tensile and compressive strengths of the corresponding panel, respectively. If two adjacent panels present different tensile or compressive strengths or different geometry, the yielding forces in tension F_{yc} and compression

F_{yc} of the equivalent link are defined as the minimum and maximum values between the two corresponding forces of the links in series as expressed in equations 3-18 and 3-19. Finally, the tensile and compressive yielding displacement u_{yt} and u_{yc} are associated with the yielding forces and initial stiffness of the equivalent nonlinear link as given by equations 3-20 and 3-21.
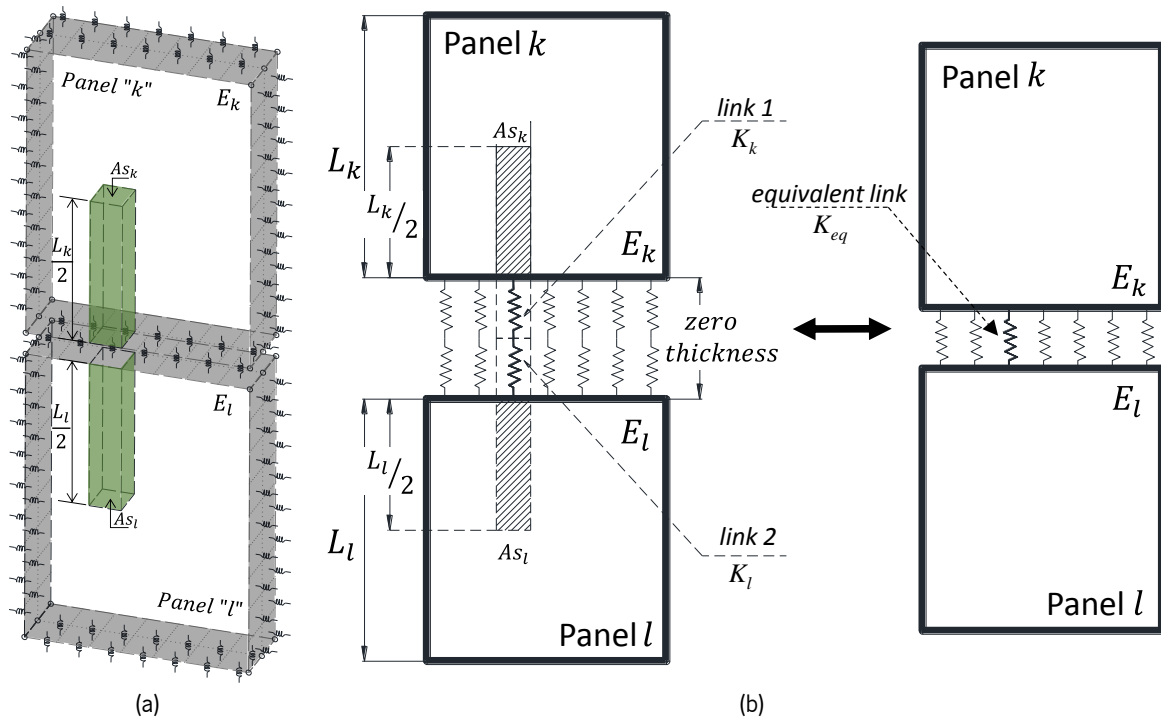
Figure 3.12 Transversal nonlinear links: (a) discretised interface element and definition of masonry strips, and (b) equivalence based on a fibre calibration procedure.

$$K_{i_n} = 2\frac{E_n \cdot As_n}{L_n}$$

3-14

$$K_i = \frac{K_{i_k} \cdot K_{i_l}}{K_{i_k} + K_{i_l}}$$

3-15

$$F_{yt_n} = As_n \cdot f_{t_n}$$

3-16

$$F_{yc_n} = As_n \cdot f_{c_n}$$

3-17

$$F_{yt} = \min\left(F_{yt_k}, F_{yt_l}\right)$$

3-18

$$F_{yc} = \max\left(F_{yc_k}, F_{yc_l}\right)$$

3-19

$$u_{yt} = \frac{F_{yt}}{K_i}$$

3-20

$$u_{yc} = \frac{F_{yc}}{K_i}$$

3-21

The nonlinearity of the transversal links can be characterised according to any uniaxial constitutive law, in the application reported in the following three different constitutive laws for tensile and compressive responses have been adopted. The first one is related to an elasto-plastic behaviour in which the post-yielding stiffness is defined by means of a ratio α_t or α_c that affects the initial stiffness in tensile or compressive phase as illustrated in Figure 3.13a. The ultimate displacements for tension u_{ut} and compression u_{uc} are described by means of the ductility of the material. It is worth noting that an infinity ductility can also be established by means of this constitutive law. The remaining constitutive laws, depicted in Figure 3.13b and Figure 3.13c, are based on a fracture energy approach ruling a softening post-yielding behaviour. The tensile response can be simulated by means of linear and exponential softening curves in which the ultimate displacement is associated with the yielding force F_{yt} and fracture energy G_f^I in tension. The ultimate tensile displacement u_{ut} corresponding to linear and exponential softening curves are expressed in equations 3-22 and 3-24, respectively. The response in compression can be simulated by two curves, namely linear and parabolic. In the case of the ultimate compressive displacement u_{uc}, its value in accordance with a linear softening is also related to the corresponding yielding force F_{yc} and fracture energy G_c, and it is given by equation 3-23. When the behaviour in compression is based on a parabolic curve, the compressive yielding displacement u_{yc} requires a different definition as reported in equation 3-25. Nevertheless, the ultimate displacement in compression is still governed by yielding force and fracture energy as expressed in equation 3-26. It is worth noting that the mesh refinement does not influence the determination of ultimate displacements (ductility) since an agreement between the adopted discretization and the crack bandwidth is considered by means of this calibration procedure.

$$u_{ut} = \frac{2 \cdot G_f^I}{\left(\dfrac{F_{yt}}{As}\right)} + u_{yt} \qquad \text{3-22}$$

$$u_{uc} = \frac{2 \cdot G_c}{\left(\dfrac{F_{yc}}{As}\right)} + u_{yc} \qquad \text{3-23}$$

$$u_{ut} = \frac{G_f^I}{\left(\dfrac{F_{yt}}{As}\right)} + u_{yt} \qquad \text{3-24}$$

$$u_{yc} = \frac{5 \cdot F_{yc}}{3 \cdot K_i} \qquad \text{3-25}$$

$$u_{uc} = \frac{3 \cdot G_c}{2 \cdot \left(\dfrac{F_{yc}}{As}\right)} + u_{yc} \qquad \text{3-26}$$

where As corresponds to the influence area of each transversal nonlinear link.
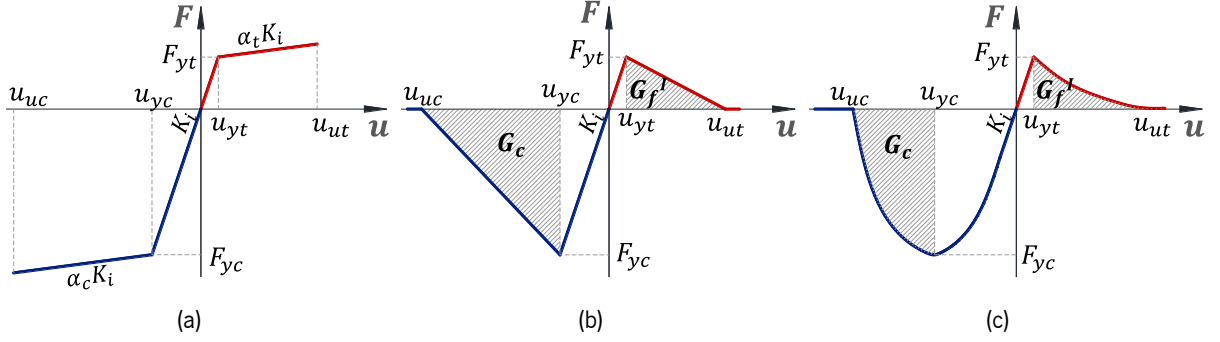
Figure 3.13 Constitutive laws defined for the transversal nonlinear links: (a) elasto-plastic, (b) linear softening, and (c) exponential and parabolic softening.

It is worth mentioning that the constitutive laws depicted in Figure 3.13c correspond to a recent upgrade regarding the nonlinear response of the transversal links. The tensile response based on an exponential softening presents an initial linear behaviour until reaching its corresponding yielding displacement which is given by equation 3-27. Subsequently, the exponential function, provided in equation 3-28, describes the softening post-peak branch as a function of the current displacement u. On the other hand, the compressive response is characterized by four stages when defined by a parabolic curve. The first one, given by equation 3-29, is associated with a linear behaviour of the transversal link until it reaches a third of the compressive yielding force. The following two stages are described by quadratic functions (equations 3-30 and 3-31) until the yielding and ultimate displacements in compression are reached, respectively. It is worth noting that the definition of the current force in also expressed as a function of the current displacement u in compression. Finally, the compressive behaviour after reaching the ultimate displacement is characterised by a zero force as expressed in equation 3-32.

$$0 < u < u_{yt} \qquad\qquad F = K_i \cdot u \tag{3-27}$$

$$u_{yt} < u \qquad\qquad F = F_{yt} \cdot e^{\left(-\frac{u - u_{yt}}{u_{yt} - u_{ut}}\right)} \tag{3-28}$$

$$0 < u < u_{F_{yc}/3} = F_{yc}/(3 \cdot K_i) \qquad F = K_i \cdot u \tag{3-29}$$

$$u_{F_{yc}/3} < u < u_{yc} \qquad F = \frac{F_{yc}}{3} \cdot \left(1 + 4 \cdot \left(\frac{u - u_{F_{yc}/3}}{u_{yc} - u_{F_{yc}/3}}\right) - 2 \cdot \left(\frac{u - u_{F_{yc}/3}}{u_{yc} - u_{F_{yc}/3}}\right)^2\right) \tag{3-30}$$

$$u_{yc} < u < u_{uc} \qquad F = Fyc \cdot \left(1 - \left(\frac{u - u_{yc}}{u_{uc} - u_{yc}}\right)^2\right) \tag{3-31}$$

$$u_{uc} < u \qquad\qquad F = 0 \tag{3-32}$$

The cyclic behaviour associated with the transversal nonlinear links was adapted from the hysteretic model introduced by Takeda [151] and implemented in the OpenSees framework [152]. This hysteretic model is characterised by a coefficient that modifies the stiffness governing the unloading

cycles. This unloading coefficient, denoted as β, can present a value ranging between 0 and 1. Figure 3.14 illustrates the cyclic behaviour of a transversal nonlinear link in which the tensile and compressive responses are ruled by exponential and parabolic curves, respectively. Three different unloading behaviours can be observed in this figure. The first one corresponds to an unloading cycle with an initial stiffness, and it is characterised by a β coefficient equal to 0. This behaviour is described throughout segments BC and EF for tension and compression, respectively. The second one corresponds to an unloading cycle with an intermediate stiffness, in which the β coefficient presents a value different to 0 or 1. In Figure 3.14, this unloading cycle in tension is depicted by segment GH, whereas in compression segment IJ applies. The last unloading cycle is governed by a stiffness oriented to the origin (secant stiffness), and the β coefficient presents a value equal to 1 as depicted by segments KO and LO. It is worth noting that tensile and compressive behaviours may present different unloading cycles; and therefore, their corresponding unloading coefficient β_t and β_c are defined independently.

Once a nonlinear link reaches a zero force, the unloading cycle finishes, and the loading in the opposite direction begins. As illustrated in Figure 3.14, this reloading is oriented to the maximum displacement reached in the previous cycle. Segments CD, HE, and OI correspond to the compressive reloading due to unloading cycles in tension based on initial, intermediate, and secant stiffness, respective. On the other hand, segments FB and JG are the corresponding tensile reloading cycles associated with compressive unloading.
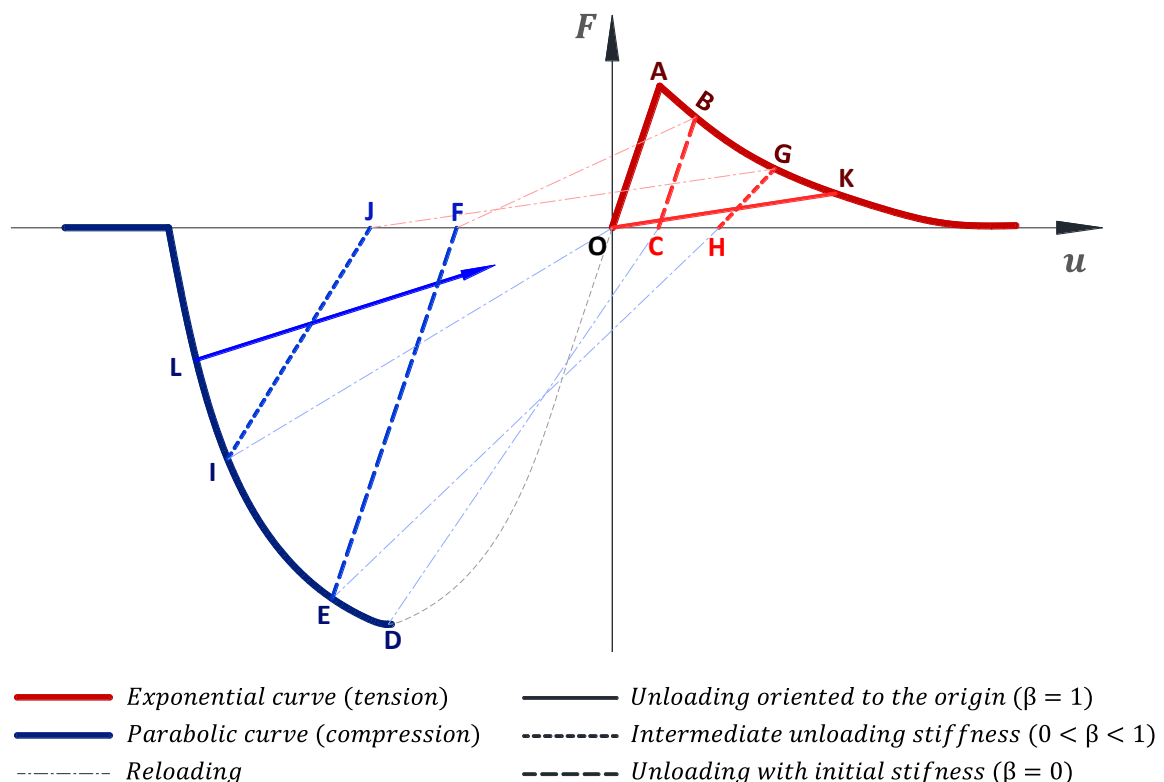
Figure 3.14 Cyclic constitutive model of the transversal nonlinear links.

The unloading cycles of a transversal link from a current tensile state are governed by the stiffness K_{un_t} given by equation 3-33. Its value is associated with the initial stiffness K_i of the equivalent transversal link by means of a coefficient denoted as k_p. This coefficient is related to the unloading coefficient in tension β_t, the tensile yielding displacement u_{yt}, and the maximum positive displacement u_{max} reached before the unloading cycle begins. An assessment of the initial value of k_p is conducted using equation 3-34. k_p is equal to 1 when its initial value is equal or lower than the unity. On the other hand, if the initial value of k_p is greater than the unity, its actual value takes into consideration the ratio between the maximum tensile force F_{max} before the unloading cycle and the tensile yielding force F_{yt}.

$$K_{un\_t} = k_p \cdot K_i \qquad\qquad 3\text{-}33$$

$$k_p = \left(\frac{u_{max}}{u_{yt}}\right)^{\beta_t}
\begin{cases}
k_p <= 1 & k_p = 1 \\[2ex]
k_p > 1 & k_p = \dfrac{\left(\dfrac{F_{max}}{F_{yt}}\right)}{k_p}
\end{cases} \qquad\qquad 3\text{-}34$$

On the other hand, the reloading in compression from tensile unloading is ruled by the stiffness K_{re_c} whose expression is given by equation 3-35. The computation of this stiffness requires the definition of the displacement in which the transversal link finishes a tensile unloading cycle reaching a zero force. This displacement is denoted as u_{un_t} and it is expressed in equation 3-36.

$$K_{re\_c} = \frac{F_{min}}{u_{min} - u_{un\_t}} \qquad\qquad 3\text{-}35$$

$$u_{un\_t} = u_{max} - \frac{F_{max}}{K_i} \qquad\qquad 3\text{-}36$$

where F_{min} and u_{min} correspond to the minimum force and displacement reached before the previous unloading compressive cycle, respectively.

3.4 CALIBRATION OF DIAGONAL NONLINEAR LINKS

The overall in-plane shear response of URM structures is partially associated to the diagonal cracking of masonry and the slipping of mortar joints. The shear-diagonal response of these structures is simulated by means of the diagonal nonlinear link located in each macro-element. The calibration of this link in the elastic field is conducted by enforcing an equivalence between a finite portion of masonry with pure shear deformability (see Figure 3.15a) and a single macro-element (see Figure 3.15b). This finite portion of masonry is characterised by shear modulus G, transversal area A_t, height h, and base b. Such equivalence is associated to the deformation δ obtained due to the application of a shear force V. The expressions that describe this deformation are given by equation 3-37 for the finite portion of masonry

with pure shear deformability, and by equation 3-38 for the single macro-element. The initial stiffness K_D of the diagonal link is expressed in equation 3-39, in which θ is defined as $arctan\ (b/h)$. It is worth noting that since the in-plane shear response of URM structures is partially simulated by two different sets of links, the value of K_D is influence by a shear factor denoted as α_s whose value ranges between 0 and 1. If this factor presents a value equal to 1, the global in-plane shear stiffness is entirely associated with the initial stiffness of the diagonal links, and the in-plane sliding links are assumed rigid. On the other hand, if the value of α_s is different than 1, the global in-plane shear stiffness comes as a contribution between diagonal and in-plane sliding nonlinear links.

$$\delta = \frac{V \cdot h}{G \cdot A_t} \qquad\qquad\qquad \text{3-37}$$

$$\delta = \frac{V}{\cos^2 \theta \cdot K_D} \cdot \alpha_s \qquad\qquad\qquad \text{3-38}$$

$$K_D = \frac{G \cdot A_t}{h \cdot \cos^2 \theta \cdot \alpha_s} \qquad\qquad\qquad \text{3-39}$$
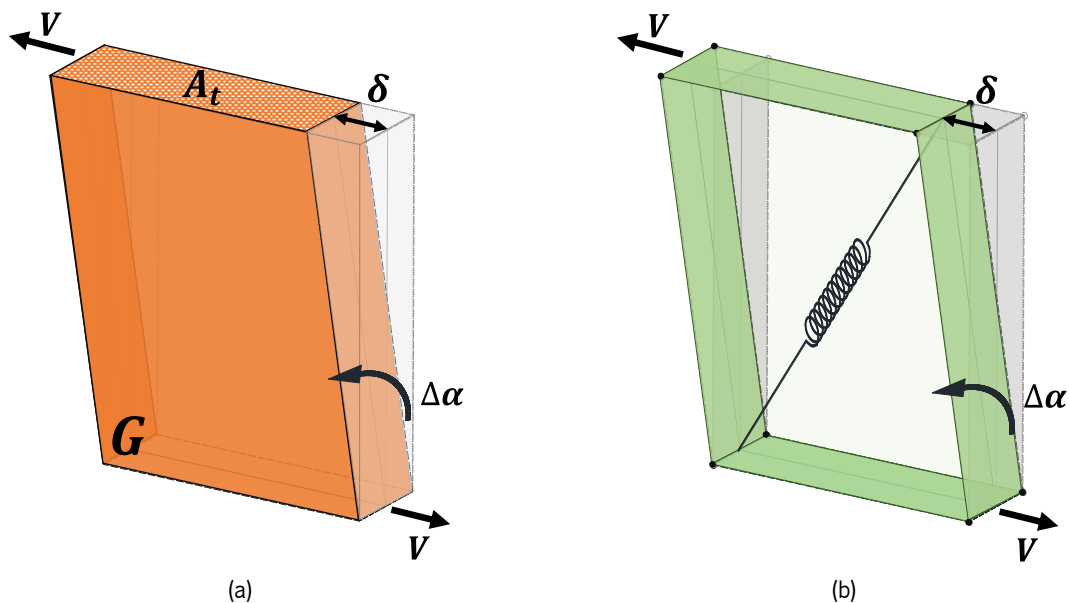
Figure 3.15 Equivalence for the calibration of the diagonal nonlinear links: (a) finite portion of masonry with pure shear deformability, and (b) single macro-element

An accurate simulation of the shear failure related to the diagonal cracking of URM structures by means of simple analytical formulations is considered a complex task [29]. Despite this, the resistance associated with the shear-diagonal mechanism of this type of structures can be estimated by means of suitable criteria [153]. In this regard, two yielding approaches can be defined for the nonlinear behaviour of the diagonal links, namely Mohr-Coulomb and Turnsek and Cacovic [154]. Based on these criteria, it is possible to simulate the influence of the normal stresses (confinement conditions) when determining

the overall shear-diagonal capacity of URM structures. The current value of yielding force F_y associated to the Mohr-Coulomb and Turnsek and Cacovic criteria are given by equations 3-40 and 3-41, respectively.

$$F_y = F_{y0} + \mu_d \cdot N$$
<div align="right">3-40</div>

$$F_y = F_{v0}\sqrt{1 + \frac{N}{1.5 \cdot F_{v0}}}$$
<div align="right">3-41</div>

where F_{y0} and F_{v0} are the yielding forces under no confinement conditions (zero normal stresses) associated with the Mohr-Coulomb and Turnsek and Cacovic criteria, respectively. In addition, N is related to the current axial forces to which the macro-element is subjected. The value of N is considered as the resultant force from the transversal nonlinear links of the contouring interface elements. Finally, μ_d corresponds to the friction coefficient of masonry, and it is associated with a shear-diagonal mechanism based on a Mohr-Coulomb criterion.

Aiming at introducing a degrading behaviour, the cyclic response of the diagonal nonlinear links is also governed by the hysteretic model introduced by Takeda [151]. However, the unloading cycles of the diagonal nonlinear links are governed by an initial stiffness, presenting a default value of unloading coefficient β_d equal to 0. Since the value of K_{un} is kept constant throughout the unloading cycles, the definition and initial assessment of k_p is not required. On the other hand, the behaviour of the reloading cycles follows a similar approach as the one defined for the transversal nonlinear links. Figure 3.16a illustrates the response of a diagonal link in which the axial force is constant, leading to an elasto-plastic behaviour, whereas Figure 3.16b depicts the response of the same link subjected to varying axial loading. It is observed that changes in the confinement conditions of the macro-element influence the reloading cycles and plasticity state of the diagonal links. In the case of the reloading cycles in which the axial load is characterised by a varying behaviour, it is necessary to update the current yielding displacement in which a new plastic phase begins in accordance with the current value of yielding force. For instance, the tensile reloading cycle described by segment FG in Figure 3.16b presents a reduction of yielding force ($F_{yB} > F_{yG}$) due to a negative increment of axial force. The estimation of the current yielding displacement u_y primarily requires determining the displacement u_{un_c} in which the compressive unloading cycle finishes as well as corresponding reloading stiffness K_{re_t}. These two variables are given by equations 3-42 and 3-43, respectively. It is worth noting that this stiffness is determined once the previous unloading cycle is concluded aiming at keeping a constant value during the reloading cycle. The current yielding displacement u_y is associated not only with the values of reloading stiffness and unloading displacement but also the current yielding force F_y as expressed in equation 3-44.

$$u_{un\_c} = u_{min} - \frac{F_{min}}{K_i}$$

3-42

$$K_{re\_t} = \frac{F_{max}}{u_{max} - u_{un\_c}}$$

3-43

$$u_y = F_y \cdot K_{re\_t} + u_{un\_c}$$

3-44

(a)

(b)
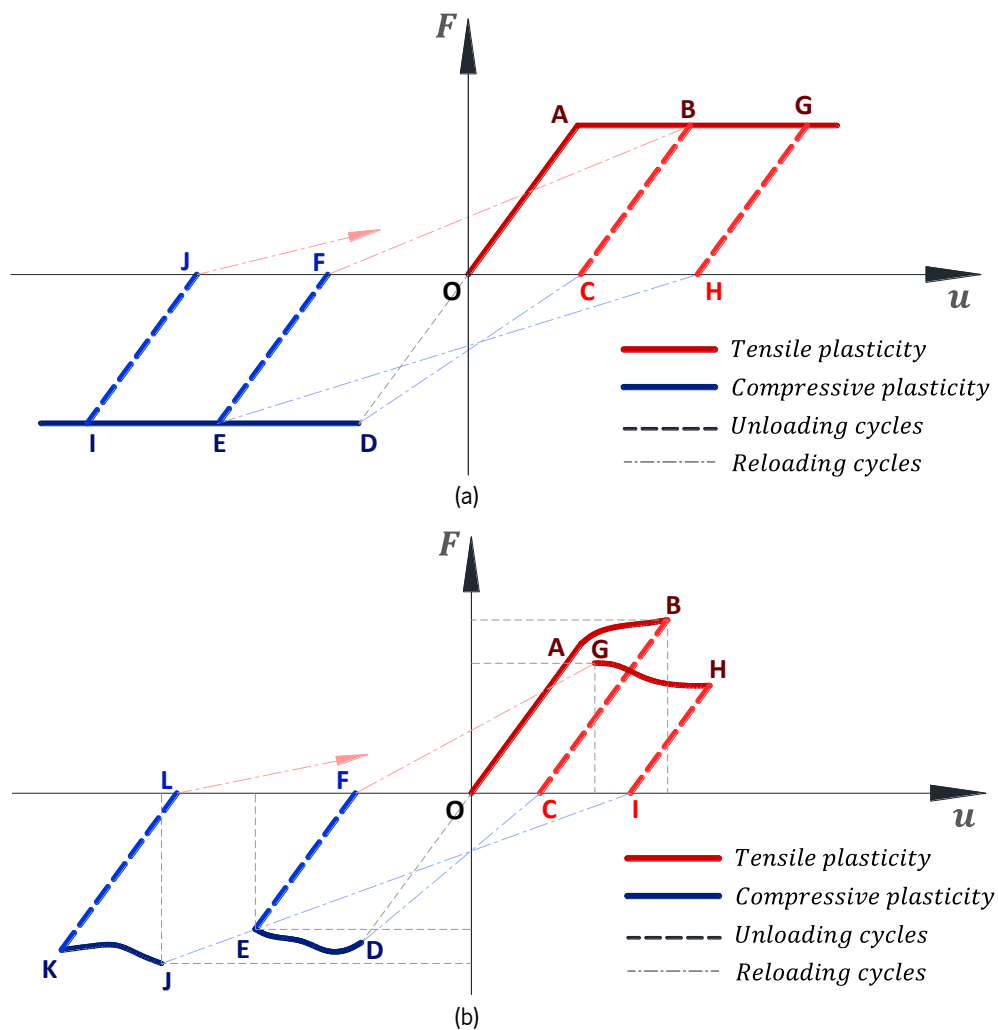
Figure 3.16 Cyclic constitutive law of diagonal nonlinear links: (a) constant, and (b) varying axial load.

3.5 CALIBRATION OF SLIDING NONLINEAR LINKS

Besides diagonal cracking, the overall in-plane shear mechanism of URM structures is also associated to the slipping of mortar joints. This mechanism is described as the relative motion between two adjacent macro-elements (panels l and k), and it is governed by the single link, denoted as in-plane sliding nonlinear link, situated along the length of the connecting interface element. On the other hand,

the out-of-plane shear mechanism is solely related to the deformability or slipping of the mortar joints. Such mechanism is simulated by a couple of nonlinear links along the thickness of the interface element, denoted as out-of-plane sliding nonlinear links. It is worth noting that these latter links also aim at the simulation of the torsion response of URM structure by means of the rotation of the macro-elements around the axis in the direction perpendicular to the surface of the interface element.

The initial stiffness K_S related to the sliding mechanism is associated to the shear modulus G of the panels, the effective length defined as the summation of half-length of adjacent panels, and the influence area As of the corresponding nonlinear link. As illustrated in Figure 3.17a, the influence area As of the in-plane sliding nonlinear link is described by the entire surface of the interface element. With reference to a single out-of-plane nonlinear link, the influence area As corresponds to half of the surface of the interface element (see Figure 3.17b). The expression that provides the definition of the initial stiffness K_S for in-plane and out-of-plane sliding links is given by equation 3-45. Since the in-plane shear mechanism is provided partially by the diagonal and in-plane sliding links, these values of stiffness are affected by the shear factor α_s. When presenting a value equal to 1, the in-plane sliding links are considered rigid (infinite stiffness). It is worth mentioning that the out-of-plane shear mechanism is solely associated with the nonlinear links along the thickness of the interface element, and there is no need to introduce a shear factor in the out-of-plane direction.
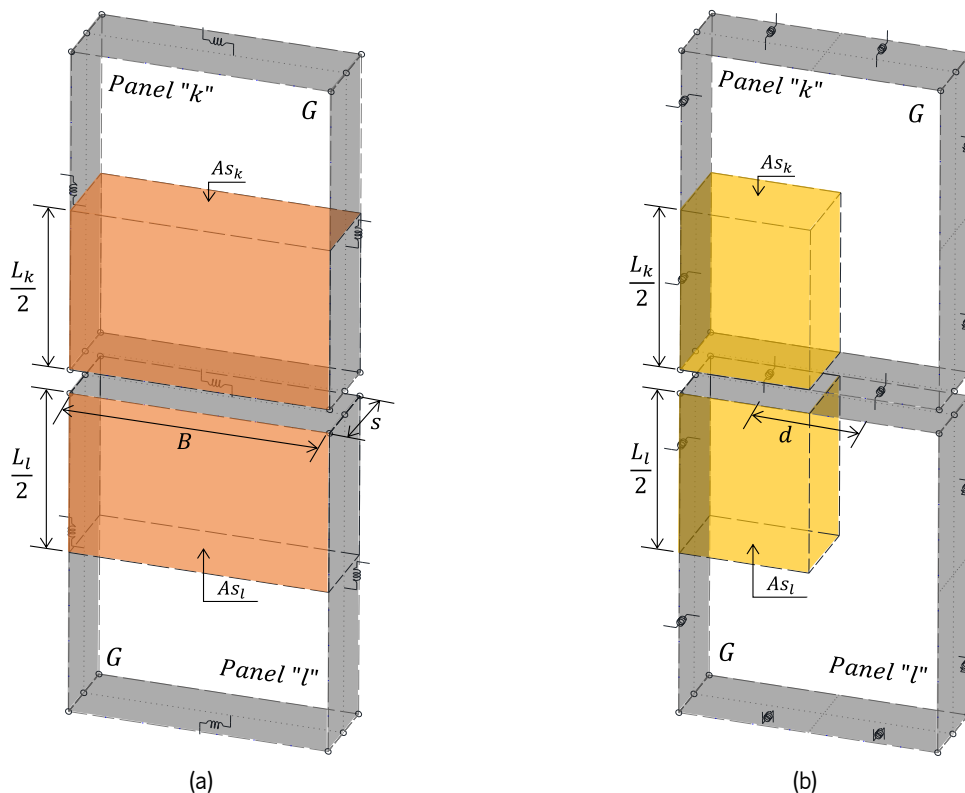
Figure 3.17 Shear-sliding mechanism: (a) in-plane, and (b) out-of-plane nonlinear links and their corresponding influence area

On the other hand, the stiffness K_ϕ that governs the torsion response of URM structures is evaluated by enforcing an equivalence between a beam model and the corresponding macro-element model. Based on this equivalence, it possible to determine the distance d between the out-of-plane nonlinear links, whose expression is given by equation 3-46, in order to simulate the torsion response. The elastic torsional stiffness (equation 3-47) is associated with a torsional rigidity factor J_ϕ given by equation 3-48, in which s corresponds to the thickness of the panel.

$$K_s = \frac{G \cdot As}{\left(\dfrac{L_k}{2} + \dfrac{L_l}{2}\right) \cdot \left(1 - \alpha_s\right)}$$

3-45

$$d = 2 \cdot s \sqrt{\frac{1}{3} - 0,21 \frac{s}{B}\left(1 - \frac{s^4}{12 \cdot B^4}\right)}$$

3-46

$$K_\phi = \frac{G \cdot J}{\left(\dfrac{L_k}{2} + \dfrac{L_l}{2}\right)}$$

3-47

$$J_\phi = B \cdot s^3 \left[\frac{1}{3} - 0,21 \frac{s}{B}\left(1 - \frac{s^4}{12 \cdot B^4}\right)\right]$$

3-48

The shear-sliding mechanism of URM structures is associated with a frictional phenomenon along the mortar joints. Such behaviour can be adequately simulated by means of a Mohr-Coulomb yielding criterion. Based on this approach, the current yielding force F_y of the in-plane and out-of-plane links is defined by means of the cohesion c and friction coefficient μ_s of the masonry material, the current contact area A, and the normal force N applied to the interface element as expressed in equation 3-49. It is worth noting that the definition of the current contact area A of the sliding links is influenced by the behaviour of the discretised matrix of transversal links. If a transversal nonlinear link has exceeded its ultimate displacement in tension or compression (rupture), its corresponding influence area As is excluded from the surface of the interface element; and therefore, from the current contact area A of the sliding link. It is worth noting that the introduction of fracture energy to define an additional softening post-yielding behaviour has also been introduced to this set of nonlinear links.

$$F_y = c \cdot A + \mu_s \cdot N$$

3-49

The cyclic behaviour of the sliding nonlinear links is characterised by an elasto-plastic hysteretic model in which the unloading and reloading cycles are ruled by the initial stiffness. The hysteretic model based on constant and varying axial forces is illustrated in Figure 3.18a, and Figure 3.18b, respectively. It is worth noting that even though there is a change in the axial load, the definition of a current yielding displacement is not required. In this regard, the loading cycles in the opposite direction (reloading) finish once the current value of yielding force is reached.

(a)

(b)
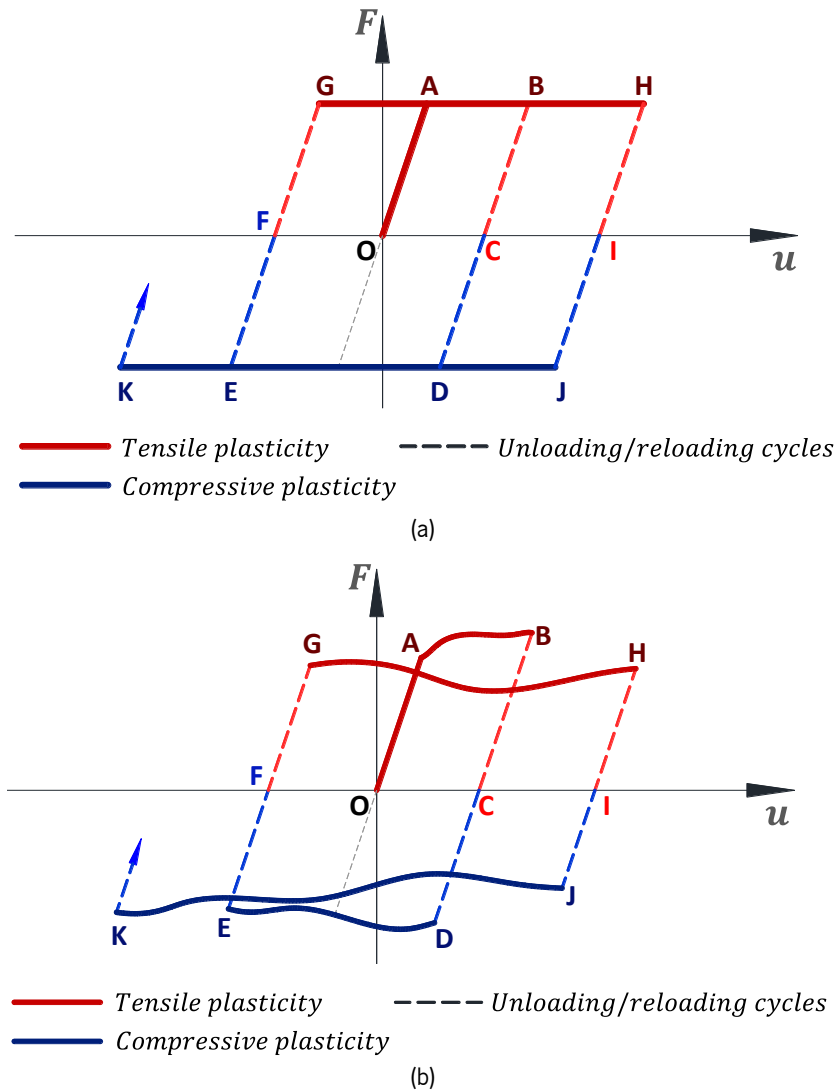
Figure 3.18 Cyclic constitutive law of sliding nonlinear links: (a) constant, and (b) varying axial load.

3.6 COMPUTATION OF MACRO-ELEMENT MASS MATRIX

The current section aims at presenting the strategy adopted for the computation of the mass matrix of a generic macro-element. A consistent mass matrix approach is followed leading to a non-diagonal element mass matrix. However, due to the adopted choice of degrees of freedom, the off-diagonal terms of the consistent mass matrix provide a negligible contribution, allowing a good representation of inertia forces when considering an approximation of the mass matrix limited to the diagonal terms. This latter consideration has been validated by comparing several numerical results obtained with and without the contribution of the off-diagonal terms.

The computation of the consistent mass matrix **m** was carried out considering the element kinematics related to the seven DOFs through the application of the principle of virtual work. For this purpose, the general case of an irregular macro-element, depicted in Figure 3.19a, was considered. The

generic term $\hat{m}_{ij}$ of the local mass matrix of a macro-element can be computed by the expression given in equation 3-50.

$$\hat{m}_{ij} = \int_V \rho \cdot \hat{\boldsymbol{\psi}}_i^T (x, y, z) \cdot \hat{\boldsymbol{\psi}}_j (x, y, z) dV$$

3-50

where $\hat{\boldsymbol{\psi}}_i$ and $\hat{\boldsymbol{\psi}}_j$ are three-component vectors of a matrix operator that allow the expression of the local displacements as a function of the DOFs i and j. In the case of the $\hat{\boldsymbol{\psi}}_j$, such expression is reported in equation 3-51.

$$\hat{\mathbf{v}}_{(x,y,z)} = \hat{\boldsymbol{\psi}}_{1_{(x,y,z)}} \cdot u_1 + \hat{\boldsymbol{\psi}}_{2_{(x,y,z)}} \cdot u_2 + \ldots + \hat{\boldsymbol{\psi}}_{6_{(x,y,z)}} \cdot u_6 + \hat{\boldsymbol{\psi}}_{7_{(x,y,z)}} \cdot u_7 = \sum_{j=1}^{7} \hat{\boldsymbol{\psi}}_j u_j$$

3-51

where u_j corresponds the DOF located at the jth component of the vector $\mathbf{u}$ reported in equation 3-1.

By concentrating the mass distribution in the middle plane of the element (see Figure 3.19b), the volume integral can be expressed as the integral over the area as given by equation 3-52.

$$\hat{m}_{ij} = \rho \cdot \int_A \hat{\boldsymbol{\psi}}_i^T (x, y) \cdot \hat{\boldsymbol{\psi}}_j (x, y) \cdot s(x, y) dA$$

3-52

where $s(x,y)$ describes the thickness variability along the four vertexes of the macro-element.

According to an isoparametric representation, the matrix operator can be conveniently expressed in an intrinsic reference system u,v by enforcing an equivalence between the middle plane of the macro-element and a square of side two as illustrated in Figure 3.19c. This equivalence allows the expression of the local displacements of any point in the macro-element assuming the meaning of a shape function. The shape function of a generic node is given by an interpolation of the values at the four vertexes of the square ($u \in [-1, 1]$, $v \in [-1, 1]$) as expressed in equation 3-53, in which $r_n(u,v)$ corresponds to the classical bi-linear function described for each vertex and it is given by equation 3-54.

$$\hat{\boldsymbol{\psi}}_j (u, v) = \sum_{n=1}^{4} \hat{\boldsymbol{\psi}}_{n,j} \cdot r_n (u, v)$$

3-53

$$r_1 (u, v) = \frac{(1-u) \cdot (1-v)}{4}$$

$$r_2 (u, v) = \frac{(1+u) \cdot (1-v)}{4}$$

$$r_3 (u, v) = \frac{(1+u) \cdot (1+v)}{4}$$

3-54

$$r_4 (u, v) = \frac{(1-u) \cdot (1+v)}{4}$$
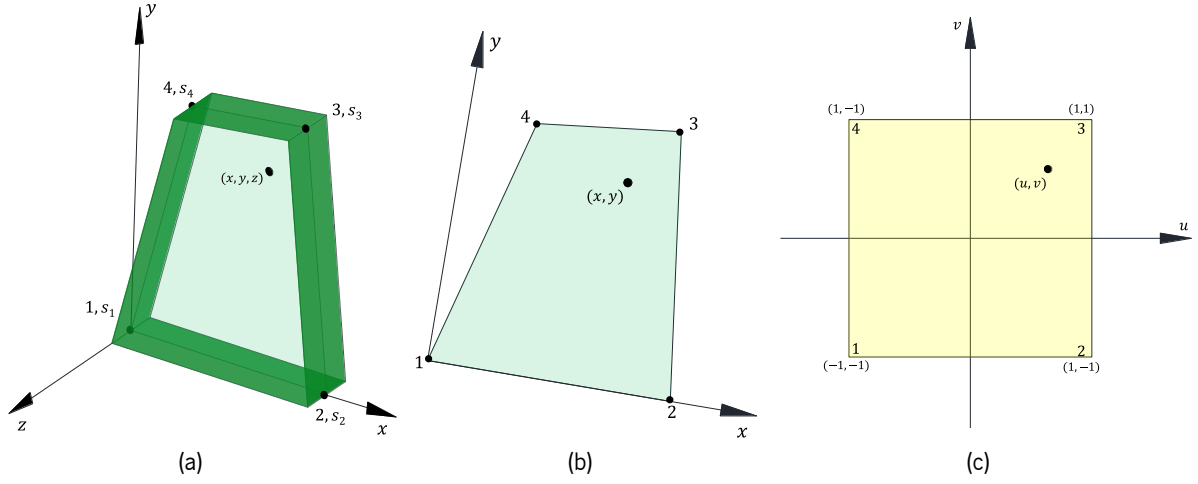
Figure 3.19. Computation of local mass matrix: (a) spatial macro-element (b) generic representation in Cartesian coordinates, and (c) intrinsic reference system.

The introduction of the isoparametric domain allows the treatment of any macro-element regardless of the characteristics of its geometric configuration. In order to define a generic formulation for any given geometry, equation 3-52 has to be expressed in the intrinsic reference system u,v. For this purpose, a Jacobian function $J(u,v)$, which allows the definition of the infinitesimal area dA, is introduced. This isoparametric transformation is given in equation 3-55.

$$dA = J(u,v)dudv = \left(\frac{\partial x}{\partial u} \cdot \frac{\partial y}{\partial v} - \frac{\partial x}{\partial v} \cdot \frac{\partial y}{\partial u} \right) dudv \qquad \text{3-55}$$

This transformation allows the formulation of each component $\hat{m}_{ij}$ of the consistent mass matrix into an intrinsic reference system as reported in equations 3-56 and 3-57 in which the Jacobian function is firstly introduced, and subsequently, the shape functions are expressed by means of the bi-linear functions, respectively. Finally, the rotational matrix $\mathbf{R}$ is introduced aiming at the formulation of the component $\hat{m}_{ij}$ in a global reference system denoted as m_{ij}, and it is expressed in equation 3-58.

$$\hat{m}_{ij} = \rho \cdot \int_{-1}^{1}\int_{-1}^{1} \left[\hat{\boldsymbol{\psi}}_i (u,v) \right]^T \cdot \hat{\boldsymbol{\psi}}_j (u,v) \cdot s(u,v) \cdot J(u,v) dudv \qquad \text{3-56}$$

$$\hat{m}_{ij} = \rho \cdot \int_{-1}^{1}\int_{-1}^{1} \sum_{n=1}^{4} \left[\hat{\boldsymbol{\psi}}_{n,i} (u,v) \right]^T \cdot r_n(u,v) \cdot \sum_{n=1}^{4} \hat{\boldsymbol{\psi}}_{n,j}(u,v) \cdot r_n(u,v) \cdot \sum_{n=1}^{4} s_n \cdot r_n(u,v) \cdot J(u,v) dudv \qquad \text{3-57}$$

$$m_{ij} = \rho \cdot \int_{-1}^{1}\int_{-1}^{1} \sum_{n=1}^{4} \left[\mathbf{R} \cdot \boldsymbol{\psi}_{n,i} (u,v) \right]^T \cdot r_n(u,v) \cdot \sum_{n=1}^{4} \left[\mathbf{R} \cdot \boldsymbol{\psi}_{n,j}(u,v) \right] \cdot r_n(u,v) \cdot \sum_{n=1}^{4} s_n \cdot r_n(u,v) \cdot J(u,v) dudv \qquad \text{3-58}$$

Based on this final formulation, a closed form solution for the estimation of the components of the global mass matrix $\mathbf{m}$ of a generic macro-element was established. Such solution is explicitly reported in Annex A.

3.7   Final considerations

The description of a simplified numerical tool based on a macro-element modelling approach as well as its various features for the assessment of the seismic response of URM structures was presented in this Chapter. Such modelling approach consisted initially four rigid edges whose interaction is conducted by hinges and a diagonal nonlinear link and the connection between these elements using interface elements. In this Chapter, it was reported that this two-dimensional model is capable of simulating the in-plane response of masonry structure successfully. Additional features have been implemented to the initial mechanical scheme of this modelling approach such as the introduction of lumped plasticity element for infilled frame structures, and the definition of reinforcement elements using rigid flat elements. Moreover, a significant enhancement carried out was the introduction of a three-dimensional macro-element capable of simulating not only the main in-plane but also the out-of-plane mechanisms that characterise the response of URM structures (flexural, shear-diagonal, shear-sliding, and torsion). It is worth noting that the latter implementation together with the definition of spatial macro-elements with irregular geometry for the modelling of curved masonry structures are some essential aspects most simplified approaches lack.

Furthermore, the procedure for the calibration of the mechanical properties of each set of nonlinear links (transversal, diagonal and sliding links) that govern the different mechanisms of URM structures was presented. As reported in this Chapter, additional constitutive laws consisting of exponential and parabolic curves were introduced for the tensile and compressive behaviours of the transversal links, respectively. On the other hand, a description of the cyclic constitutive models for the different set of links was also provided. In this sense, cyclic behaviour of transversal and diagonal links is characterised by a Takeda hysteretic model. The unloading cycles associated with the diagonal links are governed by an initial stiffness. However, it is possible to define different unloading cycles regarding the transversal link. An elasto-plastic hysteretic model rules the cyclic response of the sliding links in which both unloading and reloading cycles are characterised by the initial stiffness of the link.

A final feature presented in this Chapter corresponded to the computation of a global mass matrix based on a consistent approach. The procedure for the initial computation of local mass matrix in accordance with the DOFs of a single macro-element was carried out considering the principle of virtual work and the definition of shape functions for describing the displacement of a generic point in a macro-element. For this purpose, it was necessary to introduce an intrinsic reference system to provide a generic solution that can be used for any given geometry. The transformation from a Cartesian to an intrinsic reference system was conducted by means of a Jacobian function. Based on this isoparametric transformation, the general formulation of each component of the local mass matrix consisted of a double integration considering an intrinsic references system. Based on this formulation, a closed form solution was obtained. The validation of the closed form solution associated with the computation of a macro-element mass matrix is presented in Chapter 4.

CHAPTER 4

MODEL VALIDATION

4.1 INTRODUCTION

This Chapter is dedicated to the linear and nonlinear validation of the recently developed features associated with the macro-element modelling approach introduced by Caliò, et al. [1]. In this regard, three case studies were selected for the validation of the computation of a mass matrix as well as the cyclic behaviour of the nonlinear links. The first case study is conducted in the linear field, and it is associated with Timoshenko cantilever beams with different cross sections whose linear dynamic properties were compared to those provided by classical beam analytical formulations [155]. The capability of the modelling approach to predict the eigenproperties of these beams considering the mass matrix formulation reported in Chapter 3 is investigated. An assessment regarding the influence of the mesh discretisation in the dynamic properties is carried out. The second case study aims at validating the capability of this modelling approach to correctly describe the rocking response under the hypothesis of small displacements. In this regard, a simplified assessment of the free rocking motion of the Robert A. Millikan Memorial Library in California, USA assumed as a rigid block [156] was conducted by a macro-element model subjected to nonlinear dynamic analysis. The influence of the discretisation of transversal links at the interface element and the role of the viscous damping ratio is also assessed. The last case study is intended to validate the model to provide a satisfactory prediction of the in-plane behaviour of a masonry structure in the nonlinear field. For this purpose, a two-story benchmark masonry wall subjected to laboratory cyclic testing and numerically investigated by means of nonlinear analyses was considered. Nonlinear time-history analysis based on an artificial accelerogram is performed for investigating the capability of this modelling approach to correctly predict the hysteretic nonlinear behaviour.

4.2 CANTILEVER BEAMS

The capability of the macro-element modelling approach to predict the eingenproperties according to the stiffness and mass properties is initially validated by means of a simple but significant application. The dynamic properties of Timoshenko cantilever beams were determined by comparing the results obtained by detailed linear Finite Element (FE) and macro-element modelling approaches. The estimation of the dynamic parameters based on a FE model was conducted considering a lumped mass matrix. On the other hand, a consistent mass matrix approach with and without the contribution of the off-diagonal terms was taken into account for two macro-element models with different discretised configurations. The numerical simulations were conducted by means of the software DIANA [157] and HiStrA [149] for FE and macro-element models, respectively. The values obtained from the numerical models, namely natural frequencies, were further compared to analytical results determined using single differential equations as reported by Majkut [155].

The cantilever elements corresponded to two Timoshenko beams with a length l equal to 1.00 m and a rectangular cross-section with 20 mm of base b. These elements, denoted as Stocky and Slender beams in [155], were characterized by different height h. In the case of the Stocky beam, the height was equal to 80 mm, whereas the Slender beam presented a value of 30 mm of height as illustrated in Figure 4.1a and Figure 4.1b, respectively. On the other hand, these beams were characterized by a deformable material whose mechanical properties are summarized in Table 4-1.
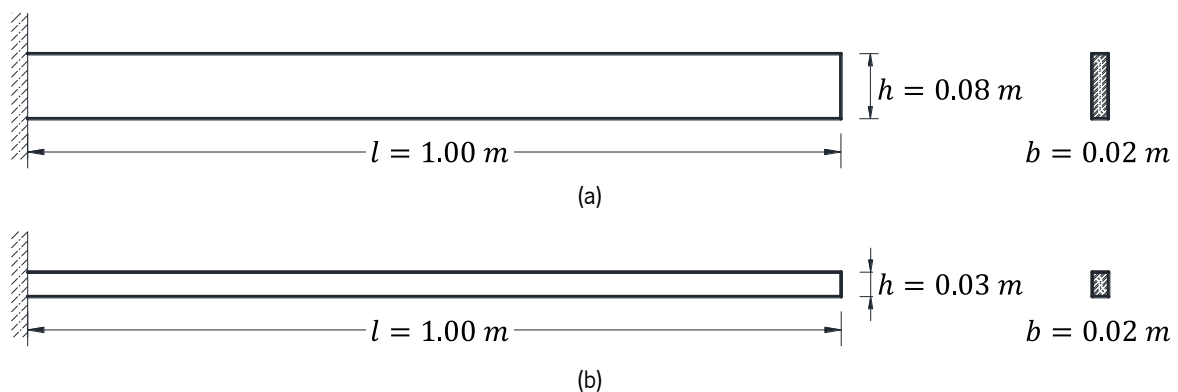
Figure 4.1. Timoshenko cantilever beams for the validation of the macro-element mass matrix: (a) Stocky beam, and (b) Slender beam

Table 4-1. Mechanical properties of the Timoshenko cantilever beams

Young's modulus E	Shear modulus G	Specific mass ρ
21x10^4 MPa	8.1 x10^4 MPa	7860 kg/m^3

Regarding the numerical simulations of the Stocky Timoshenko cantilever beam, the model based on a FE approach presented a mesh discretization of 0.02 m along the length of the cantilever beam, and a mesh size equal to 0.01 m for the rectangular cross-section. The adopted mesh refinement for this beam associated with a FE modelling approach, using linear elements (8-noded), is illustrated in Figure 4.2a. On the other hand, the macro-element model was composed of thirteen panels along the length of

the cantilever beam, with elements of approximately 0.075 m x 0.08 m. It is worth noting that the cross-section of this element did not present any mesh discretization, being characterized by a single element. The macro-element model of the Stocky Timoshenko cantilever beam is depicted in Figure 4.2b. It is worth mentioning that these models are characterised by a marked difference regarding the number of DOFs. In the case of the FE approach, the model was described by 4131 DOFs, whereas in the case of the macro-element strategy, the number of DOFs was reduced to 91 only.

(a)

(b)
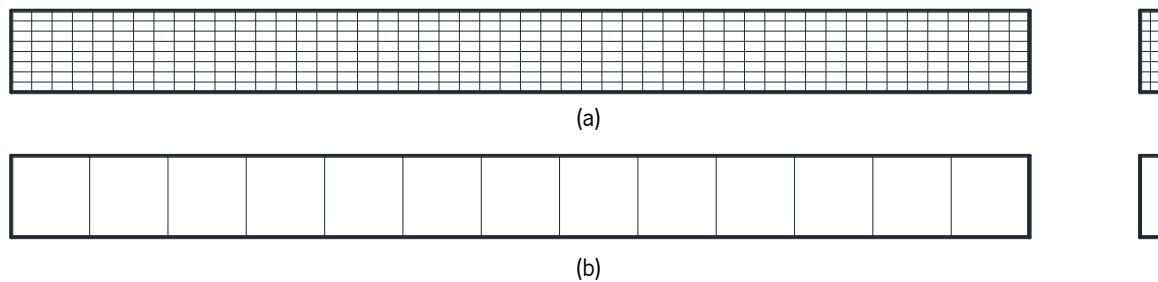
Figure 4.2. Mesh discretization of the Stocky Timoshenko cantilever beam based on a: (a) FE and (b) macro-element modelling approaches

The natural frequencies of the first five vibration modes of the Stocky cantilever beam reported by Majkut [155] together with the corresponding values obtained in the numerical simulations are summarized in Table 4-2. The error regarding the natural frequency of each vibration mode of the numerical models with respect to the analytical results was also calculated. A first comparison was conducted considering the analytical values and the result obtained from the FE model. The differences between these approaches presented maximum absolute errors of approximately 3.73% and 3.82% corresponding to the second and third vibration modes. Nevertheless, smaller errors of approximately 1.5% were obtained when comparing the remaining vibration modes. On the other hand, the results obtained from the macro-element model were characterised by absolute errors ranging between 2.18% and 5.38% which corresponded to the first and third vibration modes when considering a diagonal mass matrix. It was evidenced that the errors corresponding to lower modes did not present any substantial reduction when using a full consistent mass matrix approach. However, a more significant influence was observed in the higher modes, especially in the fifth vibration mode. This difference may be related to the behaviour of the panels associated with the DOF corresponding to the shear deformability, see also Figure 4.3.

Table 4-2. Natural frequencies of the Stocky Timoshenko cantilever beam by means of differential equation, FE and macro-element models

	Majkut [155]	FE model		Macro-element – Diagonal mass matrix		Macro-element – Full-consistent mass matrix	
	Frequency (rad/s)	Frequency (rad/s)	Error (%)	Frequency (rad/s)	Error (%)	Frequency (rad/s)	Error (%)
1st Mode	424.1	418.9	-1.23	414.9	-2.18	414.9	-2.17
2nd Mode	2653.7	2254.7	-3.73	2520.6	-5.02	2521.4	-4.99
3th Mode	7145.3	6872.5	-3.82	6760.7	-5.38	6778.4	-5.13
4th Mode	13016	12789.4	-1.74	12501.4	-3.95	12630.9	-2.96
5th Mode	19645	19955.6	1.58	19209.3	-2.22	19767.6	0.62

In this first validation, another comparison was also conducted between the results obtained by means of the numerical approaches. When considering a diagonal mass matrix, the natural frequencies also presented some variability between the FE and macro-element models ranging between 0.96% and 3.73% for the first and fifth vibration modes. On the other hand, a better agreement was obtained when considering a full-consistent mass matrix. In this case, the errors ranged between 0.96% corresponding to the first mode and 1.37% corresponding to the third mode. All in all, the macro-element model, based either on an approximate diagonal or a full-consistent mass matrix, provided results in terms of natural frequencies in acceptable agreement with the ones obtained by means of differential equations and a different numerical approach.

An additional comparison was carried out between the modal shapes of the first five vibration modes numerically obtained as depicted in Figure 4.3. In the case of the FE model, the modal shapes were illustrated by means of a simplified scheme considering the middle surface of the cantilever beam. On the other hand, the modal shapes associated with the macro-element model were plotted considering the deformed shape of the constituent panels. It is worth noting that these models are characterized by a significant difference in DOFs. Despite this, it was possible to observe a good agreement between the two numerical responses. In this regard, the macro-element model was capable of replicating successfully the modal shapes obtained by means of the FE modelling approach.
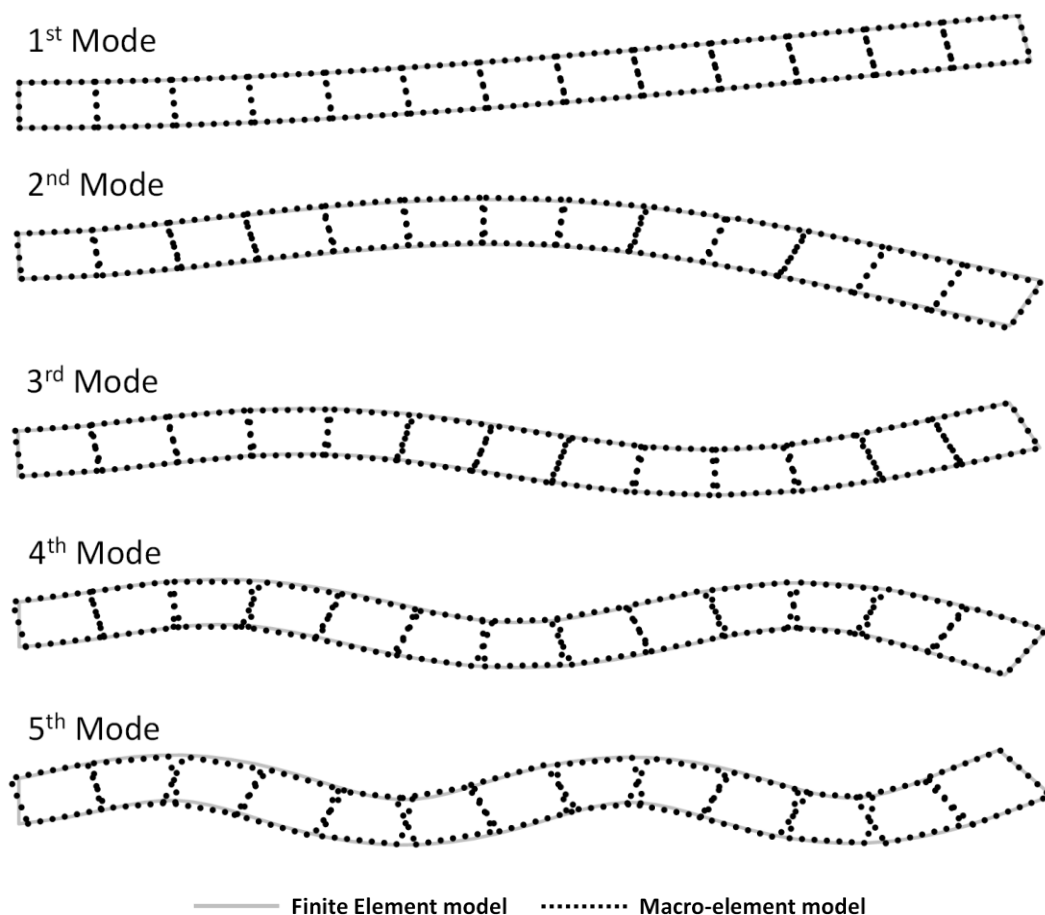
Figure 4.3. Modal shapes of FE and macro-element models of the Stocky Timoshenko cantilever beam

The influence of the mesh refinement on the dynamic response of the Stocky Timoshenko cantilever beam associated with a macro-element modelling approach was also investigated. In this sense, a model with a more refined mesh discretization along the length of the cantilever beam was taken into consideration. This *Refined* model was composed by 25 macro-elements with dimensions of approximately 0.038 m x 0.08 m as depicted in Figure 4.4. Due to the increment of panels used in this model, the number of DOFs also presented a higher value. In this case, the *Refined* model was characterised by 175 DOFs. The natural frequencies of this model were also compared not only to the values obtained by means of analytical formulation but also to the results from the initial macro-element model based on a diagonal mass matrix denoted as *Basic* model.

Figure 4.4. Mesh discretization of the *Refined* macro-element model

The natural frequencies obtained by means of the *Refined* model considering diagonal and full consistent mass approaches, together with the analytical results and the corresponding values of the *Basic* macro-element model, are reported in Table 4-3. In addition, this table also includes the differences, expressed in terms of percentage, between the results obtained by means of the *Refined* model with respect to the results from the analytical formulation. It was possible to establish a better agreement when comparing the results from this macro-element model to the ones obtained from the differential equation. In this sense, a denser mesh discretisation of the macro-element model led to an increment in the values of natural frequencies (making the structure more flexible, as expected). From these numerical simulations, it was also noted that the second and third vibration modes of the *Refined* model with a diagonal mass matrix presented the most marked differences when compared to the analytical results of approximately -4.35% and -4.40%, respectively. The approach adopted for the definition of the mass matrix did not have a significant influence on the estimation of the natural frequencies of this cantilever beam. In this regard, the difference between the natural frequencies of the first three vibration modes of macro-element models (diagonal and full-consistent mass matrices) presented comparable values. On the other hand, the values of natural frequencies of the remaining vibration modes (fourth and fifth) were characterized by errors of 0.26% and 0.73%, respectively. The similar response of these models was mainly related to the shear-diagonal deformation of the constituent panels. It was noted that, due to a more refined mesh discretisation, the DOF related to the shear deformability of the panels was not significantly involved in the kinematics of this modelling approach.

Table 4-3. Natural frequencies of the Stocky Timoshenko cantilever beam by means of differential equation, *Basic* and *Refined* macro-element models

	Majkut [155]	*Basic* model - Lumped	*Refined* model - Lumped		*Refined* model - Consistent	
	Frequency (rad/s)	Frequency (rad/s)	Frequency (rad/s)	Error (%)	Frequency (rad/s)	Error (%)
1st Mode	424.1	414.9	416.24	-1.85	416.24	-1.85
2nd Mode	2653.7	2520.6	2538.17	-4.35	2538.38	-4.34
3th Mode	7145.3	6760.7	6830.56	-4.40	6835.21	-4.34
4th Mode	13016	12501.4	12703.87	-2.40	12737.97	-2.14
5th Mode	19645	19209.3	19761.65	0.59	19907.53	1.34

A comparison of the modal shapes was also conducted for the *Refined* macro-element model. For this purpose, these results were compared to the modal shapes obtained with the FE model as illustrated in Figure 4.5. Based on these results, excellent agreement was obtained between the two numerical approaches. In general, this macro-element modelling approach provided satisfactory results in terms of natural frequencies and modal shapes of the Stocky Timoshenko cantilever beam. Even though the *Basic* model with a diagonal mass matrix presented the highest differences in terms of natural frequencies, its results can still be considered acceptable and generally preferable, due to the computational advantages related to the use of a diagonal mass matrix.
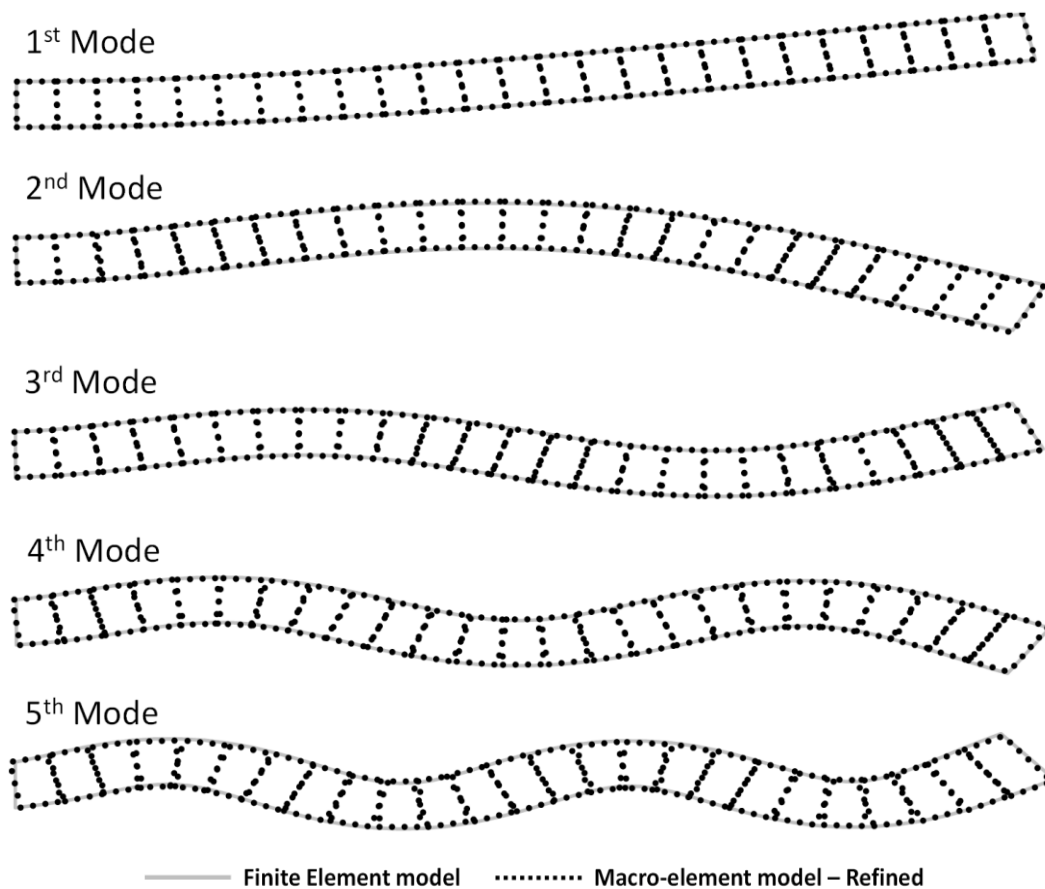
Figure 4.5. Modal shapes of FE and *Refined* macro-element models of the Stocky Timoshenko cantilever beam

In the case of the Slender Timoshenko cantilever beam, the FE model presented a similar discretisation in which mesh sizes of 0.02 m and 0.01 m were defined along the length and cross-section of the element, respectively. Based on this discretisation with linear elements (8-noded), the FE model was described by 1836 DOFs. On the other hand, the macro-element model of the Slender cantilever beam was also composed of thirteen panels along its length with dimensions of approximately 0.075 m x 0.03 m. In addition, the discretisation along the cross-section of the cantilever was conducted by means of a single panel. The number of DOFs of the macro-element model was also significantly reduced to 91. The discretised configurations of the numerical models based on FE and macro-element approaches are depicted in Figure 4.6a and Figure 4.6b, respectively.

(a)

(b)
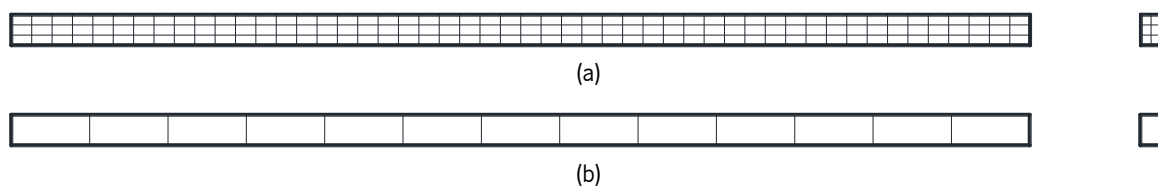
Figure 4.6. Mesh discretization of the Slender Timoshenko cantilever beam based on a: (a) FE and (b) macro-element modelling approaches

The natural frequencies of the first five vibration modes of the Slender cantilever beam obtained by analytical formulations [155] and numerical simulations are reported in Table 4-4. From these results, it was observed that the FE model was capable of successfully replicating the analytical natural frequencies of this cantilever beam. The maximum and minimum differences were associated with the fifth and first vibration modes, presenting errors of 0.73% and 0.09%, respectively. On the other hand, higher differences ranging from -3.26% to -0.93% were identified when comparing the analytical results from the ones obtained by means of the macro-element model based on a diagonal mass matrix approach. It is worth noting that, like in the FE model, these differences were also associated with the fifth and first vibration modes, respectively. An additional assessment was conducted regarding the influence of the out-of-diagonal components related to the computation of a full-consistent global mass matrix on the estimation of the natural frequencies of the Slender cantilever beam. It was evidenced that in this case, the computation of a complete consistent mass matrix provided no improvements associated with the natural frequencies of the first vibration modes. This behaviour may be related to the adopted mesh discretization and the small influence of the shear deformability in slender beams. Despite this, the results obtained by means of this macro-element model can still be considered acceptable since this approach is based on a simplified mechanical scheme characterised by a very low computational cost. The comparison regarding the modal shapes of the first vibration modes of the Slender cantilever beam by means of FE and macro-element approaches is illustrated in Figure 4.7. In this figure, the modal shapes associated with the macro-element model are plotted taking into consideration the deformed shape of the constituent panels. From these results, it was observed that despite the reduced number of panels in the macro-element model, the same was capable of successfully replicating the vibration modes obtained by a detailed FE numerical approach. No macro-element mesh refinement is considered in this case.

Table 4-4. Natural frequencies of the Slender Timoshenko cantilever beam by means of differential equation, FE and macro-element models

	Majkut [155]	FE model		Macro-element - Lumped		Macro-element - Consistent	
	Frequency (rad/s)	Frequency (rad/s)	Error (%)	Frequency (rad/s)	Error (%)	Frequency (rad/s)	Error (%)
1st Mode	157.6	157.74	0.09	156.14	-0.93	156.14	-0.93
2nd Mode	987.7	958.57	-0.22	968.63	-1.93	968.63	-1.93
3th Mode	2752.5	2747.47	-0.18	2681.33	-2.59	2681.46	-2.58
4th Mode	5344.2	5351.22	0.13	5182.09	-3.03	5183.05	-3.01
5th Mode	8716.1	8779.43	0.73	8431.65	-3.26	8435.94	-3.21

1st Mode

2nd Mode

3rd Mode

4th Mode

5th Mode

——— Finite Element model   ·········· Macro-element model
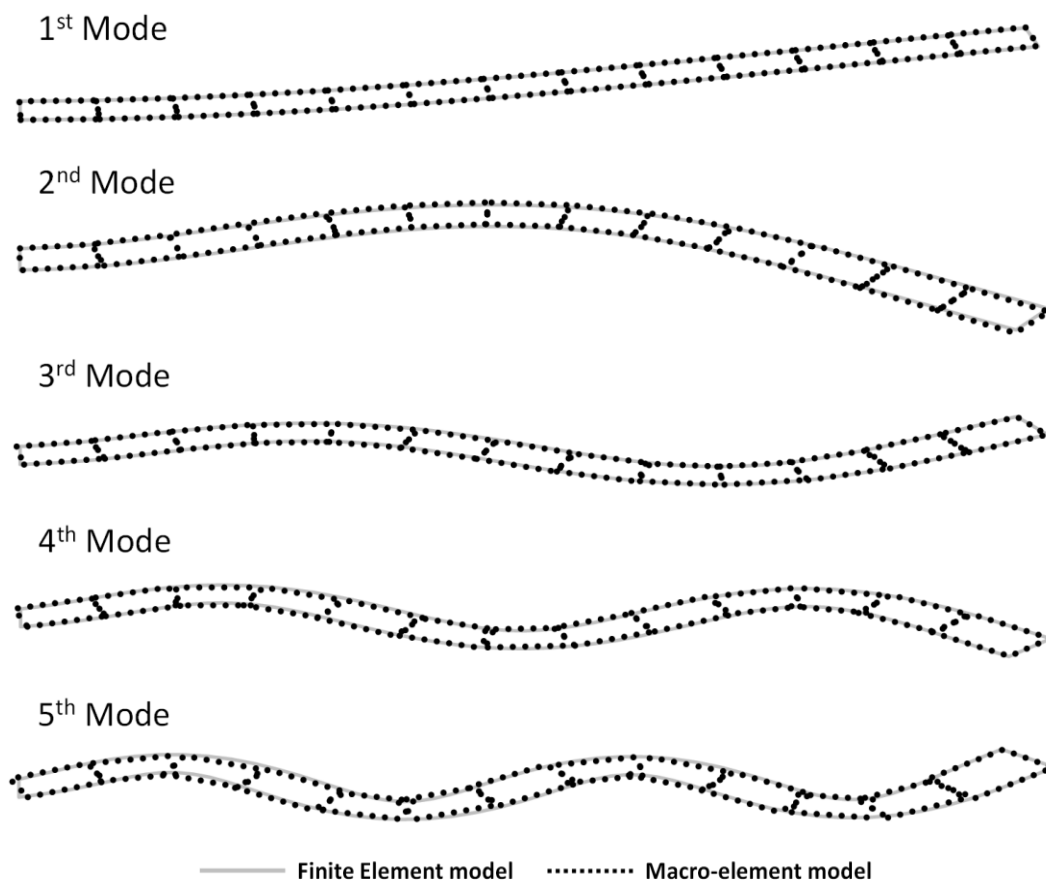
Figure 4.7. Numerical modal shapes of the Slender Timoshenko cantilever beam

4.3   ROBERT A. MILLIKAN MEMORIAL LIBRARY

The second case study for the validation of the computational resources of the macro-element in nonlinear dynamic analysis is related to the investigation of the rocking response of a building known as the Robert A. Millikan Memorial Library, in California, USA. As reported by Psycharis and Jennings [156], the free rocking motion of this structure was assessed in a simplified way as a rigid block considering different foundation models. In such investigation, the support conditions adopted for the assessment of the Robert A. Millikan Memorial Library corresponded namely to a Winkler and a 2-Spring foundation

models as depicted in Figure 4.8. It is worth noting that an equivalence between these models was also taken into consideration for such investigation. In addition, this structure modelled as a rigid block was characterized by two vibration modes. The corresponding natural frequencies and damping ratios corresponded to 4 Hz and 5.7%, and 16 Hz and 22.7% for the first and second modes, respectively.
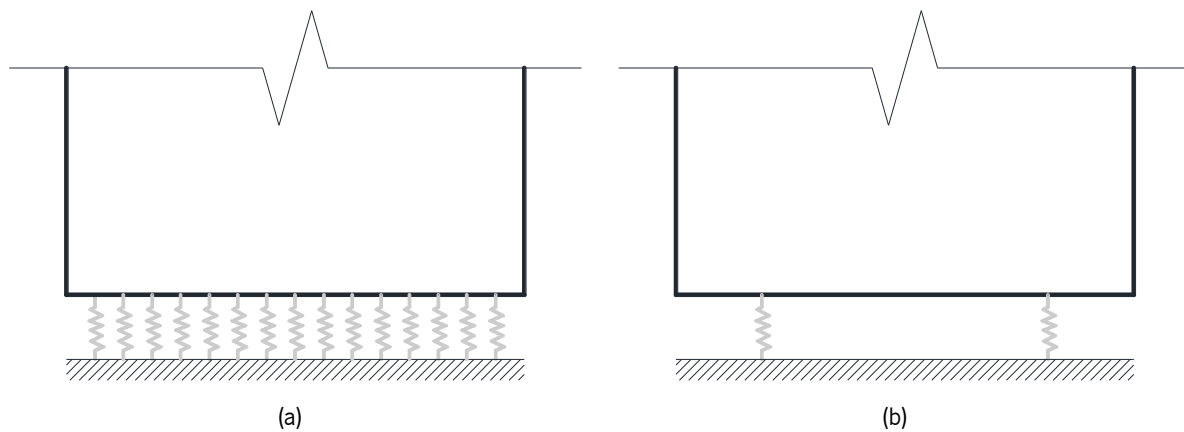
Figure 4.8. Foundation models adopted for the assessment of the free rocking motion of the Robert A. Millikan Memorial Library: (a) Winkler and (b) 2-Spring, Psycharis and Jennings [156]

For this validation, the free rocking motion of the library, based on Winkler foundation model was replicated by means of the macro-element modelling approach. The structure was modelled by a single macro-element whose interaction with the boundary conditions was conducted by means of an interface element. In this sense, the interface element with a proper discretisation of transversal links can accurately simulate the behaviour of the Winkler foundation model. The macro-element model of this structure was described by a height h of 48 m, a base b of 21 m and a width w of 22 m as illustrated in Figure 4.9. It is worth noting that due to the different mass corresponding to each of the stories in the structure, the centre of gravity (CG) was not placed at mid-height. In the macro-element model as well as in the investigation conducted by Psycharis and Jennings [156], CG was located at a height h' of 18 m from the boundary conditions. In addition, mechanical properties such as Young's modulus E and specific mass ρ associated with the macro-element model were estimated from the stiffness per unit length k_0 of the Winkler foundation model and the estimated total weight of the structure. The simulation of the rocking motion according to a single macro-element allows considering internal deformability related to the element shear deformation. Nevertheless, the shear modulus was defined aiming at simulating a rigid block. The mechanical properties of the macro-element model are summarized in Table 4-5.

Table 4-5. Mechanical properties of the numerical model of the Robert A. Millikan Memorial Library based on a macro-element approach

Young's modulus E	Shear modulus G	Specific mass ρ
4.89x10^3 MPa	4.89 x10^6 MPa	570.4 kg/m^3
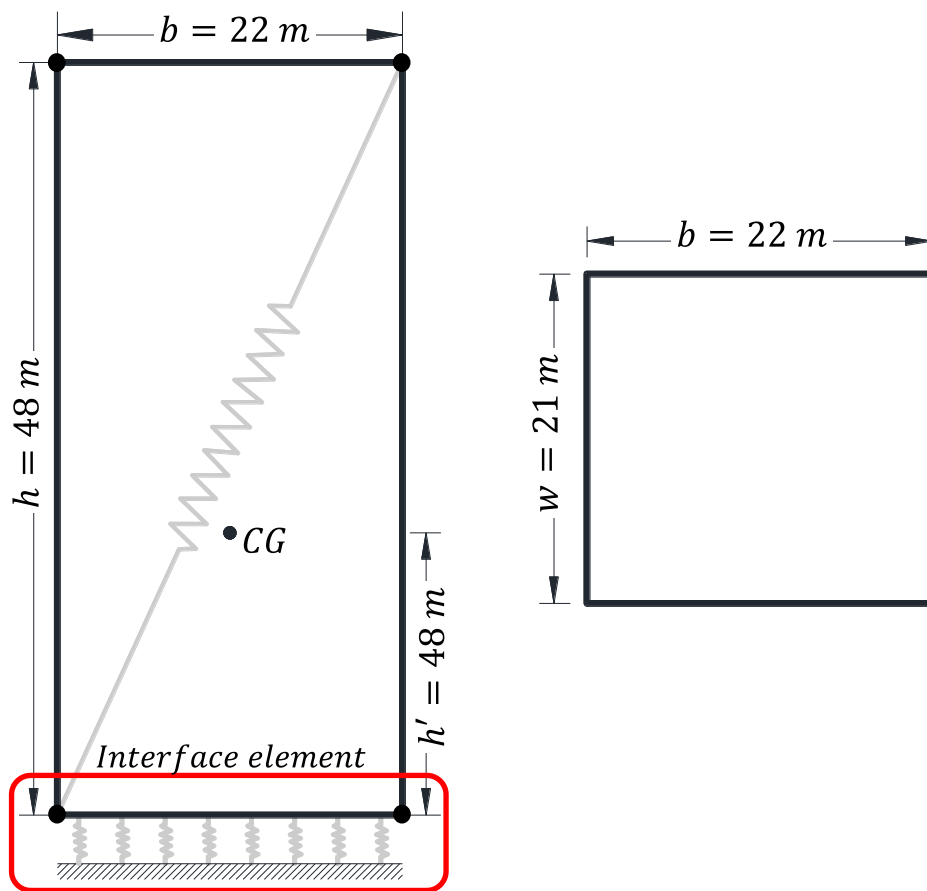
Figure 4.9. Macro-element model for the assessment of the free rocking motion of the Robert A. Millikan Memorial Library

The assessment of the free rocking motion of the macro-element model was conducted by the application of a pulse load characterised by an initial velocity of 0.61 m/s per unit mass. Such impulse was associated with an intensity load equal to 8 reported in the analytical investigation conducted by Psycharis and Jennings [156]. The solution of the dynamic equilibrium was based on the classical Newmark method [158] with an average acceleration in which the velocity and displacement of the system are characterised by the finite difference equations reported in expressions 4-1 and 4-2, respectively.

$$\dot{\mathbf{u}}_{t+\Delta t} = \dot{\mathbf{u}}_t + \left[\left(1-\gamma\right) \cdot \ddot{\mathbf{u}}_t + \gamma \cdot \ddot{\mathbf{u}}_{t+\Delta t} \right] \qquad\qquad 4\text{-}1$$

$$\mathbf{u}_{t+\Delta t} = \mathbf{u}_t + \dot{\mathbf{u}}_t \cdot \Delta t + \left[\left(\frac{1}{2}-\beta\right) \cdot \ddot{\mathbf{u}}_t + \beta \cdot \ddot{\mathbf{u}}_{t+\Delta t} \right] \cdot \Delta t^2 \qquad\qquad 4\text{-}2$$

Here, $\mathbf{u}$, $\dot{\mathbf{u}}$, and $\ddot{\mathbf{u}}$ correspond to the displacement, velocity and acceleration vectors of the system. In addition, t and Δt are associated with the current time and the time increment during the analysis. Finally, β and γ are two constants that define the variation of acceleration over a time step. In the case of an average acceleration approach, the values of these constants are $1/4$ and $1/2$, respectively.

The influence of the discretisation of the interface element on the free rocking motion of the Robert A. Millikan Memorial Library was initially assessed by the application of the pulse load to the macro-element model with an elastic foundation (without uplift of the rigid block). For this purpose, there different discretised configurations of the matrix of transversal links were taken into consideration. The discretization of interface element was characterised by square matrices composed by 4x4, 8x8 and 16x16 transversal links, as illustrated in Figure 4.10. It is worth noting that an undamped system was considered for this initial assessment.
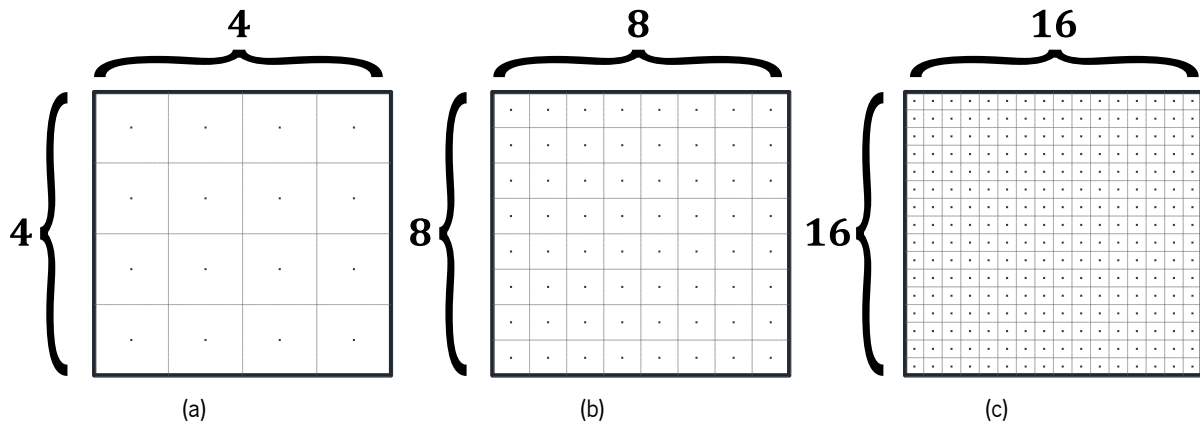
Figure 4.10. Discretization of interface element: matrix of (a) 4x4, (b) 8x8, and (c) 16x16 transversal links

The response of the undamped free rocking motion of the rigid block based on a Winkler foundation model and the macro-element models with the different discretised interface elements is illustrated in Figure 4.11. In this figure, the continuous black line is associated with the response of the rigid block obtained by means of an analytical procedure [159]. On the other hand, the remaining three grey lines are related to the free rocking motion of the macro-element models. The free rocking motion was assessed by comparing analytical and numerical results in terms of angle of rotation considered as the ratio between the horizontal top displacement and the height of the structure for a period of 1 second. It was observed that the macro-element model with a 4x4 matrix presented not only an increased value of amplitude of angle of rotation, but also a higher period that characterized its free oscillation. A better agreement in terms of amplitude of angle of rotation as well as free oscillation period was obtained when increasing the discretisation of the interface element (macro-element models with 8x8 and 16x16 matrices). The amplitude of the angle of rotation was slightly higher to the one from the rigid block, whereas the period that characterized the rocking motion of the macro-elements presented a smaller value. A very good agreement by the different formulations was observed, and the small differences, related to distinct discretised configurations, do not affect the practical relevance of the proposed approach since it has the capability to investigate the rocking behaviour of deformable structures with a very low computational burden.
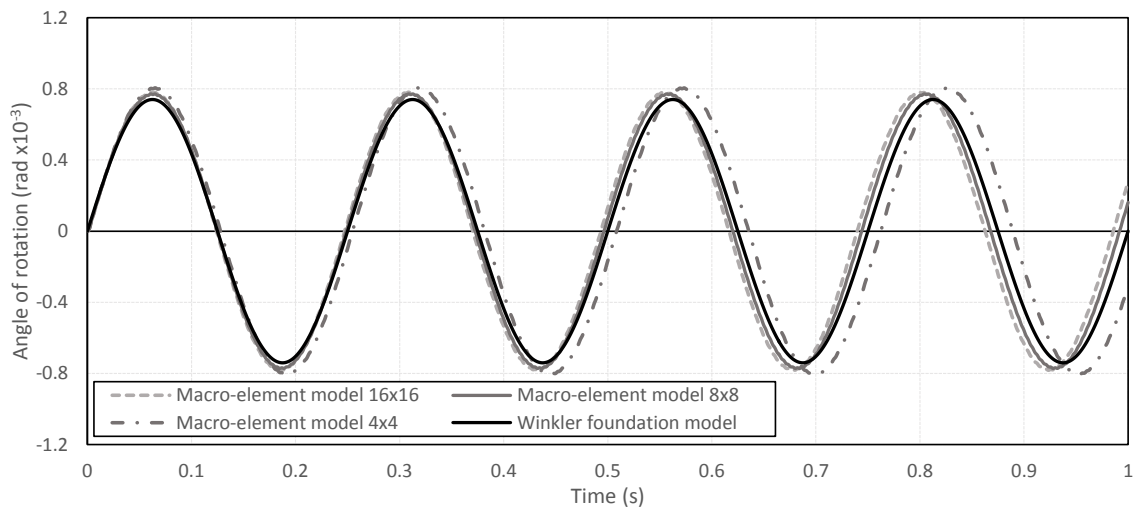
Figure 4.11. Free rocking motion of the macro-element model of the Robert A. Millikan Memorial Library based on an elastic foundation and assessment of the discretisation of the interface element

The free rocking motion was also assessed considering the uplift of the rigid block by means of a deformable foundation. This foundation was simulated by the interface element considering a zero-tensile strength f_t associated with the flexural mechanism. In this regard, the macro-element model based on an interface element with a discretisation of a matrix of 8x8 transversal links was selected for the assessment of the free rocking motion of the library. In addition, damped and undamped systems were also considered for this assessment [159]. The energy dissipation was based on a Rayleigh [160] viscous damping criterion, in which the damping matrix $\mathbf{C}$ corresponds to a linear function of the stiffness $\mathbf{K}$ and mass $\mathbf{M}$ matrices as expressed in equation 4-3. These matrices are influenced by two variables denoted as α_0 and α_1, whose expressions are given by equations 4-4 and 4-5, respectively. The damping ratio ζ and natural frequencies ω_i and ω_j related to the macro-element model presented the same values as the ones used for the analytical investigation.

$$\mathbf{C} = \alpha_0 \cdot \mathbf{M} + \alpha_1 \cdot \mathbf{K}$$

4-3

$$\alpha_0 = \zeta \cdot \left(\frac{2 \cdot \omega_i \cdot \omega_j}{\omega_i + \omega_j} \right)$$

4-4

$$\alpha_1 = \zeta \cdot \left(\frac{2}{\omega_i + \omega_j} \right)$$

4-5

The response in terms of angle of rotation associated with the free rocking motion considering the occurrence of lift-off, obtained by means of the differential formulation and the numerical model is depicted in Figure 4.12. The continuous lines are related to the analytical results of the rigid block based on a Winkler foundation model considered as an undamped or a damped medium, respectively. On the contrary, the dashed lines are associated with the response of the macro-element model. The black lines correspond to an undamped system, whereas the grey lines were obtained considering a Rayleigh viscous

damping criterion. The comparison of the history of angle of rotation related to the undamped systems presented a good agreement between the analytical and numerical approaches. It was also observed that the macro-element model was capable of replicating successfully the period of the free rocking motion of the structure based on a deformable foundation. On the other hand, the introduction of viscous damping led to slightly different results in terms of angle of rotation. It is noted that the response of the macro-element model was described by slightly higher values of angle of rotation which is related to the lower energy dissipation. This difference may be justified due to the different approaches of energy dissipation of each model. The macro-element model was characterized by a Rayleigh damping criterion, whereas in the case of the rigid block with a Winkler foundation model, the energy dissipation was considered only at a spring level. Nevertheless, the macro-element model presented an acceptable agreement, evidencing that this modelling approach, if correctly calibrated, can be applied for the assessment of the rocking behaviour of deformable structures in the dynamic field. It is worth to notice that, at this stage, the investigation of the rocking response is limited to the hypothesis of small rotations.
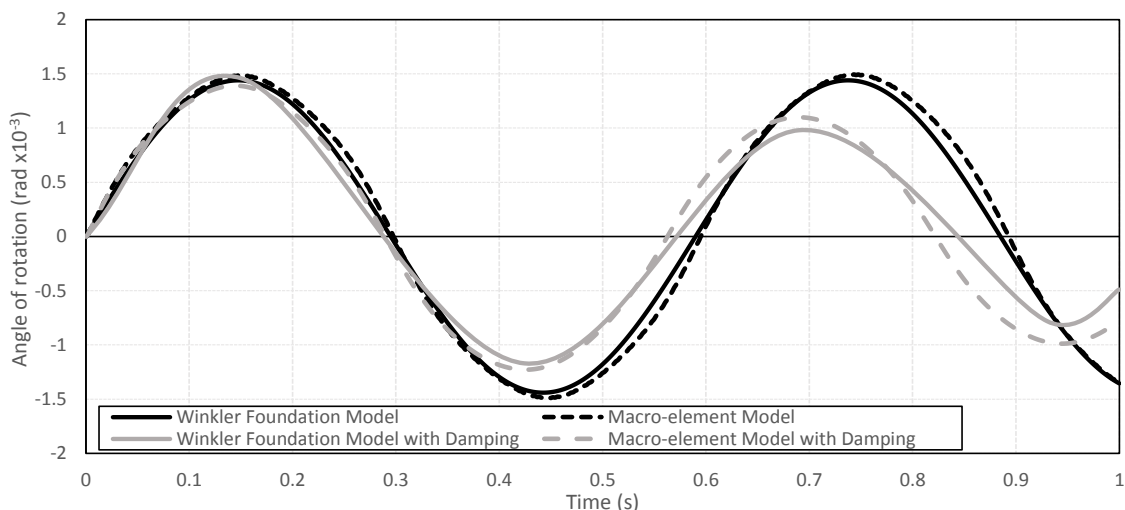
Figure 4.12 Free rocking motion of the macro-element model of the Robert A. Millikan Memorial Library based on a deformable foundation considering undamped and damped systems

4.4 TWO-STORY MASONRY WALL

The last part of this validation consisted of the assessment of the seismic response of a two-story masonry wall based on the macro-element modelling approach. Such wall corresponded to a full-scale masonry structure whose seismic response was investigated by means of cyclic static tests at the University of Pavia [161]. In addition, the masonry structure was also investigated using simplified and sophisticated numerical tools [1, 19, 162]. As depicted in Figure 4.13a, the brick masonry structure was constituted by four walls denoted as A, B, C, and D, with an equal thickness of 0.25 m. Unlike walls A and C, walls B and D presented door and window openings, and were connected by means of steel beams characterised by an I section aiming at the simulation of a flexible diaphragm. It is worth noting that wall B was perfectly connected to the lateral walls A and C, whereas wall D was slightly isolated from those lateral walls for the assessment of the seismic in-plane response. The wall investigated in this final

validation corresponded to wall D, and it is illustrated in Figure 4.13b. This wall was characterised by base and height of 6.0 m and 6.4 m, respectively.
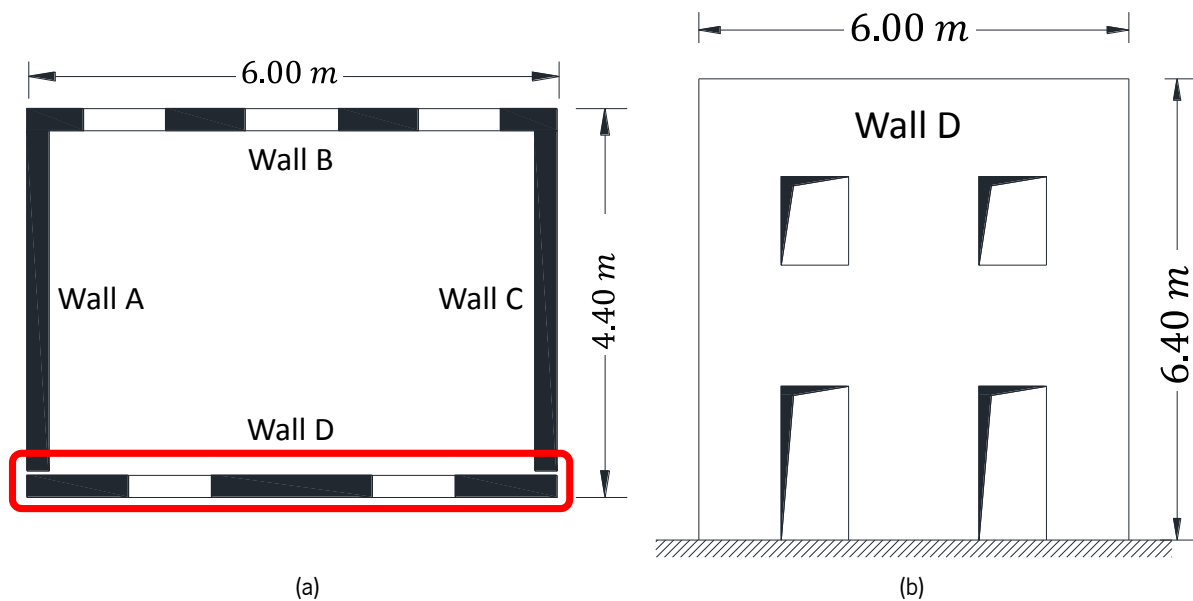
Figure 4.13 Two-story masonry building: (a) plan view, and (b) Wall D.

The seismic response of Wall D was previously investigated in the static nonlinear field by means of this macro-element modelling approach in the work conducted by Caliò, et al. [1]. Based on such investigation, the macro-element model was capable of accurately simulating the cyclic response together with the corresponding failure mechanism obtained by means of the experimental campaign. In such investigation, the shear-diagonal nonlinear behaviour was based on a Turnsek and Cacovic [154] yielding criterion. However, in this current validation, the shear-diagonal mechanism was ruled by a Mohr-Coulomb law. For this purpose, an agreement between the two yielding criteria was established by determining equivalent values of friction coefficients for piers and spandlers. In this sense, a ratio equal to 1.5 between the shear strength under no confinement conditions f_{v0}, based on the Turnsek and Cacovic [154] criterion, and the corresponding value related to a Mohr-Coulomb yielding criterion f_{y0} was considered. The remaining mechanical properties, such as Young's and shear modulus, compressive and tensile strengths, and cohesion, were defined based on a mechanical characterisation, and on values selected in other numerical investigations. The mechanical properties used for the macro-element model are reported in Table 4-6. Here, E, f_c and f_t are the Young's modulus, compressive and tensile strengths, whereas G, f_{y0}, c, μ_d and μ_s are the shear modulus, shear strength under no confinement conditions, cohesion, and friction coefficients for shear-diagonal and shear-sliding mechanisms, respectively.

Table 4-6. Mechanical properties of the macro-element model of the two-story masonry wall

	Flexural parameters			Shear-diagonal parameters			Shear-sliding parameters	
	E	f_c	f_t	G	f_{y0}	μ_d	c	μ_s
	(MPa)	(MPa)	(MPa)	(MPa)	(MPa)	-	(MPa)	-
Piers	2100	6.20	0.05	500	0.12	0.15	0.20	0.60
Spandlers					0.15			

It is worth noting that in order to assess the influence of the mesh discretisation on the overall in-plane response of the two-story masonry wall, two macro-element models with a different number of panels were taken into consideration. In this sense, the first macro-element model presented 16 panels, and it was described by 112 DOFs, whereas the second model presented a slightly higher number of elements equal to 36 panels, and it was described by 252 DOFs. Based on the degree of discretisation, these models were denoted as Basic and Refined macro-models.

For the application of nonlinear static analyses, the macro-element model of Wall D was initially subjected to additional axial loads of 124.2 kN and 118.4 kN along the first and second stories, in accordance with the experimental campaign. Subsequently, the macro-element model was subjected to two horizontal forces at each story until a drift of approximately 0.3% was achieved. The responses of these models, due to the application of static nonlinear analyses were compared to experimental results, as well as the results from three numerical approaches based on sophisticated and simplified mechanical schemes. The numerical results considered for comparison corresponded to a FE model investigated by Gambarotta and Lagomarsino [162], a rigid body spring model adopted by Casolo and Peña [2], and a previous investigation conducted by Caliò, et al. [1] using the same macro-element as in the present work. The responses of the different approaches are illustrated in Figure 4.14 by means of pushover curves which describe the behaviour of Wall D in terms of base shear capacity vs horizontal top displacement. This comparison was conducted taking into account the envelope associated with the cyclic response of the experimental and numerical investigation. From this comparison, a reasonable agreement in terms of initial stiffness, maximum load capacity and post-elastic behaviour was evidenced between the macro-element modelling approach and the other investigations. It is worth noting that the numerical models presented a slightly different maximum base shear (around 150 kN) with respect to the one from the experimental campaign. Despite this, the differences between experimental and numerical results, which may also be related to their distinct mechanical schemes, are acceptable. In addition, it was also possible to observe that the macro-element model with a more refined mesh discretisation presented a slightly increased base shear capacity when comparing it to the basic macro-element model. In the same regard, the macro-element approach, regardless of the discretization of the numerical model, was capable of effectively simulating the in-plane response of this structure, and due to the reduced number of DOFs, it can be considered as a suitable tool for the assessment of masonry structures from a practical point of view.
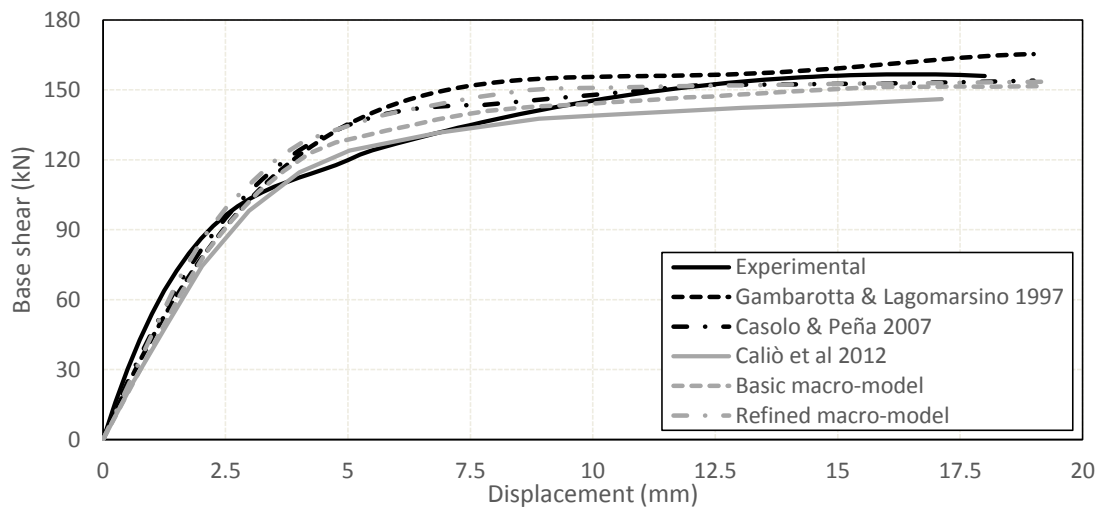
Figure 4.14. Pushover curves of Wall D due to the application of horizontal static loading: (a) experimental campaign, (b) FE model [162], (c) rigid body spring model [19], (d) macro-element model conducted by Caliò, et al. [1], and macro-models based on (e) basic and (f) refined mesh refinement.

In addition to the pushover curves, the failure mechanisms of Wall D obtained from the experimental campaign and from the numerical models due to the application of horizontal loading were also considered for comparison. In this regard, Figure 4.15a presents the collapse mechanism associated with the cyclic tests, whereas Figure 4.15b and Figure 4.15c are associated with the numerical results obtained by means of FE [162] and RBS [19] models, respectively. On the other hand, the remaining three figures (Figure 4.15d,e,f) correspond to the failure mechanism obtained from the macro-element approach (Caliò, et al. [1], Basic, and Refined macro-models).

From this comparison, it was observed that there was a good resemblance between experimental and numerical failure mechanisms. In all models, the masonry piers and spandrels of the first story were governed by an in-plane shear mechanism which was in good agreement with the experimental collapse. In addition, some numerical models (FE and macro-element approaches) also presented failure associated with the rocking of the masonry elements. This flexural behaviour was mainly localized at the base of the masonry wall, and around the door and window openings. It is worth noting that this behaviour was also identified after the application of the laboratory cyclic test. A comparison between Basic and Refined macro-element models was also conducted in terms of failure mechanisms. Some small differences were obtained between these models, which were mainly associated with the occurrence of rocking in some parts of the masonry wall. An additional difference was related to the left spandrel in the first story since in the Refined macro-element, this structural component did not present any nonlinear behaviour associated with a shear mechanism. Nevertheless, the overall responses of the two macro-element models are in reasonable agreement.
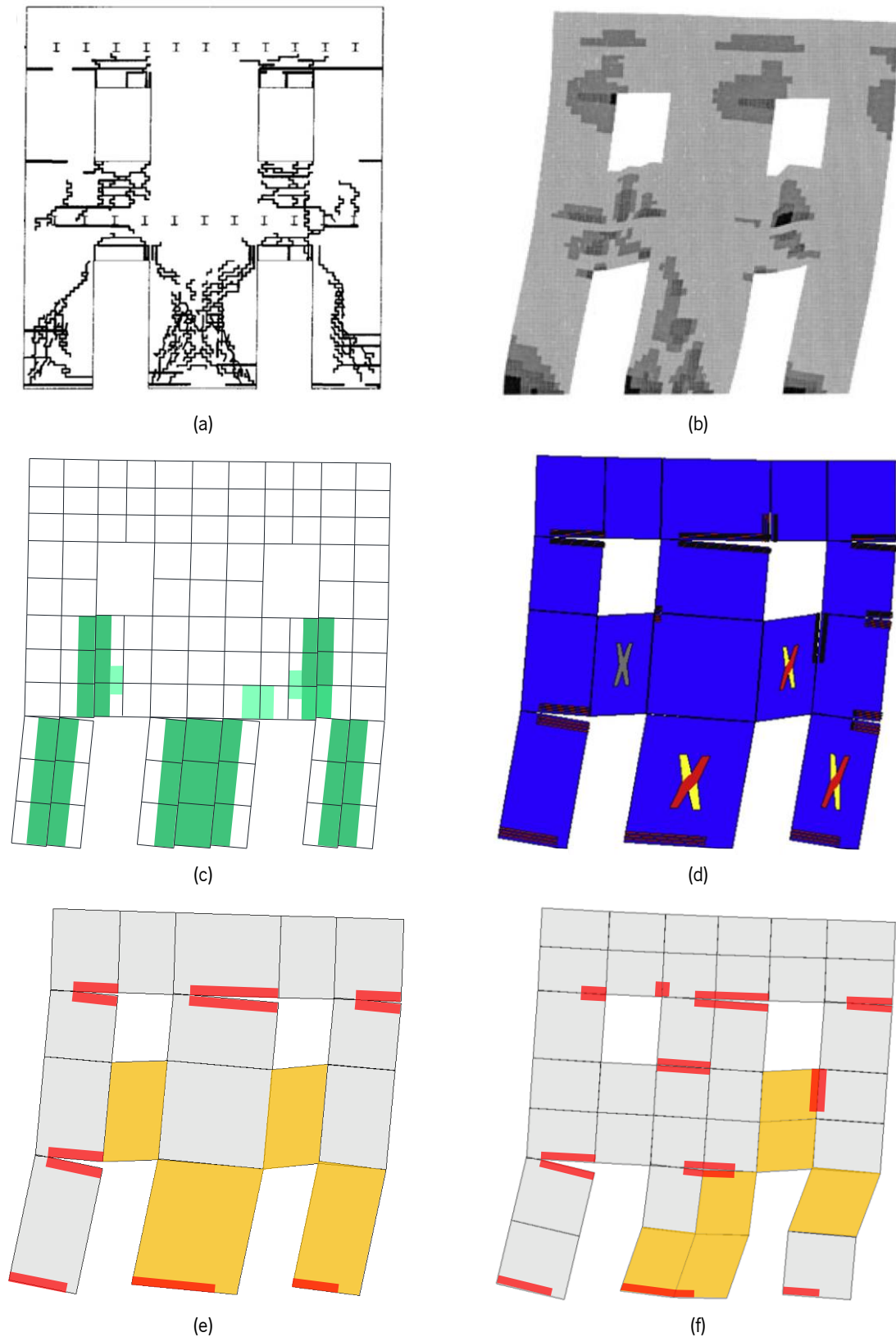
Figure 4.15. Failure mechanisms of Wall D due to the application of horizontal static loading: (a) experimental campaign, (b) FE model [162], (c) rigid body spring model [19], (d) macro-element model conducted by Caliò, et al. [1], and macro-models based on (e) basic and (f) refined mesh refinement.

The two-story masonry wall was also subjected to time history analysis aiming at validating the hysteretic behaviour of the nonlinear links of this macro-element modelling approach in a dynamic context. For this purpose, the dynamic responses of the Basic and Refined macro-models were compared to the one obtained by means of a FE approach. In the investigation conducted by Gambarotta and Lagomarsino [162], the two-story masonry wall was subjected to a uniaxial artificial accelerogram with a PGA of 0.35 g (see Figure 4.16a). For this validation, as the horizontal record was not available, an additional uniaxial artificial accelerogram was generated based on the spectrum of accelerations (see Figure 4.16b) reported in [162] aiming at validating a similar frequency content. In this sense, the post-processed generated accelerogram and its corresponding spectrum of acceleration are illustrated in Figure 4.16c and Figure 4.16d, respectively.
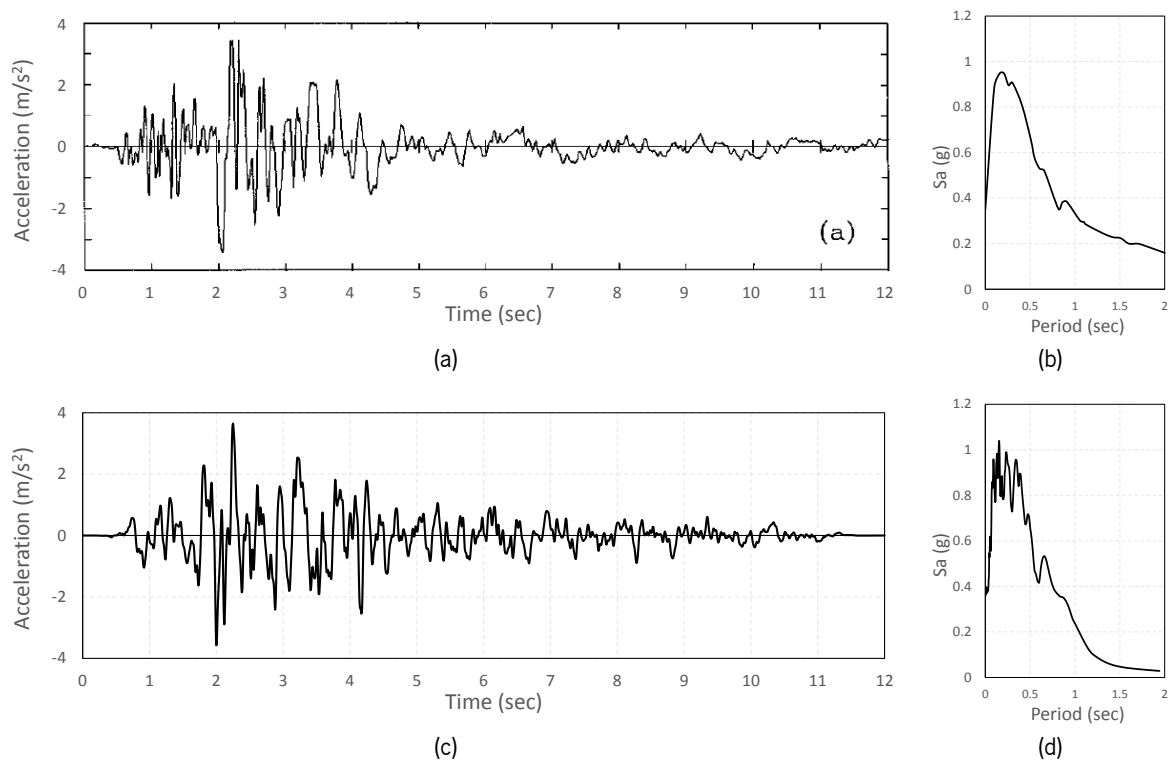
Figure 4.16. Time history analysis on two-story masonry wall: (a) artificial accelerogram and (b) spectrum of acceleration used by Gambarotta and Lagomarsino [162], and (c) artificial accelerogram and (d) spectrum of acceleration used for the validation of the macro-element model in the dynamic nonlinear field.

The uniaxial artificial accelerogram was applied to macro-models (Basic and Refined) aiming at assessing their corresponding in-plane responses in the dynamic field. The dynamic equilibrium was solved considering a Newmark method based on constant acceleration [158] and a Rayleigh viscous damping criterion [160]. It is worth noting that these analyses were conducted taking into consideration a diagonal mass matrix as reported in Chapter 3, and as validated in the previous sections. On the other hand, the unloading cycles associated with the tensile flexural response was governed by a stiffness oriented to the origin (unloading coefficient $\beta_t = 1$), or secant, whereas for the compressive, and shear-diagonal responses, such behaviour was governed by an initial stiffness (unloading coefficients $\beta_c = \beta_d = 0$).

The comparison regarding the dynamic response between the FE and macro-models was conducted taking into consideration the base shear vs displacement hysteresis curve at the second story. Figure 4.17a illustrates the response of the second story in which the top of the second story was considered as control node for the hysteresis curve. It is observed that these models were able to replicate the response of a FE model with a good agreement in terms of hysteretic loop and maximum base shear capacity. There is a slight difference of displacement since the FE model reached a minimum negative displacement of approximately 17 mm, whereas the corresponding displacement associated with the Basic macro-model presented a value of around 15.7 mm (7.5% less). On the other hand, the macro-model reached a slightly higher maximum displacement in the positive direction when compared to the one from the FE model. Figure 4.17b depicts the comparison of the dynamic response of the FE model and the Refined macro-model when subjected to the uniaxial artificial accelerogram. It is observed that these models were characterised by a similar hysteresis loop and maximum load capacity. In the negative branch, the Refined macro-model reached a minimum displacement of approximately 16 mm (5.9% less than the FE model). This value was slightly higher than the one obtained with the Basic model. A similar behaviour in the positive branch (slightly higher maximum horizontal displacement) was also identified in the Refined macro-model. Based on these comparisons, it was possible to evidence that the discretisation of the macro-element model did not have any significant influence on the in-plane nonlinear dynamic response of the two-story masonry wall.
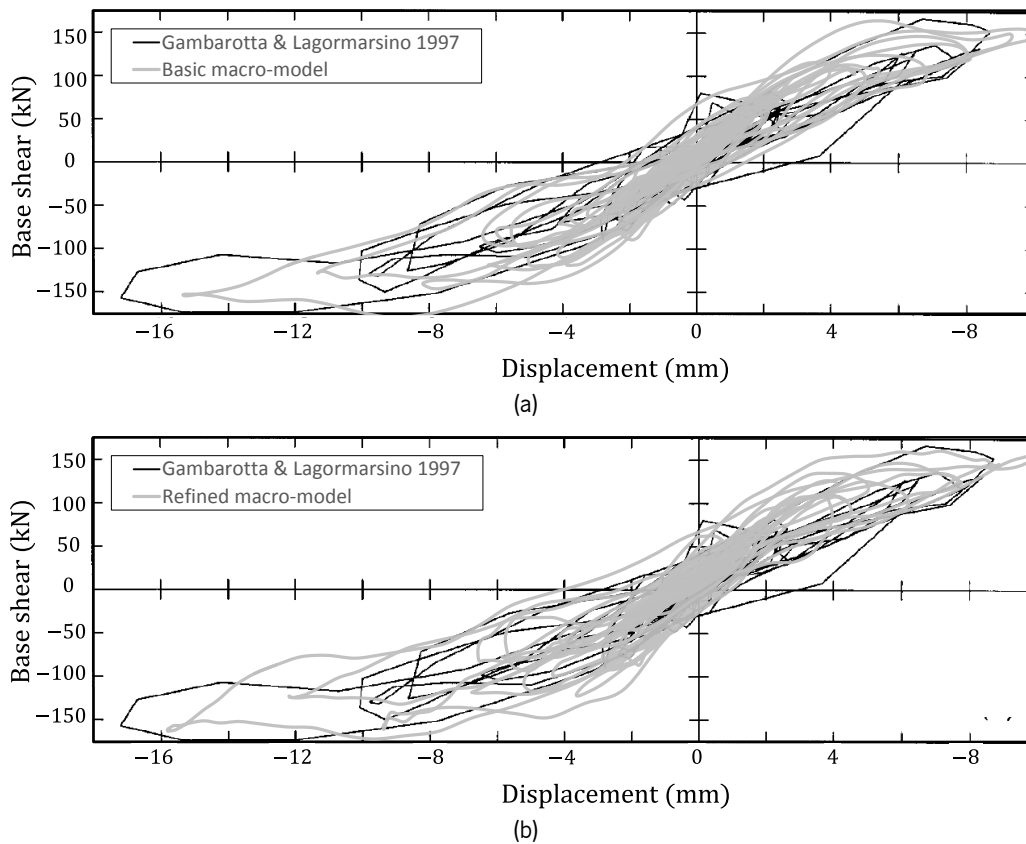
Figure 4.17. Comparison of hysteretic behaviour between FE and macro-element models due to the application of nonlinear dynamic analysis: (a) Basic, and (b) Refined macro-models

An additional comparison regarding the overall failure mechanisms due to the application of time history analysis obtained by means of the macro-element approach was also conducted. Schematic representations of the components (panels and interface elements) which presented a significant concentration of damage are illustrated in Figure 4.18a and Figure 4.18b associated with the Basic and Refined macro-models, respectively. It was observed that both models were characterized by a similar mechanism which consisted of the failure of masonry piers and spandrels at the first story, as well as failure along the interface elements at the base and around door and window openings. The mechanisms were related to the shear-diagonal behaviour of the panels in the rocking response of the interface elements. Nevertheless, small differences between the two discretised mesh refinements were also identified. For instance, it was noted that the right pier of the Basic macro-model did not exceed its elastic branch, whereas the Refined model cracked. In addition, the Refined macro-model presented additional concentration of damage propagating vertically along the interface elements of the spandrel elements. In general, the results from the macro-element models associated with the application of nonlinear dynamic analysis can be considered reasonably acceptable in terms of base shear vs displacement hysteresis curve and failure mechanisms. It is worth noting that a reduced computational burden was required for the application of time history analyses. In this regard, this macro-element modelling approach can be considered as a reliable and practical computational tool for the static and dynamic seismic assessment of masonry structures for practical applications.

(a)   (b)
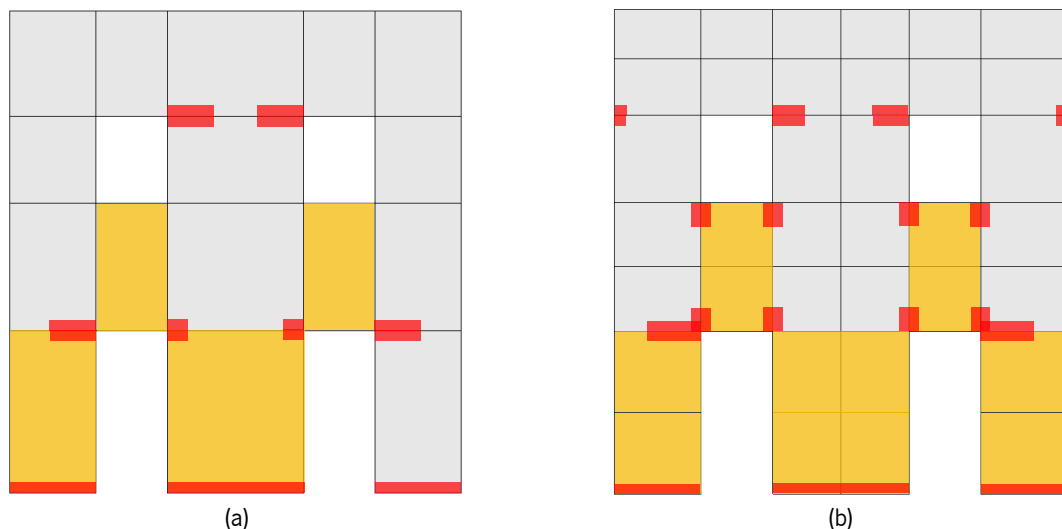
Figure 4.18. Failure mechanisms due to the application of nonlinear dynamic analysis: (a) Basic, and (b) Refined macro-models

4.5 FINAL CONSIDERATIONS

The present Chapter was dedicated to the validation in a dynamic context of the latest upgrades conducted to the macro-element modelling approach introduced by Caliò, et al. [1]. For this purpose, three case studies were taken into consideration for the validation of the procedure for the computation of a macro-element in the context of nonlinear dynamics, with particular reference to the mass properties as well as the geometrical and material nonlinearities. The first case study was related to the estimation

of the dynamic properties of two Timoshenko cantilever beams. In this regard, the values of natural frequencies obtained by macro-element models were compared to the ones obtained from analytical formulations and sophisticated computational tools (FE approach). Based on this comparison, it was noted that the macro-element model was capable of replicating well the values of natural frequencies from analytical and numerical procedures. The performed investigation focused on the inertia force representation had shown that the adoption of an approximate diagonal-consistent mass matrix leads to sufficiently accurate results for practical purposes since the use of a full-consistent mass matrix leads to only a small enhancement in terms of accuracy but increases the computational cost of step by step procedures.

The capability of the proposed approach of correctly grasping the nonlinearities related to the rocking motion, under the hypothesis of small rotations, has been investigated by comparing the rocking behaviour of a rigid block on a stiff a deformable soil making reference to a benchmark reported in the literature. This is the case study relative to the rocking behaviour of the Robert A. Millikan Memorial Library. The free rocking motion of the macro-element model was compared to the results obtained in an analytical investigation considering a Winkler foundation model. An initial comparison was conducted taking into account an elastic foundation. In this regard, the free rocking motion of the macro-element model, as well as the influence of the discretisation of the interface element, were investigated. Furthermore, a second comparison was conducted considering a deformable foundation. In this last comparison, assessment of the macro-element model also involved the definition of undamped and damped systems (based on a Rayleigh viscous damping criterion). A good agreement in terms of amplitude of rotation and period of the response was obtained when comparing the free rocking motion of the undamped systems. On the contrary, a slight difference was obtained when considering damped systems. Such difference may be associated with the distinct approaches defined for the dissipations of viscous damping energy. Nevertheless, the results obtained from the macro-element model considering elastic and deformable foundations, as well as damped and undamped systems, were considered acceptable.

The last case study corresponded to a two-story masonry wall which was previously investigated by means of cyclic laboratory testing, as well as numerical simulations with simplified and sophisticated computational tools. An initial validation of the macro-element modelling approach was carried out by the application of in-plane horizontal forces at the top of each stories. A comparison was performed between the pushover curves and their corresponding failure mechanisms associated with different experimental and numerical investigations. In this first validation, the assessment of the mesh refinement related to the macro-element model was taken into account in order to determine its influence of the in-plane response of the two-story masonry wall. For the application of time history analyses, an artificial accelerogram was generated, and further processed, based on the spectrum of acceleration of a previous investigation. A final comparison between the dynamic behaviour of a FE model and two macro-element models with different mesh refinements in terms of hysteresis loops, maximum shear capacity and top horizontal displacements. Based on this comparison, a good agreement was demonstrated between the modelling approaches regarding base shear and hysteresis loops, and a reasonable agreement in terms

of top horizontal displacements. It was evidenced that there a minor influence of increasing discretisation of the macro-element model.

Based on this validation, it was demonstrated that, due to its simple mechanical scheme, the adopted modelling approach could be considered as a valuable alternative computational tool for the assessment of the seismic behaviour of masonry structures in the static and dynamic nonlinear ranges. The results obtained by means of this validation showed that the modelling approach can effectively simulate the in-plane behaviour of masonry structures, successfully capturing their corresponding collapse mechanisms. Another advantage related to this modelling approach is the low computational burden required for sophisticated analysis, making it a suitable tool for practical applications.

CHAPTER 5

ANALYSIS OF URM STRUCTURES

5.1 INTRODUCTION

In this Chapter, the out-of-plane behaviour of two URM structures was investigated by means of numerical simulations. These structures corresponded to U-shape specimens made of brick and stone masonry units. Out of the scope of this investigation, these structures, denoted as brick and stone masonry prototypes, were subjected to shaking table tests up to collapse [77]. However, a description of these tests and the discussion on the results are briefly reported next.

For the purpose of this investigation, two computational tools were taken into consideration, namely Finite Element (FE) and macro-element modelling approaches. Aiming at the assessment of the out-of-plane response of the numerical models, static and dynamic nonlinear analyses were conducted by means of the application of an incremental mass distributed lateral force and a uniaxial seismic input, respectively. It is worth noting that the influence of the mesh and material dependency on the overall failure mechanisms of these models was also evaluated.

Subsequently, the results from the numerical simulations were compared to the corresponding collapse mechanisms obtained experimentally by the shaking table tests. An additional comparison between these modelling approaches as well as the computational demand required for the application of sophisticated simulations such as nonlinear dynamic analyses was carried out. Finally, the conclusions of the numerical simulation and the applicability of these modelling approaches are reported.

5.2   Brick masonry prototype

The brick masonry prototype corresponded to a full-scale structure made of hydraulic lime mortar and fired clay units based on an English bond arrangement as illustrated in Figure 5.1a. This U-shape structure was composed of three walls with 0.235 m of thickness. The façade consisted of a main gable wall that presented a centred window opening of 0.80 m x 0.80 m. The dimensions of the main gable wall corresponded to 2.75 m of height, and 3.50 m of length. On the other hand, the two remaining walls, denoted as return walls, were placed orthogonally to the main gable wall. Both walls presented a height of 2.25 m, and a length of 2.50 m. One of the return walls presented an additional window opening with dimensions of 0.80 m of length and 1.00 m of height leading to a non-symmetric response of the structure. Furthermore, it is worth noting that this structure lacked a horizontal rigid diaphragm; hence, it did not present a box-type behaviour.

| (a) | (b) |

Figure 5.1 Brick masonry: (a) U-shape full-scale prototype, and (b) square wallets

The characterization of the mechanical properties of this type of masonry was conducted by means of vertical and diagonal compressive tests on six square wallets (see Figure 5.1b). Three samples were subjected to vertical compressive tests aiming at determining the Young's modulus E and compressive strength f_c. Mean values of 5170 MPa and 2.48 MPa were obtained for Young's modulus and compressive strength, respectively. The remaining three samples were subjected to diagonal compressive tests in order to determine the tensile strength f_t, presenting an average value of 0.10 MPa. The mean values and coefficient of variance CoV of the mechanical properties of the brick masonry prototype are summarized in Table 5-1. These values will be used for the subsequent numerical simulations. Further details regarding the mechanical characterization of this material can be found in [77].

Table 5-1. Mechanical properties of brick masonry obtained from experimental campaign

	Specific mass ρ	Young's Modulus E	Compressive strength f_c	Tensile strength f_t
Mean	1890 kg/m^3	5170 MPa	2.48 MPa	0.10 MPa
CoV	3%	29%	14%	19%

5.2.1 SHAKING TABLE TESTS

The U-shape brick masonry prototype was subjected to unidirectional ground motions by means of shaking table tests at the LNEC (National Laboratory for Civil Engineering) in Lisbon [77]. The seismic input used for these experiments consisted of the 2011 Christchurch earthquake in New Zealand. After a filtering process, the brick masonry prototype was subjected to eight consecutive tests with three different amplification factors aiming at the out-of-plane collapse of the main gable wall. The seismic response of this structure in terms of displacement and acceleration was measured by means of six LVDTs and nineteen accelerometers, respectively. Figure 5.2 illustrated the setup of transducers established for the brick masonry prototype.
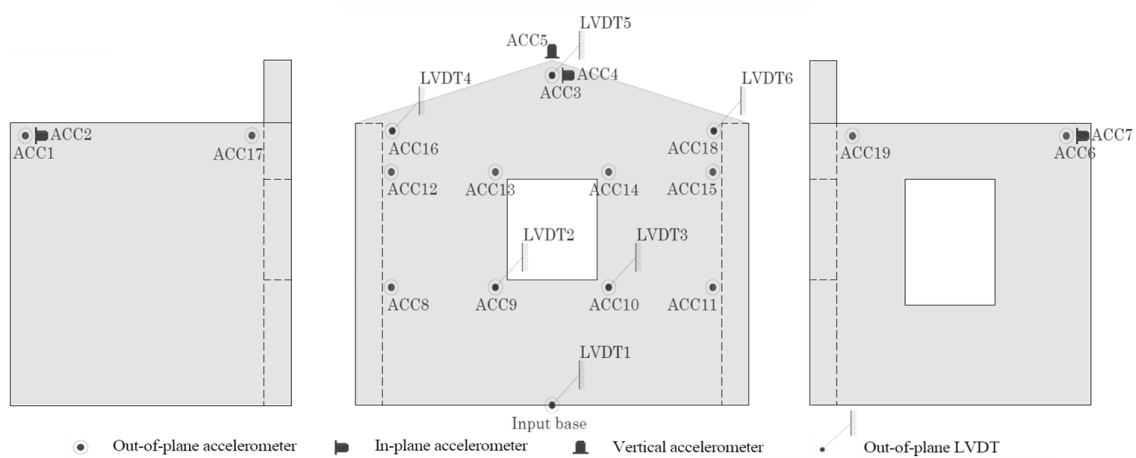
Figure 5.2 Measurement setup for the brick masonry prototype

Throughout the first five seismic inputs, the brick masonry prototype did not experience significant damage. On the other hand, visible damage was observed in the main gable wall and the return wall with opening after the sixth and seventh ground motions. The collapse of the brick masonry prototype was obtained after the last seismic input in which a peak ground acceleration PGA equal to 1.27 g was registered. No visible damage was observed in the remaining return wall (see Figure 5.3a). The overall collapse mechanism was composed by the out-of-plane failure of the main gable wall, and the in-plane failure of the return wall with window opening. The out-of-plane failure mechanism corresponded to the overturning of the tympanum, and additional horizontal crack in the lower part of the opening towards its right corner, as illustrated in Figure 5.3b. The in-plane failure mechanism was described by the collapse of the upper part of the return wall with window opening together with a significant portion of the right pier. Additional horizontal cracks were observed towers the connection to the main gable wall as illustrated in Figure 5.3c. Due to the asymmetry of the brick masonry prototype, the collapse was localized only in the main gable wall and the return wall with opening.

<div align="center">(a)   (b)   (c)</div>
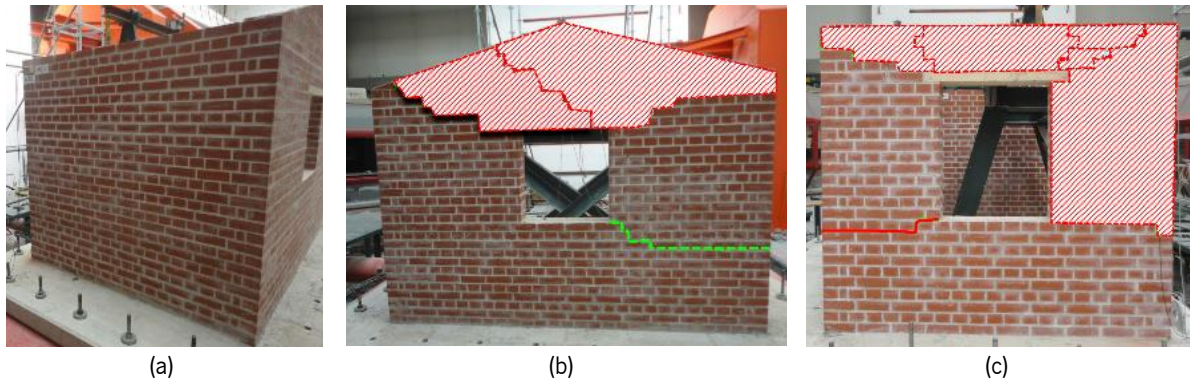
Figure 5.3 Collapse mechanisms of the brick masonry prototype from shaking table tests: (a) return wall without opening, (b) main gable wall, and (c) return wall with window opening

5.2.2 FINITE ELEMENT MODEL

The numerical simulations based on the FE method were conducted taking into consideration two different approaches, namely macro and simplified micro modelling approaches. In the former, masonry was modelled as a homogeneous and continuum material, whereas the latter corresponds to a discretized representation in which masonry units are considered as elastic elements, and the interaction between units and mortar joints is modelled by means of interface elements. The brick masonry prototype was subjected to nonlinear static and dynamic analyses in order to investigate its out-of-plane response. Nonlinear static analyses or pushover analyses consisted of the application of a mass distributed lateral force in the direction perpendicular to the main gable wall. On the other hand, nonlinear dynamic analyses or time-history analyses consisted of the application of the last unidirectional seismic input recorded from the shaking table tests.

a. Macro-modelling approach

The FE model associated with a macro-modelling approach was built using twenty-node solid brick elements CHX60 which are based on quadratic interpolation and Gauss integration as reported in [157]. Material properties used for this model were based on the ones obtained from the mechanical characterization. The nonlinearity of the material was governed by the total strain crack model in which a single stress-strain relation characterizes the tensile and compressive behaviours. Fixed and rotating crack models were defined aiming at the assessment of the influence of the nonlinear behaviour in the overall response of the brick masonry prototype. In this investigation, exponential and parabolic curves based on a fracture energy approach were selected for the nonlinear behaviour in tension and compression, respectively. The tensile fracture energy G_f^I presented a recommended value of 0.012 N/mm, whereas the compressive fracture energy G_c was determined using a ductility index d_{uc} equal to 1.6 mm. On the other hand, the post-cracking shear behaviour associated with fixed models is described by a retention factor denoted as β_s. For these analyses, two constant retention factors of 0.20 and 0.05 were established for the simulation of the shear behaviour. The mechanical properties defined for this model are summarized in Table 5-2.

Table 5-2. Mechanical properties of the FE-model of the brick masonry prototype

Linear parameters			Tensile parameters		Compressive parameters	
Young's modulus E	Poisson's ratio ν	Specific weight γ	Tensile strength f_t	Fracture energy G_f^I	Compressive strength f_c	Fracture energy G_c
5170 MPa	0.20	18.9 kN/m³	0.10 MPa	0.012 N/mm	2.48 MPa	3.97 N/mm

The mesh dependency was initially assessed by means of the application of nonlinear static analyses in a positive direction perpendicular to the main gable wall (pushing). Such assessment consisted of determining the optimum number of elements the FE model should have so that its out-of-plane response does not experience significant variation. For this purpose, models with different mesh refinements consisting of one, two and four elements along the wall thickness were taken into consideration. It is worth noting that the mesh refinement was mainly focused on the main gable wall since its out-of-plane response was the object of the investigation. These models were denoted as Brickx1, Brickx2, and Brickx4 and are illustrated throughout Figure 5.4a-c. The loading corresponding to these analyses consisted of the application of an incremental mass distributed lateral force.

(a)   (b)   (c)
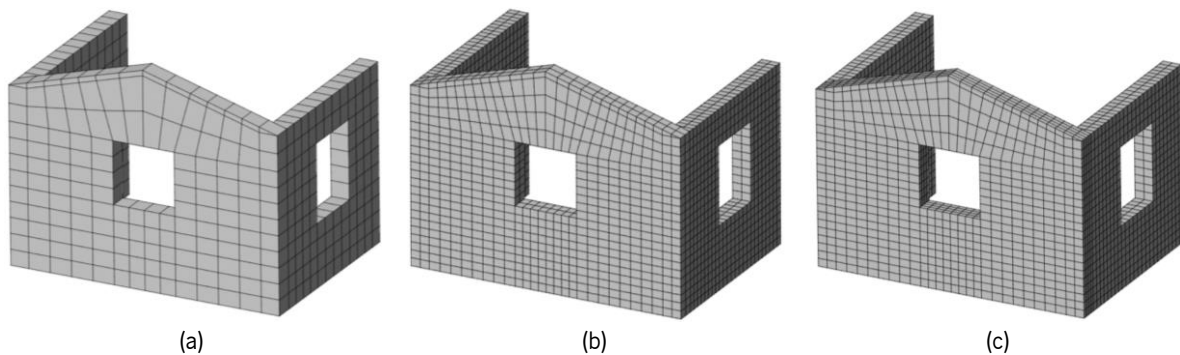
Figure 5.4 FE models of the brick masonry prototype: (a) Brickx1, (b) Brickx2, and (c) Brickx4

The results of each analysis are presented by means of principal strains together with the corresponding pushover curve, which describes the response of the structure in terms of load factor (ratio between horizontal load and self-weight) vs the horizontal displacement of a control node. In this case, the control node corresponded to the top of the tympanum. The response of the brick masonry prototype subjected to a pushing lateral load and the influence of the mesh refinement are illustrated throughout Figure 5.5a-c. From the pushover curves, it was possible to observe that, regardless the constitutive law, the model Brickx1 presented the lowest maximum load capacity. On the other hand, it was evidenced that the remaining models with two and for elements in thickness (Brickx2 and Brickx4) were in good agreement, not only in terms of maximum load capacity but also post-peak behaviour. The influence of the constitutive model on the post-peak behaviour of the brick masonry prototype was also assessed. As illustrated in Figure 5.5a, an increment of the shear capacity after the elastic phase was obtained when using a fixed model with a shear retention factor equal to 0.20 (hardening behaviour). When the shear retention factor β_s was reduced from 0.20 to 0.05, there was a slight influence on the out-of-plane response of the structure. In this case, the post-peak branch was not characterized by a hardening behaviour since the maximum load capacity did not experience any significant variation (see Figure 5.5b).

Finally, the rotating model was governed by a post-peak behaviour with a substantial reduction of the load capacity (about 50%). In addition, it was also possible to observe that the residual base shear remained constant after reaching a horizontal displacement of approximately 7.5 mm as depicted in Figure 5.5c. It is worth noting that this abrupt softening behaviour is characteristic of quasi-brittle materials such as unreinforced masonry.
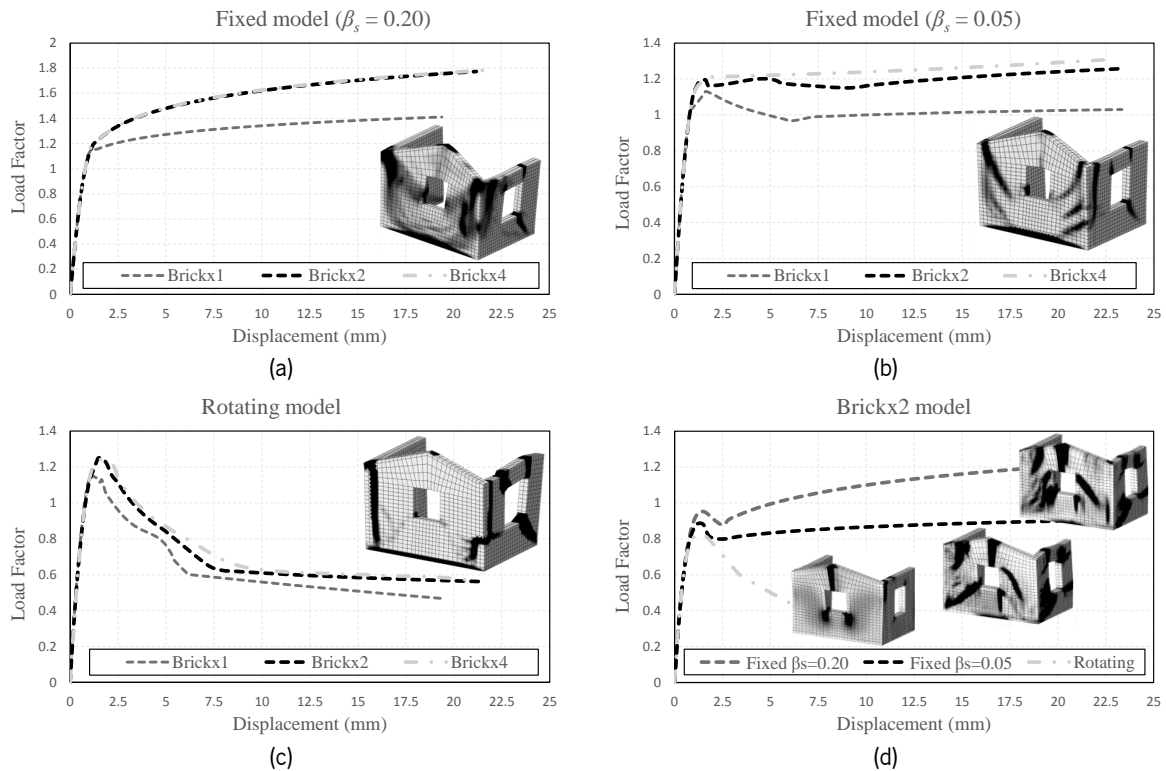
Figure 5.5 Static nonlinear analyses of the brick masonry prototype FE model in (a-c) positive, and (d) negative directions

The collapse mechanism of the FE models was assessed according to the different constitutive models, and further compared to the experimental results. The comparison in terms of principal strains, again depicted in in Figure 5.5 as an indicator of cracks or damage, was conducted separately for in-plane and out-of-plane mechanisms. The in-plane mechanism of the fixed model with a shear retention factor equal to 0.20 was constituted by concentration of principal strains propagating vertically in the upper part of the return wall, and diagonally from the lower right corner of the window opening. Additional damage was concentrated in the connection between main gable wall and return wall with window opening. Regarding the fixed model with a shear retention factor of 0.05, damage is also localized in the upper part of the return wall, on the lower right corner of the window opening, and on the connection between walls. Finally, the in-plane mechanism of the rotating model was also characterized by concentration of strains in similar locations of the return wall as the fixed models with 0.20 and 0.05 of shear retention factor. However, it was also possible to observe horizontal concentration of strain at the lower height of the window opening of the return wall. These responses were in good agreement with the experimental results since the vertical damage in the upper part of the return wall with window opening was accurately simulated. On the other hand, the experimental results showed horizontal cracks at the

lower height of the window opening. The corresponding response was reproduced by the diagonal cracking in the FE models. The out-of-plane mechanism of the brick masonry prototype with the different constitutive models presented damage concentration at the base of the wall as well as on the centre of the tympanum. Additional strains propagating diagonally from the top corners of the main gable wall were also evidenced in the fixed model with a retention factor of 0.20 and 0.05. The rotating model presented vertical strains in the connection of the main gable wall with the remaining return wall. When comparing these results to the experimental response, it is possible to observe that the FE models were not capable of simulating the complex out-of-plane of unreinforced masonry structures since there is a lack of resemblance between these mechanisms.

The FE model Brickx2 was subsequently subjected to a mass distributed lateral force pulling the main gable wall (negative direction) in order to assess the out-of-plane behaviour of the brick masonry prototype in its weakest direction. The responses in terms of pushover curves and principal strains for the different constitutive models are illustrated in Figure 5.5d. Since there was a considerable difference of strength of the main gable wall when subjected to a lateral load in a negative direction, the responses were characterized by a lower maximum load capacity (33% reduction using the rotating model as reference). The post-peak behaviour was still controlled by the constitutive models in a similar manner as in the one obtained when pushing the main gable wall. The fixed models were characterized by locking and over strength after reaching the peak, whereas the rotating model described a softening post-peak behaviour. The in-plane mechanism was constituted by vertical damage in the upper part of the return wall with window opening as well as horizontal strains localized in the right side of the wall. Such mechanism was in good agreement with the results obtained from the shaking table tests. Regarding the out-of-plane mechanism, the damage was accumulated in the base, the centre part of the tympanum, and the corner that connected the main gable wall and the return walls. These analyses demonstrated that this model was not capable of accurately reproducing the experimental out-of-plane response of the brick masonry prototype, in terms of collapse mechanisms [163].

The FE model Brickx2 was also subjected to time history analyses aiming at the evaluation of the out-of-plane response and the corresponding failure mechanism associated with dynamic loading. The solution of the dynamic equilibrium was based on the Hilber-Hughes-Taylor (HHT) method, also known as the α-method [164]. This method is capable of considering numerical dissipation without degrading the order of accuracy by the introduction of the variable α. For these analyses, the value of α was defined equal to -0.10. The structural damping was simulated by means of a Rayleigh viscous damping criterion [160] with a damping ratio ζ equal to 5%. On the other hand, the seismic input used for the time history analyses corresponded to the last ground motion recorded from the shaking table tests and illustrated in Figure 5.6. The uniaxial accelerogram with a PGA equal to 12.47 m/s^2 (1.27 g) was applied in the direction perpendicular to the main gable wall. The influence of the constitutive models on the seismic behaviour of the brick masonry prototype was assessed in terms of the hysteretic response. In addition, the failure mechanisms from the different constitutive models were compared to the one from the shaking table tests.
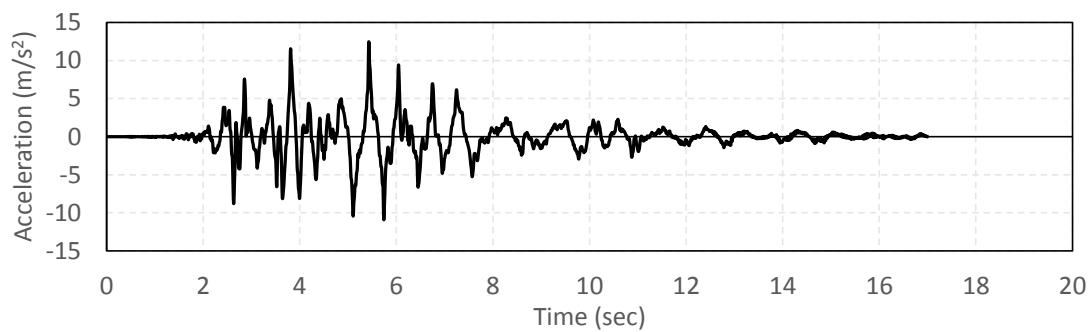
Figure 5.6 Uniaxial accelerogram applied to the brick masonry prototype

The behaviour of the FE model of the brick masonry prototype subjected to nonlinear dynamic analysis is presented in Figure 5.7. The fixed model with retention factor of 0.20 reached a maximum horizontal displacement of approximately 5 mm at the top of the tympanum. The in-plane mechanism of this model was described by vertical strains in the upper part of the return wall, as well as horizontal and diagonal crack patterns at the lower height of the window opening in the right and left sides of the return wall, respectively. On the other hand, the out-of-plane mechanism presented damage concentration mainly in the centre of the tympanum as illustrated in Figure 5.7a. However, it was possible to evidence additional damage at the base of the main gable wall and at the lower part of its window opening. The fixed model with a shear retention factor of 0.05 experienced a higher horizontal displacement (8 mm) when compared to the fixed model with 0.20 of shear retention factor. As shown in Figure 5.7b, in-plane and out-of-plane mechanisms are characterized by a similar behaviour as the one obtained from the fixed model with a shear retention factor of 0.20. However, due to the reduction of the shear retention factor, it was observed that the model presented a higher concentration of principal tensile strains. The rotating model reached a maximum horizontal displacement at the top of the tympanum of approximately 17.5 mm. Figure 5.7c shows a high concentration of principal strains in the main gable wall, in the return wall with window opening and in the connection of these two elements. In addition, damage propagating diagonally from the window opening of the main gable wall to the corner that connected it to the return wall with no opening was also evidenced. The influence of the constitutive model adopted for each analysis on the dynamic response of the brick masonry prototype is presented in Figure 5.7d. It was noted that the reduction of the shear stiffness after cracking played a fundamental role in the overall response of the structure mainly in terms of horizontal displacements; and therefore, the concentration of principal strains. Finally, the comparison between the seismic behaviour of the FE model with the different constitutive laws and the response from the shaking table test demonstrated acceptable agreement regarding the in-plane mechanism since some similarities were identified (horizontal and vertical damage propagating from the window opening). On the contrary, the out-of-plane responses obtained from the numerical models and the experimental campaign lacked resemblance, which might be due to the fact that different collapse mechanisms are possible with similar capacity, e.g. by slight changes in properties, geometry or input, even if this sensitivity analysis is outside the scope of the present work [165]. As it is clear from the rotating crack model, the FE model exhausted all its capacity, meaning that a good representation of the experimental capacity was obtained and this model can be assumed as representative of the experimental behaviour.
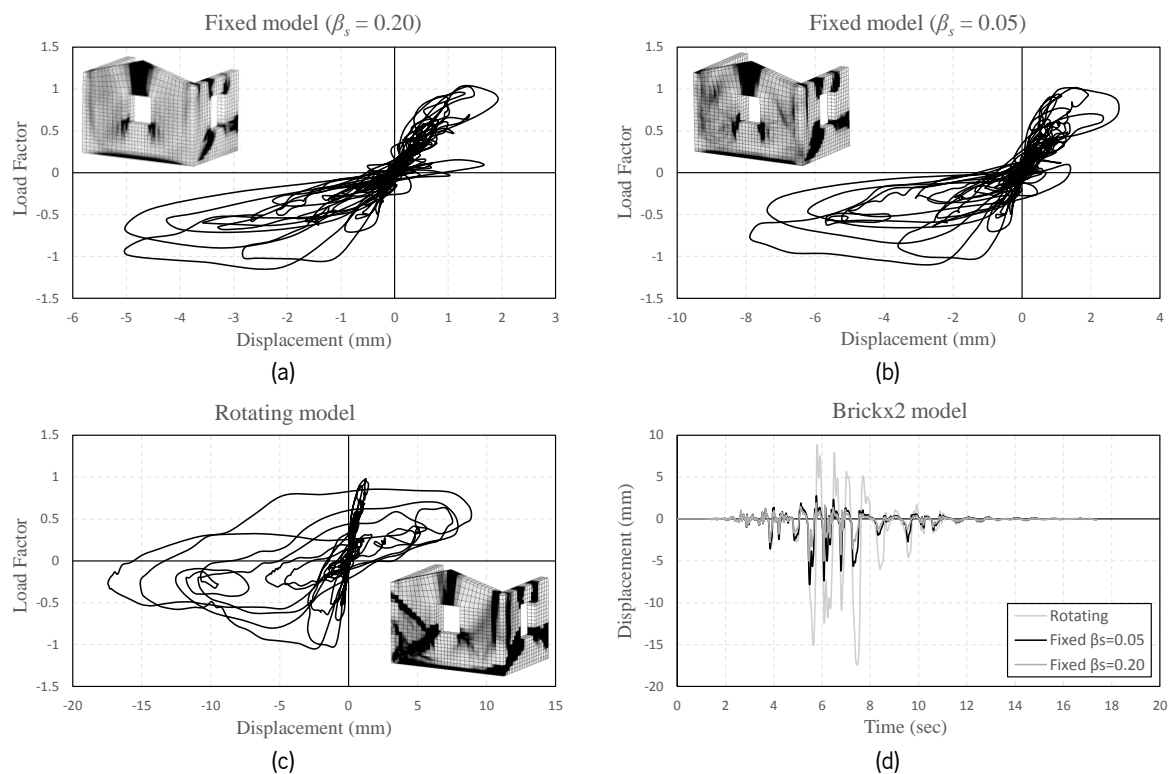
Figure 5.7 Dynamic nonlinear analyses of the brick masonry prototype FE model: hysteretic response based on fixed models with (a) 0.20, (b) 0.05 of shear retention factor, and (c) rotating model, and (f) history of displacements

b. Simplified micro-modelling approach

The modelling of masonry structures based on this approach corresponds to a discrete representation in which masonry units are considered as continuum elements, whereas the interaction between the mortar joints and the masonry units are considered as interface elements [5-8]. This advanced numerical tool corresponds to a suitable and reliable approach for the assessment of the behaviour of masonry structures since it is capable of simulating not only the different material properties of mortar joints and masonry units but also the various failure mechanisms of the constituent elements [4].

The simplified micro model of the brick masonry prototype was constituted by twenty-node solid brick elements CHX60 together with fifteen-node solid wedge elements CTP45 for the simulation of fired clay masonry units. The timber lintels above both window openings were also modelled by means of solid brick elements CHX60. Finally, mortar joints or the interaction between masonry units was modelled by means of 8+8-node plane quadrilateral 3D interface elements CQ48I. As depicted in Figure 5.8, an approximate geometric configuration of the brick masonry prototype was considered for this investigation.
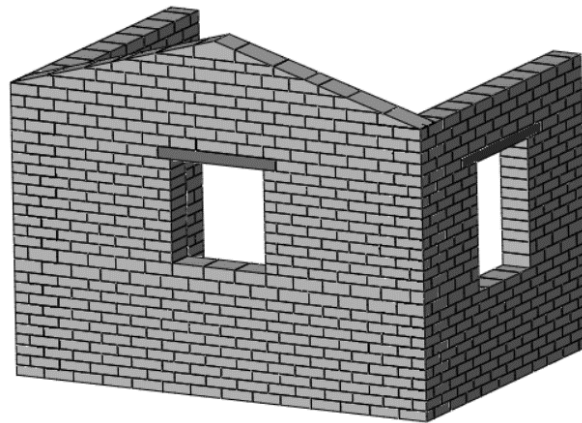
Figure 5.8 Simplified micro model of the brick masonry prototype

The behaviour of the masonry units was considered as linear elastic, whereas the nonlinearity was focused solely on the interface elements. Such nonlinearity was governed by a Combined Cracking-Shearing-Crushing interface material model which is capable of simulating fracture, frictional slip and crushing along elements as reported in [8, 166]. This material model is characterized by normal and shear stiffness of the interface elements denoted as k_n and k_t, respectively. Fracture and crushing the interface elements is described by means of tensile f_t and compressive f_c strengths, and their corresponding values of fracture energy (G_f^I and G_c) for the definition of a softening behaviour. The frictional slipping is determined by mechanical parameters such as cohesion c, friction angle φ, and fracture energy G_f^{II}. It is worth noting that the effect of dilatancy was not taken into consideration (as a zero value was adopted). The material properties of the solid and interface elements defined for the simplified micro model of the brick masonry prototype are summarized in Table 5-3 and Table 5-4, respectively.

Table 5-3. Mechanical properties of masonry units and timber lintels for the simplified micro model of the brick masonry prototype

	Young's modulus (MPa)	Poisson's ratio (-)	Specific weight (kN/m³)
Brick units	20,000	0.2	18.9
Timber lintel*	10,000		12.0

Table 5-4. Mechanical properties of interface elements for the simplified micro model of the brick masonry prototype

Linear parameters	Normal stiffness	k_n	N/mm³	72
	Shear stiffness	k_t		30
Tensile parameters	Tensile strength	f_t	MPa	0.10
	Fracture energy (mode I)	G_f^I	N/mm	0.012
Shear parameters	Cohesion	c	MPa	0.15
	Friction coefficient	$tan\,\varphi$	-	0.75
	Dilatancy coefficient	$tan\,\psi$	-	0
	Fracture energy (mode II)	G_f^{II}	N/mm	0.050
Compressive parameters	Compressive strength	f_c	MPa	2.84
	Shear traction contribution to compressive failure	C_s	-	9
	Fracture energy	G_{fc}	N/mm	3.97
	Equivalent plastic relative displacement	k_p	mm	1

The simplified micro model of the brick masonry prototype was also subjected to an incremental lateral mass distributed force in positive (pushing) and negative (pulling) directions perpendicular to the main gable wall. The response of the application of static nonlinear analyses is presented in terms of pushover curves, interface "strains" (or relative displacements), and deformed shapes of the corresponding direction as illustrated in Figure 5.9. The response of the simplified micro model when pushing the main gable wall presented a ductile behaviour with no significant variation of the maximum load capacity. The in-plane mechanism of this model was described by cracking propagating diagonally from the top left and bottom right corners of the window opening of the return wall. Additional damage was localized in the top right corner of the window opening. On the other hand, the out-of-plane mechanism when subjected to a positive lateral load presented damage at the base of the main gable wall, and horizontal crack pattern in the connection of the main gable wall and the return wall with window opening. The response of the simplified micro model when pulling the main gable wall also experienced a reduction of the maximum load capacity due to the difference in strength. Furthermore, the behaviour after the linear range was characterized by a hardening response. The in-plane mechanism corresponded to diagonal cracking around the window opening and additional horizontal detachment of masonry courses. Damage was slightly concentrated in the centre of the tympanum related to the out-of-plane response of the simplified micro model. The results from the static nonlinear analyses demonstrated good resemblance with the experimental results regarding the in-plane mechanism of the brick masonry structure mainly associated with horizontal and diagonal cracks. The horizontal crack located at the connection of the main gable wall and the return wall with window opening was a similarity associated with the out-of-plane mechanism. However, the partial collapse of the tympanum was not successfully reproduced.
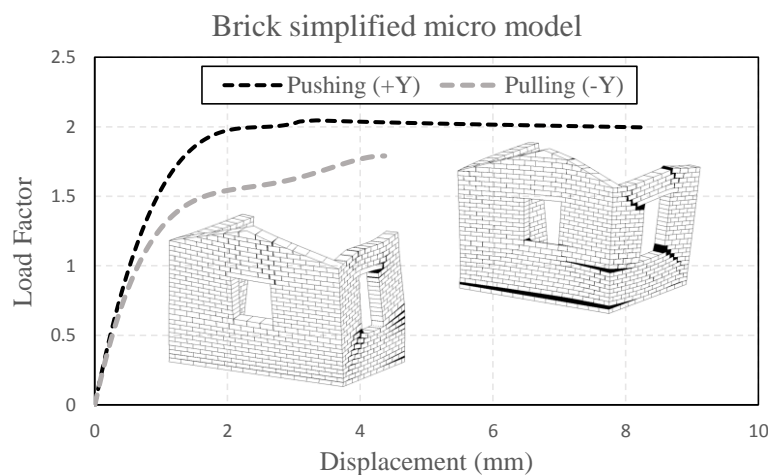
Figure 5.9 Static nonlinear analyses of the simplified micro model of the brick masonry prototype

In the case of the brick masonry simplified micro model, nonlinear dynamic analysis was also conducted by means of the HHT method. The results in terms of hysteresis curve and failure mechanisms due to the application of a uniaxial accelerogram are presented in Figure 5.10. The in-plane failure mechanism of this model consisted on the detachment of some horizontal courses at the right pier of the return wall. It was possible to determine that this mechanism was also captured experimentally

throughout the shaking table tests. Additional diagonal cracking was identified in the left pier of the same wall. It is worth noting that such crack pattern led to a diagonal partial over-turning of the main gable wall. Despite this, the out-of-plane mechanism did not accurately resemble the collapse of the tympanum obtained experimentally. The FE model experiences residual displacements and seems to have reached the maximum capacity, again in agreement with the experimental results.
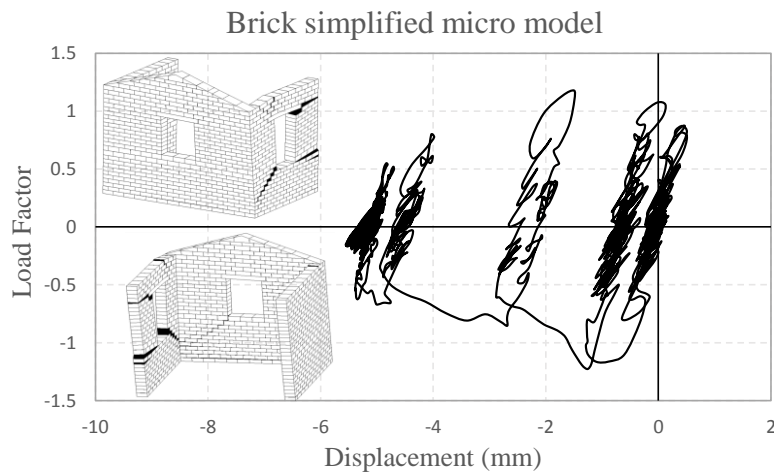
Figure 5.10 Dynamic nonlinear analyses of the simplified micro model of the brick masonry prototype

5.2.3 MACRO-ELEMENT MODEL

The out-of-plane response of the brick masonry prototype was also investigated by means of a simplified macro-element modelling approach capable of simulating the main in-plane and out-of-plane mechanisms of URM structures. The numerical model of the brick masonry prototype was built using the HiStrA software [149] by means of regular and irregular macro-elements as illustrated in Figure 5.11. The assessment of the out-of-plane response of the macro-element model in the static field was conducted by applying an incremental mass distributed lateral force. Subsequently, the macro-element model was subjected to a uniaxial accelerogram aiming at assessing the corresponding response in the dynamic field.
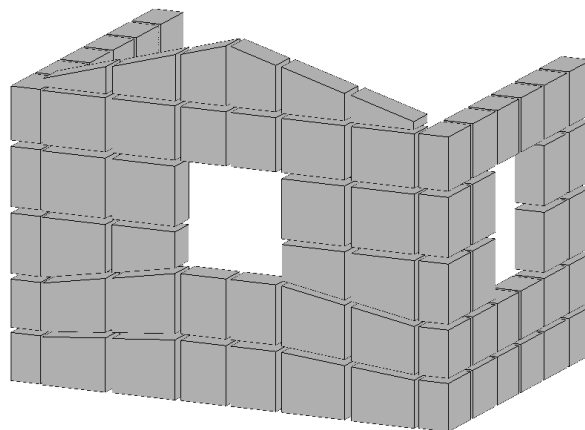
Figure 5.11 Macro-element model of the brick masonry prototype

The definition of the mechanical properties of the macro-element model was conducted considering each of the mechanisms in an independent manner. Parameters such as Young's modulus E, specific weight γ, tensile f_t, and compressive f_c strengths were established based on the mechanical characterization of the masonry wallets, as before. The flexural response was based on a fracture energy approach in which the tensile and compressive behaviours were ruled by exponential and parabolic curves, respectively. It is worth noting that the values of fracture energy in tension G_f^I and compression G_c used in the FE models were as assumed for the macro-element model. The simulation of the overall shear mechanism required the definition of additional mechanical properties. Regarding the shear-sliding, the cohesion c under no confinement conditions was considered equal to the tensile strength assuming a uniform shear stress during the diagonal compression tests [167, 168]. The post-yielding behaviour associated with the shear-sliding mechanism was also influenced by fracture energy G_f^{II} assumed 1.5 times G_f^I. On the other hand, the shear strength f_s related to the shear-diagonal mechanism was also established according to the tensile strength and a ratio of 0.67. A summary of the mechanical properties defined for the macro-element model is presented in Table 5-5.

Table 5-5. Mechanical properties of the macro-element model of the brick masonry prototype

Linear parameters	Young's modulus	E	GPa	5.17
	Shear modulus	G	GPa	2.15
	Specific weight	γ	kN/m^3	18.9
Tensile parameters	Tensile strength	f_t	MPa	0.10
	Fracture energy	G_f^I	N/mm	0.012
Compressive parameters	Compressive strength	f_c	MPa	2.48
	Fracture energy	G_{fc}	N/mm	3.97
Shear-diagonal parameters	Shear strength	f_s	MPa	0.067
	Friction coefficient	μ_d	-	0.60
Shear-sliding parameters	Cohesion	c	MPa	0.10
	Friction coefficient	μ_s	-	0.70
	Fracture energy	G_f^{II}	N/mm	0.018

The assessment of the out-of-plane response of the macro-element model was also conducted by means of the application of an incremental mass distributed lateral force in positive and negative directions. The pushover curves and the failure mechanisms of this model in accordance with the application of these analyses in the corresponding given direction are illustrated in Figure 5.12. The response of the macro-element model when pushing the main gable wall (positive direction) was characterized by a maximum load capacity of approximately 1.27 times the structure's self-weight. It was also possible to observe that this response was described by a high ductility and a softening post-peak behaviour. The mechanism associated with this direction consisted mainly of the out-of-plane failure of the main gable wall since tensile strains were concentrated in the corners and in the centre of the tympanum.

Due to the lower strength in the negative direction, the macro-element model also experienced a significant reduction of its maximum load capacity of around 30%. The post-peak branch was described by a softening response in which a constant residual force was reached at approximately 10 mm. The mechanism obtained when pulling the main gable wall corresponded to horizontal and vertical damage

in the window opening associated with an in-plane flexural failure of the return wall. It was also possible to observe a partial overturning of the main gable wall and concentration of strains in the centre of the tympanum. The mechanisms obtained due to static nonlinear analyses were compared to the response from the shaking table tests. It was noted that there were good similarities between both in-plane responses since the localization of damage in the macro-element model was in agreement with the collapse of the return wall. In addition, it was possible to observe the partial detachment of the left side of the tympanum (failure in along the interface elements) which may resemble the experimental collapse mechanism.
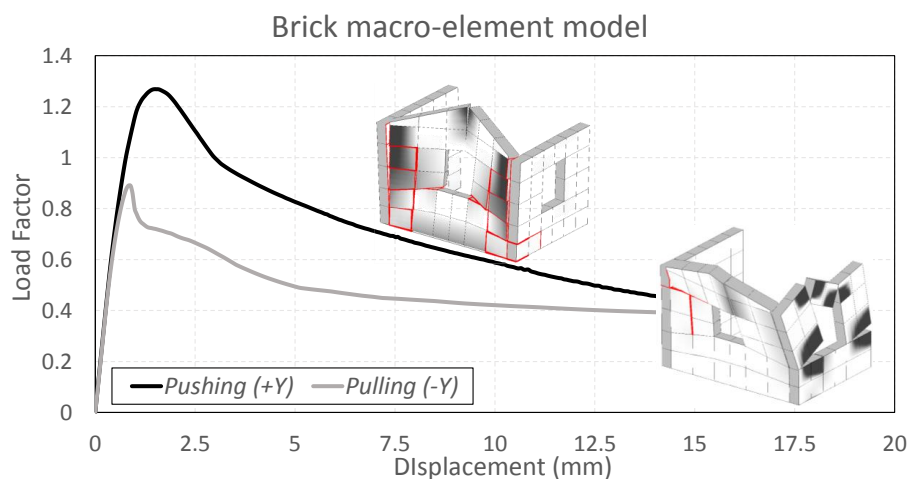
Figure 5.12 Static nonlinear analyses of the macro-element model of the brick masonry prototype

Nonlinear dynamic analysis was conducted to the macro-element model considering a Newmark method [158] based on a constant acceleration, and a Rayleigh viscous damping criterion with a damping ratio ζ of 5%. The cyclic behaviour associated with the tensile response was described by a stiffness oriented to the origin (secant stiffness) in which the unloading coefficient β_t presented a value of 1. On the other hand, the unloading cycles in compression and shear-diagonal were governed by an initial stiffness ($\beta_c = \beta_d = 0$). The definition of the mass properties was based on a lumped approach in which the components of the mass matrix were defined along its diagonal. Figure 5.13 illustrates the load factor-displacement hysteresis curve of the macro-element model together with the deformed shapes corresponding to the maximum and minimum displacements due to the application of the uniaxial accelerogram. The maximum displacements obtained at the top of the tympanum presented values of approximately 10 mm and16 mm in positive and negative directions, respectively. The overall failure mechanism of the macro-element model consisted of damage propagating vertically in the upper part of the return wall, and horizontally in the lower part of the same wall. The out-of-plane mechanism of the macro-element model consisted of the failure in the connection of the main gable wall with the return ones, and additional damage along the tympanum.
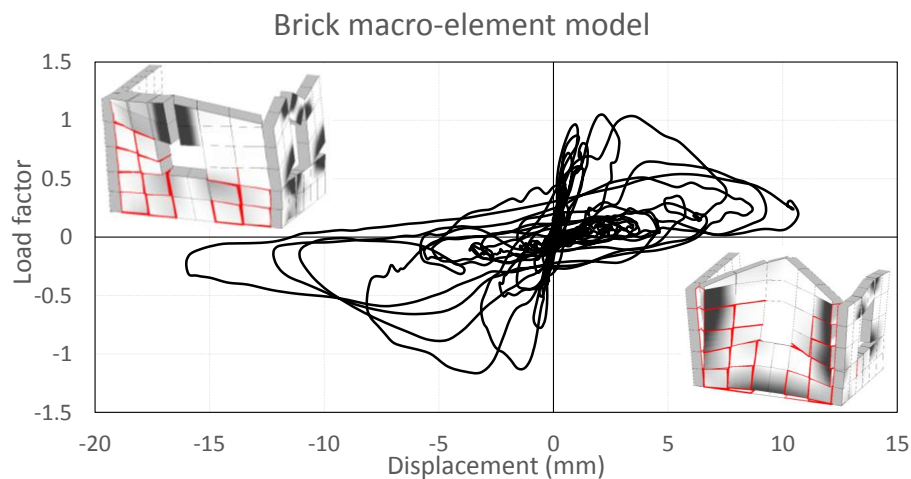
Figure 5.13 Dynamic nonlinear analyses of the macro-element model of the brick masonry prototype

A comparison between FE and macro-element models was conducted in order to investigate the suitability of this simplified modelling approach for the assessment of URM structures for practical applications. Taking into consideration the post-peak behaviour, residual force, and the failure mechanisms of the different constitutive laws adopted for the FE models, it was noted that the rotating total strain crack model was more appropriate for such comparison, as stated before. Similar maximum load capacities, as well as coinciding initial softening post-peak branches, were obtained in both models when pushing the main gable wall. As illustrated in the pushover curve of Figure 5.14a, the post-peak response of the FE model after a displacement of approximately 7.5 mm consisted of a constant residual force. However, in the case of the macro-element model, such response was still governed by a softening behaviour. Regarding the failure mechanisms, a similar response was obtained in the main gable wall (concentration of strains in the connection between main gable wall and return walls, and at the centre of the tympanum). Unlike the macro-element model, the response of FE model was also characterized by an in-plane failure mechanism. Figure 5.14b presents the pushover curves and failure mechanisms of the FE and macro-element models due to the application of a negative lateral load. From these results, it was observed that the macro-element model presented a slight increment of the maximum load capacity. In addition, the macro-element model experienced a more pronounced initial softening response. Despite the lower ductility obtained with the FE model, it can be stated that the overall post-peak branch of both models may be in good agreement. It is worth noting that the localization of strains in the return wall and in the centre of the tympanum coincide between the two models.

The comparison in the dynamic nonlinear field by means of load-displacement hysteresis curves together with their corresponding failure mechanisms are depicted in Figure 5.14c. A small difference in the displacement at the top of the tympanum in the negative direction was obtained between the FE and macro-element modelling approaches presenting values of 17.5 mm and 16 mm, respectively (difference of 10%). Such difference in terms of peak displacement was slightly higher when considering the positive direction. Moreover, the assessment of the out-of-plane response of these models was also conducted by means of the history of displacements at the top of the tympanum illustrated in Figure 5.14d. It was also possible to observe not only the difference of maximum displacement but also a residual displacement

that characterized the dynamic response of the macro-element model. On the other hand, a similar concentration of strains was identified in the return wall with window opening. A reasonable agreement was found regarding the main gable wall since both models presented damage in the centre of the tympanum, and in the right corner.
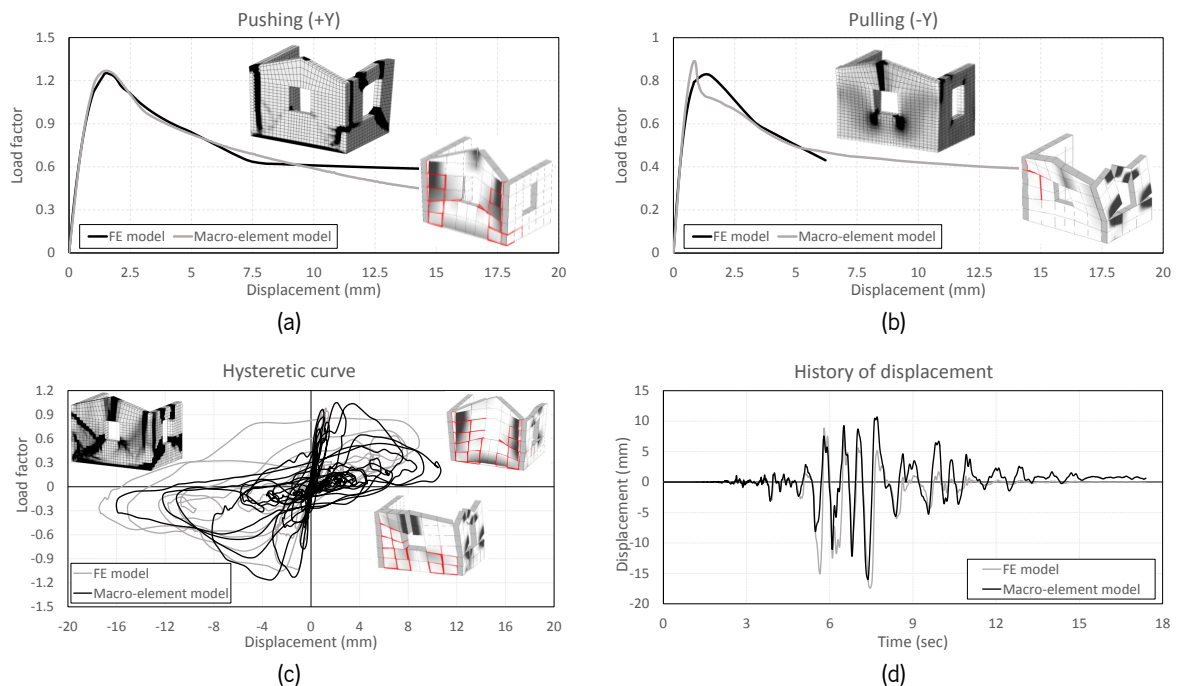
Figure 5.14 Comparison of the out-of-plane response of the brick masonry prototype based on FE and macro-element models: pushover analyses in (a) positive and (b) negative direction, (c) load-displacement hysteresis curve, and (d) history of displacement

Finally, an assessment of the mesh dependency of the macro-element model was conducted taking into consideration a more discretized representation of the brick masonry prototype. For comparison purposes, the initial model was denoted as *MeshA* (see Figure 5.15a), whereas the macro-element with a more refined mesh discretization was denoted as *MeshB* (see Figure 5.15b). Pushover analysis along the weakest direction (pulling) and time history analysis were conducted to the macro-element model *MeshB*. The comparison due to the application of an incremental lateral force is illustrated in Figure 5.15c. A slight increment of the maximum load capacity was identified between the different mesh discretization. It was also noted that the maximum load capacity was reached at a higher displacement. On the contrary, both models were characterized by a softening post-peak behaviour, reaching the same residual force. *MeshA* was characterised by nonlinearity along some interface elements associated with the sliding mechanism (red lines), whereas this behaviour was not identified in model *MeshB*. Despite this, a good agreement in terms of failure mechanisms was obtained from the mesh refinements. Figure 5.15d depicts the history of displacement due to the application of the uniaxial accelerogram. It can be observed that the macro-element model *MeshB* presented a coinciding response like the one obtained from the initial model especially in the negative direction. The response of the refined model presented a small difference associated with a residual displacement in the positive

direction. In this regard, it can be stated that the mesh refinement did not play a meaningful role in the out-of-plane response of the brick masonry structure by means of a macro-element model.
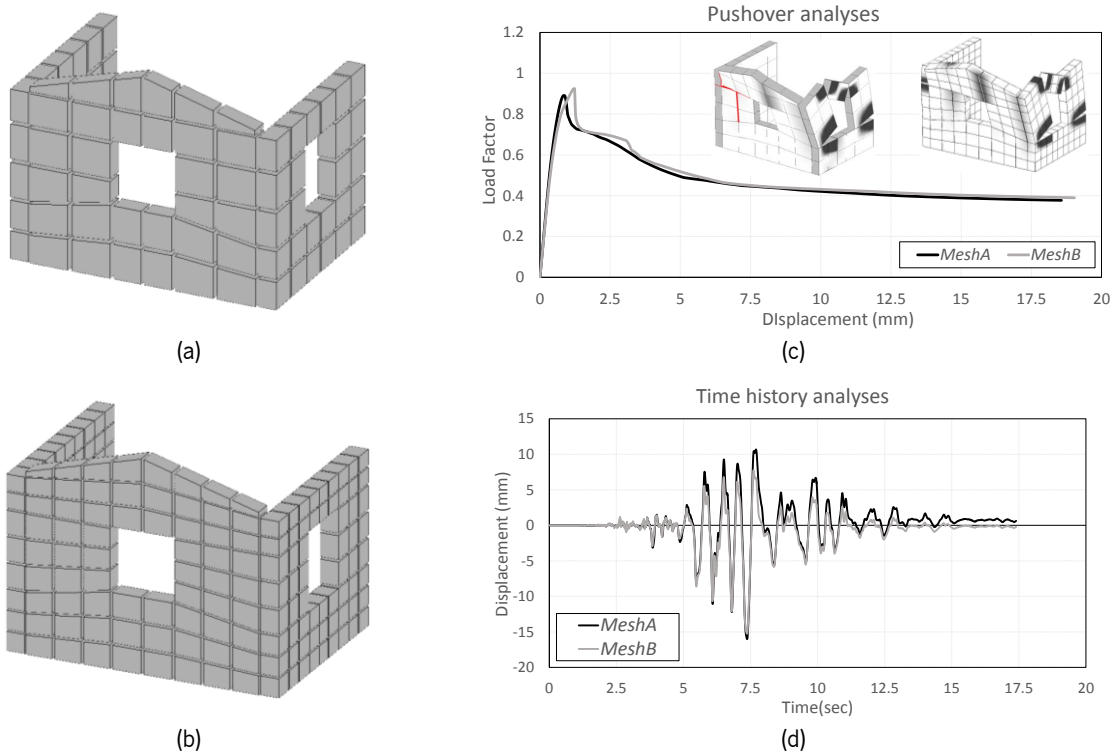
Figure 5.15 Assessment of the influence of the mesh refinement in the out-of-plane response of the macro-element model: (a) *MeshA*, (b) *MeshB*, comparison by means of nonlinear (c) static, and (d) dynamic analyses

A substantial reduction of the computational effort when conducting sophisticated numerical simulations, namely time history analyses, was obtained with the macro-element modelling approach. This decrease was related to the difference in DOFs that the two modelling approaches presented. In the case of the FE model, the number of DOFs corresponded to 54477, and the application of nonlinear dynamic analyses required a computation demand of approximately 18 hours. On the other hand, macro-element models *MeshA* and *MeshB* were characterized by 616 and 1407 DOFs, respectively. The computational requirements corresponding to these models were around 40 and 90 minutes. A summary of the required computational time and the reduction obtained by means of the macro-element modelling approach are reported in Table 5-6.

Table 5-6. Computation effort for the application of time history analyses on the FE and macro-element models of the brick masonry prototype

FE model	Macro-element model – *MeshA* (Reduction)	Macro-element model – *MeshB* (Reduction)
18 hours	40 minutes (−96%)	90 minutes (−92%)

Figure 5.16 illustrates a compilation of the failure mechanisms of the FE macro models and the corresponding macro-element models due to the application of static and dynamic nonlinear analyses, as well as a scheme of the collapse mechanism obtained from the shaking table tests. Again, globally a

reasonable agreement as found between FE rotating crack model, macro-element model *MeshA* and experimental results.
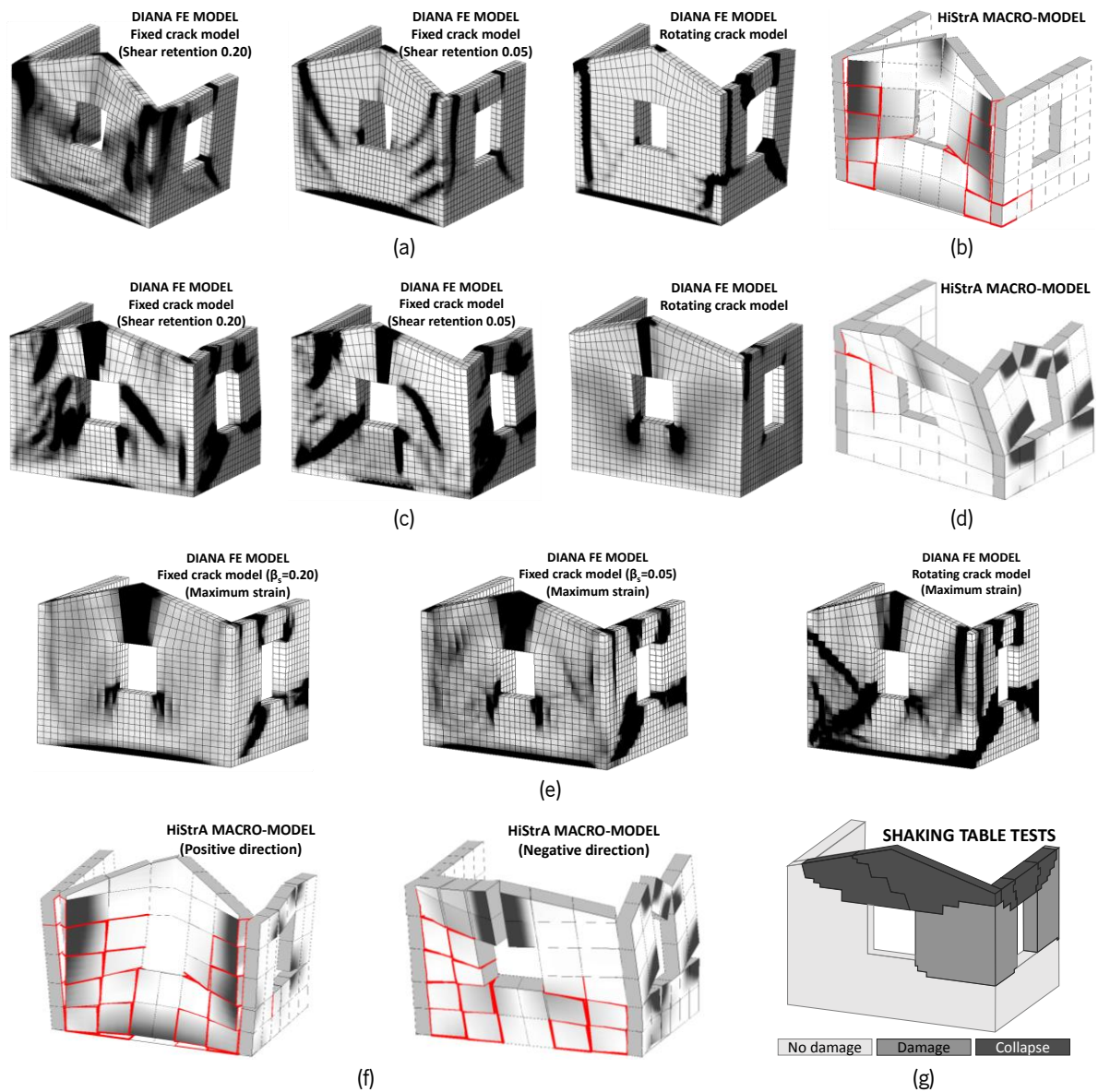
Figure 5.16 Failure mechanisms of brick masonry prototype: pushover analyses in positive and negative directions of (a, c) FE and (b, d) macro-element models; dynamic analyses of (e) FE and (f) macro-element models, and (g) shaking table tests.

5.3   STONE MASONRY PROTOTYPE

The stone masonry prototype also corresponded to a U-shape full-scale structure made of an irregular arrangement of stone units with lime-based mortar as illustrated in Figure 5.17a. The three walls that composed this structure presented a thickness equal to 0.50 m. Unlike the brick masonry prototype, the stone one presented a 1.00 m x2.00 m centred door opening in the main gable wall. Such wall was characterized by 3.0 m of height and 4.15 m of length, whereas the return walls placed orthogonally presented a height of 2.45 m and a length of 2.50 m. In addition, one return wall also presented a window

opening with the same dimensions as the one from the brick masonry prototype (0.80 m of length and 1.00 m of height). This structure was also characterized by an asymmetric response due to the presence of the window opening, and by the lack of a box-type behaviour as a result of the absence of a horizontal rigid diaphragm.

| (a) | (b) |

Figure 5.17 Stone masonry: (a) U-shape full-scale prototype, and (b) square wallets

Vertical and diagonal compressive tests were conducted in the stone masonry square wallets shown in Figure 5.17b. A total of six samples were experimentally tested. Three of them were subjected to vertical compressive tests in order to determine mechanical parameters such as Young's modulus E and compressive strength f_c. The remaining samples were subjected to diagonal compressive tests aiming at the estimation of tensile strength f_t. Table 5-7 summarizes the mean values and CoV of the mechanical parameters of the stone masonry obtained from these tests. Mean values of 2080 MPa, 5.44 MPa, and 0.22 MPa were obtained for Young's modulus, compressive, and tensile strengths, respectively. A specific mass equal to 2360 kg/m³ was also determined for this type of material. Further details regarding the mechanical characterization of this material can be found in [77].

Table 5-7. Mechanical properties of stone masonry obtained from experimental campaign

	Specific mass ρ	Young's Modulus E	Compressive strength f_c	Tensile strength f_t
Mean	2360 kg/m³	2080 MPa	5.44 MPa	0.22 MPa
CoV	1%	43%	15%	17%

5.3.1 SHAKING TABLE TESTS

Shaking table tests consisting on the application of uniaxial accelerograms to the main gable wall along its perpendicular direction were again conducted to the stone masonry prototype at the LNEC (National Laboratory for Civil Engineering) in Lisbon as reported by Candeias, et al. [77]. Aiming at the assessment of the out-of-plane response of the stone masonry prototype, the structure was subjected to six consecutive seismic inputs considering two amplification factors until near collapse was reached. The transducers used for the measurement and recording of the seismic response (six LVDTs and nineteen

accelerometers) presented a similar configuration to the brick masonry prototype. The setup for these experimental tests is illustrated in Figure 5.18.
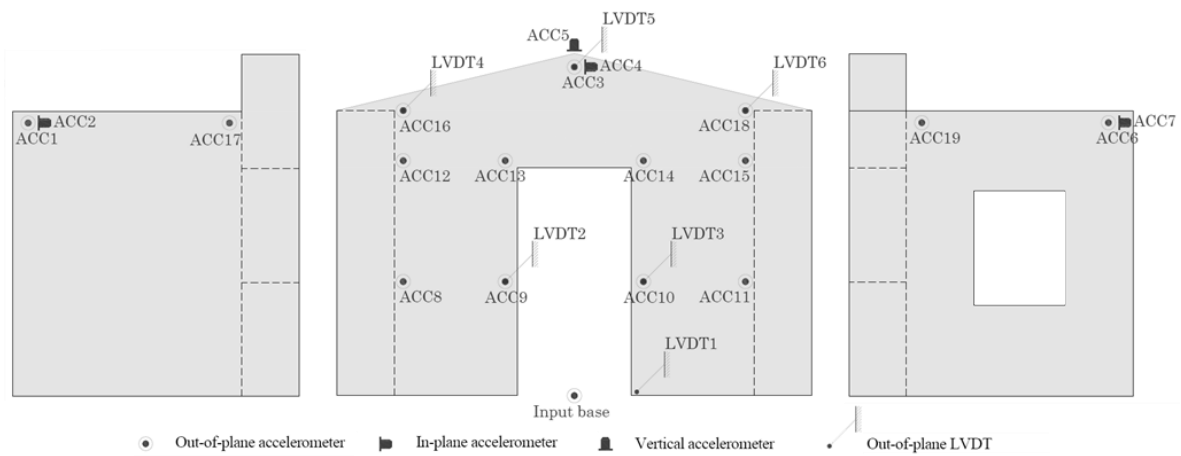
Figure 5.18 Measurement setup for the stone masonry prototype

Before the application of shaking table tests, the stone masonry prototype already presented horizontal cracking at the base, due to the transport to the shaking table. However, the structure did not experience significant additional damage during the first three seismic inputs. Due to the application of the fourth ground motion, the structure presented vertical and horizontal cracking along the mortar joints in the upper part of the return wall with window opening. The main gable wall also experienced damage in terms of a vertical crack propagating from the top right corner of the door opening. Additional cracking along mortar joint was induced diagonally from the window opening in the return wall as well as in the left part of the main gable wall after the application of the fifth seismic input. Vertical cracking propagating from the top left corner of the door opening was also identified. During the last seismic input with a registered PGA of 1.07 g, the stone masonry structure experienced severe damage along the mortar joints in the main gable wall and both return walls. It is worth noting that the structure almost reached collapse state due to the application of the last seismic input. Partial collapse of the right corner of the return wall with window opening was observed. The seismic response of the stone masonry prototype is illustrated in Figure 5.19.

| (a) | (b) | (c) |
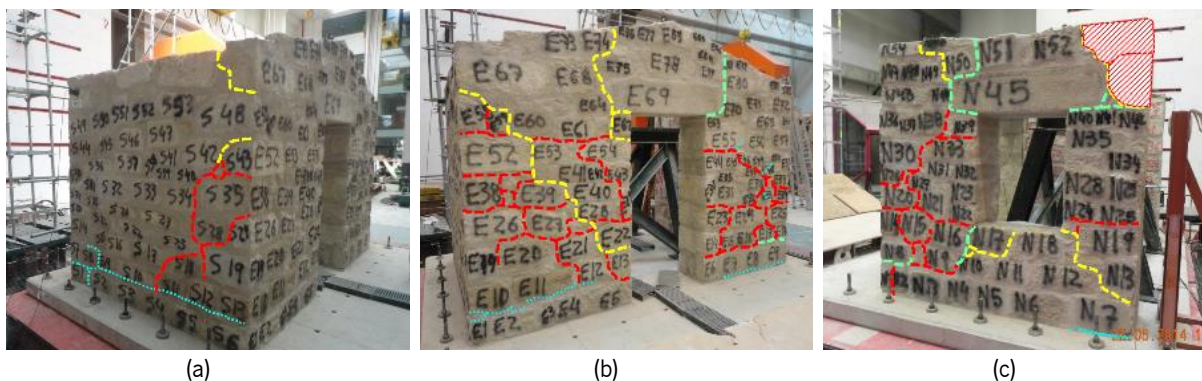
Figure 5.19 Collapse mechanisms of the stone masonry prototype from shaking table tests: (a) return wall without opening, (b) main gable wall, and (c) return wall with window opening

5.3.2 FINITE ELEMENT MODEL

The assessment of the out-of-plane behaviour of the stone masonry prototype by means of FE numerical simulations was also conducted considering macro and simplified micro-modelling approaches. An incremental mass distributed lateral force and a uniaxial accelerogram were applied to the stone masonry prototype in the perpendicular direction to the main gable wall in order to investigate its out-of-plane response in the nonlinear static and dynamic fields, respectively. The uniaxial accelerogram used for the nonlinear dynamic analyses corresponded to the last seismic input from the shaking table tests.

a. Macro-modelling approach

The FE model of the stone masonry prototype as a continuum material was also built using solid brick elements CHX60. The values obtained from the mechanical characterization (vertical and diagonal compressive tests) were used for the definition of the mechanical properties of masonry, namely Young's modulus E, specific weight γ, compressive f_c, and tensile f_t strength. Fixed and rotating total strain crack models were selected for the assessment of the nonlinear behaviour of this structure in the static and dynamic fields. The tensile response was governed by an exponential softening curve, whereas the compressive response was ruled by a parabolic one. In this case, the fracture energy in tension G_f^I corresponded to 0.048 N/mm, whereas the corresponding value in compression G_c was also defined by means of a ductility index d_{uc} equal to 1.6 mm. Again, shear retention factors β_s of 0.20 and 0.05 were established for the fixed total crack models for the shear response. The mechanical properties defined for this model are summarized in Table 5-8.

Table 5-8. Mechanical properties of the FE model of the stone masonry prototype

Linear parameters			Tensile parameters		Compressive parameters	
Young's modulus E	Poisson's ratio ν	Specific weight γ	Tensile strength f_t	Fracture energy G_f^I	Compressive strength f_c	Fracture energy G_c
2080 MPa	0.20	23.6 kN/m³	0.22 MPa	0.048 N/mm	5.44 MPa	8.70 N/mm

Static nonlinear analyses were initially conducted on the positive direction of the main gable wall aiming at assessing the influence of the mesh refinement on the out-of-plane response of the of FE model of the stone masonry prototype. In a similar approach as the one followed for the brick masonry prototype, the mesh dependency was evaluated considering one, two and four elements along the thickness of the main gable wall denoted as Stonex1, Stonex2, and Stonex4, respectively. The different mesh refinements used for the FE model of the stone masonry prototype are illustrated throughout Figure 5.20a-c. The analyses also consisted of the application of an incremental mass distributed lateral force pushing the main gable wall against the return walls.

(a)   (b)   (c)
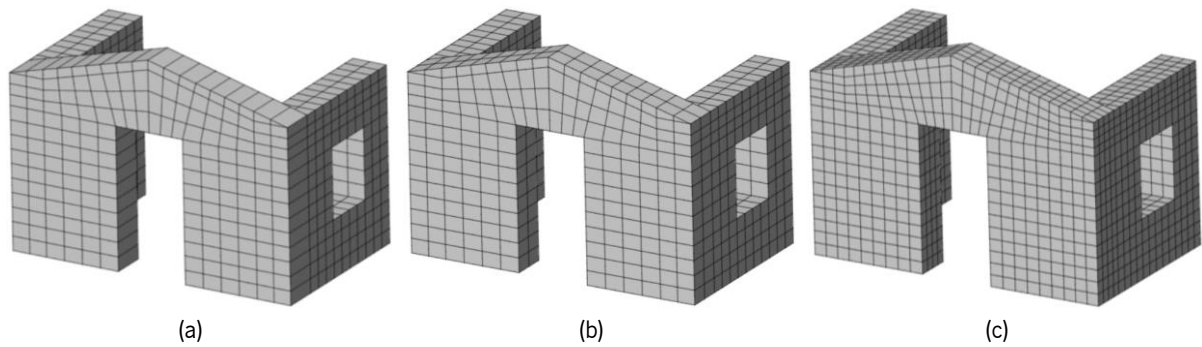
Figure 5.20 FE models of the stone masonry prototype: (a) Stonex1, (b) Stonex2, and (c) Stonex4

The results of the pushover analyses for the assessment of the mesh dependency are illustrated throughout Figure 5.21a-c. It could be observed that in the case of the fixed model with 0.20 of shear retention, the model Stonex1 presented a limited ductility due to difficulties in convergence. However, larger displacements were obtained when increasing the number of elements along the thickness of the main gable wall (Stonex2 and Stonex4). In addition, the last two models were also characterized by a hardening behaviour in the post-peak branch as illustrated in Figure 5.21a. The mesh refinement played a significant role in the peak capacity of the FE models since a small increment of base shear was evidenced when increasing the number of elements in thickness. On the other hand, the FE models Stonex1 and Stonex2 were characterized by a similar response when the material nonlinearity was governed by a fixed crack model with a shear retention of 0.05. The response of these models was described by a ductile behaviour with a reduction (25%) of the shear capacity at approximately 5 mm of displacement at the top of the tympanum. Such reduction of the shear capacity was not evidenced in the FE model Stonex4 since its response was also characterized by a hardening post-peak behaviour (see Figure 5.21b). Finally, the response in terms of maximum load capacity of the FE models based on rotating cracks was also slightly influenced by the mesh refinement. Model Stonex4 presented the higher base shear (load factor equal to 1.6) when compared to the other models, and its response was described by a softening post-peak behaviour. It is worth noting that these models presented a lower ductility as depicted in Figure 5.21c.

The assessment of the collapse mechanism according to the different constitutive models was conducted considering the FE model Stonex4 since it presented the smoothest response. Regarding the fixed crack model with a shear retention factor of 0.20, the in-plane mechanism of the return wall was described by concentration of damage originating from the window opening. A slight concentration of strains was also identified in the corner that connects the main gable wall to the return wall. On the other hand, the out-of-plane mechanism of the main gable wall was composed of damage concentrating along its base, and at the lower height of the window opening. It was also possible to identify additional strains in the centre of the tympanum, as well as cracking propagating along the left side of the main gable wall. The overall mechanism of the FE model based on a fixed crack model with a shear retention factor of 0.05 was characterized by a similar response, consisting of cracking around the window opening, concentration of strains along the main gable wall and in the centre of the tympanum. It is worth noting that this model presented a higher concentration of strains which may be associated with the different shear behaviour between the two fixed crack models. In the case of the FE model with rotating cracks,

the in-plane mechanism related to the return wall consisted on high concentration of strains propagating diagonally and horizontally from the window opening. Due to the low ductility obtained for the response, the out-of-plane mechanism was not characterized by a significant damage pattern. However, it was possible to observe concentration of strains at the base of the main gable wall and at the centre of the tympanum.

Static nonlinear analyses were conducted using the FE model Stonex4 in order to assess its out-of-plane response in the negative direction as well as the influence of the different adopted constitutive laws. An incremental lateral force was applied perpendicularly to the main gable wall pulling it from the return walls. The results from these analyses in terms of pushover curves and damage pattern are illustrated in Figure 5.21d. The pushover analyses also demonstrated the weak behaviour the structure presented when pulling the main gable wall. The stone masonry structure experienced a reduction of 25% of maximum load capacity as a result of the difference in strength between positive and negative directions considering the rotating crack model as reference. Regarding the material dependency, the out of plane response based on a fixed crack model with 0.20 of shear retention factor was characterized by an initial reduction of the maximum load capacity and a subsequent hardening behaviour. A similar ductile response was evidenced in the fixed crack model with a shear retention factor of 0.05. However, a higher reduction of the maximum load capacity was obtained due to the difference in terms of shear retention factors. Finally, the FE model governed by rotating cracks also presented a significant reduction of its maximum load capacity (approximately 50%). It is worth noting that the softening post-peak branch associated with this constitutive law was not characterized by a high ductility when compared to the fixed crack models.

(a)

(b)

(c)

(d)
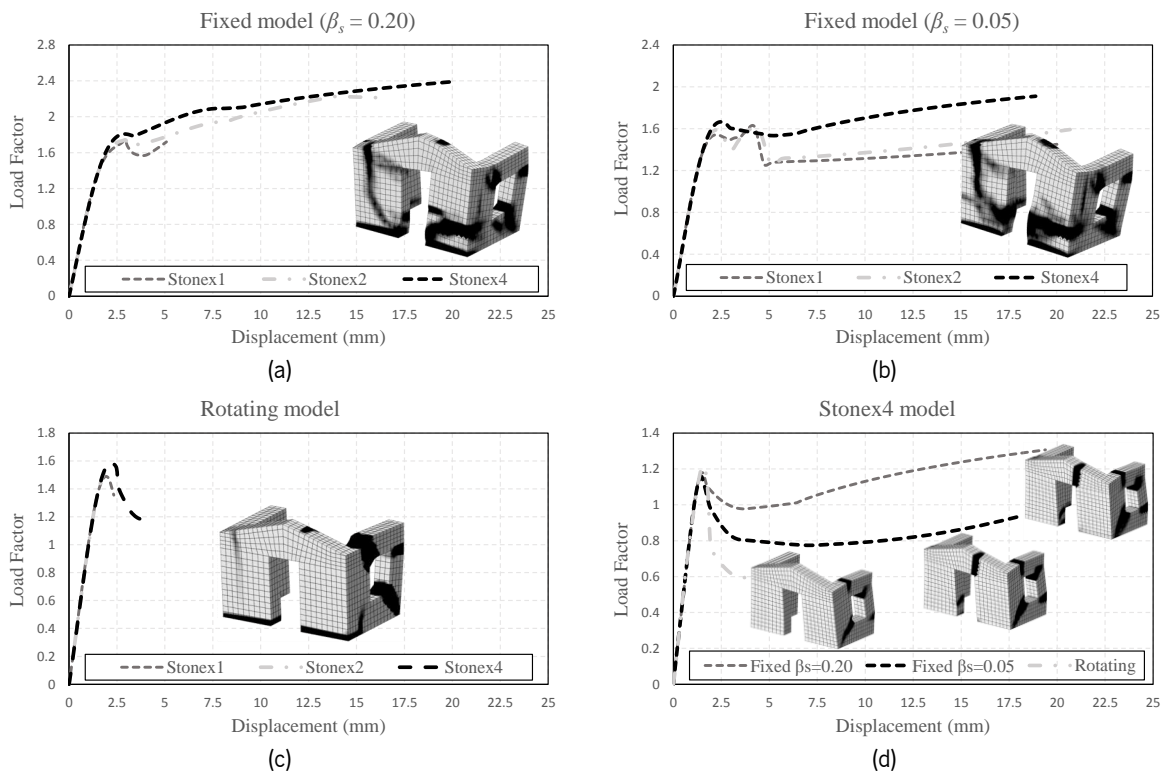
Figure 5.21 Static nonlinear analyses of the stone masonry prototype FE model in (a-c) positive, and (d) negative directions

The collapse of these models was mainly associated with an in-plane mechanism of the return wall consisting on vertical and diagonal cracks in the top and bottom corners of the right side of the opening, as well as horizontal cracks in the left side of the opening. Both fixed crack models presented additional damage related to the out-of-plane mechanism. Such mechanism was related to concentration of strains at the centre of the tympanum, and close to the base of the main gable wall. On the contrary, the rotating crack model did not experience an out-of-plane mechanism. A comparison between the collapse mechanisms of these models and the response obtained from the shaking table tests was also conducted. Reasonable agreement was obtained in terms of in-plane mechanisms since the cracking around the window opening of the return wall coincided with the failure of the mortar joints of the stone masonry prototype. It is worth noting that an acceptable resemblance was evidenced in the out-of-plane mechanism of the main gable wall also associated with the failure of the mortar joints.

The out-of-plane response of the stone masonry prototype was also investigated in the nonlinear dynamic field by means of the application of time history analysis. In this regard, the FE model Stonex4 was subjected to a uniaxial accelerogram in the direction perpendicular to the main gable wall. The seismic input used in this investigation is depicted in Figure 5.22, and it corresponded to the last ground motion recorded from the shaking table tests with a PGA of 10.5 m/s^2 (1.07 g). For the time history analyses, the HHT method [164] (α = -0.10) and a Rayleigh viscous damping criterion [160] (ζ = 5%) were defined for the solution of the dynamic equilibrium, and for the dissipation of energy, respectively. The response of the different constitutive models was assessed by means of hysteretic response and history of displacements. Subsequently, the corresponding failure mechanisms were compared to the one obtained from the shaking table tests.
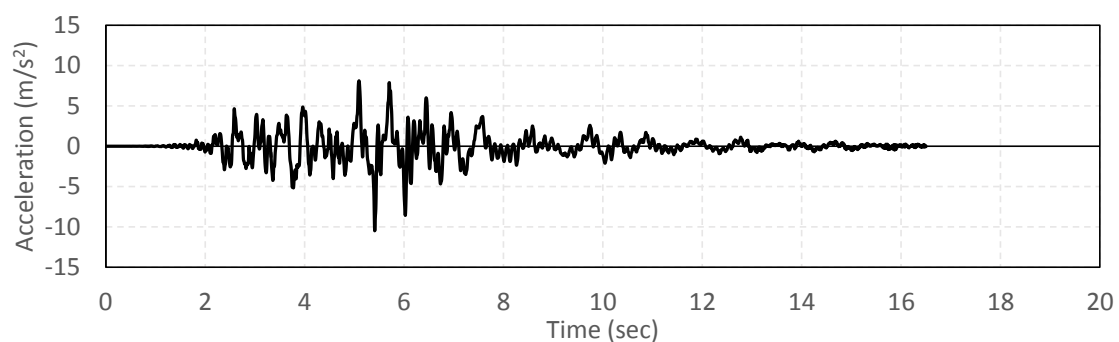
Figure 5.22 Uniaxial accelerogram applied to the stone masonry prototype

An initial assessment of the seismic response of the FE models of the stone masonry prototype was conducted considering the original seismic input. However, such response was characterized by an elastic behaviour. In this regard, an amplification factor was applied to the original seismic input (1.5 was adopted as a round figure). The out-of-plane response due to the amplified seismic input (PGA = 1.60 g) in accordance with the corresponding constitutive models is illustrated in Figure 5.23. The response of the fixed model with 0.20 of shear retention factor was described by a maximum displacement of approximately 6 mm at the top of the tympanum in its weakest direction. The mechanism of this model consisted on concentration of strains around the window opening related to its in-plane response, and damage at the base and centre of the tympanum related to its out-of-plane response (see Figure 5.23a).

The response fixed model with a shear retention factor of 0.05 presented a higher displacement (around 10 mm) at the top of the tympanum.

The in-plane mechanism consisted of a pattern in which the cracks are located around the opening of the return wall. On the other hand, a more extensive concentration of strains was evidenced in the left side and at the base of the main gable wall. Additional damage was identified in the centre of the tympanum as shown in Figure 5.23b. In the case of the rotating model, a maximum horizontal displacement of approximately 11 mm was reached at the top of the tympanum due to the application of the amplified seismic input. As illustrated in Figure 5.23c, the overall mechanism of the rotating model presented a significant resemblance to the one obtained from the fixed model with 0.05 of shear retention. It is worth noting that the two latter models showed a reasonable agreement when comparing their corresponding response to the collapse obtained in the shaking table tests. The out-of-plane response and its dependency on the material nonlinearity were also assessed by means of the histories of displacements depicted in Figure 5.23d. It was observed that the history of displacements associated with the fixed model with a shear retention factor of 0.05 and the rotating model presented a similar behaviour. On the other hand, a ratio of approximately 2 was obtained when comparing the horizontal top displacements of the two fixed models in which the shear retention factors a significant influence on the dynamic response.
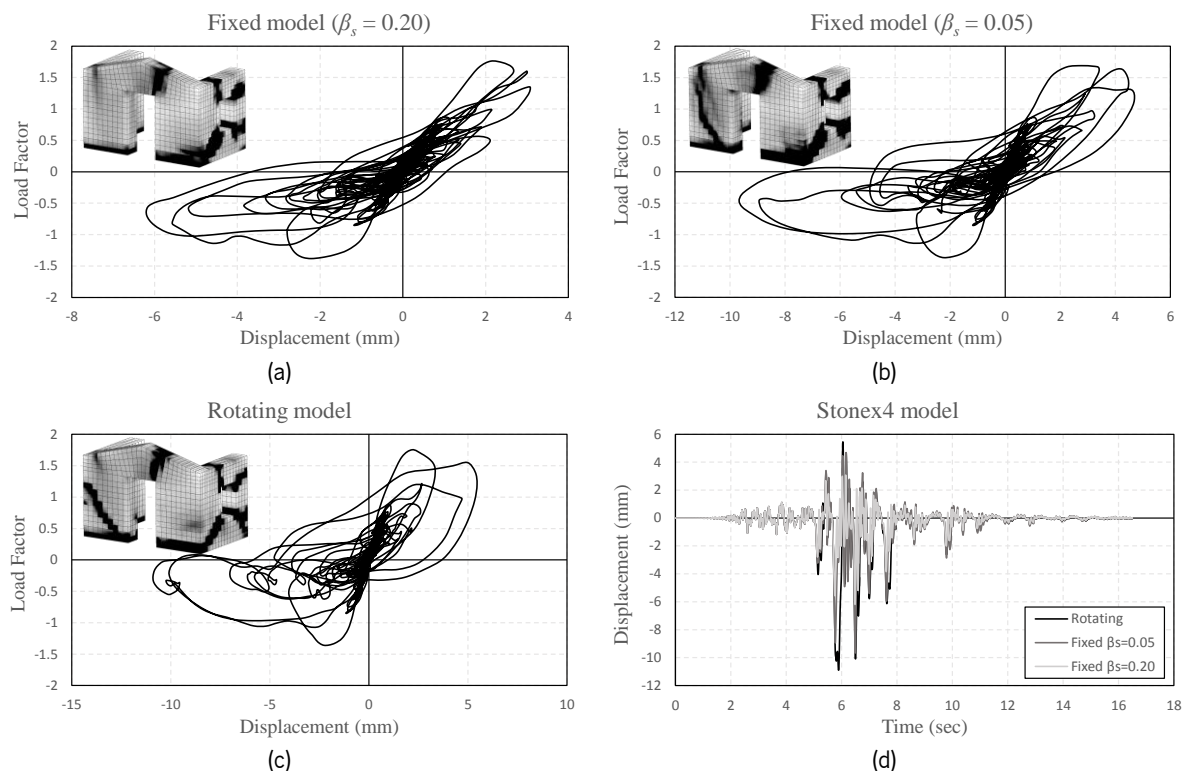
Figure 5.23 Dynamic nonlinear analyses of the stone masonry prototype FE model: hysteretic response based on fixed models with (a) 0.20, (b) 0.05 of shear retention factor, and (c) rotating model, and (d) history of displacements

b. Simplified micro-modelling approach

In a similar approach as the one followed for the brick masonry prototype, this simplified micro model was built by means of solid brick and wedge elements for the simulation of stone units, and interface elements for the interaction between units and mortar joints. Based on the DIANA software [157], these components corresponded to twenty-node (CHX60) and fifteen-node (CTP45) solid elements, and 8+8-node plane quadrilateral 3-dimensional (CQ48I) interface elements. An approximate geometric configuration was defined for the construction of the simplified micro model taking into account the actual unit arrangement of the stone masonry prototype as shown in Figure 5.24.
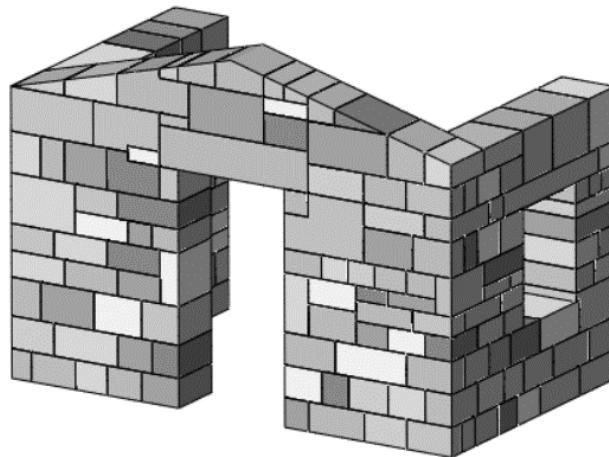
Figure 5.24 Simplified micro model of the stone masonry prototype

The simplified micro model of the stone masonry prototype was subjected to nonlinear static and dynamic analyses in order to investigate its out-of-plane response. For these analyses, the behaviour of the solid elements was kept linear elastic, whereas as the Combined Cracking-Shearing-Crushing material model was defined for the interface elements. The linear elastic material properties defined for the brick and wedge solid elements are summarized in Table 5-9. On the other hand, the material model chosen for the interface elements require the definition of nonlinear parameters for the simulation of mechanisms such as fracture, crushing, and frictional slipping. These nonlinear parameters together with the elastic properties of the interface elements are reported in Table 5-10.

Table 5-9. Mechanical properties of stone units for the simplified micro model of the stone masonry prototype

	Young's modulus (MPa)	Poisson's ratio (-)	Specific weight (kN/m^3)
Stone units	31,500	0.2	23.6

Table 5-10. Mechanical properties of interface elements for the simplified micro model of the stone masonry prototype

Linear parameters	Normal stiffness	k_n	N/mm³	48
	Shear stiffness	k_t		20
Tensile parameters	Tensile strength	f_t	MPa	0.22
	Fracture energy (mode I)	G_f^I	N/mm	0.048
Shear parameters	Cohesion	c	MPa	0.33
	Friction coefficient	$tan\,\varphi$	-	0.75
	Dilatancy coefficient	$tan\,\psi$	-	0
	Fracture energy (mode II)	G_f^{II}	N/mm	0.050
Compressive parameters	Compressive strength	f_c	MPa	5.44
	Shear traction contribution to compressive failure	C_s	-	9
	Fracture energy	G_{fc}	N/mm	8.70
	Equivalent plastic relative displacement	k_p	mm	1

A lateral force proportional to the mass was applied perpendicularly to the main gable wall in positive and negative directions aiming at evaluating the out-of-plane response of the simplified micro model in the static field. The results from these analyses in terms of pushover curves and deformed shapes are illustrated in Figure 5.25. It was observed that when pulling the gable wall against the return wall, the model reached a maximum load capacity of approximately 1.2 times its weight. In addition, this response was characterized by a softening response in the post-peak branch. The mechanism obtained from this model consisted of the failure of the interface element around the opening of the return wall, as well as additional damage along horizontal bed joints in the main gable wall. On the other hand, the simplified micro model experienced a reduction of its maximum load capacity (around 35%) when pulling the main gable wall. In this case, this response presented a low ductility, in which the post-peak behaviour was governed by a smooth loss of the shear capacity. The mechanism that characterized the response of this model involved the formation of horizontal cracks in the left side of the return wall and vertical and diagonal cracks in the right side of the same wall. It was also evidenced that the application of the load in the negative direction produced the failure of vertical mortar joints in the tympanum. Some similarities were identified when comparing the mechanisms from the numerical simulations and the collapse from the shaking table tests mainly related to the crack pattern in the return wall, and in the tympanum.
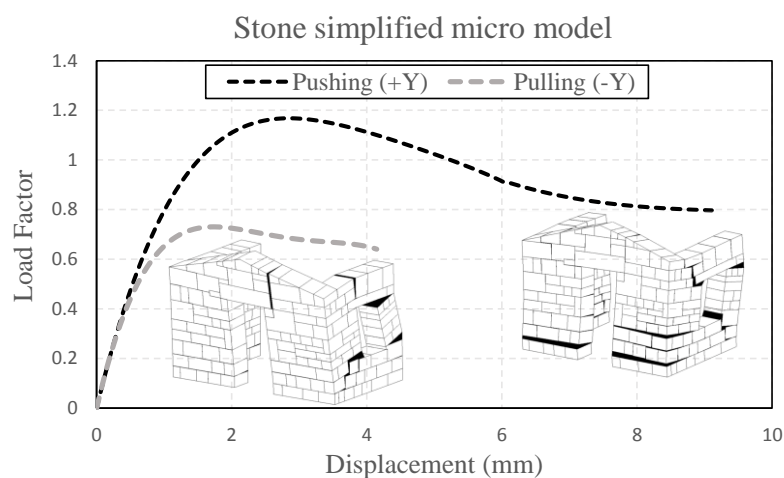
Figure 5.25 Static nonlinear analyses of the simplified micro model of the brick masonry prototype

The simplified micro model of the stone masonry prototype was also subjected to a uniaxial seismic input. Due to the application of time history analysis, the model reached a maximum horizontal displacement of approximately 17 mm at the top of the tympanum as illustrated in Figure 5.26. It is worth noting that the failure mechanism of this model consisted of cracking at the mortar joints generating from the window opening of the return wall. Such in-plane crack pattern was in good agreement with the experimental response. An acceptable resemblance was obtained when comparing the failure mechanism of the main gable wall. Due to the seismic input, the simplified micro model presented vertical cracking at the tympanum. In addition, a stepped detachment of units was observed around the right corner of the main gable wall, leading to a partial overturning of the tympanum.
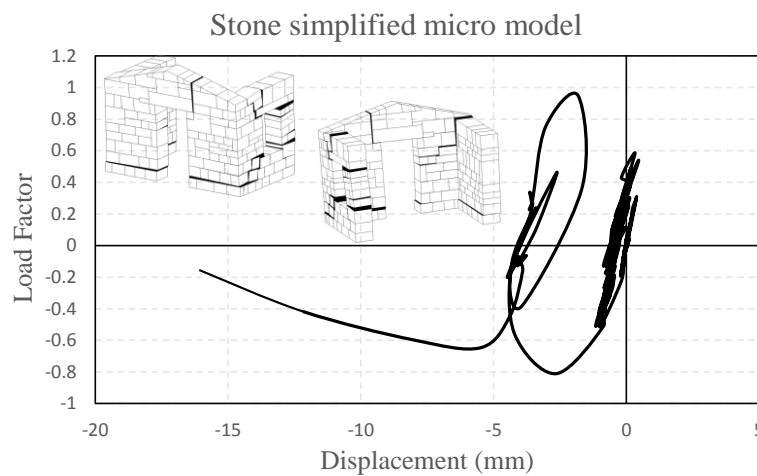
Figure 5.26 Dynamic nonlinear analyses of the simplified micro model of the brick masonry prototype

5.3.3 MACRO-ELEMENT MODEL

The macro-element modelling approach implemented in the HiStrA software [149] was also employed for the assessment of the out-of-plane response of the stone masonry prototype. The numerical model, depicted in Figure 5.27, was composed of regular and irregular 3-dimensional macro-elements. The assessment of the out-of-plane response in the static field was also conducted by applying an incremental lateral force to the main gable wall. On the other hand, such assessment in the dynamic field required the application of time history analysis based on a uniaxial accelerogram.

For the definition of the mechanical properties of the macro-element model, the values obtained from the mechanical characterization of the stone masonry wallets were considered for Young's modulus E, specific weight γ, tensile f_t, and compressive f_c strengths. The tensile and compressive behaviour were also governed by exponential and parabolic curves, respectively. The values for fracture energy in tension G_f^I and compression G_c were defined in accordance with the FE macro model. Following the same approach as the brick masonry prototype, the cohesion c was considered equal to the tensile strength, and the value for fracture energy for shear-sliding G_f^{II} was adopted as 1.5 times the value of fracture energy in tension G_f^I. Similarly, the ratio between shear strength f_s under no confinement conditions and tensile strength f_t was considered as 0.67. These mechanical properties are detailed in Table 5-11.
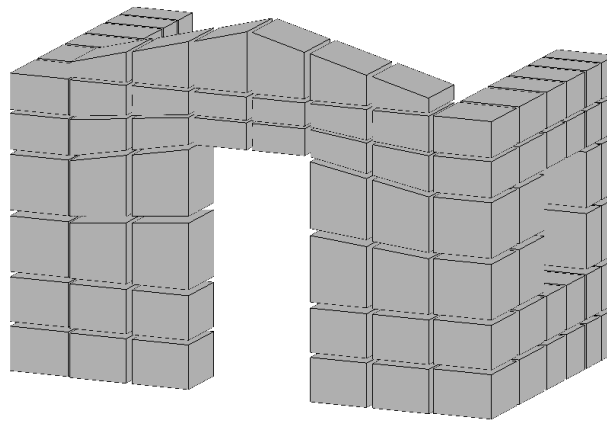
Figure 5.27 Macro-element model of the brick masonry prototype

Table 5-11. Mechanical properties of the macro-element model of the stone masonry prototype

Linear parameters	Young's modulus	E	GPa	2.08
	Shear modulus	G	GPa	0.87
	Specific weight	γ	kN/m³	23.6
Tensile parameters	Tensile strength	f_t	MPa	0.22
	Fracture energy	G_f^I	N/mm	0.048
Compressive parameters	Compressive strength	f_c	MPa	5.44
	Fracture energy	G_{fc}	N/mm	8.70
Shear-diagonal parameters	Shear strength	f_s	MPa	0.15
	Friction coefficient	μ_d	-	0.60
Shear-sliding parameters	Cohesion	c	MPa	0.22
	Friction coefficient	μ_s	-	0.70
	Fracture energy	G_f^{II}	N/mm	0.072

The results from the application of an incremental mass distributed lateral force in directions perpendicular to the main gable wall are illustrated in Figure 5.28. These results were provided in terms of pushover curves and failure mechanisms for positive and negative directions. A maximum load factor of approximately 1.72 was obtained when pushing the main gable wall. The post-peak branch was characterized by a sudden loss of the maximum load capacity (around 35%) and a subsequent smooth softening behaviour. The failure mechanism of the macro-element model consisted of concentration of strains in the return wall around the window opening. Additional damage was obtained horizontally in the main gable wall, and diagonally along the connection between the main gable wall and the return wall. A reduction of 30% of the maximum load capacity was obtained when applying the incremental lateral force in the negative direction (load factor of approximately 1.2). In addition, the response of the macro-element model was described by a softening post-peak behaviour. In this case, a similar concentration of strains was evidenced in the return wall with window opening. However, the out-of-plane collapse consisted of the detachment of the left side of the return wall.
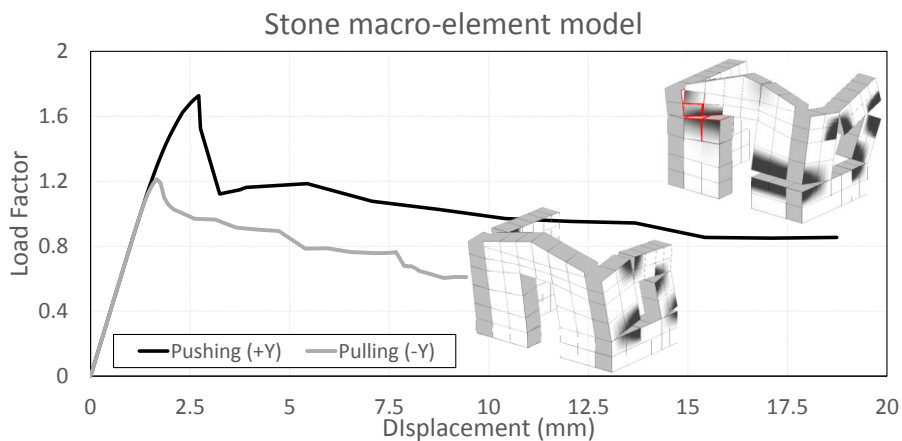
Figure 5.28 Static nonlinear analyses of the macro-element model of the brick masonry prototype

The assessment of the out-of-plane response of the stone masonry prototype by means of the macro-element modelling approach was conducted by means of the application of time history analysis. The numerical procedure for the solution of the dynamic equilibrium and the dissipation of energy were also based on a Newmark method [158] and a Rayleigh viscous damping criterion (damping ratio ζ = 5%). In the same manner as the brick masonry prototype, the unloading cycles of this model were governed by a secant stiffness for the tensile behaviour (β_t = 1), and an initial stiffness for the compressive and shear-diagonal behaviours ($\beta_c = \beta_d = 0$). Due to the application of time history analysis, the macro-element model experienced maximum displacements of approximately 5 mm and 9 mm in positive and negative directions, respectively. The return wall presented an in-plane mechanism which consisted on concentration of strains along the window opening. On the other hand, the out-of-plane failure mechanism of the main gable wall was characterized by its detachment from the remaining return wall. It was possible to observe that additional damage was concentrated in the centre of the tympanum. The mechanism of this macro-element model, as well as the load factor-displacement hysteresis curve, are illustrated in Figure 5.29. It was evidenced that the in-plane mechanism was in good agreement with the experimental response. Some similarities such as damage in the tympanum and the concentration of strains in the right side of the main gable wall were identified regarding the out-of-plane mechanism. However, it is worth noting that the detachment of the main gable wall obtained in the macro-element model did not correspond to the out-of-plane collapse due to the shaking table tests. Still, an acceptable agreement between these responses was determined.
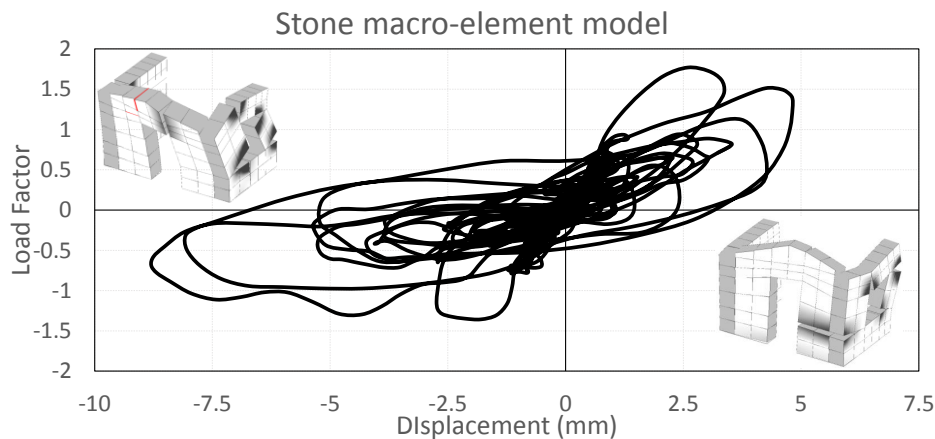
Figure 5.29 Dynamic nonlinear analyses of the macro-element model of the brick masonry prototype

The comparison between the FE and macro-element models of the stone masonry prototype was also conducted taking into consideration the rotating total strain crack model since it also simulated the quasi-brittle response of URM structures. From the pushover curves when applying an incremental lateral load in the positive direction (pushing the main gable wall), a slight difference in the initial stiffness was evidenced (see Figure 5.30a). It was also observed that the macro-element model presented a higher maximum load capacity (around 6% more). Both models are characterized by a softening behaviour. Unlike the macro-element model, the post-peak branch of the FE model was marked by a low ductile response. Both in-plane mechanisms of the return wall are in good agreement, presenting concentration of damage around the opening. But these two models were characterized by slightly different out-of-plane mechanisms related to the small displacement reached in the pushover analysis of the FE model. When applying the lateral load in a negative direction (pulling the main gable wall), both models presented a similar maximum load capacity (see Figure 5.30b). It was noted that both responses were characterized by a softening behaviour. However, in the case of the FE model presented a rapid decrement of the load capacity. Nevertheless, a similar residual force was obtained with both models. Regarding the in-plane mechanism, the failure of the return wall in the FE model coincided with the one obtained in the macro-element model. This similarity was not established when comparing the out-of-plane response of the main gable wall.

From the application of time history analyses, it was possible to observe a significant coincidence in terms of hysteric response between the two models. In addition, a similar maximum displacement of approximately of 5 mm at the top of the tympanum was reached in a positive direction as illustrated in Figure 5.30c and Figure 5.30d. On the contrary, the corresponding displacement in the negative direction presented a lower value for the macro-element model. Regarding the failure mechanisms of these models, the in-plane responses were characterized by an acceptable agreement consisting of strains located in the opening of the return wall. The out-of-plane mechanisms presented slightly different behaviour when comparing the FE and macro-element models.
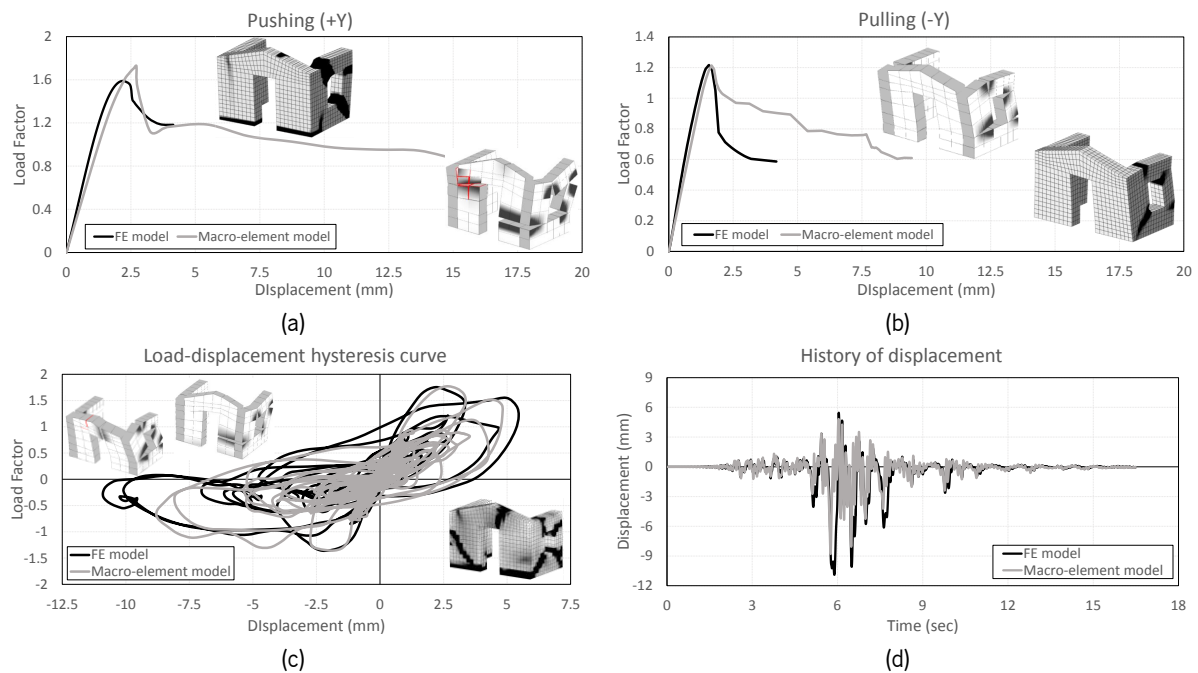
Figure 5.30 Comparison of the out-of-plane response of the stone masonry prototype based on FE and macro-element models: pushover analyses in (a) positive and (b) negative direction, (c) load-displacement hysteresis curve, and (d) history of displacement

It is worth noting that an assessment of the computational demand was also conducted for the stone masonry prototype. The FE model of the stone masonry prototype, characterized by 40545 DOFs, required approximately 21 hours for the application of time history analysis. On the other hand, the corresponding computational demand needed for the application of dynamic nonlinear analysis to the macro-element model was around 45 minutes, leading to a reduction of 96%. In this regard, the macro-element model was characterized by a significantly low number of DOFs equal to 714. A brief description of the computation effort of both modelling approaches is summarized in Table 5-12.

Table 5-12. Computation effort for the application of time history analyses on the FE and macro-element models of the stone masonry prototype

FE model	Macro-Element model
Duration	Duration (reduction)
21 hours	45 minutes (–96%)

The failure mechanisms of the different numerical models (FE and macro-element approaches) subjected to static and dynamic nonlinear analyses, as well as a simplified schematic configuration of the collapse mechanism obtained experimentally from the shaking table tests are depicted in Figure 5.31.

DIANA FE MODEL
Fixed crack model
(Shear retention 0.20)

DIANA FE MODEL
Fixed crack model
(Shear retention 0.05)

DIANA FE MODEL
Rotating crack model

HiStrA MACRO-MODEL

(a)　　　　　　　　　　　　　　　　　　　(b)

DIANA FE MODEL
Fixed crack model
(Shear retention 0.20)

DIANA FE MODEL
Fixed crack model
(Shear retention 0.05)

DIANA FE MODEL
Rotating crack model

HiStrA MACRO-MODEL

(c)　　　　　　　　　　　　　　　　　　　(d)

DIANA FE MODEL
Fixed crack model (β_s=0.20)
(Maximum strain)

DIANA FE MODEL
Fixed crack model (β_s=0.05)
(Maximum strain)

DIANA FE MODEL
Rotating crack model
(Maximum strain)

(e)

HiStrA MACRO-MODEL
(Positive direction)

HiStrA MACRO-MODEL
(Negative direction)

SHAKING TABLE TESTS

No damage　Damage　Collapse

(f)　　　　　　　　　　　　　　　　　　　(g)

Figure 5.31 Failure mechanisms of the stone masonry prototype: pushover analyses in positive and negative directions of (a, c) FE and (b, d) macro-element models, dynamic analyses of (e) FE and (f) macro-element models, and (g) shaking table tests.

5.4 FINAL CONSIDERATIONS

The results of the numerical simulations for the assessment of the out-of-plane response of two URM structures are presented in this Chapter. These structures, made of fired brick and stone units, were experimentally tested by means of shaking table tests up to collapse. The numerical assessment of the out-of-plane response of these structures was conducted considering two different computational tools. Both masonry structures were investigated by means of the FE method considering macro and simplified micro modelling approaches. The latter computational tool corresponded to the simplified macro-element model described in Chapter 3. The numerical models were subjected to an incremental mass distributed lateral force in positive and negative directions aiming at assessing the out-of-plane response of the gable

wall in the static field. In addition, the evaluation of this response in the dynamic field was carried out by applying the last ground motion registered from the shaking table tests to the numerical models.

The influence of mesh and material dependencies on the out-of-plane response of the FE macro model was investigated by means of pushover analyses conducted to the masonry prototypes. The mesh dependency was assessed by considering different discretized configurations along the thickness of the gable wall. It was noted that the mesh refinement influenced only moderately the maximum load capacity and post-peak behaviour of the FE models. On the other hand, the material dependency was evaluated by the selection of different constitutive models, evidencing a high influence mainly on the post-peak branch in positive and negative directions. A high resemblance was identified regarding the in-plane response of the return wall of the FE models when comparing it to the collapse due to the shaking table tests. Nevertheless, the out-of-plane collapse mechanism was not so successfully reproduced by means of this modelling approach. The material dependency was also assessed by means of time history analyses. It was possible to observe the high influence that it played on the ductility of the dynamic response. It is worth noting that the in-plane failure mechanisms obtained in the dynamic nonlinear field coincided with the experimental results. Based on the results obtained from the simplified micro models, a small difference on the maximum load capacity was evidenced when comparing them to the ones from the FE macro models. This difference may be related to an anisotropic behaviour of masonry that characterizes this modelling approach. The results obtained from the simplified micro models provided a more accurate resemblance to the experimental response. In this model, the failure mechanisms, especially for the stone masonry prototype, were concentrated along the mortar joints. Despite this, such sophisticated modelling approach requires a high expertise not only for a proper definition of the material properties but also for the interpretation of the numerical results.

Finally, it was possible to simulate the results from the FE macro models by means of the simplified macro-element modelling approach. For this purpose, a comparison was carried out considering the FE model based on rotating cracks since it resembled better the quasi-brittle behaviour that characterizes URM structures. Good agreement in terms of maximum load capacity, post-peak behaviour, and in-plane failure mechanisms in the static field was obtained between the two modelling approaches. Reasonably similar results were obtained in the dynamic field, such as maximum horizontal displacement at the top of the tympanum, hysteretic response, and in-plane failure mechanisms. Nevertheless, some differences regarding the out-of-plane mechanisms were also identified. It is worth noting that an assessment of the mesh dependency of the macro-element modelling approach was carried out to the brick masonry prototype by means of static and dynamic nonlinear analyses. It was evidenced that no strong influence was obtained when increasing the number of elements since a good agreement in terms of maximum load capacity, post-peak behaviour, failure mechanisms, and maximum top displacements was obtained. To conclude, a comparison between the computational demands required for the application of time history analyses was conducted. A significant reduction of the time (1 to 20) was attained by means of the macro-element modelling approach making it a rather suitable computational tool for the seismic assessment of URM structures in engineering applications.

CHAPTER 6

SEISMIC VULNERABILITY OF URM STRUCTURE

6.1 INTRODUCTION

The current Chapter aims at the assessment of the seismic vulnerability of one URM structure characterized by a marked out-of-plane failure mechanism. Such assessment was conducted by means of the application of nonlinear dynamic analyses using a software based on a simplified macro-element modelling approach characterized by a reduced computational burden. The assessment of the seismic vulnerability of this structure begins with the definition of three limit states in accordance with the EC8-Part3, namely Damage Limitation, Significant Damage, and Near Collapse, respectively. For this purpose, an alternative procedure consisting on the estimation of the displacement capacity for each limit state due to the application of nonlinear static analyses is employed. Subsequently, the seismic vulnerability assessment was carried out taking into consideration two approaches, namely deterministic and probabilistic, respectively. In the first one, the uncertainty was focused on the seismic input composed by artificial accelerograms. For this purpose, the artificial accelerograms were generated in accordance with the EC8-Part 1 together with the Portuguese National Annex. In this regard, over 840 artificial accelerograms based on far- and near-field earthquakes were generated and further subjected to a baseline correction process. In the second approach, the uncertainty was focused on the mechanical properties of the model, together with the thickness of the wall and the viscous damping ratio. It is worth noting that in this case the application of time history analyses was also based on artificial accelerograms. The derivation of fragility curves considered a fitting process based on a maximum likelihood approach.

6.2 CAPACITY DOMINIUM

The proper definition of Limit States (LSs) corresponds to one of the key aspects when assessing seismic vulnerability. These LSs can be defined based on inter-story drifts, damaged area, shear capacity or hysteretic energy, as established in several standards or codes [114-116, 118, 119, 123] and proposed by different authors [128, 144, 169, 170]. Inter-story drift-based procedures are commonly used for the assessment of the behaviour of masonry structures when subjected to seismic loading. For instance, the EC8-Part3 proposes three LSs together with their corresponding drift capacities. The first LS, named Damage Limitation, presents a drift capacity associated with the yielding displacement of the masonry structure. The second LS, denoted as Significant Damage, presents a drift capacity whose definition is associated with the type of mechanism that characterises the failure of the masonry structure. In this regard, a drift capacity of 0.4% is established for a shear failure, whereas 0.8% (H_0/L) is related to a flexural failure, being H_0 the distance between the section in which the flexural capacity is attained and the contra-flexure point, and L the in-plane length of the wall. The remaining one, denoted as Near Collapse, is described by a drift capacity which can be estimated as 4/3 time the one associated with a Significant Damage LS. The Italian Code [119] establishes an Ultimate Limit State (ULS) in which the drift capacity is defined in a similar manner as the Significant Damage LS from the EC8-Part3 [116]. In this sense, the value associated with a shear failure mechanism corresponds to 0.4%, whereas the one related to a flexural failure mechanism does not take into consideration the slenderness ratio H_0/L (drift capacity equal to 0.8%).

In addition, a Heavy Damage LS proposed by FEMA 306 [115] also provides different drift capacities associated with failure mechanisms. A drift capacity of 0.8% (H_S/L) is established when the failure of the structure is characterised by horizontal cracking due to rocking, being H_S the free height between two stories. In the case of sliding failure along the mortar joints, FEMA 306 provides a drift capacity of 0.4%. FEMA 306 also establishes drift capacities for mixed failure mechanisms, mainly related to squat walls. In this sense, when the failure is described by toe crushing, flexural cracking and bed joint sliding, the drift capacity presents a value of 1.2%, whereas, for a combined flexural cracking and toe-crushing failure, the drift capacity corresponds to 0.3%. It is worth noting that when the failure of a structure is described by diagonal cracking, this LS is not determined by drift capacity, but as a function of ductility capacities. On the other hand, FEMA 273 [114] also defines drift capacities based on failure mechanisms in accordance with a Near Collapse LS. In this case, the drift capacities are established as 0.4% (H_S/L) and 0.4% for flexural and shear failure mechanisms, respectively. It is worth mentioning that these drift capacities present a lower value when compared to the ones proposed by EC8-Part3. A detailed comparison between the different proposal regarding inter-story drift capacities and the definition of LSs can be found in the work conducted by Petry and Beyer [171].

The definition of these drift capacities is mainly associated with the in-plane behaviour of masonry structures with a box-type behaviour. Nevertheless, the estimation of ultimate drift capacities representative of the complex and predominant out-of-plane collapse mechanisms of URM structures becomes a subjective choice. For this reason, a more rational approach for the definition of the structural capacity and corresponding LSs is needed. In this sense, the EC8-Part3 together with the Italian code

also establish LSs based on the shear capacity of the structure. These LSs, denoted respectively as Near Collapse and Life Safety for EC8-Part3 and the Italian code, are defined by an ultimate horizontal displacement reached when the structure experiences a 20% loss of its shear capacity.

Taking into consideration this shear capacity-based formulation, this Chapter aims at presenting an alternative procedure for the identification of the LSs of the brick masonry prototype, a URM structure characterised by an out-of-plane collapse mechanism. This procedure, denoted as *Capacity Dominium*, consists initially on the application of nonlinear static analyses along different directions of the structure as reported by Cannizzaro, et al. [172]. For this purpose, the brick masonry prototype was subjected to sixteen pushover analyses, with an incremental angular step of 22.5° as illustrated in Figure 6.1. For these analyses, the applied load consisted of an incremental mass distributed lateral force in the given directions. In addition, three points in the brick masonry prototype were considered as control nodes for the application of nonlinear static analyses: one located at the top of the tympanum, and two placed at the top of the end of both return walls. The selection of these points was based on the occurrence of out-of-plane failure mechanisms of this structure.
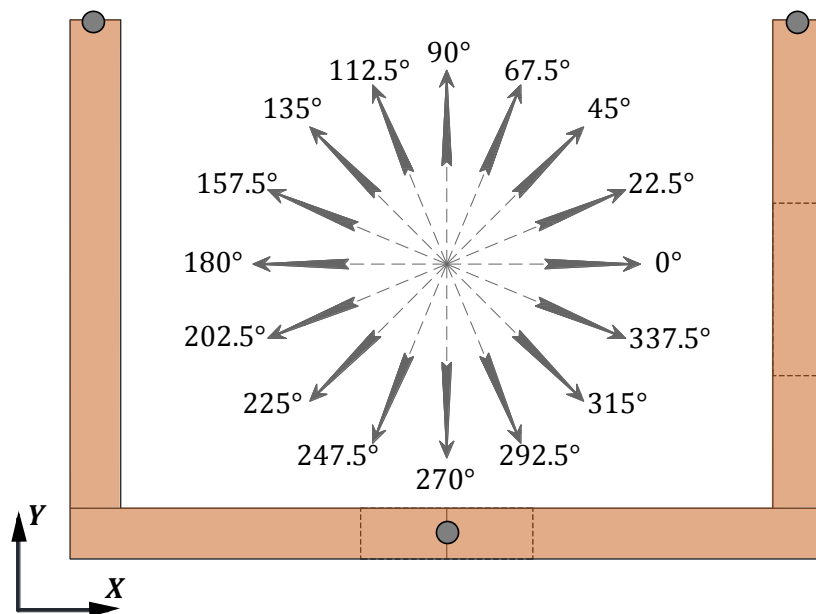
Figure 6.1. Procedure for the computation of a Capacity Dominium by means of the application of static nonlinear analyses to brick masonry prototype with an angular step of 22.5°.

The response of the brick masonry prototype due to the application of these pushover analyses is given by the load factor vs horizontal displacement curves depicted in Figure 6.2 and Figure 6.3. From these results, it was possible to observe that this structure presented load factors ranging between 0.8 and approximately 1.3. In addition, the failure mechanisms were basically characterised by the out-of-plane collapse of the main gable wall or the return walls. The pushover curves presented a sudden reduction of the maximum load capacity which confirms the quasi-brittle behaviour of this typology of structures.
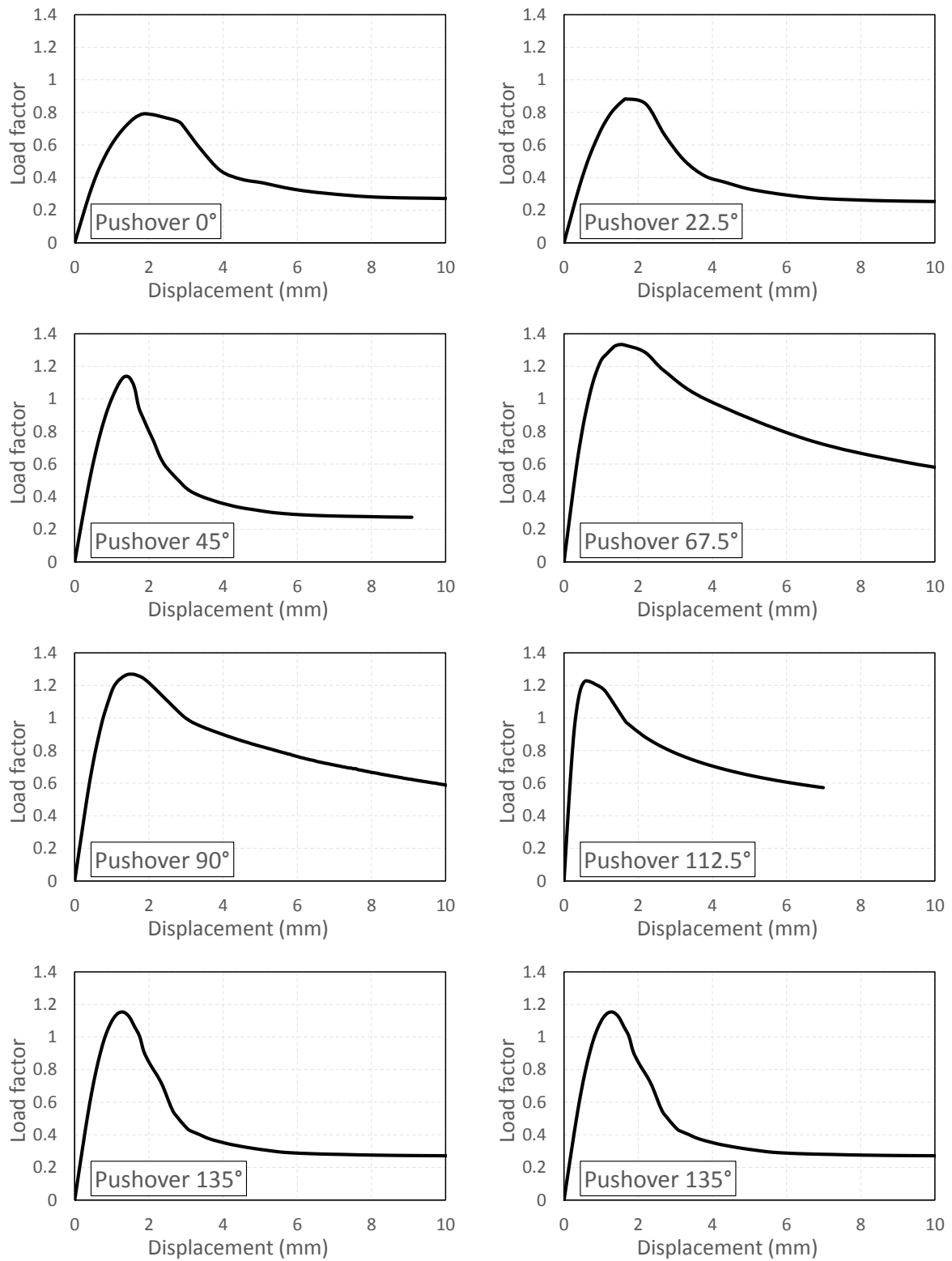
Figure 6.2. Pushover curves due to the application of lateral forces with angles of 0°, 22.5°, 45°, 67.5°, 90°, 112.5°, 135°, and 157.5°, with respect to façade wall.
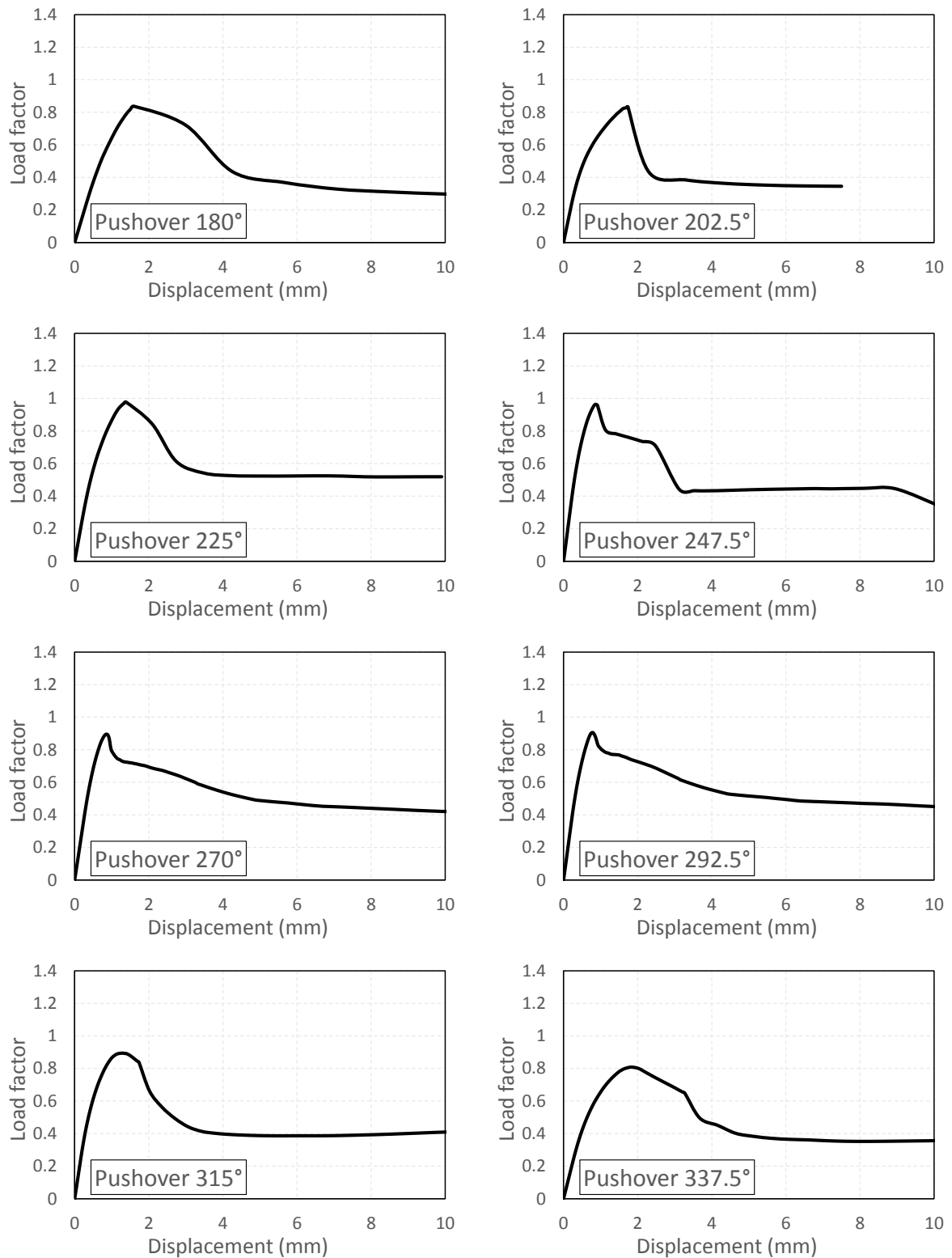
Figure 6.3. Pushover curves due to the application of lateral forces with angles of 180°, 202.5°, 225°, 247.5°, 270°, 292.5°, 355°, and 337.5°, with respect to façade wall.

For the construction of the *Capacity Dominium*, the definition of ultimate displacements associated with a Near Collapse LS was required. In this sense, the pushover curves were limited until the structure experienced a 20% reduction of its maximum load capacity as stated by the EC8-Part3 [116] and the Italian code [119]. Subsequently, the pushover curves were drawn backwards along their corresponding directions and at an equal distance from the origin. As illustrated in Figure 6.4a, the sixteen pushover curves were drawn backwards, at a distance of 8 mm from the origin point O. Afterward, the pushover curves were connected by means of patches aiming at the creation of a basket domain as illustrated in Figure 6.4b. This basket domain corresponded to a three-dimensional representation of the capacity of the brick masonry prototype associated with a Near Collapse LS. In this figure, the horizontal axes are associated with to the displacement in X and Y directions, whereas the vertical axis is related to the load factor (ratio between base shear and self-weight).

(a)

(b)
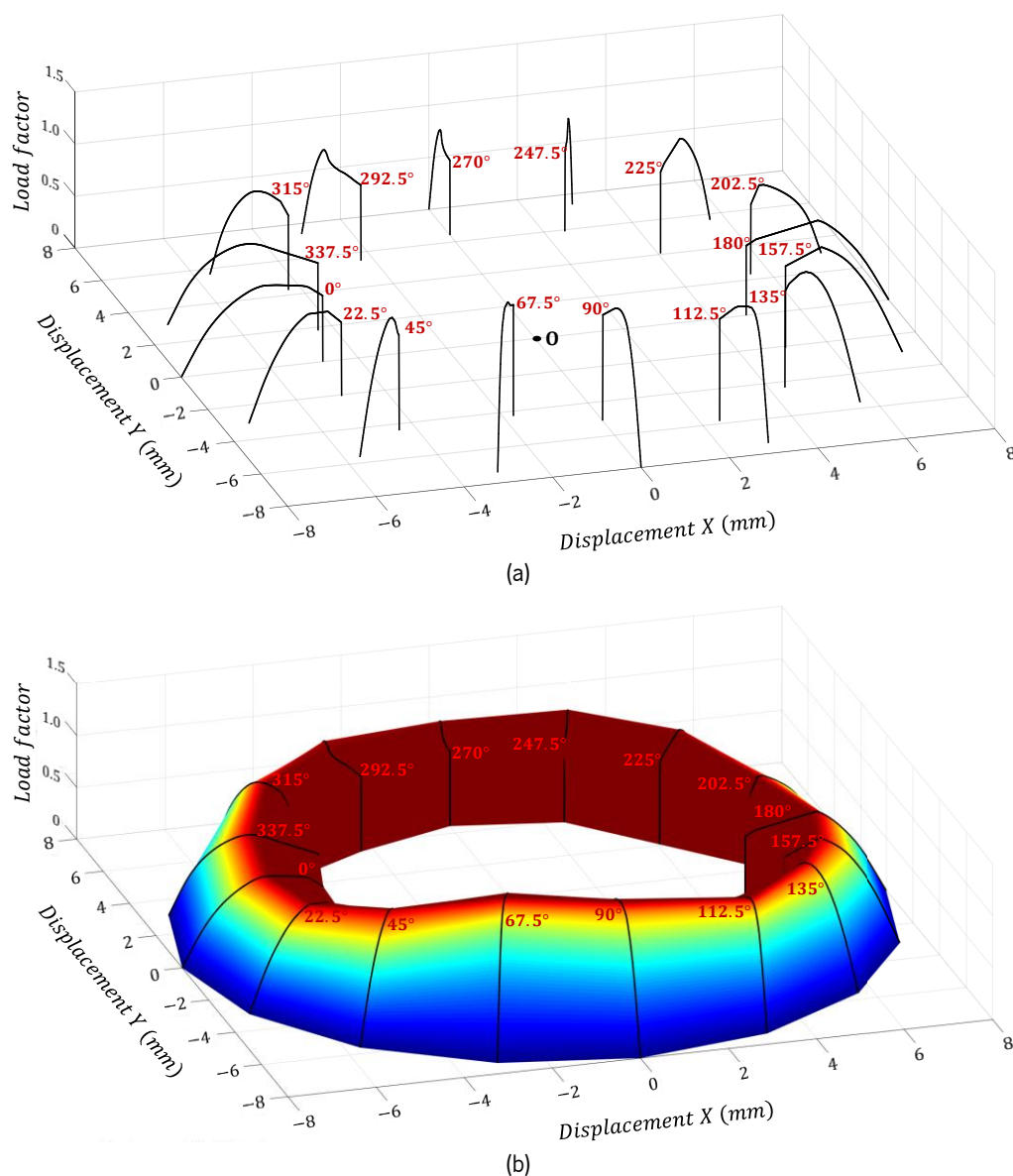
Figure 6.4. Construction of *Capacity Dominium*: (a) pushover curves drawn backwards, and (b) creation of a basket domain associated with a Near Collapse LS.

The *Capacity Dominium* associated with a Near Collapse LS can be properly identified from this three-dimensional representation of the capacity of the structure when subjected to nonlinear static analyses. As illustrated in Figure 6.5a, the *Capacity Dominium* of such LS is defined by the area generated by the connection of the nodes placed at a distance (from the origin O) equal to the effective horizontal displacement in the basket domain along their corresponding direction. In a similar manner, the *Capacity Dominium* for a Damage Limitation LS was defined by the area composed by the nodes located at a distance in the basket domain associated with yielding displacement, and it is given by the blue area in Figure 6.5b. Besides these LSs, a Significant Damage LS was also taken into consideration for the assessment of the seismic vulnerability of the brick masonry prototype. In this regard, a ratio of 4/3, as provided by the EC8-Part3 [116], was established between the displacement capacity of Near Collapse and Significant Damage LSs. The *Capacity Dominium* associated with this LS is depicted in the red area in Figure 6.5b. Based on this displacement capacity formulation, it was assumed that a certain LS was reached or exceeded when the response of the structure is located outside the area of its corresponding *Capacity Dominium*.
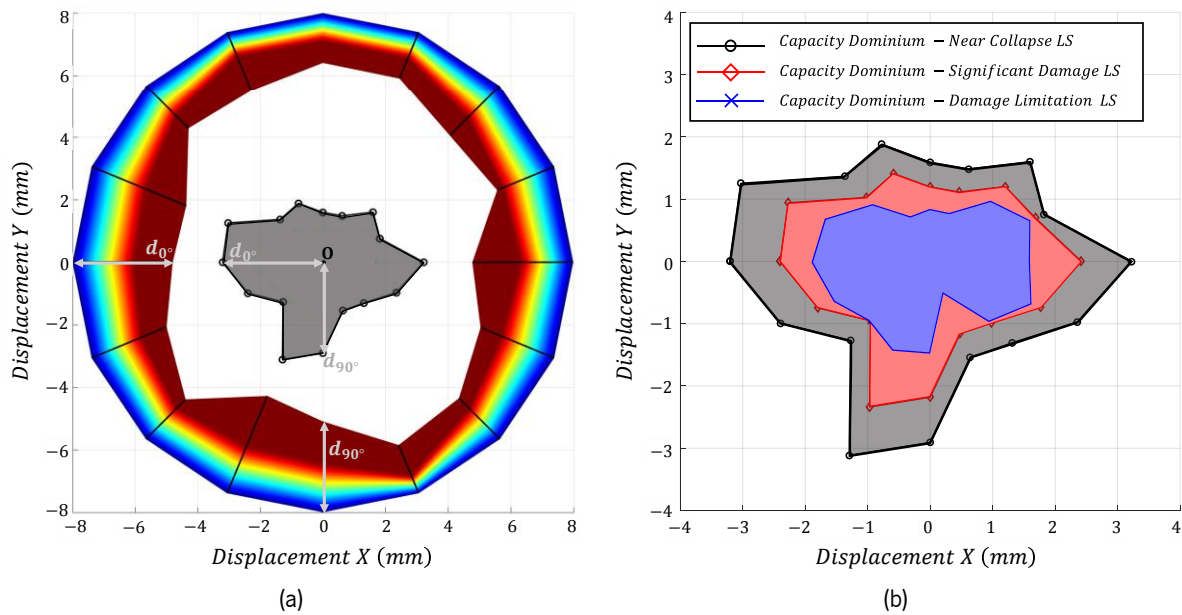
Figure 6.5. *Capacity Dominium*: (a) definition of displacement capacity of a Near Collapse LS by the definition of the effective horizontal displacement along each direction, and (b) displacement capacities associated with the three LSs defined for this investigation.

6.3 DERIVATION OF FRAGILITY CURVES

The assessment of the seismic vulnerability of the brick masonry prototype was conducted by means of the analytical derivation of fragility curves. This statistical approach is considered a suitable tool since it is capable of estimating the probability of reaching or exceeding a certain LS in accordance with an Intensity Measure IM. The fragility curves are defined by the normal cumulative distribution function Φ given by equation 6-1 in which θ and β correspond to the mean value and standard deviation, respectively. As reported in the previous section, the seismic vulnerability of the brick masonry prototype

was investigated taking into consideration three LSs, namely Damage Limitation, Significant Damage, and Near Collapse, respectively. Moreover, the IM defined for this investigation corresponded to the PGA since it can provide a clearer mechanical meaning of the intensity and severity of a given ground motion.

$$P(LS|IM = x) = \Phi\left(\frac{\ln\left(x/\theta\right)}{\beta}\right)$$

6-1

In the scope of this investigation, the brick masonry prototype was subjected to nonlinear dynamic analyses based on three-component accelerograms artificially generated according to the EC8-Part1. In addition, the seismic vulnerability of this URM structure was assessed considering two different approaches. The first one, denoted as deterministic approach, consisted of the application of a variety of artificial accelerograms with values of PGA ranging between 0.45 g and 0.80 g. In this first assessment, the uncertainty was focused solely on the seismic input, whereas the mechanical and geometrical parameters presented a deterministic value. On the other hand, in the second investigation, denoted as probabilistic approach, the uncertainty was focused on the mechanical and geometrical parameters which were defined by probability density functions. It is worth noting that in this last assessment, the seismic input also consisted of the application of nonlinear dynamic analyses based on artificial accelerograms with values of PGA ranging between 0.45 g and 0.80 g.

6.3.1 GENERATION OF SEISMIC INPUT

The assessment of the seismic vulnerability of the brick masonry prototype consisted on the application of time history analyses based on three-component artificial accelerograms. The generation of these artificial accelerograms was based on the specifications provided by the EC8-Part1 [173]. The code states that the accelerograms should be generated so that they match the elastic response spectrum with a 5% of viscous damping. For this investigation, elastic response spectra associated with far- and near-field earthquakes were taken into consideration. In this sense, the definition of the horizontal component of the elastic response spectrum corresponding to far- and near-field earthquakes, also denoted as Type 1 and Type 2, respectively, is given throughout equations 6-2, 6-3, 6-4, and 6-5.

$$0 \leq T \leq T_B \qquad S_e(T) = a_g \cdot S \cdot \left(1 + \frac{T}{T_B} \cdot (2.5 \cdot \eta - 1)\right)$$

6-2

$$T_B \leq T \leq T_C \qquad S_e(T) = a_g \cdot S \cdot 2.5 \cdot \eta$$

6-3

$$T_C \leq T \leq T_D \qquad S_e(T) = a_g \cdot S \cdot 2.5 \cdot \eta \cdot \left(\frac{T_C}{T}\right)$$

6-4

$$T_D \leq T \leq 4s \qquad S_e(T) = a_g \cdot S \cdot 2.5 \cdot \eta \cdot \left(\frac{T_C \cdot T_D}{T^2}\right)$$

6-5

where $S_e(T)$ is associated with a horizontal component of the elastic response spectrum associated with a horizontal component, a_g is the design ground acceleration on a type A ground, S corresponds to the soil factor, T is the vibration period, η is the damping correction factor equal to 1 for 5% of viscous damping, T_B and T_C are related to the lower and upper limit of period presenting a constant spectral acceleration branch, and T_D is related to the period in which a spectral displacement begins.

For the generation of the artificial accelerograms, the design ground acceleration a_g was considered equal to 1 g, whereas the soil factor presented a value of 1 based on the assumption that the brick masonry prototype was located in a Lisbon area characterized by a soil type A. On the other hand, the definition of the periods T_B, T_C and T_D was also associated with the characteristics of the soil type, and their corresponding value varies according to the specifications reported by each country. In this sense, the values of these periods are provided by the Portuguese National Annex [174]. The values of these periods together with additional parameters for the definition of horizontal elastic response spectra Type 1 and Type 2 are summarised in Table 6-1.

Table 6-1. Parameters for the definition of horizontal elastic response spectrum

Elastic response spectrum	Soil type	S	η	T_B(s)	T_C(s)	T_D(s)
Type 1	A	1	1	0.10	0.60	2.00
Type 2	A	1	1	0.10	0.25	2.00

In a similar way, the definition of the vertical component of the elastic response spectra associated with far- and near-field earthquakes is expressed throughout equations 6-6, 6-7, 6-8, and 6-9. In this case, the elastic response spectrum $S_e(T)$ is associated with a vertical design ground acceleration a_{vg}, together with the vibration period T, the periods that describe the constant spectral acceleration (T_B and T_C) and spectral displacement (T_D), and the damping correction factor η (equal to 1). The values proposed by the Portuguese National Annex [174] for the vertical design ground acceleration a_{vg} as a function of the horizontal acceleration a_g, as well as the periods that describe the elastic response spectrum, are reported in Table 6-2.

$$0 \leq T \leq T_B \qquad S_e(T) = a_{vg} \cdot \left(1 + \frac{T}{T_B} \cdot (3.0 \cdot \eta - 1)\right) \qquad \text{6-6}$$

$$T_B \leq T \leq T_C \qquad S_e(T) = a_{vg} \cdot 3.0 \cdot \eta \qquad \text{6-7}$$

$$T_C \leq T \leq T_D \qquad S_e(T) = a_{vg} \cdot 3.0 \cdot \eta \cdot \left(\frac{T_C}{T}\right) \qquad \text{6-8}$$

$$T_D \leq T \leq 4s \qquad S_e(T) = a_{vg} \cdot 3.0 \cdot \eta \cdot \left(\frac{T_C \cdot T_D}{T^2}\right) \qquad \text{6-9}$$

Table 6-2. Parameters for the definition of vertical elastic response spectrum

Elastic response spectrum	a_{vg}	η	T_B (s)	T_C (s)	T_D (s)
Type 1	0.75 a_g	1	0.05	0.25	1
Type 2	0.95 a_g	1	0.05	0.15	1

The generation of artificial accelerograms was conducted based on the elastic response spectra associated with far-field (see Figure 6.6a) and near-field (see Figure 6.6b) earthquakes. For this purpose, the EC8-Part1 [173] also states that the artificial accelerograms should present a minimum duration of stationary part according to site specifications. In accordance with the Portuguese National Annex [174], stationary times of 30 seconds and 10 seconds should be considered when generating artificial accelerograms based on elastic response spectra Type 1 and Type 2, respectively. Based on these specifications, the duration of the artificial accelerograms corresponded to 40 seconds and 20 seconds for far- and near-field earthquakes, respectively.
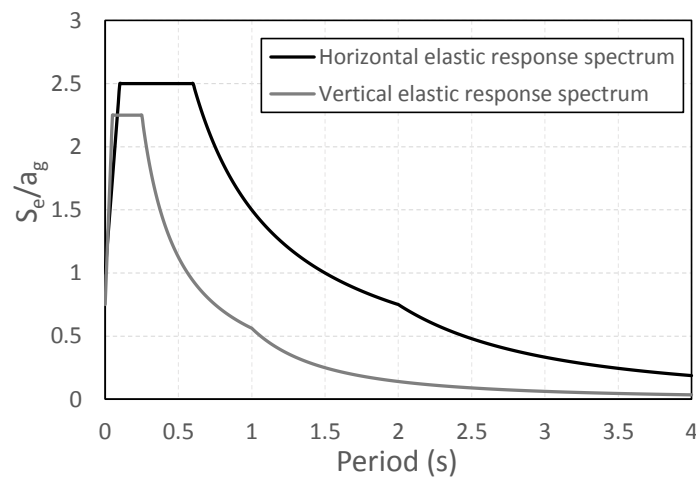
(a)
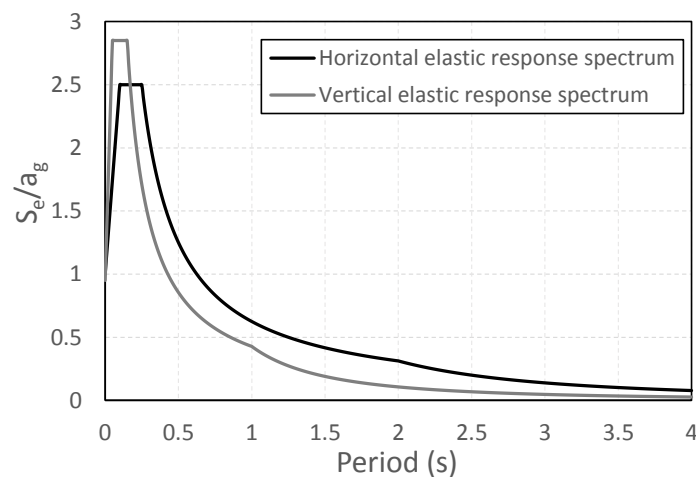
(b)

Figure 6.6. Horizontal and vertical elastic response spectra used for the generation of artificial accelerograms based on (a) far-field (Type 1), and (b) near-field (Type 2) earthquakes

Over 1200 horizontal and 600 vertical artificial accelerograms, based on a horizontal PGA of 1.0 g, were initially generated using the software SIMQKE [175]. It is worth noting that for a horizontal component of the elastic response spectrum, artificial accelerograms in X and Y directions should be uncorrelated; and therefore, their generation was conducted separately. An initial assessment regarding the accuracy of the artificial accelerograms was conducted based on their response spectrum. From this initial assessment, the artificial accelerograms whose spectrum did not present a good resemblance with the elastic response spectrum used for their generation were discarded. After this comparison, 560 horizontal and 280 vertical artificial accelerograms associated with far- and near-field earthquakes were selected for the application of time history analyses aiming at the assessment of the seismic vulnerability of the brick masonry prototype. These artificial accelerograms were subsequently subjected to a baseline correction using the software LNEC-SPA [176]. The signal processing of these accelerograms was conducted taking into consideration a bandpass Fourier filter of 0.20 Hz, together with a cosine-based windowing approach.

6.3.2 DETERMINISTIC APPROACH

The deterministic approach consisted of the application of 280 nonlinear dynamic analyses to the macro element model of the brick masonry prototype aiming at assessing its seismic vulnerability. From these analyses, 140 were associated with artificial accelerograms generated based on an elastic response spectrum Type 1, whereas the remaining were related to an elastic response spectrum Type 2. Since the artificial accelerograms were generated considering a design acceleration equal to 1 g, it was necessary to apply scale factors aiming at comprising a wider range of accelerations. In this sense, the brick masonry prototype was subjected to artificial accelerograms characterised by different values of PGA. These values ranged between 0.45 g and 0.80 g with an incremental step of 0.05 g, reaching a total of eight PGAs. For this initial investigation, the uncertainty was only focused on the seismic input which consisted on the definition of different horizontal and vertical artificial accelerograms throughout each analysis. It is worth noting that the mechanical and geometrical properties of the macro-element model were characterised by a deterministic behaviour, presenting the same values used for the assessment of the brick masonry prototype in Chapter 5.

The performance of the brick masonry prototype due to the application of time history analyses was evaluated considering the *Capacity Dominium* described in Section 6.2. It is worth noting that this evaluation was focused only on the main gable wall assuming that the return walls are not characterized by an out-of-plane failure mechanism. This assumption was based on the hypothesis that in real structures, these walls may be properly connected to other structural elements which limit their out-of-plane behaviour. In this regard, the dynamic response of the macro-element model in terms of displacements at the top of the tympanum was plotted together with the *Capacity Dominium* of a corresponding LS. For instance, Figure 6.7a illustrates the dynamic response the brick masonry prototype subjected to Type 2 artificial accelerograms with a PGA of 0.60 g together with the *Capacity Dominium* associated with a Damage Limitation LS. It can be observed that the response at the top of the tympanum of the macro-element model in both horizontal directions (X and Y) was located outside the area of the

LS due to the application of such seismic input. In a similar way, the dynamic responses of the macro-element model subjected to Type 2 artificial accelerograms with a PGA of 0.70 g are depicted in Figure 6.7b and Figure 6.7c for a Significant Damage LS and Near Collapse LS, respectively. It is worth noting that the *Capacity Dominium* is capable of assessing the displacement capacity of a structure considering both horizontal directions. Nevertheless, the dynamic responses at the top of the tympanum of the brick masonry prototype depicted in Figure 6.7 presented a behaviour which was characterised mainly by displacements in the Y direction. This was associated with the intensity of the seismic inputs which did not allow the occurrence of in-plane mechanisms of the main gable wall.
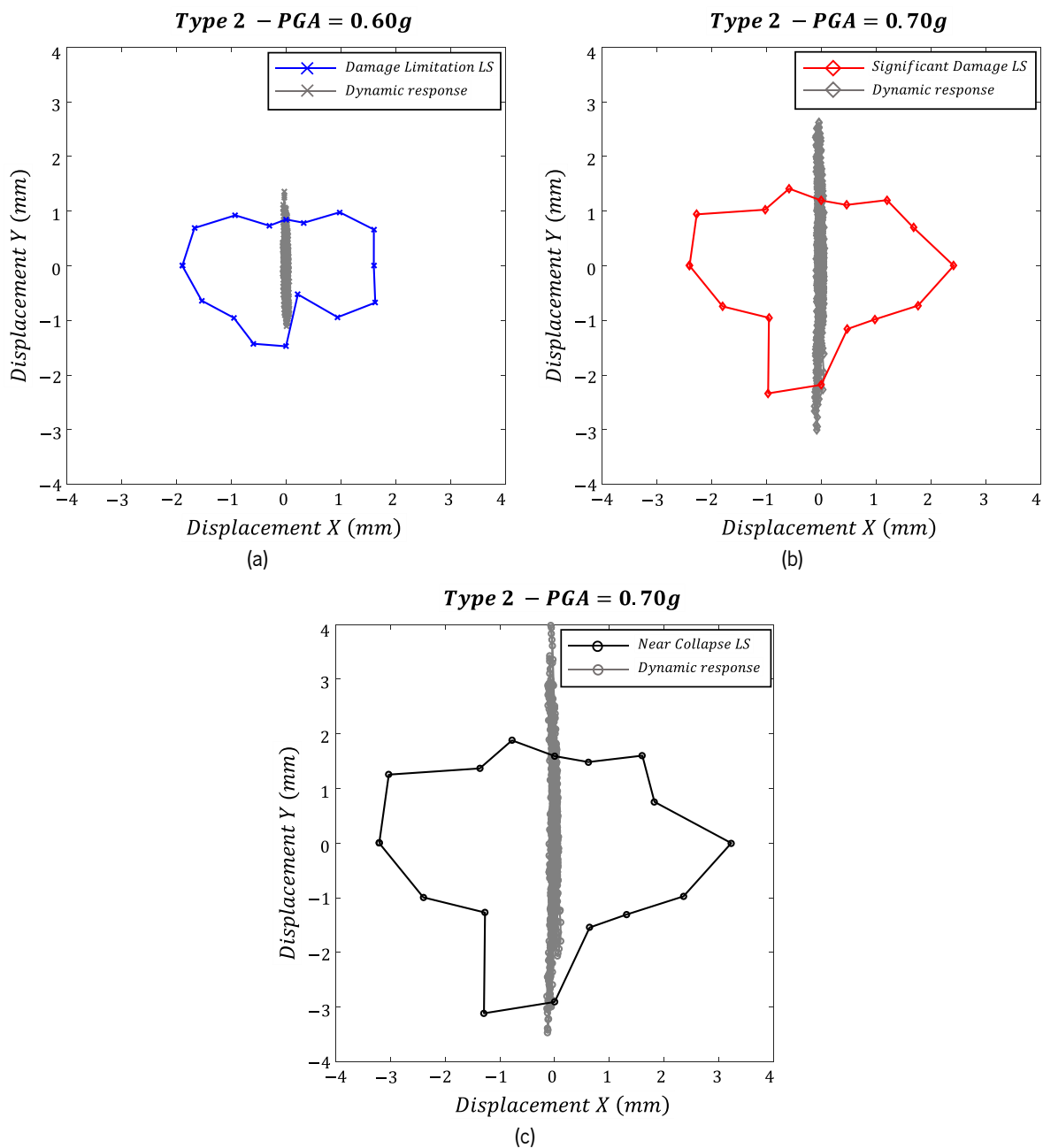
Figure 6.7. Evaluation of the dynamic response of the macro-element model of the brick masonry prototype based on a *Capacity Dominium* approach: (a) Damage Limitation LS, (b) Significant Damage LS, and (c) Near Collapse LS.

The derivation of analytical fragility curves was conducted considering a fitting process involving the number of nonlinear dynamic analyses in which a LS was exceeded. A nonlinear dynamic analysis, considered as an event in the hereafter, was excluded from the fitting process when the response of the macro-element model remained inside the effective area of the *Capacity Dominium* since the LS was not reached. In addition, the events in which the dynamic response surpassed only once the area of the *Capacity Dominium* were also discarded from the fitting process since it may not be considered a proper indicator of exceeding a LS. In this regard, the events considered in the fitting process were the ones in which the displacement at the top of the tympanum surpassed at least twice the area of the *Capacity Dominium*. It is worth mentioning that this approach may be considered slightly conservative since structures present a different behaviour in a dynamic context [177]. The number of exceeding events considered for the fitting process regarding the derivation of analytical fragility curves associated with Type 1 and Type 2 artificial accelerograms is summarized in Table 6-3 and Table 6-4, respectively.

Table 6-3. Exceeding events for the derivation of analytical fragility curves due to the application of Type 1 artificial accelerograms based on a deterministic approach

IM	Number of events	Number of exceeding events		
		Damage Limitation LS	Significant Damage LS	Near Collapse LS
0.45 g	14	0	0	0
0.50 g	14	0	0	0
0.55 g	21	18	2	0
0.60 g	21	21	19	9
0.65 g	21	21	21	18
0.70 g	21	21	21	21
0.75 g	14	14	14	14
0.80 g	14	14	14	14

Table 6-4. Exceeding events for the derivation of analytical fragility curves due to the application of Type 2 artificial accelerograms based on a deterministic approach

IM	Number of events	Number of exceeding events		
		Damage Limitation LS	Significant Damage LS	Near Collapse LS
0.45 g	14	0	0	0
0.50 g	14	0	0	0
0.55 g	21	10	0	0
0.60 g	21	19	8	2
0.65 g	21	21	16	5
0.70 g	21	21	21	19
0.75 g	14	14	14	14
0.80 g	14	14	14	14

The fitting of the fragility functions was based on a maximum likelihood procedure in which optimum mean values and standard deviations were determined in accordance with the number of exceeding events [178]. In this sense, the probability of a given number of events to exceed a certain LS was assessed by the introduction of a binomial distribution. This binomial distribution, denoted as P, is expressed in equation 6-10 in which n and z correspond to the total and exceeding number of events, respectively, and p relates to the true probability of exceedance associated with a given IM. As reported in equation 6-11, the true probability p was further replaced by the expression associated with the normal cumulative distribution function of the fragility curves (equation 6-1).

$$P = \binom{n}{z} p^{z} \left(1 - p\right)^{n-z} \qquad\qquad 6\text{-}10$$

$$P = \binom{n}{z} \Phi\left(\frac{\ln\left(x/\theta\right)}{\beta}\right)^{z} \left(1 - \Phi\left(\frac{\ln\left(x/\theta\right)}{\beta}\right)\right)^{n-z} \qquad\qquad 6\text{-}11$$

Aiming at considering multiple values of IM, the product of the binomial distributed probabilities of each IM was subsequently computed. This product corresponds to a likelihood function given by equation 6-12 in which j and m are associated with the range of IMs. Finally, the estimation of optimum values associated with the parameters that describe a fragility curve, namely mean value θ and standard deviation β, is conducted by maximizing the likelihood function.

$$Likelihood = \prod_{j=1}^{m} \binom{n}{z} \Phi\left(\frac{\ln\left(x_{j}/\theta\right)}{\beta}\right)^{z} \left(1 - \Phi\left(\frac{\ln\left(x_{j}/\theta\right)}{\beta}\right)\right)^{n-z} \qquad\qquad 6\text{-}12$$

The fitter fragility curves associated with the application of seismic inputs based on far-field earthquakes associated with the three LSs are illustrated in the continuous lines in Figure 6.8. It was observed that a small increment of PGA could lead to the collapse of the brick masonry prototype. For instance, the application of a seismic input with a PGA of 0.50 g presented a probability of approximate 13% of exceeding the Damage Limitation LS, whereas the probability of exceeding this LS when the structure was subjected to a seismic input with a PGA of 0.60 g corresponded to 99%. In this sense, an increment of the PGA of around 0.10 g presented a significant influence on the dynamic response of the brick masonry prototype, with an almost deterministic response. It was noted that the additional LSs, namely Significant Damage and Near Collapse, were also characterised by a similar behaviour.

In addition, the probability of exceedance associated with the application of near-field seismic inputs was also strongly influenced by the variation of PGA regardless of the LSs as illustrated by the dashed lines in Figure 6.8. Considering a Near Collapse LS, a 20% of probability of exceedance was obtained with a PGA of 0.59 g; however, this probability increased to 80% when considering a PGA of 0.69 g. An assessment regarding the influence of the different seismic inputs (Type 1 and Type 2) on the estimation of the probability of exceedance was also conducted. For this purpose, the value of PGA associated with a probability of exceedance for Type 1 and Type 2 seismic inputs was compared. In the case of the Damage Limitation LS, a 50% of probability of exceedance was obtained when applying a seismic input of 0.530 g and 0.555 g based on far- and near-field earthquakes. In addition, these values associated with seismic inputs (Type 1/Type 2) corresponded to 0.575 g/0.615 g, and 0.610 g/0.660 g for Significant Damage and Near Collapse LSs, respectively. It was evidenced that a slightly higher value of PGA based on near-field earthquakes is required for exceeding the LSs when applying seismic inputs based on Type 2 earthquakes. This behaviour can be related to the different characteristics of the inputs such as response spectrum an effective duration of the ground motion. The results from the deterministic approach may not be considered very reliable or useful regarding the fragility-based loss assessment

since the uncertainty regarding this structure is limited. In this sense, a more thorough assessment of the seismic vulnerability is required increasing the uncertainty parameters of the numerical model.

Figure 6.8. Analytical fragility curves of the brick masonry prototype based on a deterministic approach due to the application of Type 1 artificial accelerograms

6.3.3 PROBABILISTIC SEISMIC VULNERABILITY ASSESSMENT

The assessment of the seismic vulnerability of the brick masonry prototype based on a probabilistic approach consisted of the application of a larger number of nonlinear dynamic analyses, and additional sources of uncertainty. The macro-element model was subjected to 2000 analyses: one half based on far-field artificial accelerograms, and the other half associated with near-field artificial accelerograms. The analyses were characterised by values of PGA ranging between 0.45 g and 0.80 g since similar scaling procedure as the one used in the determinist approach was adopted for this assessment. In this sense, a set of 125 nonlinear dynamic analyses were conducted to the structure for each value of PGA.

For this investigation, the uncertainty was mainly associated with mechanical and geometric properties of the macro-element model. For this purpose, Probability Density Functions (PDF) together with mean values and coefficients of variation were defined for each of these parameters. The statistical characteristics defined for the mechanical properties of the macro-element model are reported in Table 6-5. In the case of Young's modulus, specific weight, compressive and tensile strengths, mean values and coefficients of variation were defined based on the mechanical characterization conducted by Candeias, et al. [77] and reported in Chapter 5. The mean values of other mechanical properties such as shear modulus, tensile fracture energy, cohesion, shear strength and friction coefficients were associated with the ones defined for the assessment in brick masonry prototype in the static and dynamic nonlinear fields. Nevertheless, fracture energies associated with compressive and sliding mechanisms were given as a function of ductility indexes denoted as d_{uc} and d_{us}, respectively. In this sense, the definition of the mean values for these mechanical properties was based on the average values reported by Lourenço [179]. The definition of the coefficients of variation associated with cohesion, shear strength

and friction coefficients for shear-diagonal and shear-sliding mechanisms was conducted based on the specifications regarding masonry structures provided by the JCSS Probability Model Code [180]. Due to the lack of information associated with the remaining mechanical properties (tensile fracture energy, ductility index in compression and sliding), it was assumed that they were characterised by a coefficient of variation of 30%. On the other hand, the uncertainty associated with geometric properties of the model was oriented to solely the thickness of the walls. For this parameter, a normal PDF was assumed together with a mean value and coefficient of variation of 23.5 cm and 5%, respectively. It is worth noting that the uncertainty was also oriented to the viscous damping ratio ζ in which a mean value of 3%, a coefficient of variation of 30% and a lognormal PDF were assumed.

Table 6-5. Probabilistic models associated with the mechanical properties of the macro-element model

Parameter				Mean	Coefficient of Variation	Probability Density Function
Elastic behaviour	Young's modulus	E	N/mm²	5170	29%	Lognormal
	Shear modulus	G	N/mm²	2133	30%	Lognormal
	Specific weight	γ	N/mm³	18.9x10⁻⁶	3%	Lognormal
Tensile behaviour	Tensile strength	f_t	N/mm²	0.1	19%	Lognormal
	Fracture energy	G_f^I	N/mm	0.012	30%	Lognormal
Compressive behaviour	Compressive strength	fc	N/mm²	2.48	14%	Lognormal
	Compressive ductility index	d_{uc}	mm	1.6	30%	Lognormal
Shear-sliding behaviour	Cohesion	c	N/mm²	0.1	40%	Lognormal
	Friction coefficient	μ_s	-	0.7	19%	Lognormal
	Shear-sliding ductility index	d_{us}	mm	0.09	30%	Lognormal
Shear-diagonal behaviour	Shear strength	f_{y0}	N/mm²	0.07	40%	Lognormal
	Friction coefficient	μ_d	-	0.6	19%	Lognormal

For the application of one set of nonlinear dynamic analyses associated with a single PGA, 125 values of mechanical properties, together with thicknesses and damping ratios were randomly generated based on their corresponding PDF. The generated random values of the parameters used for one set of analyses can be found in Annex B. On the other hand, from the initial set of seismic inputs composed by 840 artificial accelerograms, 375 were randomly selected for assessment of the seismic vulnerability based on a probabilistic approach. From this new set, 125 seismic inputs were assembled taking into consideration three components of artificial accelerograms (250 for horizontal and 125 for vertical directions). In this sense, the 125 seismic inputs remained the same throughout the eight sets of nonlinear dynamic analyses; however, they were subjected to a different scaling factor.

The assessment of the dynamic response of the macro-element model in terms of horizontal displacements at the top of the tympanum was also assessed by means of the *Capacity Dominium* for each of the LSs. Aiming at conducting a fitting process based a maximum likelihood approach, the number of events which led to the exceedance of a certain LS was estimated. Following the similar procedure as in the deterministic approach, the events in which the displacement surpassed the area of the *Capacity Dominium* at least twice were taken into consideration for the derivation and fitting of analytical fragility curves. On the contrary, the events in which the history of displacement in X and Y directions remained inside area of the *Capacity Dominium* or surpassed it only once were discarded from the fitting process. In this sense, Table 6-6 and Table 6-7 summarise the number of exceeding events for

the three LSs associated with the application of far- and near-field seismic inputs, respectively. It was noted that a significant number of events exceeded the three LSs when the structure was subjected to artificial accelerograms with a PGA of 0.45 g. This behaviour was not identified when assessing the seismic vulnerability of the structure based on a deterministic approach. This may be related to the limited uncertainty of the deterministic approach mainly associated with the number of time history analysis as well as the lack of definition of probabilistic models associated with mechanical properties, wall thickness, and damping ratio.

Table 6-6. Exceeding events for the derivation of analytical fragility curves due to the application of Type 1 artificial accelerograms based on a probabilistic approach

IM	Number of events	Number of exceeding events		
		Damage Limitation LS	Significant Damage LS	Near Collapse LS
0.45 g	125	79	57	43
0.50 g	125	104	85	67
0.55 g	125	113	104	89
0.60 g	125	121	116	107
0.65 g	125	124	123	119
0.70 g	125	125	124	122
0.75 g	125	125	125	124
0.80 g	125	125	125	125

Table 6-7. Exceeding events for the derivation of analytical fragility curves due to the application of Type 2 artificial accelerograms based on a probabilistic approach

IM	Number of events	Number of exceeding events		
		Damage Limitation LS	Significant Damage LS	Near Collapse LS
0.45 g	125	72	38	21
0.50 g	125	99	70	43
0.55 g	125	108	92	74
0.60 g	125	117	108	97
0.65 g	125	125	118	111
0.70 g	125	125	124	120
0.75 g	125	125	124	122
0.80 g	125	125	125	124

Figure 6.9 illustrates the fitted fragility curves of the brick masonry prototype associated with the application of far-field earthquakes in which the continuous and dashed lines correspond to the assessment of the seismic vulnerability based on probabilistic and deterministic approaches, respectively. From the probabilistic approach, it was observed that the brick masonry prototype presented a probability of exceeding the three LSs when subjected to seismic inputs with a PGA lower than the minimum value defined for this investigation. In this sense, it presented a 10% of probability of exceeding the Damage Limitation LS when considering a PGA of 0.33 g. In the case of the remaining two LSs (Significant Damage, and Near Collapse), this probability was reached when applying a seismic input with approximately 0.37 g and 0.39 g of PGA, respectively. It was also observed that there is a small branch regarding the probability of exceedance between the three LSs which was mainly associated with displacement capacities defined by means of the *Capacity Dominium*. It was observed from this

procedure that the displacement capacities of the LSs were significantly close to each other due to the rapid decrement of the shear capacity and the associated low ductility.

In addition, a comparison between the fragility curves obtained by means of deterministic and probabilistic approaches was conducted. The increment of the uncertainty associated with the definition of the different probabilistic models was clearly evidenced based on the shape of the fragility functions (continuous vs dashed lines). It was also possible to observe that, in the case of the probabilistic approach, it was required to apply a seismic input with a lower PGA in order to obtain the same probability of exceedance associated with a certain LS. In the case of Damage Limitation LS, a seismic input with a PGA of 0.425 g led to a probability of exceedance of 50%, which corresponded to 20% less when compared to 0.53 g of the deterministic approach. The same behaviour was identified when comparing the remaining two LSs.
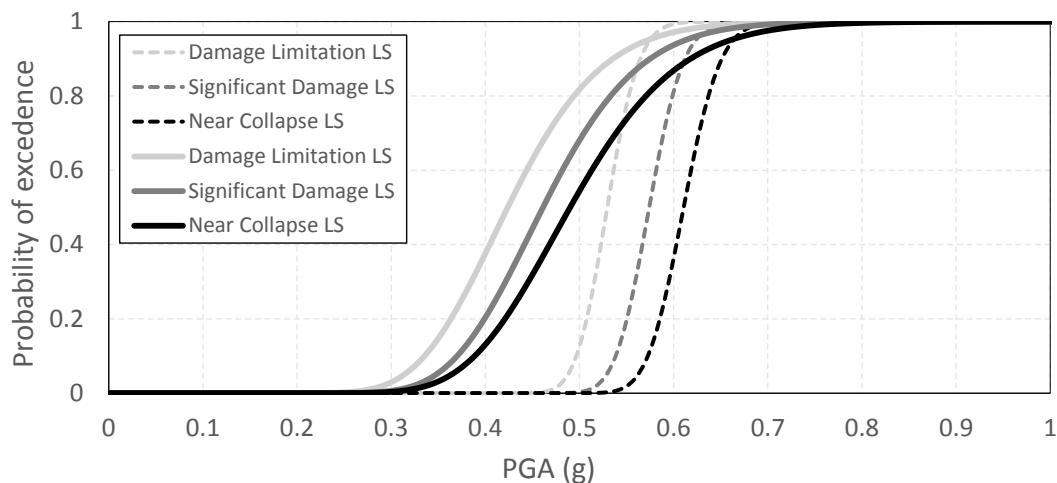
Figure 6.9. Analytical fragility curves of the brick masonry prototype based on a probabilistic approach due to the application of Type 1 artificial accelerograms

On the other hand, the fragility curves corresponding the application of near-field seismic inputs is illustrated in Figure 6.10. From these results, the influence of the probability density functions defined for the mechanical properties, thickness and damping ratio, on the probability of exceedance was also evidenced. An initial comparison was conducted between the application of far- and near-field seismic inputs considering a probabilistic approach. In this sense, a similar response was obtained when comparing the fragility curve associated with the Damage Limitation LS. On the other hand, the structure required to be subjected to Type 2 seismic inputs with higher PGA (<10% increment) aiming at reaching the same probability of exceedance. Another comparison was conducted considering both approaches for the derivation of the fragility functions. In this regard, these fragility functions (continuous and dashed lines) were also characterised by the same behaviour evidenced when assessing the seismic vulnerability associated with the application of far-field seismic inputs.
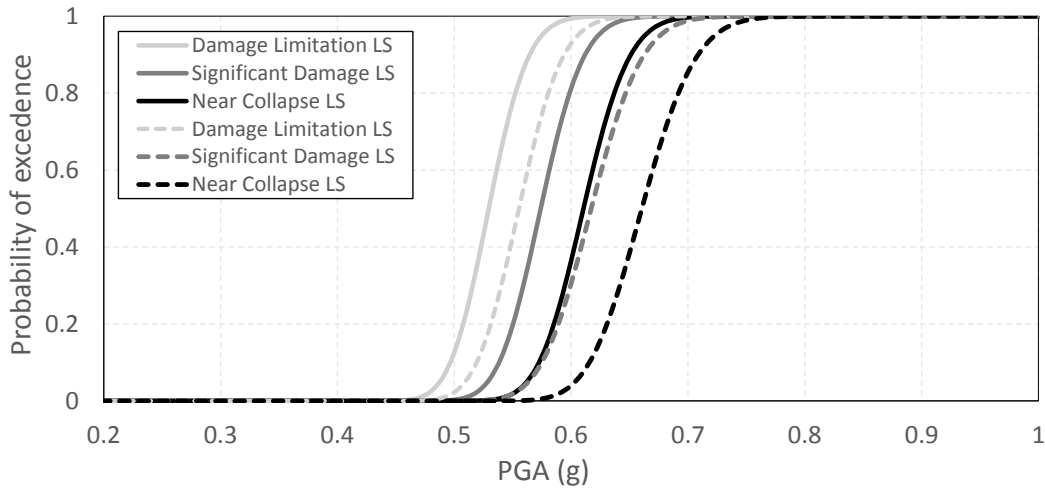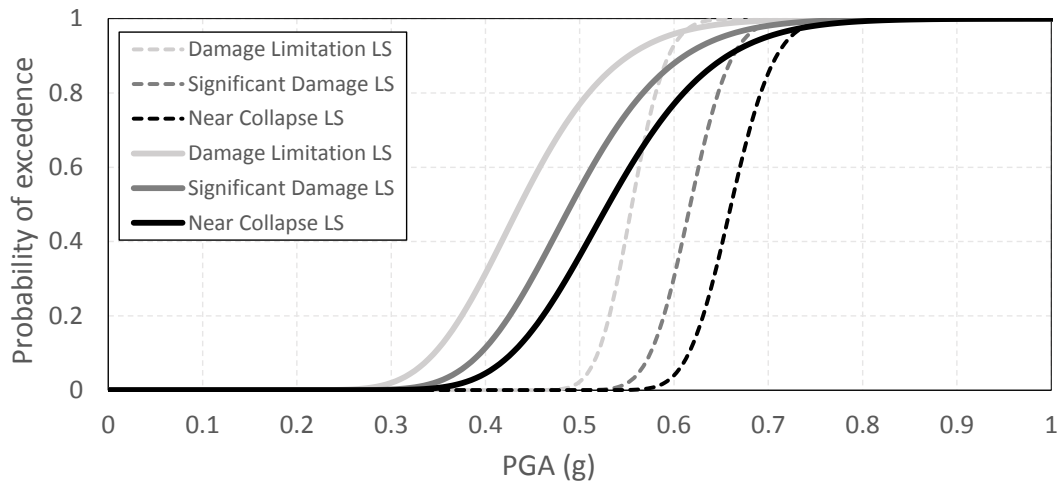
Figure 6.10. Analytical fragility curves of the brick masonry prototype based on a probabilistic approach due to the application of Type 2 artificial accelerograms

The results obtained in terms of mean values and standard deviations obtained by means of the probabilistic approach were further compared to the ones provided by Hazus [140] as reported in Table 6-8. The building type denoted as URML was selected for this comparison since it is related to URM structures with low-height bearing walls. Three equivalent LSs, namely Slight, Moderate, and Extensive Damage LS were defined for this comparison. In accordance with Hazus [140], the Slight Damage LS corresponds to diagonal and stair-step cracking on masonry walls and around door and window openings. The Moderate Damage LS consists of diagonal cracking in most masonry walls, and visible separation from diaphragms. Finally, the Extensive Damage LS consists of extensive cracking in most walls, the overturning of parapets and gable end walls, and the relative motion of beam or trusses from their supports. Besides these LSs, two seismic design levels, denoted as low-code and pre-code, were also taken into consideration. It was noted that there were significant differences when comparing the properties of the fragility curves obtained by means of analytical and expert-based formulations. The analytical mean values θ were higher from the ones provided by Hazus regardless of the seismic design level. On the other hand, the analytical standard deviations β presented an average value of 0.17, whereas the value provided by Hazus corresponds to 0.64. These differences are mainly associated with the definition of the displacement capacity of each LS. In the case of the fragility functions estimated by Hazuz, the capacity was associated with inter-story drifts presenting values of 0.24% (6.6 mm), 0.48% (13.2 mm), and 1.2% (33 mm) for Slight, Moderate, and Extensive Damage LSs based on a Pre-code seismic design level. The capacities of these LSs were characterised by a slightly higher value when considering a Low-code seismic design level presenting inter-story drifts of 0.3%, 0.6% and 1.5%. The difference between these formulations is also depicted in Figure 6.11 in which the fragility curves associated with a probabilistic approach based on Type 2 seismic inputs were plotted together with the corresponding Hazus fragility curves. It was observed that the fragility curves obtained by Hazus presented a higher uncertainty, and a small probability of exceeding the LSs when subjected to low values of PGA.

Table 6-8 Comparison of obtained standard deviation with

Limit state	Far-field earthquake (Type 1)		Near-field earthquake (Type 2)		Equivalent limit state	Equivalent PGA Low-code seismic design level		Equivalent PGA Pre-code seismic design level	
	θ	β	θ	B		θ	β	θ	β
Damage Limitation	0.42	0.18	0.43	0.18	Slight Damage	0.14	0.64	0.13	0.64
Significant Damage	0.46	0.17	0.49	0.17	Moderate Damage	0.20	0.64	0.17	0.64
Near Collapse	0.49	0.18	0.53	0.17	Extensive Damage	0.32	0.64	0.26	0.64
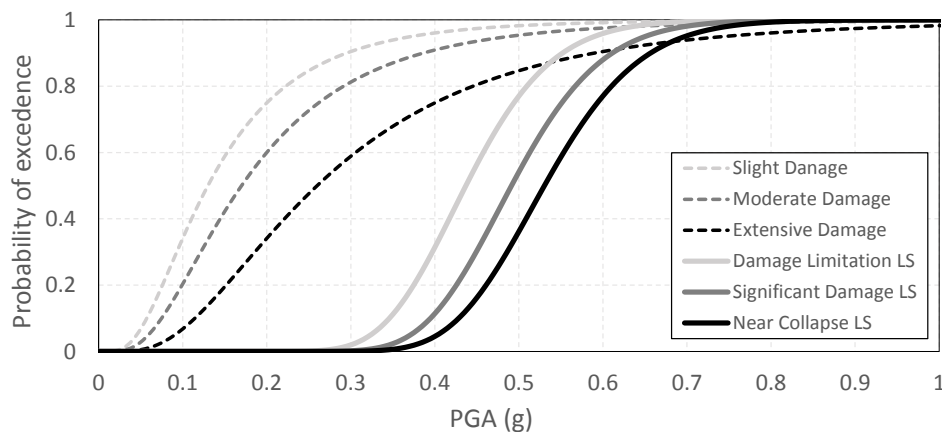
Figure 6.11. Comparison of fragility curves obtained by means analytical (Type 2) and expert-based formulations.

6.4 FINAL CONSIDERATIONS

The present Chapter was focused on the assessment of the seismic vulnerability of a URM structure by means of the application of nonlinear dynamic analyses and the derivation of analytical fragility functions. This masonry structure corresponded to the brick masonry prototype whose out-of-plane failure mechanism was investigated in the static and dynamic nonlinear fields by means of a macro-element modelling approach as reported in Chapter 5.

In this investigation, three limit states LSs were taken into consideration in accordance with the EC8-Part3 for the assessment of the seismic vulnerability of this structure, namely Damage Limitation, Significant Damage, and Near Collapse, respectively. For this purpose, an alternative procedure denoted as *Capacity Dominium* was carried out for the proper definition of the displacement capacities of each of the LSs. This *Capacity Dominium* consists of the application of a set of nonlinear static analyses along different directions of a structure. In this regard, the macro-element model of the brick masonry prototype was subjected to sixteen pushover analyses at an angular step of 22.5°. The *Capacity Dominium* of each LS was defined by estimating their corresponding displacement capacity. In the case of a Damage Limitation LS, this capacity corresponded to the yielding displacement, whereas as for a Near Collapse LS the capacity was associated with the displacement reached with a 20% loss of shear capacity. In the case of a Significant Damage LS, a ratio between the capacity of this LS and a Near Collapse LS was considered as 3/4 as proposed by the EC8-Part3.

Moreover, the assessment of the seismic vulnerability of the brick masonry prototype required the generation of artificial accelerograms as input for the application of time history analyses. In this regard, over 560 horizontal and 280 vertical accelerograms were artificially generated based on elastic response spectra associated with far- and near-field earthquakes in accordance with the EC8-Part1 and the Portuguese National Annex. These artificial accelerograms were further subjected to a signal processing consisting of a bandpass Fourier filter of 0.20 Hz.

Two different approaches were taken into consideration for the assessment of the seismic vulnerability of this structure. The first one, denoted as deterministic approach, focused the uncertainty on the seismic input, whereas other parameters presented a deterministic value. In addition, it consisted of the application of 280 nonlinear dynamic analyses in which the artificial accelerograms were scaled aiming at comprising a range of PGA between 0.45 g and 0.80 g. It is worth noting that in this assessment, different horizontal and vertical artificial accelerograms were defined for each time history analysis. On the other hand, the second one, denoted as probabilistic approach, focused the uncertainty on a wider number of parameters, namely mechanical properties, the thickness of walls and damping ratio. In this case, 2000 time history analyses, divided into 16 sets of 125 analyses between far- and near-field earthquakes were conducted to the macro-element model of the brick masonry prototype. For each set, 125 random values of mechanical properties, thickness, and damping ratio were generated based on the definition of probability density functions, mean values and coefficients of variation. In addition, from the initial set of artificial accelerograms, 375 between horizontal and vertical components were selected for a single set of analyses.

The derivation of fragility curves was subjected to a fitting process based on a maximum likelihood approach. For this purpose, it was necessary to estimate the number of nonlinear dynamic analyses which led to the exceedance of a certain LS. The dynamic response in terms of maximum horizontal displacement at the top of the tympanum was plotted together with the *Capacity Dominium* of a LS. In this sense, the analyses in which the response of the structure surpasses at least two times the effective area of the CP were taken into consideration for the fitting process. It is worth noting that these results may be considered somehow conservative since the displacement capacity associated with the different LSs was establish in a static context, and it is well-known that structures are capable of bearing larger displacements in the dynamic field.

From these fragility curves, it was possible to determine the probability of exceedance of the three LSs when the structure is subjected to seismic input. It was evidenced that the results associated with the deterministic approach were not capable of providing reliable information for fragility loss assessment. On the other hand, the probabilistic approach led to more consistent results when assessing the seismic vulnerability of the brick masonry prototype when subjected to far- and near-field seismic inputs. Nevertheless, further investigations regarding the seismic vulnerability of URM structures considering their out-of-plane mechanisms are required not only due to their complex behaviour, but to a proper risk assessment. The comparison between expert-based and analytical fragility curves has evidenced the necessity of conducting further investigations regarding the assessment of the seismic vulnerability of URM structures, as well as a more rigorous definition of the displacement capacity which is suitable in a dynamic context and it considers the occurrence of in-plane and out-of-plane failure mechanisms.

CHAPTER 7

CONCLUSIONS AND FUTURE WORK

7.1 CONCLUSIONS

This thesis aimed at the assessment of the seismic vulnerability of URM structures characterised by out-of-plane collapse mechanism. The approach for assessment was conducted by means of the application of nonlinear dynamic analyses based on a macro-element modelling approach, and the subsequent derivation of analytical fragility curves. For this purpose, this investigation has been divided into five main topics. The first one was associated with the state of the art regarding the assessment of the out-of-plane behaviour of masonry structures as well as the different available computational tools for assessing the seismic vulnerability of this typology of structures. The second topic was focused on the description of a macro-element modelling approach together with the introduction of cyclic constitutive laws and the formulation of a generic expression for the computation of a consistent mass matrix. The third topic was devoted to the validation of these features considering three case studies. The fourth topic was associated with the numerical assessment of the out-of-plane response of two URM structures subjected to shaking table tests. Finally, the last topic was focused on the assessment of the seismic vulnerability of one URM structure, incorporating the tools and knowledge gathered in the thesis.

From the literature review, it was possible to acknowledge the vast range of available computational tools used for the assessment of masonry structures. For instance, the Finite Element method corresponds to one of the most popular numerical approaches for the assessment of the seismic behaviour of this type of structures. However, it requires the definition of complex constitutive laws for the mechanical behaviour of the material and a detailed mesh refinement of the numerical model which

lead to a high computational burden when performing sophisticated analyses. On the contrary, approaches based on simplified procedures have been developed aiming at the assessment of masonry structures taking into consideration the limitations of refined methodologies. Nevertheless, the accuracy of these modelling approaches is in some cases questionable due to the oversimplifications. Besides, most of these approaches are only focused on the in-plane response and are not suitable for representing masonry structures with complex geometry.

The assessment of the out-of-plane behaviour of masonry structures has been conducted by means of analytical formulations as well as experimental programmes. The analytical formulations can be classified in force- and displacement-based approaches. In this regard, displacement-based approaches correspond to a more accurate formulation for the assessment of URM since their out-of-plane behaviour can be described as a rigid block. Different mechanisms, with associated collapse multipliers, have been proposed for the assessment this type of behaviour. On the other hand, there is a limited number of investigations focused on the experimental assessment of the out-of-plane behaviour of masonry structures. The findings of most of those investigations were obtained as a by-product of extensive experimental programmes or were focused on retrofitting techniques. In a similar way, the investigations related to the assessment of the seismic vulnerability of masonry structures is also limited. In such investigations, masonry buildings were usually modelled using simplified numerical tools in which the out-of-plane mechanisms are neglected. In this sense, further investigations regarding the assessment of the out-of-plane behaviour and the seismic vulnerability of masonry structures by means of a suitable numerical approach are required.

An alternative and innovative computational tool was introduced by Caliò, et al. [1] and further upgraded by Pantò, et al. [2] aiming at the assessment of the seismic response of masonry structures. This macro-element modelling approach is capable of simulating the main in-plane and out-of-plane mechanisms of this type of structures with a low computational burden. In addition, it is also able to simulate the response of infilled frame structures by the introduction of beam-column plasticity elements as well as the complex behaviour of curved masonry structures as reported by Caliò and Pantò [147] and Cannizzaro [150], respectively. This modelling approach has been employed for the assessment of the seismic behaviour of different masonry structures, demonstrating significant accuracy on the results. Nevertheless, these investigations were conducted in a static context. As part of this thesis, this modelling approach was extended into the dynamic field by the introduction of cyclic constitutive laws and the formulation of a generic expression for the computation of a consistent macro-element mass matrix. This formulation was conceptualised aiming at its applicability regardless of the geometric configuration of the elements. For this purpose, a proper definition of the kinematics associated with irregular elements and the introduction of an isoparametric transformation based on an intrinsic reference system were taken into consideration. Based on this procedure, a closed form solution for the computation of each component of the global mass matrix was formulated.

These additional aspects regarding the macro-element modelling approach, namely consistent mass matrix and cyclic constitutive laws, were validated taking into consideration three case studies. The first one was associated with the estimation of the dynamic properties of Timoshenko cantilever beams by means of this modelling approach, and the comparison of the results with the ones obtained by means

of differential equations and additional numerical simulations. This case study constituted an initial validation of the computation of a consistent mass matrix as well as the influence of the off-diagonal components. It was demonstrated that the off-diagonal terms presented a small impact regarding the estimation of natural frequencies. In addition, the influences associated with the discretisation of this macro-element modelling approach was investigated. Even though a more discretised model provided improvements in terms of natural frequencies, a less refined model was capable of properly replicate the dynamic properties of the beam elements. The second case study was related to the assessment of the free rocking motion of a rigid block aiming at the simulation of a building known as the Robert A. Millikan Memorial Library in California, USA. Such structure was modelled by a single macro-element which was subjected to dynamic analyses by means of a pulse load. The assessment of the rocking motion was investigated in the linear and nonlinear fields. Based on the linear assessment, it was possible to determine an efficient discretization of the interface element so that the response of the macro-element was in good agreement with the analytical one. On the other hand, a foundation with zero tensile strength was taken into consideration for the nonlinear assessment of the free rocking motion of the macro-element model. Based on this assessment, the influence of energy dissipation was also investigated considering a Rayleigh viscous damping criterion. The results obtained from these analyses also demonstrated the applicability and efficiency of this macro-element modelling approach with respect to the assessment of free rocking motion. Finally, the last case study corresponded to a full-scale benchmark masonry wall tested by cyclic static tests and investigated by means of numerical models. This final validation was oriented not only to the formulation of a consistent mass matrix but also to the definition of appropriate cyclic constitutive laws. Macro-element models of the two-story masonry wall were subjected to artificial accelerograms aiming at evaluating the in-plane seismic response in the nonlinear dynamic field. The capability of this modelling approach for assessing the in-plane seismic response of masonry structures was evidenced, with an acceptable agreement in terms of hysteresis loops, maximum load capacity and maximum horizontal top displacements. In addition, these analyses required a low computational burden making this modelling approach a practical computational tool.

These features were further applied for the assessment of the out-of-plane response of two URM structures investigated by means of shaking table tests. These structures, denoted as brick and stone masonry prototypes, were modelled considering two different numerical strategies. The first one corresponded to a FE model, whereas as the second one was related to the adopted macro-element modelling approach. The out-of-plane behaviour of the numerical models was initially assessed in the static field by means of the application of a mass distributed lateral force. Based on these results, it was possible to obtain a good agreement in terms of maximum load capacity and in-plane collapse mechanisms. Nevertheless, the experimental out-of-plane collapse was not properly reproduced. The application of nonlinear static analyses also allowed evaluating the material and mesh dependency of the numerical models. The out-of-plane behaviour of these models was also investigated in the dynamic field by the application of a seismic input recorded in the experimental campaign. These results provided a good agreement in terms of in-plane collapse mechanisms, whereas the out-of-plane collapse was not fully simulated. A comparison in terms of load factor vs displacement hysteresis loops was conducted between the two numerical strategies noticing a significant resemblance. In this regard, the macro-

element modelling approach seems as a better alternative since the computational demand for the application of these analyses was significantly reduced.

Finally, the seismic vulnerability of one of these URM structures was assessed by means of the application of nonlinear dynamic analyses. For this purpose, the macro-element model of the brick masonry prototype was selected since it required a low computational burden for the application of this type of analysis. The seismic vulnerability of this structure was assessed by means of the derivation of fragility curves characterized by a cumulative normal distribution function. The fragility curves correspond to a statistical tool capable of providing the probability of reaching or exceeding a limit state due to a given intensity measure. In this sense, the assessment of the seismic vulnerability of this structure required the definition of different limit states and their corresponding displacement capacities. The displacement capacities of three limit states were established by means of an alternative procedure denoted as *Capacity Dominium* which consists of the application of a set of nonlinear static analyses along different directions. In addition, the seismic vulnerability assessment also required the generation of artificial accelerograms based on the specifications provided by the EC8-Part1 [173] and the Portuguese National Annex [174]. In this regard, the macro-element model was subjected to three-component artificial accelerogram, and the dynamic response in terms of horizontal top displacement was assessed by means of the *Capacity Dominium*. The number of nonlinear dynamic analyses that exceeded a certain limit state was determined aiming at the fitting of the analytical fragility curves based on a maximum likelihood approach. It is worth noting that the uncertainty of the model was focused initially on the seismic input, denoted as deterministic approach, and subsequently on other parameters, and it was denoted as probabilistic approach. In the latter, the definition of probabilistic models for parameters such as mechanical properties, wall thickness and damping ratio was required. The results from the deterministic approach were characterised by a low uncertainty regarding the probability of exceedance of the limit states. The behaviour of this fragility curves cannot be considered reliable for conducting fragility loss assessment. On the other hand, this uncertainty was increased due to the definition of probability density functions for the different parameters associated with the probabilistic approach. Nevertheless, these results were considered somehow conservative since the displacement capacity was determined in a static context. All in all, the applicability of this modelling approach was demonstrated, not only for the assessment of the seismic response of URM structures, but also as a favourable numerical tool for the assessment of the seismic vulnerability due to its low computational demand.

7.2 FUTURE WORK

This investigation provided additional insight regarding the assessment of the seismic vulnerability of a masonry structure characterised by predominant out-of-plane failure mechanisms. Nevertheless, there are still several aspects that need to be taken into consideration due to the complexity of this behaviour and, therefore, further investigations should be conducted. In this sense, a set of future actions are proposed:

- A more rigorous definition of the parameters that determine the capacity of the different limit states in terms of base shear or displacements, when considering masonry structures in which a box-type behaviour cannot be guaranteed.

- Assessment of the seismic vulnerability taking into consideration different sources of seismic input aiming at providing additional uncertainty when deriving analytical fragility curves. These sources could be related to a database of real earthquakes or more detailed formulations based on attenuation laws.

- Assessment of the seismic vulnerability taking into consideration different typologies of masonry structures. In this sense, the variability associated with the distribution of structural elements in plan, the number of stories, the position of door and window openings or the influence of flexible diaphragms can be taken into account. This will not only increase introduce additional uncertainty when deriving fragility curves but will provide reliable information for the risk assessment and loss estimation.

- Proposal of retrofitting techniques aiming at preventing the out-of-plane collapse of this typology of structures, and the further evaluation of the effectiveness of these techniques by means of seismic vulnerability assessment and the derivation of analytical fragility curves.

REFERENCES

[1]   I. Caliò, M. Marletta, and B. Pantò, "A new discrete element model for the evaluation of the seismic behaviour of unreinforced masonry buildings," Engineering Structures, vol. 40, pp. 237-338, (2012).

[2]   B. Pantò, F. Cannizzaro, I. Caliò, and P. B. Lourenço, "Numerical and experimental validation of a 3D macro-model for the in-plane and out-of-plane behaviour of unreinforced masonry walls," International Journal of Architectural Heritage, (2017). doi: 10.1080/15583058.2017.1325539

[3]   P. B. Lourenço, "Computations on historic masonry structures," Progress in Structural Engineering and Materials, vol. 4, pp. 301-319, (2002). doi: 10.1002/pse.120

[4]   P. B. Lourenço, "Computational strategies for masonry structures," PhD Thesis, Delft University, Delft, The Netherlands, (1996).

[5]   S. K. Arya and G. A. Hegemier, "On nonlinear response prediction of concrete masonry assemblies," in North American Masonry Conference, Boulder, Colorado, USA, pp. 19.1-19.24 (1978).

[6]   A. W. Page, "Finite element model for masonry," Journal of the Structural Division, vol. Vol. 104, pp. 1267-1285, (1978).

[7]   V. Lotfi and P. B. Shing, "Interface Model Applied to Fracture of Masonry Structures," ASCE, vol. Vol. 120, pp. 63-80, (1994).

[8]   P. B. Lourenço and J. G. Rots, "A Multisurface Interface Model for Analysis of Masonry Structures," Journal of Engineering Mechanics, vol. Vol. 123, pp. 660-668, (1997).

[9]   CUR, Structural masonry: An experimental/numerical basis for practical design rules. Balkema: Rotterdam, (1997).

[10]   R. Senthivel and P. Lourenço, "Finite element modelling of deformation characteristics of historical stone masonry shear walls," Engineering Structures, vol. 31, pp. 1930-1943, (2009).

[11]   P. B. Lourenço, J. G. Rots, and J. Blaauwendraad, "Continuum model for masonry: Parameter estimation and validation," Journal of Structural Engineering, vol. 124, pp. 642-652, (1998).

[12]   P. B. Lourenço, "Anisotropic softening model for masonry plates and shells," Journal of Structural Engineering, vol. 126, pp. 1008–1016, (2000).

[13]   P. A. Cundall, "A computer model for simulating progressive large scale movements in blocky rock systems," in Symposium on Rock Fracture (ISRM), Nancy, France (1971).

[14]   P. A. Cundall, "Formulation of a three-dimensional distinct element model – Part I: A scheme to detect and represent contacts in a system composed of many polyhedral blocks," International Journal of Rock Mechanics and Mining Sciences, vol. 25, pp. 107-116, (1988).

[15]   R. D. Hart, P. A. Cundall, and J. V. Lemos, "Formulation of a three-dimensional distinct element model – Part II: mechanical calculations," International Journal of Rock Mechanics and Mining Sciences, vol. 25, pp. 117-125, (1988).

[16]   P. A. Cundall and R. D. Hart, "Numerical modeling of discontinua," in 1st US Conference on Discrete Element Methods, Colorado, United States of America (1989).

[17]   G. Boffi and S. Casolo, "Non-linear dynamic analysis," in Monument 98 - Workshop on Seismic Performance of Monuments, Lisbon, Portugal (1998).

[18]   S. Casolo, "Modelling in-plane micro-structure of masonry walls by rigid elements," International Journal of Solids and Structures, vol. 41, pp. 3625-3641, (2004).

[19]   S. Casolo and F. Peña, "Rigid element model for in-plane dynamics of masonry walls considering hysteretic behaviour and damage," Earthquake Engineering and Structural Dynamics, vol. 36, pp. 1029-1048, (2007).

[20]   R. E. Barbosa, "Discontinuous structural analysis," in 11th European Conference on Earthquake Engineering, Paris (1996).

[21]   N. Petrinic, "Aspects of discrete element modelling involving facet-to-facet contact detection and interaction," PhD Thesis, University of Wales, UK, (1996).

[22]   A. Munjiza, The combined finite-discrete element method. Chichester, (2004).

[23]   M. A. Ma, A. D. Pan, M. Luan, and J. M. Gebara, "Seismic analysis of stone arch bridges using discontinuous deformation analysis," in 11th World Conference on Earthquake Engineering, Amsterdam (1996).

[24]   G. H. Shi and R. E. Goodman, "Discontinuous deformation analysis—Anew method for computing stress, strain and sliding of block systems," in Key Questions in Rock Mechanics, P. A. Cundall, R. Sterling, and A. Starfield, Eds., ed Rotterdam: Balkema, (1988).

[25]   J. V. Lemos, "Discrete Element Modeling of Masonry Structures," International Journal of Architectural Heritage: Conservation, Analysis, and Restoration, vol. 1, pp. 190-213, (2007).

[26]   M. Tomaževič, "The computer program POR," Ljubljana, Slovenia(1978).

[27]   G. Magenes and G. M. Calvi, "Prospettive per la calibrazione di metodi semplificati per l'analisi sismica di pareti murarie," in Convegno Nazionale La Meccanica delle Murature tra Teoria e Progetto, Bologna, Italy (1996).

[28]   G. Magenes and A. Della Fontana, "Simplified non-linear seismic analysis of masonry buildings," Proc British Masonry Society, vol. 8, pp. 190-5, (1998).

[29]   G. Magenes and G. M. Calvi, "In plane seismic response of brick masonry walls," Earthquake Engineering and Structural Dynamics, vol. 26, pp. 1091-1112, (1997).

[30]   F. Braga and D. Liberatore, "A finite element for the analysis of the response of masonry buildings," in 5th North American masonry conference, Urbana, pp. 201-12 (1990).

[31]   F. Braga, D. Liberatore, and G. Spera, "A computer program for the seismic analysis of complex masonry buildings," in Computer Methods in Structural Masonry - 4th International Symposium, Firenze, pp. 309-316 (1997).

[32]   P. D'Asdia and A. Viskovic, "Analyses of a masonry wall subjected to horizontal actions on its plane, employing a non-linear procedure using changing shape finite elements," Transactions on Modelling and Simulation, vol. 10, pp. 519–26, (1993).

[33]   P. D'Asdia and A. Viskovic, "Analisi tridimensionale della resistenza di edifici in muratura, storici o recenti, soggetti ad azioni orizzontali di tipo sismico," presented at the Convegno Nazionale La meccanica delle murature tra teoria e progetto, Messina, (1996).

[34]   A. Brencich, L. Gambarotta, and S. Lagomarsino, "A macroelement approach to the three-dimensional seismic analysis of masonry buildings," in 11th European Conference on Earthquake Engineering, Paris (1998).

[35]   A. Penna, "A macro-element procedure for the dynamic non-linear analysis of masonry buildings," PhD Thesis, Politecnico di Milano, Milano, Italy, (2002).

[36]   S. Lagomarsino, A. Galasco, and A. Penna, "Non linear macro-element dynamic analysis of masonry buildings," in ECCOMAS COMPDYN Conference, Crete, Greece (2007).

[37]   A. Galasco, S. Lagomarsino, A. Penna, and S. Resemini, "Non-linear Seismic Analysis of Masonry Structures," in 13th World Conference on Earthquake Engineering, Vancouver, Canada (2004).

[38]   A. Penna, S. Lagomarsino, and A. Galasco, "A nonlinear macroelement model for the seismic analysis of masonry buildings," Earthquake Engineering and Structural Dynamics, vol. 43, pp. 159-179, (2014). doi: 10.1002/eqe.2335

[39]   R. Marques and P. B. Lourenço, "Possibilities and comparison of structural component models for the seismic assessment of modern unreinforced masonry buildings," Computers and Structures, vol. 89, pp. 2079–91, (2011).

[40]   P. Foraboschi and A. Vanin, "Non-linear static analysis of masonry buildings based on a strut-and-tie modeling," Soil Dynamics and Earthquake Engineering, vol. 55, pp. 44-58, (2013).

[41]   T. M. Ferreira, A. A. Costa, and A. Costa, "Analysis of the out-of-plane seismic behaviour of unreinforced masonry: A literature review," International Journal of Architectural Heritage: Conservation, Analysis, and Restoration, (2014). doi: 10.1080/15583058.2014.885996

[42]   J. Heyman, "The stone skeleton," International Journal of Solids and Structures, vol. 2, pp. 249-256, (1966).

[43]   M. Giaquinta and E. Giusti, "Researches on the equilibrium of masonry structures," Archive for Rational Mechanics and Analysis, vol. 84, pp. 359-392, (1985).

[44] G. Del Piero, "Constitutive equation and compatibility of the external loads for linear elastic masonry-like materials," Meccanica, vol. 24, pp. 150-162, (1989).

[45] S. Stevin, De Beghinselen der Weeghconst vol. Volume 1. Leiden, (1586).

[46] M. J. DeJong, "Seismic Assessment Strategies for Masonry Structures," PhD Thesis, Department of Architecture, Massachusetts Institute of Technology, United States, (2009).

[47] P. Block, M. DeJong, and J. Ochsendorf, "As hangs the flexible line: Equilibrium of masonry arches," Nexus Network Journal, vol. 8, pp. 13-24, (2006).

[48] P. Block, T. Ciblac, and J. Ochsendorf, "Real-time limit analysis of vaulted masonry buildings," Computers and Structures, vol. 84, pp. 1841-1852, (2006).

[49] D. D'Ayala and E. Speranza, "Definition of Collapse Mechanisms and Seismic Vulnerability of Historic Masonry Buildings," Earthquake Spectra, vol. 19, pp. 479–509, (2003).

[50] A. Giuffrè, Letture sulla meccanica delle murature storiche. Rome, Italy, (1990).

[51] B. Hobbs, M. Ting, and M. Gilbert, "An analytical approach for walls subjected to static and dynamic out-of-plane point loads," in 10th International Brick and Block Masonary Conference, Alberta, Canada (1994).

[52] C. Casapulla, "Resistenze attritive in una parete muraria soggetta ad azioni normali al suo piano medio," in L'Ingegneria Sismica in Italia, Atti IX Convegno Nazionale ANIDIS, Torino, Italy (1999).

[53] L. Picchi, "Risposta Sismica per Azioni Fuori dal Plano di Parete Murarie," Università degli studi di Pavia, Pavia, Italy, (2002).

[54] L. F. Restrepo-Vélez, Seismic risk of unreinforced masonry buildings. ROSE School Pavia, Italy, (2004).

[55] D. P. Abrams, R. Angel, and J. Uzarski, "Out-of-plane strength of unreinforced masonry infill panels," Earthquake Spectra, vol. 12, pp. 825-844, (1996).

[56] K. Doherty, M. C. Griffith, N. T. K. Lam, and J. L. Wilson, "Displacement-based analysis for out-of-plane bending of seismically loaded unreinforced masonry walls," Earthquake Engineering and Structural Dynamics, vol. 31, pp. 833-50, (2002).

[57] M. C. Griffith, G. Magenes, G. Melis, and L. Picchi, "Evaluation of out-of-plane stability of unreinforced masonry walls subjected to seismic excitation," Journal of Earthquake Engineering, vol. 7, pp. 141-169, (2003).

[58] G. W. Housner, "The behavior of inverted pendulum structures during earthquakes," Bulletin of the Seismological Society of America, vol. 53, pp. 403-417, (1963).

[59] M. Aslam, D. T. Scalise, and W. G. Godden, "Earthquake rocking response of rigid bodies," Journal of the Structural Division, vol. 106, pp. 377-392, (1980).

[60] C. S. Yim, A. K. Chopra, and J. Penzien, "Rocking response of rigid blocks to earthquakes," Earthquake Engineering & Structural Dynamics, vol. 8, pp. 565-587, (1980).

[61] L. Sorrentino, "Dinamica di muri sollecitati fuori del piano come sistemi di corpi rigidi," University of Rome "La Sapienza", Italy, (2003).

[62] O. Al Shawa, G. De Felice, M. Mauro, and L. Sorrentino, "Out-of-plane seismic behaviour of rocking masonry walls," Earthquake Engineering and Structural Dynamics, vol. 41, pp. 949-968, (2012).

[63] I. N. Psycharis, "Dynamic behaviour of rocking two-block assemblies," Earthquake Engineering & Structural Dynamics, vol. 19, pp. 555-575, (1990).

[64] P. D. Spanos, P. C. Roussis, and N. P. A. Politis, "Dynamic analysis of stacked rigid blocks," Soil Dynamics and Earthquake Engineering, vol. 21, pp. 559-578, (2001).

[65] D. D'Ayala and Y. Shi, "Modeling Masonry Historic Buildings by Multi-Body Dynamics," International Journal of Architectural Heritage, vol. 5, pp. 483-512, (2011).

[66] R. Gabellieri, L. Landi, and P. P. Diotallevi, "A 2-DOF model for the dynamic analysis of unreinforced masonry walls in out-of-plane bending," in 4th ECCOMAS Thematic Conference on Computational Methods in Structural Dynamics and Earthquake Engineering, Kos Island, Greece (2013).

[67] H. Derakhshan, M. C. Griffith, and J. M. Ingham, "Out-of-plane behavior of one-way unreinforced masonry walls," Journal of Engineering Mechanics, vol. 139, pp. 409-417, (2013).

[68] T. M. Ferreira, A. A. Costa, R. Vicente, and H. Varum, "A simplified four-branch model for the analytical study of the out-of-plane performance of regular stone URM walls," Engineering Structures, vol. 83, pp. 140-153, (2015).

[69] H. Derakhshan, Y. Nakamura, J. M. Ingham, and M. C. Griffith, "Simulation of shake table results on out-of- plane masonry buildings. Part (I): Displacement-based approach using simple failure mechanisms," International Journal of Architectural Heritage, vol. 11, pp. 72-78, (2017).

[70] ABK, "Methodology for mitigation of seismic hazards in existing unreinforced masonry buildings: The Methodology," El Segundo, California, USA(1984).

[71] M. Tomaževič, P. Weiss, and T. Velechovsky, "The influence of rigidity of floors on the seismic behaviour of old stone-masonry buildings," European Earthquake Engineering, vol. 5, pp. 28-41, (1991).

[72] D. Benedetti, P. Carydis, and P. Pezzoli, "Shaking table tests on 24 simple masonry buildings," Earthquake Engineering and Structural Dynamics, vol. 27, pp. 67-90, (1998).

[73] N. T. K. Lam, M. C. Griffith, J. L. Wilson, and K. Doherty, "Time-history analysis of URM walls in out-of-plane flexure," Engineering Structures, vol. 25, pp. 743-754, (2003).

[74] M. C. Griffith, J. Vaculik, N. T. K. Lam, J. Wilson, and E. Lumantarna, "Cyclic testing of unreinforced masonry walls in two-way bending," Earthquake Engineering and Structural Dynamics, vol. 36, pp. 801-821, (2007).

[75] A. Ghobarah and K. El Mandooh Galal, "Out-of-plane strengthening of unreinforced masonry walls with openings," Journal of Composites for Construction, vol. 8, pp. 298-305, (2004).

[76] J. Vaculik, M. C. Griffith, B. Hogarth, and J. Todd, "Out-of-plane flexural response tests using dry-stack masonry," in Australian Earthquake Society Conference, Mt Gambier, South Australia (2004).

[77] P. X. Candeias, A. Campos Costa, N. Mendes, A. A. Costa, and P. B. Lourenço, "Experimental Assessment of the Out-of-Plane Performance of Masonry Buildings Through Shaking Table Tests," International Journal of Architectural Heritage, vol. 11, pp. 31-58, (2017).

[78] A. A. Costa, A. Arêde, A. Campos-Costa, A. Penna, and A. Costa, "Out-of-plane behaviour of a full scale stone masonry façade. Part 2: shaking table tests," Earthquake Engineering and Structural Dynamics, vol. 42, pp. 2097-2111, (2013).

[79] S. Hamoush, M. McGinley, P. Mlakar, and M. J. Terro, "Out-of-plane behavior of surface-reinforced masonry walls," Construction and Building Materials, vol. 16, pp. 341-351, (2002).

[80] L. Anania, G. D'Agata, C. Giaquinta, and A. Badalà, "Out of Plane Behavior of Calcareous Masonry Panels Strengthened by CFRP," APCBEE Procedia, vol. 9, pp. 401-406, (2014).

[81] A. S. Mosallan, "Out-of-plane flexural behavior of unreinforced red brick walls strengthened with FRP composites," Composites Part B: Engineering, vol. 38, pp. 559-574, (2007).

[82] Ö. Anil, M. Tatayoğlu, and M. Demirhan, "Out-of-plane behavior of unreinforced masonry brick walls strengthened with CFRP strips," Construction and Building Materials, vol. 35, pp. 614-624, (2012).

[83] D. Dizhur, M. Griffith, and J. Ingham, "Out-of-plane strengthening of unreinforced masonry walls using near surface mounted fibre reinforced polymer strips," Engineering Structures, vol. 59, pp. 330-343, (2014).

[84] A. Costa, "Determination of mechanical properties of traditional masonry walls in dwellings of Faial Island, Azores," Earthquake Engineering and Structural Dynamics, vol. 31, pp. 1361-1382, (2002).

[85] J. G. Tumialan, N. Galati, and A. Nanni, "Field assessment of unreinforced masonry walls strengthened with fiber reinforced polymer laminates," Journal of Structural Engineering, vol. 129, pp. 1047-1056, (2003).

[86] A. Arêde, A. Costa, A. A. Costa, C. Oliveira, and F. Neves, "Experimental In-Situ Testing of Typical Masonry Constructions of Faial Island-Azores," in 14th World Conference on Earthquake Engineering, Beijing, China (2008).

[87] D. Dizhur, H. Derakhshan, J. M. Ingham, and M. C. Griffith, "In-situ out-of-plane testing of an unreinforced masonry partition walls," in 11th Canadian Masonry Symposium, Toronto (2009).

[88] N. Ismail and J. M. Ingham, "In-situ and laboratory based out-of-plane testing of unreinforced clay brick masonry walls strengthened using near surface mounted twisted steel bars," Construction and Building Materials, vol. 36, pp. 119-128, (2012).

[89] A. Cecchi, G. Milani, and A. Tralli, "A Reissner–Mindlin limit analysis model for out-of-plane loaded running bond masonry walls," International Journal of Solids and Structures, vol. 44, pp. 1438–1460, (2006).

[90] F. A. Zuccarello, G. Milani, R. S. Olivito, and A. Tralli, "A numerical and experimental analysis of unbonded brickwork panels laterally loaded," Construction and Building Materials, vol. 23, pp. 2093–2106, (2009).

[91]   G. Milani, F. A. Zuccarello, R. S. Olivito, and A. Tralli, "Heterogeneous upper-bound finite element limit analysis of masonry walls out-of-plane loaded," Computational Mechanics, vol. 40, pp. 911–931, (2007).

[92]   G. Milani, P. B. Lourenço, and A. Tralli, "Homogenization approach for the limit analysis of out-of-plane loaded masonry walls," Journal of Structural Engineering, vol. 132, pp. 1650–1663, (2006).

[93]   L. Macorini and B. A. Izzuddin, "A non-linear interface element for 3D mesoscale analysis of brick-masonry structures," International Journal for Numerical Methods in Engineering, vol. 85, pp. 1584–1608, (2011).

[94]   A. Cecchi and K. Sab, "Out of plane model for heterogeneous periodic materials: The case of masonry," European Journal of Mechanics—A/Solids, vol. 21, pp. 715–746, (2002).

[95]   G. Milani, M. Pizzolato, and A. Tralli, "Simple numerical model with second order effects for out-of-plane loaded masonry walls," Engineering Structures, vol. 48, pp. 98–120, (2013).

[96]   S. Casolo and G. Milani, "Simplified out-of-plane modelling of threeleaf masonry walls accounting for the material texture," Construction and Building Materials, vol. 40, pp. 330–351, (2013).

[97]   M. Gams, A. Anžlin, and M. Kramara, "Simulation of shake table results on out-of-plane masonry buildings. Part (III): Two-step FEM approach," International Journal of Architectural Heritage, vol. 11, pp. 94-102, (2017).

[98]   C. Chácara, N. Mendes, and P. B. Lourenço, "Simulation of Shake Table Tests on Out-of-Plane Masonry Buildings. Part (IV): Macro and Micro FEM Based Approaches," International Journal of Architectural Heritage, vol. 11, pp. 103-116, (2017).

[99]   J. V. Lemos, "Discrete element modelling of the seismic behaviour of stone masonry arches," in Computer Methods in Structural Masonry. vol. 4, J. M. a. G. N. Pande, Ed., ed Swansea: Books & Journals International, (1998), pp. 220-227.

[100]   G. E. Sincraian, C. S. Oliveira, and J. V. Lemos, "Assessment of the seismic behaviour of a stone masonry aqueduct using the discrete element method," in 11ᵗʰ European Conference on Earthquake Engineering, Rotterdam, Netherlands (1998).

[101]   A. Drei and C. S. Oliveira, "The seismic behaviour of the 'Aqueduto da Amoreira' in Elvas using distinct element modeling," in Historical Constructions, P. B. Lourenço and P. Roca, Eds., ed Guimaraes, (2001), pp. 903–911.

[102]   S. Casolo, "Rigid element model for non-linear analysis of masonry facades subjected to out-of-plane loading," Communications in Numerical Methods in Engineering, vol. 15, pp. 457–468, (1999).

[103]   S. Casolo, "Modelling the out-of-plane seismic behaviour of masonry walls by rigid elements," Earthquake Engineering & Structural Dynamics, vol. 29, pp. 1797–1813, (2000).

[104]   S. Casolo and G. Uva, "Nonlinear analysis of out-of-plane masonry facades: Full dynamic versus pushover methods by rigid body and spring model," Earthquake Engineering & Structural Dynamics, vol. 42, pp. 499–521, (2013).

[105]   G. M. Roberti and O. Spina, "Discrete element analysis on the Sardinian' Nuaraghe," in 3rd International Seminar on Historical Constructions, Guimarães, Portugal, pp. 719–727 (2001).

[106] A. Alexandris, E. Protopapa, and I. N. Psycharis, "Collapse mechanisms of masonry buildings derived by the distinct element method," in 13th World Conference on Earthquake Engineering, Vancouver, Canada (2004).

[107] J. V. Lemos and A. Campos Costa, "Simulation of shake table results on out-of-plane masonry buildings. Part (V): Discrete element approach," International Journal of Architectural Heritage, vol. 11, pp. 117-124, (2017).

[108] O. AlShawa, L. Sorrentino, and D. Liberatore, "Simulation Of Shake Table Tests on Out-of-Plane Masonry Buildings. Part (II): Combined Finite-Discrete Elements," International Journal of Architectural Heritage, vol. 11, pp. 79-93, (2017).

[109] A. A. Costa, "Seismic assessment of the out-of-plane performance of traditional stone masonry walls," PhD thesis, University of Porto, Portugal, (2012).

[110] F. Cannizzaro and P. B. Lourenço, "Simulation of Shake Table Tests on Out-of-Plane Masonry Buildings. Part (VI): Discrete Element Approach," International Journal of Architectural Heritage, vol. 11, pp. 125-142, (2017).

[111] B. R. Ellingwood, "Earthquake risk assessment of building structures," Reliability Engineering & System Safety, vol. 74, pp. 251-62, (2001).

[112] ATC-13, Earthquake damage evaluation data for California, Applied technology council FEMA contract no. EMW-C-0912, (1985).

[113] M. Rota, A. Penna, and C. L. Strobbia, "Processing Italian damage data to derive typological fragility curves," Soil Dynamics and Earthquake Engineering, vol. 28, pp. 933–947, (2008).

[114] ATC, FEMA-273: NEHRP Guidelines for the seismic rehabilitation of buildings. Basic procedures manual, Applied Technology Council (ATC), (1997).

[115] ATC, FEMA-306: Evaluation of earthquake damaged concrete and masonry wall buildings. Basic Procedures Manual, Applied Technology Council (ATC), (1998).

[116] Eurocode 8: Design of structures for earthquake resistance – Part 3: General rules, seismic actions and rules for buildings, Design Code EN 1998-3, (2005).

[117] SIA, SIA 266: Masonry. Swiss code, Swiss Society of Engineers and Architects, (2005).

[118] NZSEE: Assessment and improvement of the structural performance of buildings in earthquakes. New Zealand Society of Earthquake Engineering., University of Auckland, (2006).

[119] (2008). NTC 2008, Decreto Ministeriale 14/1/2008: Norme tecniche per le costruzioni. Ministry of Infrastructures and Transportations.

[120] MIT, Ministry of Infrastructures and Transportation, Circ. C.S.Ll.Pp. No. 617 of 2/2/2009: Istruzioni per l'applicazione delle nuove norme tecniche per le costruzioni di cui al Decreto Ministeriale 14 Gennaio 2008. G.U. S.O. n. 27 of 26/2/2009, No. 47, (2008).

[121] National Annex – Nationally determined parameters – Eurocode 8. Design of structures for earthquake resistance – Part 1: General rules, Seismic actions and rules for buildings, National Annex of Germany, DIN EN 1998-1/NA: 2011-, (2011).

[122] NZSEE: Assessment and improvement of unreinforced masonry buildings for earthquake resistance. In: Ingham J, editor. New Zealand Society of Earthquake Engineering, Supplement to

Assessment and improvement of the structural performance of buildings in earthquakes, University of Auckland, (2011).

[123] SIA, SIA D0237: Evaluation de la sécurité parasismique des bâtiments en maçonnerie. Documentation, Swiss Society of Engineers and Architects, (2011).

[124] M. Rota, "Advances in the derivation of fragility curves for masonry buildings," PhD thesis, European School for Advanced Studies in Reduction of Seismic Risk (ROSE School), Pavia, Italy, (2007).

[125] M. Rota, A. Penna, and G. Magenes, "A methodology for deriving analytical fragility curves for masonry buildings based on stochastic nonlinear analyses," Engineering Structures, vol. 32, pp. 1312-23, (2010).

[126] D. D'Ayala, "Force and displacement based vulnerability assessment for traditional buildings," Bulletin of Earthquake Engineering vol. 3, pp. 235-65, (2005).

[127] S. Cattari, S. Frumento, S. Lagomarsino, S. Parodi, and S. Resemini, "Multi-level procedure for the seismic vulnerability assessment of masonry buildings: The case of Sanremo (north-western italy)," in 1st European Conference on Earthquake Engineering and Seismology (ECEES), Geneva, Switzerland (2006).

[128] A. J. Kappos, G. Panagopoulos, C. Panagiotopoulos, and G. Penelis, "A hybrid method for the vulnerability assessment of R/C and URM buildings.," Bulletin of Earthquake Engineering, vol. 4, pp. 421-44, (2006).

[129] M. A. Erberik, "Generation of fragility curves for Turkish masonry buildings considering in-plane failure modes," Earthquake Engineering & Structural Dynamics, vol. 37, pp. 387-405, (2008).

[130] J. Park, P. Towashiraporn, J. I. Craig, and B. J. Goodno, "Seismic fragility analysis of low-rise unreinforced masonry structures," Engineering Structures, vol. 2009, pp. 125-37, (2009).

[131] L. Pasticier, C. Amadio, and M. Fragiacomo, "Non-linear seismic analysis and vulnerability evaluation of a masonry building by means of the SAP2000 V.10 code," Earthquake Engineering & Structural Dynamics, vol. 37, pp. 467–485, (2008).

[132] CSI (Computers and Structures Inc.), "SAP2000 v10 Integrated Finite Element Analysis and Design of Structures," (2004), Berkeley,

[133] M. Altug Erberik, "Generation of fragility curves for Turkish masonry buildings considering in-plane failure modes," Earthquake Engineering & Structural Dynamics, vol. 37, pp. 387-405, (2008).

[134] Y. Mengi, H. D. McNiven, and A. D. Tanrıkulu, "Models for nonlinear earthquake analysis of brick masonry buildings.," University of California at Berkeley(1992).

[135] Z. V. Milutinovic and G. S. Trendafiloski, "ISK-UE: An advanced approach to earthquake risk scenarios with applications to different European towns. WP4: Vulnerability of current buildings," (2003).

[136] G. Grünthal, "European macroseismic scale 1998 (EMS 1998). Council of Europe, Cahiers du Centre Europe´en de Géodynamique et de Sismologie," p. 15.

[137] B. Omidvar, B. Gatmiri, and S. Derakhshan, "Experimental vulnerability curves for the residential buildings of Iran," Natural Hazards, vol. 60, pp. 345–365, (2012). doi: 10.1007/s11069-011-0019-y

[138] S. Lagomarsino, A. Penna, A. Galasco, and S. Cattari, "TREMURI program: An equivalent frame model for the nonlinear seismic analysis of masonry buildings," Engineering Structures, vol. 56, pp. 1787-1799, (2013).

[139] T. Yi, " Experimental investigation and numerical simulation of an unreinforced masonry structure with flexible diaphragms," Ph.D. thesis, Georgia Institute of Technology, (2004).

[140] HAZUS 99 earthquake loss estimation methodology, technical manual, N.-N. I. o. B. Science, (1999).

[141] Y. K. Wen and C. L. Wu, "Uniform hazard ground motions for Mid-America cities," Earthquake Spectra, vol. 17, pp. 359-84, (2001).

[142] A. J. Kappos and V. K. Papanikolaou, "Nonlinear Dynamic Analysis of Masonry Buildings and Definition of Seismic Damage States," The Open Construction and Building Technology Journal, vol. 10, pp. 192-209, (2016).

[143] P. G. Asteris, M. P. Chronopoulos, C. Z. Chrysostomou, H. Varum, V. Plevris, N. Kyriakides, and V. Silva, "Seismic vulnerability assessment of historical masonry structural systems," Engineering Structures, vol. 62-63, pp. 118-134, (2014).

[144] P. G. Asteris, "On the structural analysis and seismic protection of historical masonry structures," The Open Construction and Building Technology Journal, vol. 2, pp. 124-33, (2008).

[145] G. Milani and G. Venturini, "Automatic fragility curve evaluation of masonry churches accounting for partial collapses by means of 3D FE homogenized limit analysis," Computers and Structures, vol. 89, pp. 1628-1648, (2011).

[146] Gruppo Sismica s.r.l., "3DMacro (3D Computer program for seismic assessment of masonry buildings)," (2014), Catania, Italy, Release 3.0, http://www.3dmacro.it.

[147] I. Caliò and B. Pantò, "A macro-element modelling approach of Infilled Frame Structures," Computers and Structures, vol. 143, pp. 91-107, (2014).

[148] B. Pantò, F. Cannizzaro, S. Caddemi, I. Caliò, C. Chácara, and P. B. Lourenço, "Nonlinear Modelling of Curved Masonry Structures after Seismic Retrofit through FRP Reinforcing," Buildings, vol. 7, p. 79, (2017). doi: 10.3390/buildings7030079

[149] Gruppo Sismica s.r.l., "HiStrA (Historical Structure Analysis)," (2015), Catania, Italy, Release 17.2.3, http://www.histra.it.

[150] F. Cannizzaro, "The seismic behavior of historical buildings: a macro-element approach," PhD Thesis, Department of Civil and Environmental Engineering, University of Catania, Catania, Italy, (2010).

[151] T. Takeda, M. A. Sozen, and N. N. Nielsen, "Reinforced concrete response to simulated earthquakes," Journal of the Structural Division, vol. 96, pp. 2557-2573, (1970).

[152] S. Mazzoni, F. Mckenna, M. H. Scott, and G. L. Fenves, "OpenSees User Manual," (2000), University of California, Berkeley, U.S.A,

[153]   V. Turnsek and P. Sheppard, "The shear and flexural resistance of masonry walls," in International research conference on earthquake engineering, Skopje, pp. 517-573 (1981).

[154]   V. Turnsek and F. Cacovic, "Some experimental result on the strength of brick masonry walls," in 2nd International Brick Masonry Conference, Stoke-on-Trent, UK (1971).

[155]   L. Majkut, "Free and Forced Vibrations of Timoshenko Beams Described by Single Difference Equation," Journal of Theoretical and Applied Mechanics, vol. 47, pp. 193-210, (2009).

[156]   I. N. Psycharis and P. C. Jennings, "Rocking of Slender Rigid Bodies Allowed to Uplift," Earthquake Engineering & Structural Dynamics, vol. 11, pp. 57-76, (1983).

[157]   TNO, "DIANA - DIsplacement method ANAlyser," (2013), Delft, Netherlands,

[158]   N. M. Newmark, "A Method of Computation for Structural Dynamics," ASCE Journal of Engineering Mechanics Division, vol. 85, pp. 67-94, (1959).

[159]   I. N. Psycharis, "Dynamic Behavior of Rocking Structures Allowed to Uplift," PhD, California Institute of Technology, Pasadena, California, (1981).

[160]   L. Rayleigh, Theory of Sound. New York, (1877).

[161]   G. Magenes, C. M. Calvi, and G. R. Kingsley, "Seismic Testing of a Full-Scale, Two-Story Masonry Building: Test Procedure and Measured Experimental Response," University of Pavia, Department of Structural Mechanics(1995).

[162]   L. Gambarotta and S. Lagomarsino, "Damage Models for the Seismic Response of Brick Masonry Shear Wall. Part II: The Continuum Model and its Applications," Earthquake Engineering & Structural Dynamics, vol. 26, pp. 441-462, (1997).

[163]   N. Mendes and P. B. Lourenço, "Seismic Assessment of Masonry "Gaioleiro" Buildings in Lisbon, Portugal," Journal of Earthquake Engineering, vol. 14, pp. 80-101, (2009). doi: 10.1080/13632460902977474

[164]   H. M. Hilber, T. J. R. Hughes, and R. L. Taylor, "Improved numerical dissipation for time integration algorithms in structural dynamics.," Earthquake Engineering and Structural Dynamics, vol. 5, pp. 283-292, (1977).

[165]   N. Mendes and P. B. Lourenço, "Sensitivity analysis of the seismic performance of existing masonry buildings," Engineering Structures, vol. 80, pp. 137-146, (2014).

[166]   G. Van Zijl, "Computational Modelling of Masonry Creep and Shrinkage," PhD thesis, Delft University of Technology, (2000).

[167]   J. Milosevic, A. Sousa Gago, M. Lopes, and R. Bento, "Experimental assessment of shear strength parameters on rubble stone masonry specimens," Construction and Building Materials, vol. 47, pp. 1372-1380, (2013).

[168]   C. Calderini, S. Cattari, and S. Lagomarsino, "The use of the diagonal compression test to identify the shear mechanical parameters of masonry," Construction and Building Materials, vol. 24, pp. 677-685, (2010).

[169]   G. M. Calvi, "A displacement-based approach for vulnerability evaluation of classes of buildings," Journal of Earthquake Engineering, vol. 3, pp. 411-38, (1999).

[170]   A. Mouyiannou, M. Rota, A. Penna, and G. Magenes, "Identification of suitable limit states for nonlinear dynamic analyses of masonry structures," Journal of Earthquake Engineering, vol. 18, pp. 231-63, (2014).

[171]   S. Petry and K. Beyer, "Influence of boundary conditions and size effect on the drift capacity of URM walls," Engineering Structures, vol. 65, pp. 76-88, (2014).

[172]   F. Cannizzaro, B. Pantò, M. Lepidi, S. Caddemi, and I. Caliò, "Multi-directional seismic assessment of historical masonry buildings by means of macro-element model-ling: Application to a building damaged during the L'Aquila earthquake (Italy)," Buildings, vol. 7, (2017).

[173]   Eurocode 8: Design of structures for earthquake resistance – Part 1: General rules, seismic actions and rules for buildings, EN 1998-1, (2004).

[174]   NP EN 196-8, Eurocode 8: Design of structures for earthquake resistance Part 1: General rules, seismic actions and rules for buildings -Portuguese Institute for Quality, (2010).

[175]   D. A. Gasparini and E. H. Vanmarcke, "SIMQKE, A Program for Artificial Motion Generation: User's Manual and Documentation," (1976), Department of Civil Engineering, MIT, USA,

[176]   L. Mendes, "LNEC-SPA: Signal Processing and Analysis Tools for Civil Engineers," Lisbon, Portugal Patent, (2008).

[177]   C. M. Calvi, G. R. Kingsley, and G. Magenes, "Testing of masonry structures for seismic assessment," Earthquake Spectra, vol. 12, pp. 145-65, (1996).

[178]   J. W. Baker, "Efficient Analytical Fragility Function Fitting Using Dynamic Structural Analysis," Earthquake Spectra, vol. 31, pp. 579-99, (2015).

[179]   P. B. Lourenço, "Recent advances in masonry modelling : micromodelling and homogenisation," I. C. Press, Ed., ed, (2009).

[180]   JCSS Probability Model Code Part 3: Resistance Models, Joint Committee of Structural Safety, (2011).

Annex A

FORMULATION FOR CONSISTENT MASS MATRIX

$$m_{ij} = 4 \cdot \rho \cdot \left(\begin{array}{l} \dfrac{\left(V_{15} \cdot V_{11} + V_{14} \cdot V_8 + V_{16} \cdot V_6\right) \cdot V_4}{9} + \dfrac{\left(V_{14} \cdot V_{12} + V_{15} \cdot V_8 + V_{16} \cdot V_5\right) \cdot V_2}{9} + \dfrac{\left(V_{16} \cdot V_{10} + V_{15} \cdot V_6 + V_{14} \cdot V_5\right) \cdot V_3}{9} + \\[3mm] \dfrac{\left(V_{14} \cdot V_{13} + V_{15} \cdot V_7\right) \cdot V_2}{3} + \dfrac{\left(V_{15} \cdot V_{10} + V_{14} \cdot V_7\right) \cdot V_4}{3} + \dfrac{\left(V_{15} \cdot V_{12} + V_{16} \cdot V_9\right) \cdot V_4}{3} + \dfrac{\left(V_{16} \cdot V_{13} + V_{15} \cdot V_9\right) \cdot V_3}{3} + \dfrac{V_{14} \cdot V_{10} \cdot V_2}{5} + \\[3mm] \dfrac{V_{14} \cdot V_{11} \cdot V_2}{15} + V_{15} \cdot V_{13} \cdot V_4 + \dfrac{V_{16} \cdot V_{11} \cdot V_3}{15} + \dfrac{V_{16} \cdot V_{12} \cdot V_3}{5} + \dfrac{V_{14} \cdot V_1 \cdot V_6}{15} + \dfrac{V_{14} \cdot V_1 \cdot V_9}{9} + \dfrac{V_{16} \cdot V_1 \cdot V_7}{9} + \dfrac{V_{16} \cdot V_1 \cdot V_8}{15} + \dfrac{V_{15} \cdot V_1 \cdot V_5}{9} \end{array} \right)$$

where

$$V_1 = \frac{s_1 - s_2 + s_3 - s_4}{4} \qquad V_2 = \frac{s_1 - s_2 - s_3 + s_4}{4} \qquad V_3 = \frac{s_1 + s_2 - s_3 - s_4}{4} \qquad V_4 = \frac{s_1 + s_2 + s_3 + s_4}{4}$$

$$V_5 = V_{22} \cdot V_{33} + V_{28} \cdot V_{39} + V_{34} \cdot V_{21} + V_{40} \cdot V_{27} + V_{20} \cdot V_{31} + V_{26} \cdot V_{37} + V_{32} \cdot V_{19} + V_{38} \cdot V_{25} + V_{18} \cdot V_{29} + V_{24} \cdot V_{35} + V_{30} \cdot V_{17} + V_{36} \cdot V_{23}$$

$$V_6 = V_{22} \cdot V_{27} + V_{28} \cdot V_{21} + V_{20} \cdot V_{25} + V_{26} \cdot V_{19} + V_{18} \cdot V_{23} + V_{24} \cdot V_{17}$$

$$V_7 = V_{22} \cdot V_{39} + V_{40} \cdot V_{21} + V_{20} \cdot V_{37} + V_{38} \cdot V_{19} + V_{18} \cdot V_{35} + V_{36} \cdot V_{17}$$

$$V_8 = V_{28} \cdot V_{33} + V_{34} \cdot V_{27} + V_{26} \cdot V_{31} + V_{32} \cdot V_{25} + V_{24} \cdot V_{29} + V_{30} \cdot V_{23}$$

$$V_9 = V_{34} \cdot V_{39} + V_{40} \cdot V_{33} + V_{32} \cdot V_{37} + V_{38} \cdot V_{31} + V_{30} \cdot V_{35} + V_{36} \cdot V_{29}$$

$$V_{10} = V_{22} \cdot V_{21} + V_{20} \cdot V_{19} + V_{18} \cdot V_{17}$$

$$V_{11} = V_{28} \cdot V_{27} + V_{26} \cdot V_{25} + V_{24} \cdot V_{23}$$

$$V_{12} = V_{34} \cdot V_{33} + V_{32} \cdot V_{31} + V_{30} \cdot V_{29}$$

$$V_{13} = V_{40} \cdot V_{39} + V_{38} \cdot V_{37} + V_{36} \cdot V_{35}$$

$$V_{14} = V_{42} \cdot V_{43} - V_{45} \cdot V_{41}$$

$$V_{15} = V_{42} \cdot V_{44} - V_{46} \cdot V_{41}$$

$$V_{16} = V_{45} \cdot V_{44} - V_{46} \cdot V_{43}$$

$$V_{17} = \frac{\left(\hat{\psi}_{1j}(1) - \hat{\psi}_{2j}(1) - \hat{\psi}_{3j}(1) + \hat{\psi}_{4j}(1)\right) \cdot K_x + \left(\hat{\psi}_{1j}(2) - \hat{\psi}_{2j}(2) - \hat{\psi}_{3j}(2) + \hat{\psi}_{4j}(2)\right) \cdot K_y + \left(\hat{\psi}_{1j}(3) - \hat{\psi}_{2j}(3) - \hat{\psi}_{3j}(3) + \hat{\psi}_{4j}(3)\right) \cdot K_z}{4}$$

$$V_{18} = \frac{\left(\hat{\psi}_{1i}(1) - \hat{\psi}_{2i}(1) - \hat{\psi}_{3i}(1) + \hat{\psi}_{4i}(1)\right) \cdot K_x + \left(\hat{\psi}_{1i}(2) - \hat{\psi}_{2i}(2) - \hat{\psi}_{3i}(2) + \hat{\psi}_{4i}(2)\right) \cdot K_y + \left(\hat{\psi}_{1i}(3) - \hat{\psi}_{2i}(3) - \hat{\psi}_{3i}(3) + \hat{\psi}_{4i}(3)\right) \cdot K_z}{4}$$

$$V_{19} = \frac{\left(\hat{\psi}_{1j}(1) - \hat{\psi}_{2j}(1) - \hat{\psi}_{3j}(1) + \hat{\psi}_{4j}(1)\right) \cdot J_x + \left(\hat{\psi}_{1j}(2) - \hat{\psi}_{2j}(2) - \hat{\psi}_{3j}(2) + \hat{\psi}_{4j}(2)\right) \cdot J_y + \left(\hat{\psi}_{1j}(3) - \hat{\psi}_{2j}(3) - \hat{\psi}_{3j}(3) + \hat{\psi}_{4j}(3)\right) \cdot J_z}{4}$$

$$V_{20} = \frac{\left(\hat{\psi}_{1i}(1) - \hat{\psi}_{2i}(1) - \hat{\psi}_{3i}(1) + \hat{\psi}_{4i}(1)\right) \cdot J_x + \left(\hat{\psi}_{1i}(2) - \hat{\psi}_{2i}(2) - \hat{\psi}_{3i}(2) + \hat{\psi}_{4i}(2)\right) \cdot J_y + \left(\hat{\psi}_{1i}(3) - \hat{\psi}_{2i}(3) - \hat{\psi}_{3i}(3) + \hat{\psi}_{4i}(3)\right) \cdot J_z}{4}$$

$$V_{21} = \frac{\left(\hat{\psi}_{1j}(1) - \hat{\psi}_{2j}(1) - \hat{\psi}_{3j}(1) + \hat{\psi}_{4j}(1)\right) \cdot I_x + \left(\hat{\psi}_{1j}(2) - \hat{\psi}_{2j}(2) - \hat{\psi}_{3j}(2) + \hat{\psi}_{4j}(2)\right) \cdot I_y + \left(\hat{\psi}_{1j}(3) - \hat{\psi}_{2j}(3) - \hat{\psi}_{3j}(3) + \hat{\psi}_{4j}(3)\right) \cdot I_z}{4}$$

$$V_{22} = \frac{\left(\hat{\psi}_{1i}(1) - \hat{\psi}_{2i}(1) - \hat{\psi}_{3i}(1) + \hat{\psi}_{4i}(1)\right) \cdot I_x + \left(\hat{\psi}_{1i}(2) - \hat{\psi}_{2i}(2) - \hat{\psi}_{3i}(2) + \hat{\psi}_{4i}(2)\right) \cdot I_y + \left(\hat{\psi}_{1i}(3) - \hat{\psi}_{2i}(3) - \hat{\psi}_{3i}(3) + \hat{\psi}_{4i}(3)\right) \cdot I_z}{4}$$

$$V_{23} = \frac{\left(\hat{\psi}_{1j}(1) - \hat{\psi}_{2j}(1) + \hat{\psi}_{3j}(1) - \hat{\psi}_{4j}(1)\right) \cdot K_x + \left(\hat{\psi}_{1j}(2) - \hat{\psi}_{2j}(2) + \hat{\psi}_{3j}(2) - \hat{\psi}_{4j}(2)\right) \cdot K_y + \left(\hat{\psi}_{1j}(3) - \hat{\psi}_{2j}(3) + \hat{\psi}_{3j}(3) - \hat{\psi}_{4j}(3)\right) \cdot K_z}{4}$$

$$V_{24} = \frac{\left(\hat{\psi}_{1i}(1) - \hat{\psi}_{2i}(1) + \hat{\psi}_{3i}(1) - \hat{\psi}_{4i}(1)\right) \cdot K_x + \left(\hat{\psi}_{1i}(2) - \hat{\psi}_{2i}(2) + \hat{\psi}_{3i}(2) - \hat{\psi}_{4i}(2)\right) \cdot K_y + \left(\hat{\psi}_{1i}(3) - \hat{\psi}_{2i}(3) + \hat{\psi}_{3i}(3) - \hat{\psi}_{4i}(3)\right) \cdot K_z}{4}$$

$$V_{25} = \frac{\left(\hat{\psi}_{1j}(1) - \hat{\psi}_{2j}(1) + \hat{\psi}_{3j}(1) - \hat{\psi}_{4j}(1)\right) \cdot J_x + \left(\hat{\psi}_{1j}(2) - \hat{\psi}_{2j}(2) + \hat{\psi}_{3j}(2) - \hat{\psi}_{4j}(2)\right) \cdot J_y + \left(\hat{\psi}_{1j}(3) - \hat{\psi}_{2j}(3) + \hat{\psi}_{3j}(3) - \hat{\psi}_{4j}(3)\right) \cdot J_z}{4}$$

$$V_{26} = \frac{\left(\hat{\psi}_{1i}(1) - \hat{\psi}_{2i}(1) + \hat{\psi}_{3i}(1) - \hat{\psi}_{4i}(1)\right) \cdot J_x + \left(\hat{\psi}_{1i}(2) - \hat{\psi}_{2i}(2) + \hat{\psi}_{3i}(2) - \hat{\psi}_{4i}(2)\right) \cdot J_y + \left(\hat{\psi}_{1i}(3) - \hat{\psi}_{2i}(3) + \hat{\psi}_{3i}(3) - \hat{\psi}_{4i}(3)\right) \cdot J_z}{4}$$

$$V_{27} = \frac{\left(\hat{\psi}_{1j}(1) - \hat{\psi}_{2j}(1) + \hat{\psi}_{3j}(1) - \hat{\psi}_{4j}(1)\right) \cdot I_x + \left(\hat{\psi}_{1j}(2) - \hat{\psi}_{2j}(2) + \hat{\psi}_{3j}(2) - \hat{\psi}_{4j}(2)\right) \cdot I_y + \left(\hat{\psi}_{1j}(3) - \hat{\psi}_{2j}(3) + \hat{\psi}_{3j}(3) - \hat{\psi}_{4j}(3)\right) \cdot I_z}{4}$$

$$V_{28} = \frac{\left(\hat{\psi}_{1i}(1) - \hat{\psi}_{2i}(1) + \hat{\psi}_{3i}(1) - \hat{\psi}_{4i}(1)\right) \cdot I_x + \left(\hat{\psi}_{1i}(2) - \hat{\psi}_{2i}(2) + \hat{\psi}_{3i}(2) - \hat{\psi}_{4i}(2)\right) \cdot I_y + \left(\hat{\psi}_{1i}(3) - \hat{\psi}_{2i}(3) + \hat{\psi}_{3i}(3) - \hat{\psi}_{4i}(3)\right) \cdot I_z}{4}$$

$$V_{29} = \frac{\left(\hat{\psi}_{1j}(1) + \hat{\psi}_{2j}(1) - \hat{\psi}_{3j}(1) - \hat{\psi}_{4j}(1)\right) \cdot K_x + \left(\hat{\psi}_{1j}(2) + \hat{\psi}_{2j}(2) - \hat{\psi}_{3j}(2) - \hat{\psi}_{4j}(2)\right) \cdot K_y + \left(\hat{\psi}_{1j}(3) + \hat{\psi}_{2j}(3) - \hat{\psi}_{3j}(3) - \hat{\psi}_{4j}(3)\right) \cdot K_z}{4}$$

$$V_{30} = \frac{\left(\hat{\psi}_{1i}(1) + \hat{\psi}_{2i}(1) - \hat{\psi}_{3i}(1) - \hat{\psi}_{4i}(1)\right) \cdot K_x + \left(\hat{\psi}_{1i}(2) + \hat{\psi}_{2i}(2) - \hat{\psi}_{3i}(2) - \hat{\psi}_{4i}(2)\right) \cdot K_y + \left(\hat{\psi}_{1i}(3) + \hat{\psi}_{2i}(3) - \hat{\psi}_{3i}(3) - \hat{\psi}_{4i}(3)\right) \cdot K_z}{4}$$

$$V_{31} = \frac{\left(\hat{\psi}_{1j}(1) + \hat{\psi}_{2j}(1) - \hat{\psi}_{3j}(1) - \hat{\psi}_{4j}(1)\right) \cdot J_x + \left(\hat{\psi}_{1j}(2) + \hat{\psi}_{2j}(2) - \hat{\psi}_{3j}(2) - \hat{\psi}_{4j}(2)\right) \cdot J_y + \left(\hat{\psi}_{1j}(3) + \hat{\psi}_{2j}(3) - \hat{\psi}_{3j}(3) - \hat{\psi}_{4j}(3)\right) \cdot J_z}{4}$$

$$V_{32} = \frac{\left(\hat{\psi}_{1i}(1) + \hat{\psi}_{2i}(1) - \hat{\psi}_{3i}(1) - \hat{\psi}_{4i}(1)\right) \cdot J_x + \left(\hat{\psi}_{1i}(2) + \hat{\psi}_{2i}(2) - \hat{\psi}_{3i}(2) - \hat{\psi}_{4i}(2)\right) \cdot J_y + \left(\hat{\psi}_{1i}(3) + \hat{\psi}_{2i}(3) - \hat{\psi}_{3i}(3) - \hat{\psi}_{4i}(3)\right) \cdot J_z}{4}$$

$$V_{33} = \frac{\left(\hat{\psi}_{1j}(1) + \hat{\psi}_{2j}(1) - \hat{\psi}_{3j}(1) - \hat{\psi}_{4j}(1)\right) \cdot I_x + \left(\hat{\psi}_{1j}(2) + \hat{\psi}_{2j}(2) - \hat{\psi}_{3j}(2) - \hat{\psi}_{4j}(2)\right) \cdot I_y + \left(\hat{\psi}_{1j}(3) + \hat{\psi}_{2j}(3) - \hat{\psi}_{3j}(3) - \hat{\psi}_{4j}(3)\right) \cdot I_z}{4}$$

$$V_{34} = \frac{\left(\hat{\psi}_{1i}(1) + \hat{\psi}_{2i}(1) - \hat{\psi}_{3i}(1) - \hat{\psi}_{4i}(1)\right) \cdot I_x + \left(\hat{\psi}_{1i}(2) + \hat{\psi}_{2i}(2) - \hat{\psi}_{3i}(2) - \hat{\psi}_{4i}(2)\right) \cdot I_y + \left(\hat{\psi}_{1i}(3) + \hat{\psi}_{2i}(3) - \hat{\psi}_{3i}(3) - \hat{\psi}_{4i}(3)\right) \cdot I_z}{4}$$

$$V_{35} = \frac{\left(\hat{\psi}_{1j}(1) + \hat{\psi}_{2j}(1) + \hat{\psi}_{3j}(1) + \hat{\psi}_{4j}(1)\right) \cdot K_x + \left(\hat{\psi}_{1j}(2) + \hat{\psi}_{2j}(2) + \hat{\psi}_{3j}(2) + \hat{\psi}_{4j}(2)\right) \cdot K_y + \left(\hat{\psi}_{1j}(3) + \hat{\psi}_{2j}(3) + \hat{\psi}_{3j}(3) + \hat{\psi}_{4j}(3)\right) \cdot K_z}{4}$$

$$V_{36} = \frac{\left(\hat{\psi}_{1i}(1) + \hat{\psi}_{2i}(1) + \hat{\psi}_{3i}(1) + \hat{\psi}_{4i}(1)\right) \cdot K_x + \left(\hat{\psi}_{1i}(2) + \hat{\psi}_{2i}(2) + \hat{\psi}_{3i}(2) + \hat{\psi}_{4i}(2)\right) \cdot K_y + \left(\hat{\psi}_{1i}(3) + \hat{\psi}_{2i}(3) + \hat{\psi}_{3i}(3) + \hat{\psi}_{4i}(3)\right) \cdot K_z}{4}$$

$$V_{37} = \frac{\left(\hat{\psi}_{1j}(1) + \hat{\psi}_{2j}(1) + \hat{\psi}_{3j}(1) + \hat{\psi}_{4j}(1)\right) \cdot J_x + \left(\hat{\psi}_{1j}(2) + \hat{\psi}_{2j}(2) + \hat{\psi}_{3j}(2) + \hat{\psi}_{4j}(2)\right) \cdot J_y + \left(\hat{\psi}_{1j}(3) + \hat{\psi}_{2j}(3) + \hat{\psi}_{3j}(3) + \hat{\psi}_{4j}(3)\right) \cdot J_z}{4}$$

$$V_{38} = \frac{\left(\hat{\psi}_{1i}(1) + \hat{\psi}_{2i}(1) + \hat{\psi}_{3i}(1) + \hat{\psi}_{4i}(1)\right) \cdot J_x + \left(\hat{\psi}_{1i}(2) + \hat{\psi}_{2i}(2) + \hat{\psi}_{3i}(2) + \hat{\psi}_{4i}(2)\right) \cdot J_y + \left(\hat{\psi}_{1i}(3) + \hat{\psi}_{2i}(3) + \hat{\psi}_{3i}(3) + \hat{\psi}_{4i}(3)\right) \cdot J_z}{4}$$

$$V_{39} = \frac{\left(\hat{\psi}_{1j}(1) + \hat{\psi}_{2j}(1) + \hat{\psi}_{3j}(1) + \hat{\psi}_{4j}(1)\right) \cdot I_x + \left(\hat{\psi}_{1j}(2) + \hat{\psi}_{2j}(2) + \hat{\psi}_{3j}(2) + \hat{\psi}_{4j}(2)\right) \cdot I_y + \left(\hat{\psi}_{1j}(3) + \hat{\psi}_{2j}(3) + \hat{\psi}_{3j}(3) + \hat{\psi}_{4j}(3)\right) \cdot I_z}{4}$$

$$V_{40} = \frac{\left(\hat{\psi}_{1i}(1) + \hat{\psi}_{2i}(1) + \hat{\psi}_{3i}(1) + \hat{\psi}_{4i}(1)\right) \cdot I_x + \left(\hat{\psi}_{1i}(2) + \hat{\psi}_{2i}(2) + \hat{\psi}_{3i}(2) + \hat{\psi}_{4i}(2)\right) \cdot I_y + \left(\hat{\psi}_{1i}(3) + \hat{\psi}_{2i}(3) + \hat{\psi}_{3i}(3) + \hat{\psi}_{4i}(3)\right) \cdot I_z}{4}$$

$$V_{41} = \frac{y_1 - y_2 - y_3 + y_4}{4}$$

$$V_{42} = \frac{x_1 - x_2 - x_3 + x_4}{4}$$

$$V_{43} = \frac{y_1 - y_2 + y_3 - y_4}{4}$$

$$V_{44} = \frac{y_1 + y_2 - y_3 - y_4}{4}$$

$$V_{45} = \frac{x_1 - x_2 + x_3 - x_4}{4}$$

$$V_{46} = \frac{x_1 + x_2 - x_3 - x_4}{4}$$

Annex B

PARAMETERS FOR SEISMIC VULNERABILITY

ASSESSMENT

Event	Young's Modulus	Shear Modulus	Specific weight	Tensile strength	Tensile fracture energy	Compressive strength	Ductility index	Compressive fracture energy	Shear strength	Friction coefficient	Cohesion	Friction coefficient	Ductility index	Fracture Energy	Thickness	Damping ratio
	E	G	γ x10^{-6}	f_t	$G_f{}^I$	f_c	d_{uc}	G_c	f_{y0}	μ_d	c	μ_s	d_{us}	$G_f{}^{II}$	s	ζ
	N/mm²	N/mm²	N/mm³	N/mm²	N/mm	N/mm²	mm	N/mm	N/mm²	-	N/mm²	-	mm	N/mm	mm	%
1	5068	1515	18.98	0.086	0.014	2.757	1.624	4.477	0.061	0.546	0.051	0.727	0.060	0.003	249.1	4.059
2	7617	2485	19.51	0.064	0.011	3.095	1.360	4.210	0.084	0.552	0.078	0.684	0.069	0.005	211.1	3.229
3	3564	1387	19.62	0.086	0.020	2.414	1.174	2.833	0.066	0.478	0.082	0.650	0.162	0.013	242.3	2.141
4	5406	2018	18.11	0.118	0.013	2.239	1.121	2.509	0.029	0.430	0.128	0.794	0.082	0.010	241.7	2.175
5	3116	1464	19.08	0.100	0.012	2.804	1.077	3.021	0.025	0.585	0.069	0.637	0.146	0.010	219.1	3.038
6	5603	1467	18.06	0.121	0.012	2.062	1.492	3.077	0.090	0.513	0.079	0.854	0.097	0.008	249.5	1.951
7	5342	1839	19.56	0.072	0.014	2.260	1.628	3.678	0.038	0.524	0.092	0.518	0.134	0.012	243.5	3.700
8	4237	1695	18.24	0.113	0.017	3.333	1.233	4.111	0.040	0.754	0.088	0.646	0.083	0.007	239.7	2.592
9	3648	1813	19.40	0.084	0.006	2.067	1.546	3.196	0.042	0.663	0.131	0.622	0.065	0.009	232.0	1.737
10	3455	1640	20.06	0.103	0.011	2.814	1.362	3.832	0.057	0.781	0.098	0.562	0.086	0.008	245.7	3.794
11	5067	3152	19.40	0.134	0.011	1.960	1.210	2.372	0.071	0.584	0.109	0.773	0.075	0.008	260.8	2.441
12	2795	2700	18.44	0.114	0.016	2.719	2.115	5.749	0.065	0.783	0.117	0.696	0.091	0.011	244.8	2.993
13	6889	1525	20.07	0.105	0.011	2.513	0.858	2.157	0.053	0.657	0.083	0.469	0.102	0.008	234.5	2.070
14	3407	3435	19.51	0.116	0.010	2.197	1.477	3.243	0.045	0.583	0.076	0.710	0.083	0.006	238.6	2.275
15	3642	1802	18.91	0.105	0.008	2.304	1.971	4.540	0.056	0.475	0.101	0.920	0.111	0.011	229.9	2.725
16	6781	1652	18.57	0.128	0.016	2.285	1.275	2.913	0.035	0.672	0.095	0.693	0.085	0.008	254.6	2.078
17	6855	1919	18.58	0.091	0.021	2.372	1.435	3.404	0.070	0.550	0.095	0.540	0.117	0.011	242.8	2.564
18	3851	2703	19.06	0.076	0.014	2.327	1.709	3.977	0.048	0.488	0.113	0.433	0.132	0.015	237.9	2.085
19	6027	2121	19.84	0.102	0.012	2.256	1.031	2.325	0.084	0.687	0.143	0.758	0.078	0.011	245.7	5.120
20	4166	2200	19.19	0.084	0.017	3.098	1.163	3.604	0.099	0.607	0.207	0.654	0.145	0.030	232.0	3.217
21	7047	3051	18.60	0.091	0.007	2.240	1.658	3.714	0.137	0.721	0.066	0.916	0.090	0.006	237.4	2.571
22	6424	1698	18.63	0.097	0.007	3.670	1.806	6.629	0.046	0.512	0.131	0.682	0.081	0.011	221.1	2.269
23	3957	1524	20.30	0.109	0.013	2.875	1.211	3.481	0.116	0.648	0.124	0.724	0.071	0.009	224.1	2.796
24	5289	3336	18.22	0.125	0.014	2.554	1.841	4.702	0.035	0.614	0.080	0.734	0.080	0.006	231.3	3.119
25	5335	2778	18.50	0.124	0.008	2.565	2.082	5.340	0.099	0.415	0.112	0.639	0.095	0.011	213.0	2.396
26	6455	1527	19.52	0.128	0.012	2.366	1.650	3.904	0.054	0.639	0.271	0.542	0.100	0.027	244.7	2.322
27	5907	2621	18.80	0.137	0.016	2.443	1.806	4.413	0.070	0.495	0.126	0.555	0.110	0.014	230.1	2.547
28	4827	2429	19.60	0.078	0.013	2.451	0.853	2.089	0.104	0.634	0.128	0.561	0.064	0.008	234.3	1.707
29	7162	3012	18.33	0.112	0.020	2.860	1.324	3.787	0.123	0.754	0.114	0.809	0.045	0.005	233.1	2.734

Event	Young's Modulus	Shear Modulus	Specific weight	Tensile strength	Tensile fracture energy	Compressive strength	Ductility index	Compressive fracture energy	Shear strength	Friction coefficient	Cohesion	Friction coefficient	Ductility index	Fracture Energy	Thickness	Damping ratio
	E	G	$\gamma \times 10^{-6}$	f_t	G_f^I	f_c	d_{uc}	G_c	f_{y0}	μ_d	c	μ_s	d_{us}	G_f^{II}	s	ζ
	N/mm²	N/mm²	N/mm³	N/mm²	N/mm	N/mm²	mm	N/mm	N/mm²	-	N/mm²	-	mm	N/mm	mm	%
30	5322	1759	18.34	0.106	0.009	2.395	1.790	4.288	0.063	0.511	0.114	0.553	0.073	0.008	241.0	2.123
31	3904	2035	18.12	0.065	0.008	2.601	1.757	4.570	0.042	0.746	0.101	0.926	0.075	0.008	227.9	3.250
32	3683	4424	17.94	0.126	0.013	2.646	1.374	3.637	0.084	0.671	0.174	0.708	0.086	0.015	240.1	2.604
33	3080	3061	18.93	0.088	0.009	2.469	1.370	3.383	0.067	0.427	0.089	0.703	0.082	0.007	239.2	1.896
34	6913	2015	18.44	0.094	0.013	2.385	1.266	3.019	0.096	0.524	0.103	0.605	0.047	0.005	258.7	2.741
35	4970	1734	20.21	0.090	0.012	2.713	2.356	6.393	0.056	0.519	0.129	0.635	0.052	0.007	221.4	3.502
36	4379	1725	17.74	0.085	0.013	2.363	2.756	6.513	0.062	0.500	0.054	0.560	0.056	0.003	255.3	3.085
37	6453	1859	19.25	0.096	0.011	2.271	1.351	3.068	0.083	0.584	0.205	0.649	0.081	0.017	218.6	2.905
38	5442	1403	19.12	0.158	0.009	2.723	1.017	2.769	0.062	0.731	0.113	0.777	0.096	0.011	227.0	4.813
39	3160	1389	19.34	0.092	0.011	2.037	2.572	5.241	0.062	0.705	0.095	0.488	0.117	0.011	235.8	5.039
40	5983	2527	18.82	0.102	0.010	2.338	0.900	2.103	0.070	0.559	0.184	0.706	0.175	0.032	213.6	3.703
41	6623	1333	18.94	0.115	0.009	2.261	0.669	1.512	0.072	0.535	0.103	0.922	0.068	0.007	213.3	2.067
42	5174	1479	18.71	0.102	0.010	2.407	0.992	2.389	0.048	0.723	0.084	0.757	0.143	0.012	248.8	3.527
43	4965	2472	18.58	0.093	0.009	2.699	2.693	7.269	0.091	0.577	0.065	0.586	0.079	0.005	249.9	2.071
44	3827	1720	19.09	0.099	0.013	2.741	1.562	4.281	0.077	0.588	0.133	0.561	0.060	0.008	231.2	3.307
45	6261	2489	18.51	0.112	0.012	2.556	0.942	2.407	0.044	0.574	0.062	0.485	0.070	0.004	219.2	2.664
46	3247	2289	18.74	0.126	0.020	2.056	1.403	2.884	0.054	0.587	0.076	0.850	0.108	0.008	241.7	2.908
47	4504	1050	19.08	0.113	0.009	2.330	1.598	3.724	0.071	0.420	0.080	0.736	0.071	0.006	245.8	4.330
48	3372	2300	19.36	0.140	0.015	2.411	1.483	3.575	0.039	0.720	0.072	0.647	0.098	0.007	232.9	3.426
49	2355	2577	18.81	0.105	0.008	2.695	1.509	4.067	0.044	0.567	0.102	0.437	0.091	0.009	241.7	4.327
50	5345	2867	18.49	0.084	0.009	2.455	1.874	4.600	0.105	0.509	0.125	0.605	0.128	0.016	262.3	1.976
51	3081	3196	19.14	0.107	0.009	2.277	1.412	3.216	0.047	0.532	0.068	0.662	0.054	0.004	226.4	3.474
52	5185	1705	18.81	0.111	0.012	2.751	2.013	5.537	0.046	0.853	0.086	0.799	0.088	0.008	238.3	2.284
53	8146	1875	18.59	0.098	0.008	2.243	1.913	4.291	0.026	0.547	0.080	0.557	0.083	0.007	273.2	1.811
54	3204	1663	18.38	0.109	0.014	2.124	1.258	2.672	0.125	0.620	0.109	0.660	0.128	0.014	226.1	4.479
55	5499	1447	18.20	0.122	0.012	2.816	2.016	5.677	0.107	0.447	0.053	0.822	0.054	0.003	230.4	2.832
56	4591	2157	18.44	0.075	0.011	2.403	1.254	3.012	0.047	0.540	0.111	0.670	0.079	0.009	243.0	2.983
57	3742	1526	18.51	0.096	0.011	3.098	1.298	4.022	0.068	0.666	0.081	0.765	0.064	0.005	246.5	2.482
58	6418	1815	18.65	0.103	0.011	2.578	1.385	3.570	0.049	0.600	0.074	0.770	0.098	0.007	263.5	2.406
59	8185	1706	19.60	0.113	0.013	2.776	1.154	3.205	0.101	0.649	0.101	0.666	0.084	0.008	232.2	2.635

Event	Young's Modulus	Shear Modulus	Specific weight	Tensile strength	Tensile fracture energy	Compressive strength	Ductility index	Compressive fracture energy	Shear strength	Friction coefficient	Cohesion	Friction coefficient	Ductility index	Fracture Energy	Thickness	Damping ratio
	E	G	γ x10^{-6}	f_t	G_f^I	f_c	d_{uc}	G_c	f_{y0}	μ_d	c	μ_s	d_{us}	G_f^{II}	s	ζ
	N/mm^2	N/mm^2	N/mm^3	N/mm^2	N/mm	N/mm^2	mm	N/mm	N/mm^2	-	N/mm^2	-	mm	N/mm	mm	%
60	4345	1990	18.37	0.079	0.010	2.260	2.011	4.546	0.058	0.526	0.227	0.733	0.071	0.016	234.1	3.601
61	5294	2545	19.02	0.100	0.009	2.373	0.765	1.815	0.159	0.548	0.060	0.659	0.131	0.008	234.3	3.726
62	4375	839	19.11	0.081	0.008	2.707	1.660	4.494	0.055	0.613	0.093	0.949	0.114	0.011	231.1	3.304
63	6996	2439	18.60	0.115	0.010	2.412	1.190	2.870	0.059	0.604	0.078	0.805	0.087	0.007	246.6	2.992
64	5122	2615	18.12	0.081	0.013	1.973	1.406	2.773	0.067	0.474	0.094	0.590	0.103	0.010	230.7	2.662
65	5280	1856	19.74	0.116	0.011	2.715	1.583	4.298	0.081	0.698	0.102	0.594	0.117	0.012	230.7	4.838
66	7041	3356	19.36	0.089	0.015	2.508	2.182	5.472	0.105	1.095	0.052	0.707	0.160	0.008	235.0	3.123
67	6455	1256	19.29	0.093	0.016	2.469	1.059	2.615	0.085	0.525	0.088	0.538	0.131	0.012	227.3	3.479
68	4131	1769	18.53	0.090	0.010	2.365	1.609	3.805	0.058	0.679	0.075	0.547	0.070	0.005	244.4	3.476
69	3710	1789	19.65	0.102	0.014	2.006	1.276	2.559	0.103	0.389	0.141	0.702	0.083	0.012	241.1	1.466
70	7781	2668	19.10	0.091	0.014	2.277	1.378	3.138	0.035	0.679	0.142	0.705	0.080	0.011	224.9	4.665
71	4595	1612	18.26	0.091	0.011	3.491	1.739	6.070	0.054	0.732	0.101	0.957	0.073	0.007	224.2	1.933
72	2871	1124	18.42	0.116	0.017	2.228	1.722	3.838	0.101	0.559	0.048	0.545	0.103	0.005	209.5	2.773
73	4161	1662	19.47	0.084	0.015	3.228	1.168	3.772	0.053	0.625	0.086	0.851	0.126	0.011	239.9	2.515
74	4649	2430	17.78	0.122	0.026	2.770	1.802	4.991	0.070	0.640	0.066	0.659	0.103	0.007	249.6	2.193
75	5650	2444	18.63	0.121	0.011	2.049	1.551	3.178	0.053	0.780	0.100	0.576	0.098	0.010	238.4	4.326
76	4076	2605	19.51	0.099	0.011	2.709	1.192	3.229	0.057	0.692	0.065	0.940	0.074	0.005	236.4	1.876
77	2759	1589	18.59	0.110	0.007	2.339	1.652	3.864	0.100	0.721	0.089	0.704	0.068	0.006	236.1	2.357
78	6657	2369	18.06	0.109	0.013	2.105	1.401	2.949	0.089	0.583	0.099	0.797	0.105	0.010	243.8	2.309
79	6911	1601	18.62	0.080	0.018	2.738	1.265	3.464	0.094	0.497	0.070	0.610	0.083	0.006	217.5	1.475
80	9220	2120	19.25	0.161	0.008	2.694	1.725	4.646	0.098	0.579	0.135	0.675	0.065	0.009	224.6	2.919
81	5361	4199	19.12	0.124	0.006	2.744	1.196	3.283	0.062	0.540	0.064	0.737	0.096	0.006	241.8	4.502
82	5183	1711	18.73	0.107	0.010	2.664	1.885	5.020	0.060	0.644	0.232	0.742	0.112	0.026	261.4	5.893
83	4574	2831	18.67	0.060	0.008	2.359	1.540	3.632	0.030	0.881	0.126	0.609	0.036	0.005	218.4	3.688
84	6613	2722	20.24	0.081	0.016	2.183	2.309	5.042	0.063	0.636	0.061	0.492	0.066	0.004	239.6	3.124
85	6150	1562	19.29	0.079	0.026	3.238	2.370	7.672	0.030	0.624	0.083	0.575	0.094	0.008	240.3	1.852
86	4541	1327	18.42	0.103	0.010	2.041	1.599	3.265	0.078	0.620	0.109	0.588	0.100	0.011	236.7	4.932
87	4899	2716	18.79	0.121	0.012	1.987	1.660	3.299	0.050	0.549	0.127	0.684	0.087	0.011	233.2	2.805
88	3505	1588	19.10	0.082	0.009	2.499	1.613	4.030	0.041	0.423	0.066	0.896	0.086	0.006	230.6	3.374
89	3847	2454	17.76	0.095	0.010	2.928	1.584	4.637	0.068	0.813	0.040	0.644	0.069	0.003	238.7	2.485

Event	Young's Modulus	Shear Modulus	Specific weight	Tensile strength	Tensile fracture energy	Compressive strength	Ductility index	Compressive fracture energy	Shear strength	Friction coefficient	Cohesion	Friction coefficient	Ductility index	Fracture Energy	Thickness	Damping ratio
	E	G	$\gamma \times 10^{-6}$	f_t	G_f^I	f_c	d_{uc}	G_c	f_{y0}	μ_d	c	μ_s	d_{us}	G_f^{II}	s	ζ
	N/mm²	N/mm²	N/mm³	N/mm²	N/mm	N/mm²	mm	N/mm	N/mm²	-	N/mm²	-	mm	N/mm	mm	%
90	5788	2274	18.78	0.104	0.013	2.630	1.658	4.362	0.106	0.533	0.059	0.515	0.079	0.005	236.7	3.327
91	3102	1927	18.57	0.090	0.009	2.487	1.284	3.194	0.061	0.627	0.069	1.046	0.108	0.007	239.5	2.444
92	4997	1892	18.93	0.091	0.015	2.141	3.326	7.122	0.101	0.632	0.068	0.607	0.105	0.007	224.6	2.089
93	8448	2252	18.70	0.107	0.012	2.609	1.221	3.185	0.038	0.476	0.097	0.644	0.085	0.008	217.9	1.699
94	6347	1718	20.37	0.110	0.014	2.638	1.095	2.888	0.054	0.714	0.118	0.649	0.073	0.009	221.8	2.552
95	5517	2378	19.27	0.169	0.009	2.716	1.118	3.035	0.094	0.593	0.198	0.873	0.143	0.028	227.4	4.053
96	5836	3630	19.02	0.125	0.016	2.952	1.877	5.541	0.058	0.505	0.058	0.666	0.097	0.006	235.8	3.719
97	5462	3136	19.54	0.125	0.007	2.143	1.599	3.427	0.066	0.632	0.070	0.519	0.059	0.004	224.2	2.036
98	4581	2558	19.46	0.109	0.011	2.277	1.215	2.767	0.055	0.454	0.093	0.525	0.048	0.004	233.4	3.215
99	3104	1966	19.13	0.130	0.018	2.494	1.100	2.744	0.093	0.624	0.141	0.626	0.110	0.016	247.0	2.988
100	4679	2068	18.68	0.078	0.009	2.792	1.627	4.542	0.049	0.613	0.094	0.556	0.099	0.009	231.3	3.262
101	7117	2317	17.84	0.112	0.010	2.069	2.372	4.908	0.071	0.552	0.097	0.743	0.066	0.006	240.3	3.277
102	5190	1606	19.74	0.109	0.017	2.756	1.459	4.020	0.105	0.489	0.083	0.532	0.111	0.009	232.4	2.866
103	3361	2040	18.22	0.089	0.010	1.907	1.300	2.478	0.052	0.651	0.107	0.487	0.112	0.012	249.7	3.789
104	3784	1455	17.89	0.113	0.014	2.308	1.512	3.491	0.048	0.655	0.122	0.714	0.069	0.008	218.1	2.633
105	3802	1810	18.70	0.120	0.011	2.299	1.812	4.166	0.055	0.685	0.142	0.828	0.082	0.012	258.3	2.871
106	10571	1794	17.61	0.091	0.009	2.893	1.959	5.667	0.068	0.652	0.107	0.720	0.143	0.015	237.7	2.957
107	4291	3008	17.92	0.143	0.009	2.078	1.731	3.595	0.056	0.603	0.139	0.760	0.083	0.011	229.0	2.317
108	7268	1535	17.87	0.104	0.018	2.664	1.355	3.610	0.068	0.539	0.168	0.626	0.077	0.013	225.9	1.965
109	3655	1464	19.04	0.091	0.012	2.903	1.967	5.710	0.045	0.621	0.081	0.508	0.051	0.004	234.1	4.324
110	5414	2661	18.50	0.106	0.010	2.262	1.107	2.504	0.053	0.562	0.074	0.634	0.094	0.007	224.1	2.367
111	3430	1861	18.91	0.077	0.012	2.910	1.414	4.116	0.068	0.437	0.175	0.660	0.072	0.013	241.3	2.485
112	6091	2611	19.02	0.089	0.018	3.180	1.806	5.742	0.051	0.664	0.049	0.548	0.066	0.003	228.7	2.126
113	4070	2223	18.52	0.094	0.012	2.425	1.691	4.099	0.033	0.697	0.174	0.644	0.087	0.015	234.3	2.916
114	4011	2048	18.37	0.111	0.012	2.394	1.109	2.656	0.028	0.620	0.041	0.811	0.101	0.004	226.3	1.830
115	7029	2491	20.34	0.085	0.014	1.864	1.175	2.190	0.068	0.951	0.112	0.473	0.082	0.009	236.2	2.496
116	4443	1741	19.28	0.102	0.014	2.346	2.000	4.693	0.034	0.410	0.101	0.931	0.073	0.007	237.6	3.395
117	3528	2927	19.67	0.074	0.017	2.259	1.267	2.861	0.028	0.537	0.073	0.614	0.094	0.007	230.8	3.612
118	5125	1696	19.07	0.128	0.012	2.929	1.533	4.491	0.042	0.579	0.205	0.688	0.136	0.028	247.9	1.672
119	3986	2377	18.88	0.124	0.008	2.277	1.941	4.420	0.069	0.502	0.062	0.862	0.078	0.005	211.6	3.937

Event	Young's Modulus	Shear Modulus	Specific weight	Tensile strength	Tensile fracture energy	Compressive strength	Ductility index	Compressive fracture energy	Shear strength	Friction coefficient	Cohesion	Friction coefficient	Ductility index	Fracture Energy	Thickness	Damping ratio
	E	G	γ x10^{-6}	f_t	G_f^I	f_c	d_{uc}	G_c	f_{y0}	μ_d	c	μ_s	d_{us}	G_f^{II}	s	ζ
	N/mm²	N/mm²	N/mm³	N/mm²	N/mm	N/mm²	mm	N/mm	N/mm²	-	N/mm²	-	mm	N/mm	mm	%
120	8247	3155	18.71	0.113	0.015	2.056	0.754	1.550	0.054	0.862	0.071	0.582	0.076	0.005	247.4	2.092
121	4637	2516	17.61	0.082	0.010	2.989	2.632	7.866	0.167	0.565	0.103	0.734	0.052	0.005	261.0	4.449
122	4856	1697	18.73	0.130	0.013	2.344	1.840	4.314	0.056	0.688	0.085	0.686	0.082	0.007	235.4	3.668
123	3338	1633	19.13	0.099	0.013	2.493	0.854	2.128	0.048	0.786	0.065	0.795	0.083	0.005	239.5	4.049
124	9985	2043	18.19	0.079	0.005	3.106	1.764	5.480	0.086	0.487	0.067	0.473	0.060	0.004	234.6	2.189
125	4848	2274	18.93	0.108	0.010	2.046	3.092	6.325	0.062	0.725	0.090	0.941	0.119	0.011	221.3	2.148